

## INFORMATION TO USERS

This manuscript has been reproduced from the microfilm master. UMI films the text directly from the original or copy submitted. Thus, some thesis and dissertation copies are in typewriter face, while others may be from any type of computer printer.

**The quality of this reproduction is dependent upon the quality of the copy submitted.** Broken or indistinct print, colored or poor quality illustrations and photographs, print bleedthrough, substandard margins, and improper alignment can adversely affect reproduction.

In the unlikely event that the author did not send UMI a complete manuscript and there are missing pages, these will be noted. Also, if unauthorized copyright material had to be removed, a note will indicate the deletion.

Oversize materials (e.g., maps, drawings, charts) are reproduced by sectioning the original, beginning at the upper left-hand corner and continuing from left to right in equal sections with small overlaps.

ProQuest Information and Learning  
300 North Zeeb Road, Ann Arbor, MI 48106-1346 USA  
800-521-0600

UMI<sup>®</sup>



University of Alberta

**Recent and Fossil Spring Deposits at Miette Hot Springs,  
Jasper National Park, Alberta, Canada**

by

**Sandy Marie Bonny** ©

A thesis submitted to the Faculty of Graduate Studies and Research in partial fulfillment  
of the requirements for the degree of **Master of Science**.

Department of Earth and Atmospheric Science

Edmonton, Alberta  
Fall, 2002



**National Library  
of Canada**

**Acquisitions and  
Bibliographic Services**

**395 Wellington Street  
Ottawa ON K1A 0N4  
Canada**

**Bibliothèque nationale  
du Canada**

**Acquisitions et  
services bibliographiques**

**395, rue Wellington  
Ottawa ON K1A 0N4  
Canada**

*Your file Votre référence*

*Our file Notre référence*

**The author has granted a non-exclusive licence allowing the National Library of Canada to reproduce, loan, distribute or sell copies of this thesis in microform, paper or electronic formats.**

**The author retains ownership of the copyright in this thesis. Neither the thesis nor substantial extracts from it may be printed or otherwise reproduced without the author's permission.**

**L'auteur a accordé une licence non exclusive permettant à la Bibliothèque nationale du Canada de reproduire, prêter, distribuer ou vendre des copies de cette thèse sous la forme de microfiche/film, de reproduction sur papier ou sur format électronique.**

**L'auteur conserve la propriété du droit d'auteur qui protège cette thèse. Ni la thèse ni des extraits substantiels de celle-ci ne doivent être imprimés ou autrement reproduits sans son autorisation.**

0-612-81368-1

**Canada**

**University of Alberta**

**Library Release Form**

**Name of Author:** *Sandy Marie Bonny*

**Title of Thesis:** *Recent and Fossil Spring Deposits at Miette Hot Springs, Jasper National Park, Alberta*

**Degree:** *Master of Science*

**Year this Degree Granted:** *2002*

Permission is hereby granted to the University of Alberta Library to reproduce single copies of this thesis and to lend or sell such copies for private, scholarly or scientific research purposes only.

The author reserves all other publication and other rights in association with the copyright in the thesis, and except as herein before provided, neither the thesis nor any substantial portion thereof may be printed or otherwise reproduced in any material form whatever without the author's prior written permission.

Signed: *Sandy M. Bonny*

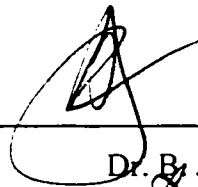
Permanent Address: 1612 3<sup>rd</sup> Avenue  
RR 4, Invermere, B.C.  
VOA 1K4

Date submitted to the Faculty of Graduate Studies and Research:: *Aug 28 / 02*

**University of Alberta**

**Faculty of Graduate Studies and Research**

The undersigned certify that they have read, and recommend to the Faculty of Graduate Studies and Research for acceptance, a thesis entitled **Recent and Fossil Spring Deposits at Miette Hot Springs, Jasper National Park, Alberta, Canada** submitted by **Sandy Marie Bonny** in partial fulfillment of the requirements for the degree of **Master of Science**.

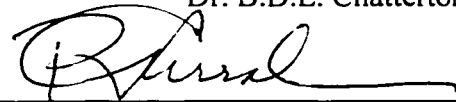


---

Dr. B. Jones (Supervisor)

---

Dr. B.D.E. Chatterton



---

Dr. R.S. Currah

Date thesis approved: Aug 27 / 08

## ABSTRACT

The Miette Hot Springs in Jasper National Park, Alberta, have an average vent temperature of 51°C, and issue Ca, CO<sub>3</sub><sup>2-</sup>, and H<sub>2</sub>S/SO<sub>4</sub><sup>2-</sup> rich water that precipitates gypsum, elemental sulphur, calcite, and strontianite, and hosts a rich microbial assemblage. Cooling and degassing induce precipitation but minerals accumulate in microbial mucus and adhere to microbial sheaths, and photosynthesis influences  $\delta^{13}\text{C}_{\text{mineral}}$  values.

Fossil tufa at Miette was generated by thermal springs issuing at 50-65°C between ~4,500 and 2,500 years BP, and a warm spring of indeterminate age, that perched ~30 m above the modern springs on an unstable slope. Variant flow path topography produced six tufa morphotypes, and differences in water temperature, style of flow, and flow path biology produced eight primary facies. Primary facies alternations are commonly sharp, representing abrupt changes in depositional conditions instigated by landslides and rockfalls. Diagenesis produced two other facies and obscured  $\delta^{13}\text{C}$  and  $\delta^{18}\text{O}$  signatures.

## ACKNOWLEDGEMENTS

Thanks are extended to Dr. Brian Jones for his guidance in the completion of this thesis, to the Carbonate Research Group (Alex MacNeil, Rong-Yu Li, Samantha Etherington, Morag Coyne and Dustin Rainey) for their friendliness, and to my family for their support.

A number of people gave advice or assistance concerning aspects of this thesis and I would particularly like to thank Dr. Karlis Muehlenbachs and Neil Banjaree (re: stable isotopes), Dr. Alex Wolfe (re: identification of microbes), and Dr. Rick Forester (re: identification of ostracodes). George Braybrook spent many hours on the SEM exploring the fossil tufa with me, Zoe Parr and Klayton Kaleta helped to map fossil tufa outcrops (in the rain!), Sheila Bonny offered proof-reading skills, Brian Jones, Liz Taylor and Morag Coyne accompanied me on field trips, and Julius Davidson and Mary Saretski supplied helpful commentary.

This research was funded by the Natural Science and Engineering Research Council of Canada (A6090 to B. Jones) and conducted under Parks Canada permit #2001-001.



## TABLE OF CONTENTS

	page
<b>Chapter 1 Background and Project Overview</b>	
1.1 Introduction	1
1.2 Background	
<i>1.2a Spring Systems and Definitions</i>	2
<i>1.2b Canadian Springs</i>	5
<i>1.2c Western Canadian Springs</i>	7
1.3 Study Site: the Miette Hot Springs	
<i>1.3a Physiogeographic Context</i>	8
<i>1.3b History and Previous Work</i>	11
1.4 Project Objectives	17
1.5 Methods	
<i>1.5a Field Methods</i>	17
<i>1.5b Laboratory Methods</i>	18
<b>Chapter 2 The Modern Miette Hot Springs</b>	
2.1 General Description	21
2.2 Water Chemistry	21
2.3 Microbial Assemblages	28
2.4 Precipitates	42
2.5 Interplays Between Microbes and Precipitates	50
2.5 Summary	56
<b>Chapter 3 The Fossil Miette Tufa Deposits</b>	
3.1 General Description	58
3.2 Tufa Morphotypes	61
3.3 Tufa Facies	
<i>3.3a Tufa/Allochthonous Lithoclast Conglomerate Facies</i>	66
<i>3.3b Stromatolitic Tufa</i>	
3.3bi Streamer Facies	68
3.3bii Porous Laminar Facies	71
3.3biii Dense Laminar Facies	79
<i>3.3c Bedded Facies</i>	87
<i>3.3d Crenulated Facies</i>	89
<i>3.3e Sheet Facies</i>	92
<i>3.3f Granular Facies</i>	95
<i>3.3g Bryophyte Facies (and Mineralized Wood)</i>	100
<i>3.3h Massive Facies</i>	111
3.4 Original Deposit Morphology and Depositional Context of the Facies	111
3.5 Facies Alternations	114
3.6 Summary	117

<b>Chapter 4</b>	<b>Stable Isotope Study of the Stromatolitic Tufa</b>	
	4.1 Introduction	118
	4.2 Stromatolitic Layering in the Fossil Miette Tufa	120
	4.3 Results and Interpretation	121
	4.4 Discussion	124
	4.5 Conclusion	130
<b>Chapter 5</b>	<b>The Fossil Miette Springs: Physiochemistry, Length of Activity and Palaeoenvironmental Context</b>	
	5.1 Introduction	132
	5.2 Physiochemistry of the Fossil Miette Springs	
	5.2a Miette South-North (MS-MN)	132
	5.2b Miette Far North End (MNN)	136
	5.3 Precipitation at the Fossil Springs	137
	5.4 Growth Rate and Age of the Fossil Miette Tufa	140
	5.5 Palaeoenvironmental Context	143
	5.6 Summary	146
<b>Chapter 6</b>	<b>Diagenesis in the Fossil Miette Tufa</b>	
	6.1 Introduction	148
	6.2 Environmental Stress	148
	6.3 Microbiological Colonization	149
	6.4 Mineralogical Changes	151
	6.5 Summary	164
<b>Chapter 7</b>	<b>Conclusions</b>	165

## Works Cited

**Appendix 1:** Key features used to identify cyanobacteria.

**Appendix 2:** Compiled stable carbon and oxygen isotope values discussed in Chapter 4.

## LIST OF TABLES

	page
1.1 Physical characteristics of Canadian springs.	6
1.2 Description of geological formations shown in figures 1.3 and 1.4.	14
2.1 Miette Hot Springs water chemistry measured at various dates.	23
2.2 Physical data collected from the Miette Hot Springs in June, 2001.	26
2.3 Variation in the water chemistry of Sulphur Creek before and after the addition of water from the Miette Hot Springs.	27
2.4 Stable carbon and oxygen isotope measurements for water and precipitates collected from the discharge paths of springs 3, 3a and seep 3b.	51
5.1 Upper temperature limits and preferred pH of organisms found in the fossil Miette tufa.	134

## LIST OF FIGURES

	page	
1.1	Distribution of thermal springs in the Canadian Cordillera.	9
1.2	Location map for the Miette Hot Springs.	10
1.3	Geologic map of the Miette Hot Springs site.	12
1.4	Cross-section of bedrock geology beneath the Miette Hot Springs.	13
2.1	Location map showing the modern hot springs and fossil tufa in Sulphur Creek Valley.	22
2.2	Photograph of spring vent 3 and the catchment basin below it.	29
2.3	Photograph of the discharge path beneath spring vent 3a.	30
2.4	Photographs of spring vent 3a and seep 3b.	31
2.5	Filamentous cyanobacteria from mats at the Miette Hot Springs.	33
2.6	Basal layer microbial mats at the Miette Hot Springs.	35
2.7	Unicellular microbes found in microbial mats at the Miette Hot Springs.	36
2.8-10	Diatom species found in spring discharge at the Miette Hot Springs.	38-40
2.11	Large gypsum crystals found in the spring flow paths.	44
2.12	Gypsum crystallites found adhering to microbial filaments at the mixing zone between spring and creek water.	45
2.13	Elemental Sulphur found in the spring flow paths.	47
2.14	Calcite crystal habits found in the spring flow paths.	48
2.15	Strontianite crystal habits found in the spring flow paths.	49
2.16	Diatom rich mucus with corroded gypsum and calcite crystals.	53
2.17	Bi-terminal calcite crystals found in microbial mats.	54
3.1	Former spring vent pools and fossil tufa at the Miette Hot Springs site.	59
3.2	General view of the fossil Miette tufa exposure.	60
3.3	Domal and roll-over tufa morphotypes in outcrop.	62

3.4	Vertical and flat banded tufa morphotypes in outcrop.	64
3.5	Wedge-shaped and mossy bed tufa morphotypes in outcrop.	65
3.6	Outcrop and thin section images of the tufa/allochthonous lithoclast conglomerate facies.	67
3.7	Outcrop and thin section images of streamer facies.	69
3.8	Microbial mediated textures in porous laminar facies.	72
3.9	Microbial filaments and filament casts in porous laminar facies.	73
3.10	Composite bi-terminal calcite crystals in porous laminar facies.	74
3.11	Upright vertical sheets in porous laminar facies.	76
3.12	Mineralised organic debris found in porous laminar facies.	77
3.13	Upright columns (filament structures) in dense laminar facies.	80
3.14	Flat-lying rods (filament structures) in dense laminar facies.	81
3.15	Composite bi-terminal calcite crystals in dense laminar facies.	82
3.16	Microbial filaments preserved by sheath impregnation in dense laminar facies.	84
3.17	Hand sample and thin section images of the bedded facies.	88
3.18	Outcrop and SEM images of the crenulated facies.	90
3.19	Crenulated sheets composed of bi-terminal calcite crystals.	91
3.20	Outcrop and SEM images of the sheet facies.	93
3.21	Sparry trigonal calcite crystals and microbial filaments found in the sheet facies.	94
3.22	Hand sample image and SEM images of gypsum and strontianite crystals found in the granular facies.	96
3.23	Trigonal sparry calcite and faceted sparry calcite in the granular facies.	97
3.24	Nodular clay coatings and microbial filaments in the granular facies.	99
3.25	Bryophyte facies tufa in outcrop, thin section and SEM.	101
3.26	Calcite crystal habits found in bryophyte facies tufa.	102

3.27	Bryophyte stem and leaf casts in bryophyte facies tufa.	104
3.28	Mineralised plant cells, microbial filaments and siliceous auxospores in bryophyte facies tufa.	105
3.29	SEM images of <i>Orthoseira roseana</i> .	106
3.30	SEM images of differentially preserved ostracode carapaces.	107
3.31	Mineralised wood found associated with bryophyte facies tufa.	108
3.32	Bubble structures found in bryophyte facies tufa.	109
3.33	Outcrop, SEM and thin section images of the massive facies.	112
3.34	Idealised profile of the fossil Miette spring mound at MS, MC and MN showing depositional environments and associated tufa facies.	113
3.35	Idealised profile of the fossil Miette spring mound at MNN showing depositional environments and associated tufa facies.	115
4.1	Hand sample drawing and stable carbon and oxygen isotope values measured from successive laminae in porous laminar facies sample M22.	122
4.2	Hand sample drawing and stable carbon and oxygen isotope values measured from successive laminae in porous laminar facies sample M29.	123
4.3	Hand sample drawing and stable carbon and oxygen isotope values measured from successive laminae in transitional stromatolitic facies sample M13.	125
4.4	Hand sample drawing and stable carbon and oxygen isotope values measured from successive laminae in dense laminar facies sample M24.	126
4.5	Stable carbon and oxygen isotope values measured from samples collected along a downslope transect at MS.	127
5.1	Photograph of bison bone, locations of sites in fig. 5.2	142
5.2	Palaeoenvironmental context of the fossil Miette Hot Springs.	144
6.1	Soft lime coating found in former spring vent pool caves images of chasmolithic microbes in the fossil Miette tufa.	150
6.2	Microborings produced by endolithic microbes in the fossil Miette tufa.	152
6.3	Calcite cements in the fossil Miette tufa.	154
6.4	Twinned needle fibre micrite in the fossil Miette tufa.	157

6.5	Micro-rod micrite in the fossil Miette tufa.	159
6.6	Nodular and rhombic micrite in the fossil Miette tufa.	161
6.7	Dodecahedral and rhombic calcium oxalate in the fossl Miette tufa.	162

# 1 Background and Project Overview

## 1.1 Introduction

The Collin's English Dictionary (1999) defines a spring as a "natural outflow of groundwater", and as "a source or origin." At the mouth of a spring, waters that have percolated through the earth, thus gaining a mineral load via dissolution of bedrock, complete their underground journey and emerge into open space. The decrease in pressure, and often temperature, concurrent with emergence of the spring water commonly results in supersaturation with one or more mineral phase. The spring vent is thus the source and origin of mineral spring deposits.

The mineralogy and texture of spring deposits are influenced by factors intrinsic to the spring water (such as temperature and mineral content) and by extrinsic environmental variables (such as flow path biology, topography, and ambient climate). As *in situ* precipitates, spring deposits have potential to record environmental information, and, because minerals are deposited on all components of the spring flow path, spring deposited rocks commonly contain textures that reflect the structure of microbial or macrophytic organisms that lived in the spring water. Thus, spring deposited rocks are of scientific interest because they may contain palaeoenvironmental information (Chafetz *et al.*, 1991b; Griffiths *et al.*, 1996; Pedley *et al.*, 1996; Andrews *et al.*, 1997) and can be used as analogues for the interpretation of ancient (and possibly extraterrestrial) fossils (Hoffman, 1975; Knoll and Barhoorn, 1975; Kazmierczak and Kempe, 1990; Bartley, 1996). Rocks formed in association with cyanobacteria have also gained attention as hydrocarbon source rocks. Bauld (1981) wrote: "Cyanobacterial mats are highly productive and the physiochemical properties of these [mat] environments confer a high preservation potential." Though spring deposits are of limited size, and would not be viable to exploit for hydrocarbon extraction, spring flow paths commonly host cyanobacteria. Thus, they provide an opportunity to examine how cyanobacterial preservation proceeds, which may be useful for identifying hydrocarbon deposits generated in intertidal sequences where cyanobacterial communities have larger extent.

At present, investigations such as those described are hampered because relatively few spring deposits have been described, and the complexity and non-uniformity of those



that have been has prevented the development of a comprehensive facies model for spring precipitates. Further investigation of modern and ancient spring deposits will facilitate and improve the accuracy of these applications.

Both modern hot springs and fossil spring deposits are found in Sulphur Creek Valley at Miette Hot Springs in Jasper National Park, Alberta. Although chemical and physical measurements from the spring waters have been recorded periodically since 1911, the extensive fossil spring deposits have never been studied. Few mineral deposits generated by Canadian springs have been studied; indeed, no literature describes any fossil spring deposits in the Southern Canadian Rockies or Foothills. This is surprising considering (1) that large deposits occur near popular tourist localities and modern hot springs in provincial and national parks (Woodsworth, 1997) that have mandates to educate the public about natural phenomena within their borders, and (2) the untapped reservoir of palaeoenvironmental information the fossil spring deposits may represent.

In ecologically oriented investigations of the Banff thermal springs, Lepitzki and Lepitzki (2001) found that the microbial assemblages living in the spring flow path are key to the entire spring ecosystem (which includes the endangered Banff Springs Snail). Further, the microbial assemblage may be specific to the spring water physiochemistry (Lepitzki and Lepitzki, 2001), and is no doubt influenced by mineral precipitation. Even a cursory examination of fossil spring deposits in the Banff and Jasper National Parks reveals the presence of microbially mediated textures in the rocks. There is, however, no precedent for an interdisciplinary geobiological investigative approach to further understanding of these delicate ecological systems. It is, thus, important to study modern and fossil Rocky Mountain spring deposits in order to facilitate ecological preservation and to apply findings to palaeoenvironmental and paleoecological interpretation.

This thesis describes and characterizes the modern and fossil spring precipitates at the Miette Hot Springs, thus, furthering knowledge of biological and physiochemical dynamics in Canadian springs, contributing towards the development of a comprehensive facies model for spring deposits, and providing a long term history of spring activity at the Miette site.

## 1.2 Background

### 1.2a Spring Systems and Definitions

Spring waters are usually derived from meteoric water that has circulated in the earth and may have undergone chemical and physical changes through interaction and exchange with buried rock (Criss and Taylor, 1986). They are described by their total-dissolved-solid (TDS) content as freshwater (TDS < 1000 mg/L) or mineral (TDS >1000 mg/L) (van Everdingen, 1991). The TDS of the spring water is determined by the solubility of the host rock, and by the corrosivity of the spring water to the host rock.

In magmatic terrains, silicate or volcanic-hosted springs typically have low TDS values that display a positive linear correlation with concentrations of dissolved silica (Grasby *et al.*, 2000a). The flow of groundwater in non-magmatic systems tends to be concentrated in permeable strata that act as aquifers. The lithology of these permeable layers is reflected in the solute content of the spring water: Ca and HCO<sub>3</sub> are derived from limestones; Ca, Mg, and HCO<sub>3</sub> from dolomites; Ca and SO<sub>4</sub> from gypsum and anhydrite beds; Na, K, Mg, and Cl from salt beds; and Ca, Na, K, Fe, Mn, and SiO<sub>2</sub> from igneous and metamorphic rocks (van Everdingen, 1991; Grasby *et al.*, 2000a). Relatively high concentrations of heavy metals and SO<sub>4</sub>, as well as low pH values, can also be derived from the subsurface oxidation and dissolution of metal sulphides. Biological reduction of sulphur to H<sub>2</sub>S is common in the subsurface. Its incomplete reoxidation as the water ascends to the spring orifice may result in a strong sulphur smell, and acid aspect to emerging spring waters (Grasby *et al.*, 2000a). The chemical composition of the spring water may also be affected by subsurface precipitation of minerals and selective exchange of cations between water and clay minerals (van Everdingen, 1991).

Springs are also classified by the temperature of the water at the spring orifice. Cold springs are commonly defined as having water temperatures that do not exceed the mean-annual air temperature by more than 5°C, whereas thermal springs exceed this (Grasby and Hutcheon, 2001). This definition fails, however, in regions where the mean-annual air temperature is near or below 0°C. For example, in the Canadian Cordillera, where the average ground water temperature is ~5°C, all springs would be considered thermal (Grasby and Hutcheon, 2001). Thus, for the purposes of this paper, thermal springs are those with temperatures greater than 10°C at the spring orifice. Thermal

springs are arbitrarily designated warm (<37°C), hot (>37°C), and very hot or boiling (>80°C) (cf. van Everdingen, 1991).

Globally, thermal springs are concentrated in areas with high heat flow and shallow permeable rock layers – especially along active rifts, plate margins, and areas of recent volcanism or plutonism. In these systems, the spring water discharges at the terminal end of convective circulation cells that occur in, and derive heat from, thermally anomalous areas of the earth's crust (Criss and Taylor, 1986). In continental areas not affected by magmatic processes, thermal springs are found where deeply circulating meteoric waters are heated by the geothermal gradient. In mountainous regions, high topographic relief provides the gravitational potential required for deep circulation (van Everdingen, 1991). The heated waters become buoyant and rise along the paths of least resistance offered them, usually through very permeable layers or fault plane conduits, emerging where gravitational potentials are low, or at formation contacts where permeability differences force the water to emerge (Gadd, 1999).

Cold springs emerge in many geologic settings where ground water circulation is shallow, dominated by young meteoric water, and controlled by the position of permeable layers and changing gravitational potentials (Woodsworth, 1997). Cold springs are found where the gravitational potential is not great enough to drive deep circulation, where strata are impermeable at depth, or where hot waters cool or are diluted before reaching the surface.

Spring waters commonly have atypical chemistries and temperatures compared to surface water, and may support species that are inviable, or marginal, in the larger environmental setting of the spring (Woodsworth, 1997). Bacteria, cyanobacteria, and filamentous fungi are prolific inhabitants of hot spring water, and larger species of arthropods, fish, orchids, and mosses are known to exploit spring habitats (Gadd, 1999; Woodsworth, 1997; Pritchard *et al.*, 1991). Minerals precipitated from spring water will coat all components in the spring habitat, and the subsequent decay of organic structures generates high porosity and numerous fossil moulds. Most spring deposits can be classified as sinter, tufa, or travertine. Sinters are the most dense, typify very hot thermal springs, and are dominantly composed of amorphous silica (Woodsworth, 1997). Tufa and travertine are usually composed of carbonate minerals. Tufa is more porous than

travertine, has a higher abundance of macrophytic components, and is usually associated with cool or warm thermal spring waters (Woodsworth, 1997). Travertines are associated with thermal springs, and are usually (but not always) hard, crystalline precipitates (Ford and Pedley, 1996). In this paper, the terms tufa and travertine refer to the texture and mineralogy of the original spring deposit. For example, a porous tufa that became heavily cemented and crystalline through diagenetic processes are still called tufa.

### *1.2b Canadian Springs*

The geographic distribution, and physical and chemical character, of Canadian springs is closely related to regional geology and geography. Canada hosts over 130 thermal springs, which are concentrated in the Canadian Cordillera where high topographic relief permits heating of ground water by deep circulation (Grasby, 1998). In central and eastern Canada, low relief and low permeability bedrock, preclude the development of large thermal springs (van Everdingen, 1991). An exception to this trend are a series of warm brine springs derived from formation waters that emerge along the eastern edge of the Williston Basin in Manitoba (Bachu and Hitchon, 1996; Grasby *et al.*, 2000b).

Surface run-off and snowmelt act as the initial source for most Canadian spring waters (van Everdingen, 1972, 1991; Grasby *et al.*, 2000a). Differences in the physical and chemical character of spring water between regions originate from differences in the depth and length of subsurface circulation, and from mineralogical differences between the host rocks they circulate through. Studies using tritium isotopes have shown that Canadian spring waters have residence times ranging from a few years in most cold springs to greater than 37 years in thermal springs (van Everdingen, 1991). The physical characteristics of Canadian springs are variable (Table 1.1). Common major anions in Canadian springs include  $\text{HCO}_3^{2-}$ ,  $\text{SO}_4^{2-}$ , and  $\text{Cl}^-$ , and dominant cations include  $\text{Ca}^{2+}$ ,  $\text{Mg}^{2+}$ ,  $\text{Na}^+$  and  $\text{K}^+$ . Dissolved gases in Canadian spring waters include  $\text{N}_2$ ,  $\text{CH}_4$ ,  $\text{CO}_2$ ,  $\text{O}_2$ ,  $\text{H}_2\text{S}$ ,  $\text{Rd}$ ,  $\text{He}$ , and other noble gases. The pH value of Canadian spring water ranges from strongly acidic to alkaline (pH 2.2 to >10.0) (van Everdingen, 1991). The lowest pH values are associated with high concentrations of dissolved iron and other heavy

**Table 1.1** Physical and chemical characteristics of Canadian springs (after van Everdingen, 1991).

<b>Parameter</b>	<b>High</b>	<b>Low</b>
Temperature	82.2 Dewar Creek, BC	-2.9 Gypsum Hill, Axel Heiberg Island
pH	>10 Unnamed Spring, NF	2.2 Location not cited
Eh	+683 mV	-252 mV
TDS	>75000 mg/L Gypsum Hill, Axel Heiberg Island	32 mg/L Sheet Harbour spring, NS
HCO <sub>3</sub>	5960 mg/L Grotto springs, BC	
SO <sub>4</sub>	17520 mg/L Saltspring Island, BC	
Cl	44300 mg/L near Norman Wells, N.W.T.	
Ca	1823 mg/L Gypsum Hill, Axel Heiberg Island	
Mg	1190 mg/L near Great Bear Lake, N.W.T.	
Na	27100 mg/L Gypsum Hill, Axel Heiberg Island	
K	1598 mg/L Brine Springs, MN	

metals, and result from the subsurface oxidation of metal sulfides. Strongly alkaline pH values have been found for springs associated with ultrabasic igneous rocks in Newfoundland. The redox potential of Canadian spring water (Eh) ranges from -252 to +683 mV (van Everdingen, 1991). The negative Eh values are usually found in spring water that contains high concentrations of dissolved H<sub>2</sub>S, produced by bacterial reduction of dissolved sulfate.

Many Canadian springs precipitate either tufa or travertine, consisting mainly of calcite with minor amounts of dolomite and other accessory minerals. Examples include the large deposits around the Rabbit Kettle Hot Springs in Nahanni National Park, N.W.T., and the Cave and Basin Spring and Big Hills Springs in Alberta. Where spring waters have high concentrations of sulfate, gypsum may be incorporated into tufa or travertine deposits, and at the Fly-By Springs in the Mackenzie Mountains, significant deposits of barite (BaSO<sub>4</sub>) travertine also form (Cecile and Jones, 1979). Bacterial reduction of dissolved sulfate can lead to the deposition of soft yellow sulfur coatings on objects in the discharge area of springs, and evaporation may also result in the precipitation of salt (NaCl) from briny spring waters (van Everdingen, 1991; Bachu and Hitchon, 1996). Rapid cooling of silica-rich water from the McArthur Hot Springs near Mayo, Yukon, produces minor encrustations of silica sinter on emergent rocks in the discharge area (Brandon, 1965). Iron precipitates are also found in some Canadian springs. The oxidation of Fe<sup>2+</sup> to Fe<sup>3+</sup> in acidic, heavy metal bearing spring waters is followed by the formation of amorphous ferric hydroxide, and/or the precipitation of jarosite (van Everdingen, 1970). The ferric hydroxide is produced as flocs that remain in suspension in the discharge channel and form reddish to dark brown coatings on banking rocks. Wherever flow velocity decreases, the flocs can settle and accumulate as beds of soft, yellow to red “ochre” which develops a hard dark brown crust when it is dried out and fully oxidized (van Everdingen, 1970). A famous example of this type of deposit are the Paint-pots in Kootenay National Park, British Columbia.

### *1.2c Western Canadian Springs*

Western Canada's thermal springs are concentrated along NW-SE trending fault zones in the Canadian Cordillera: from west to east these are the West Coast, Harrison

Lake, Okanogan Valley, Columbia River, Purcell Trench, and Rocky Mountain Trench faults (Fig. 1.1A) (Grasby and Hutcheon, 2001). In southwestern Alberta, thermal springs are concentrated in localized zones of complex deformation, mainly related to crustal scale brittle faults in the front ranges of the Rocky Mountains (Grasby and Hutcheon, 2001).

The thermal gradient varies significantly within the Cordillera (Fig. 1.1B), and there tend to be more thermal springs in the regions with higher heat flow. In the Garibaldi Volcanics of the Coast Belt, for example, anomalously high heat fluxes associated with intrusive bodies heat the groundwater, and numerous thermal springs are present (Grasby and Hutcheon, 2001). Thermal springs are, however, found throughout the Cordillera, proving that geothermal gradients are steep enough to heat deeply circulating groundwater, and that additional heat sources (i.e. radiogenic heat production or magmatic conduction) are not necessary to the development of geothermal systems (Grasby and Hutcheon, 2001).

Mineral precipitates are associated with many springs in the Cordillera, and the most substantial deposits consist of calcareous tufa (Woodsworth, 1997). Significant accumulations of fossil tufa are also found at many locations in the southern Rockies and the western Foothills (i.e. Cave and Basin Springs at Banff, petrified river near Edson, False Creek Springs, Big Hills Springs, Miette Hot Springs).

### *1.3 Study Site: the Miette Hot Springs*

#### *1.3a Physiogeographic Context*

The Miette Hot Springs are located in the Foreland Belt of the Canadian Cordillera, near the east gate of Jasper National Park, Alberta (Fig. 1.2). The springs emerge as a series of fracture springs and minor seeps with an average outflow temperature of 51°C in the narrow steep walled valley of Sulphur Creek (Baird, 1963; Borneuf, 1983). Sulphur Creek is a tributary of Fiddle River, which is in turn a tributary of the Athabasca River. This area of the Rocky mountains has an average mean annual temperature of 2.6°C, and average mean annual precipitation of 571 mm. Seasonal variation is extreme; at the nearby Jasper town site, temperatures range from -40°C in winter to +35°C in summer (Gadd, 1999).



**Figure 1.1**

(A) Regional map of Western Canada showing the five morphogeological belts in the Canadian Cordillera. The location of known thermal springs is marked with (•). (B) Variations in geothermal heat flow across the Canadian Cordillera along transect A-A' in Fig. 1.1A (after Grasby and Hutcheon, 2001).



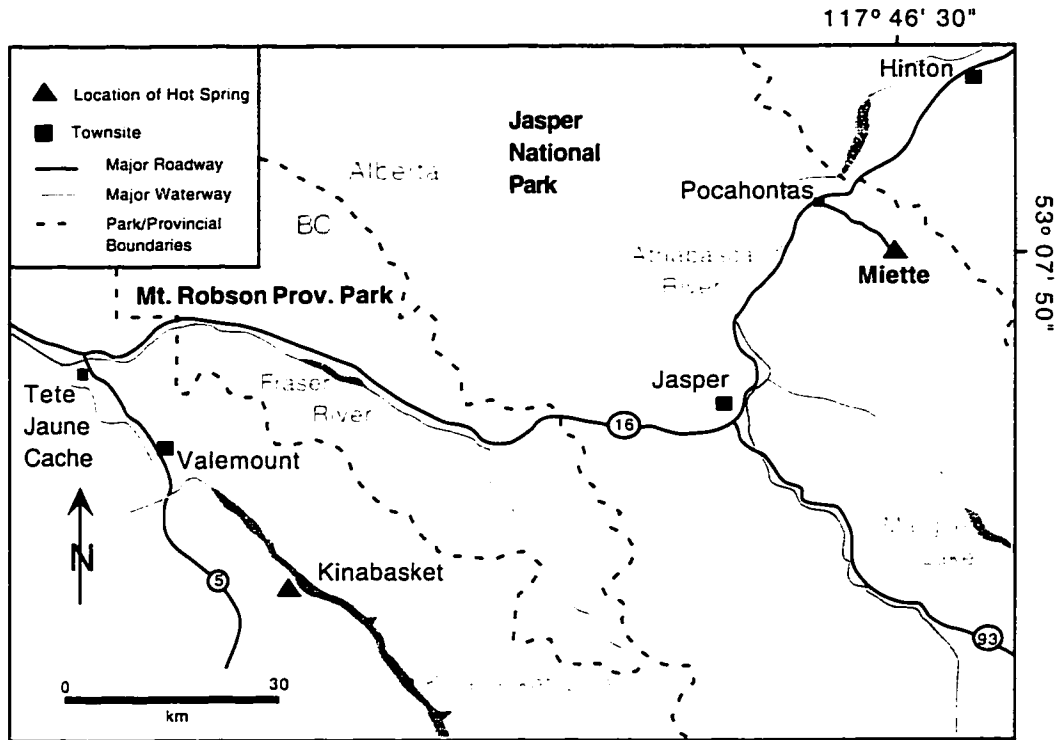


**Figure 1.2**

Location map for the Miette Hot Springs in Jasper National Park (after Woodsworth, 1997).

Sulphur Creek Valley is densely vegetated by coniferous trees (lodgepole pine and white and Engleman spruce) with deciduous trees and shrubs (trembling aspen, autumn willow, balsam poplar and red osier dogwood) becoming more prominent in open areas close to the creek bed. Ground cover consists of small shrubs and feather mosses. The valley is inhabited by small mammals (ground squirrels and rabbits), by mountain sheep, elk, deer, bears, and an abundance of tourists in the summer months.

Surficial deposits in the Miette Hot Springs area include talus and scree cones, fluvial deposits, and glacial till. The springs site is surrounded by folded and tilted metasedimentary formations (Fig. 1.3, Table 1.2); the pool parking lot offers extraordinary views of the Roche Miette Reef Complex to the North and Sulphur Ridge Mountain to the South (Gadd, 1999). The springs are positioned near the axis of a plunging anticline in the underlying Mississippian Rundle Group Carbonates, indicating that subterranean migration of water is structurally controlled (Fig. 1.4, Table 2.1) (Baird, 1963; van Everdingen, 1972). The underlying strata are cut by the Hot Spring fault, and although there are no thermal springs at the surface outcrop of this fault, it may act as an access route for deep water circulation from the northeast; or, it could act as a barrier that forces water originating in the thrust sheet to the south and southeast of the springs to come to the surface in Sulphur Creek Valley (van Everdingen, 1972). The springs emerge at the contact between Formations B and C of the Rundle Group and these units contain shale interbeds that may provide a stratigraphic cap for the confined aquifer system (van Everdingen, 1972). The Miette springs emerge at the lowest exposure of the core of the anticline, and tension fractures associated with the fold are also thought to act as flow conduits for the thermal water (van Everdingen, 1972).

### *1.3b History and previous work*

The Miette Hot Springs are a major attraction in Jasper National Park and support two restaurants, a motel, campsites, and cabins that cater to tourists during the summer. Little is known about the initial discovery of the springs, but there is anecdotal evidence that Native people and traders from the Hudson's Bay and North-West Trading Companies used them for bathing in the late 1800's (McDonald, 1978). The spring site was first developed, with the construction of a wood bathing tub, by miners from the

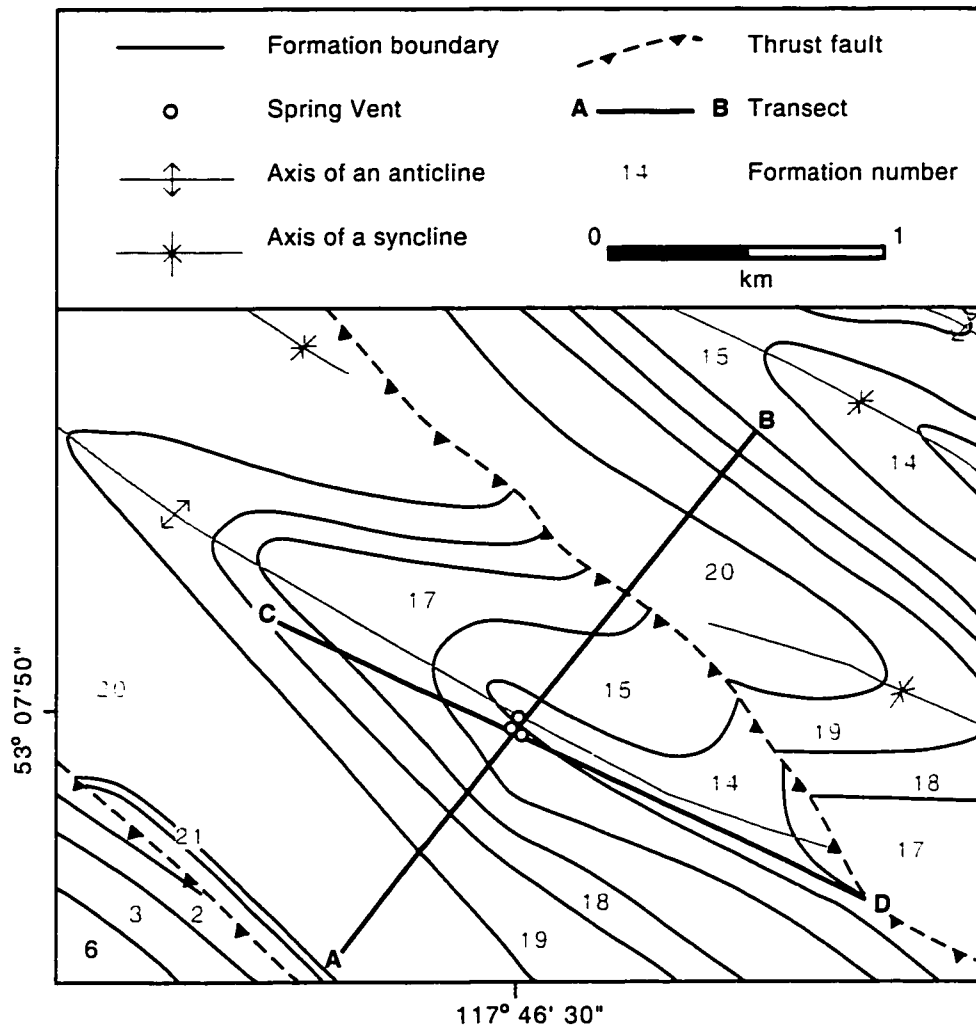


**Figure 1.3**

Geology of the Miette Hot Springs area. The transect lines indicate the orientation of the structural cross sections shown in figure 1.4. See table 1.2 for stratigraphy and formation lithology (after Mountjoy, 1959).

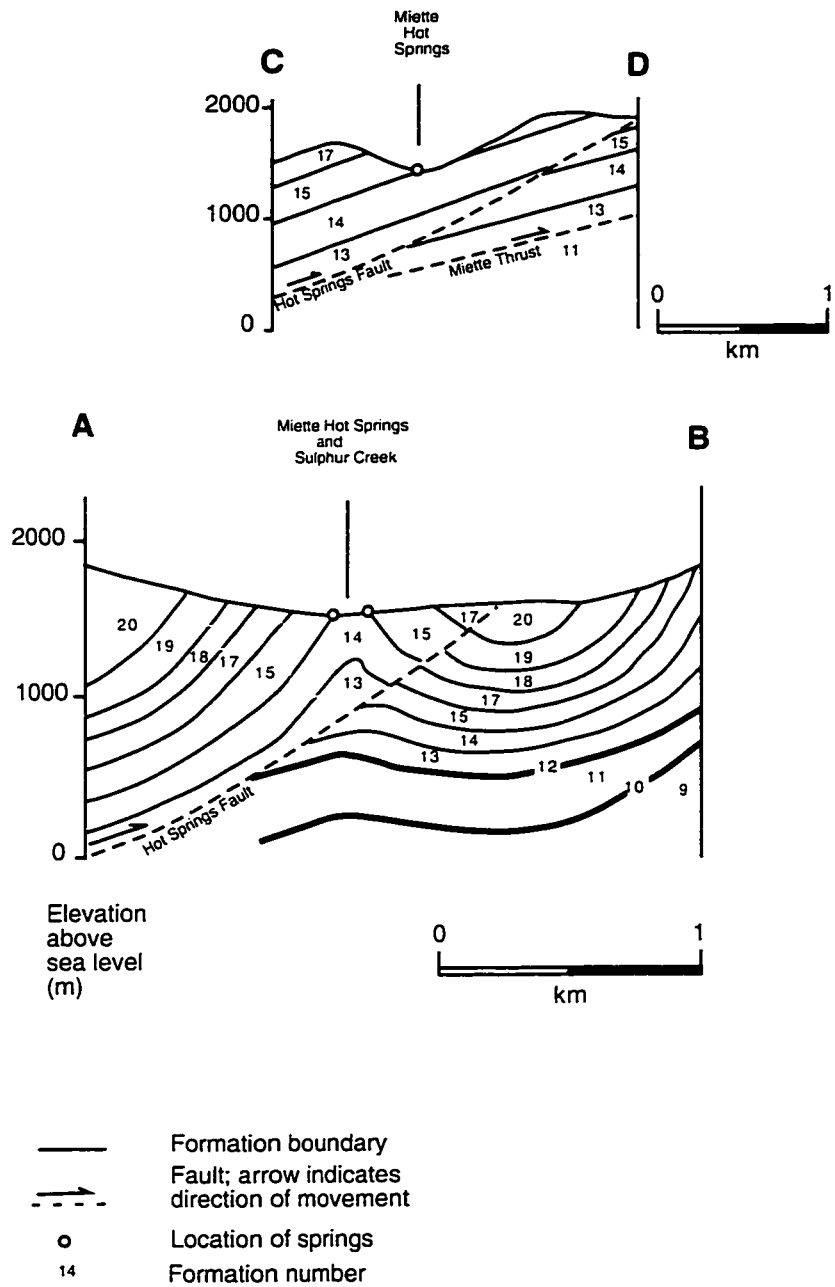


**Figure 1.4**  
 Structural cross-sections through the Miette Hot Springs area. (See table 1.2 for stratigraphy and lithology; Fig. 1.3 for the location of each transect) (after vanEverdingen, 1972).

**Table 1.2** Stratigraphy and lithology of the Miette Hot Springs area, Jasper National Park, Alberta (after van Everdingen, 1972).

Stratigraphy and Lithology		Map units on Fig. 1.3, 1.4
<b>Mesozoic</b>	<b>Lower Cretaceous/Jurassic</b> <b>Nikanassin Formation</b> - dark grey silty mudstone, siltstone, sandstone	20
	<b>Jurassic</b> <b>Fernie Group</b> - dark grey to black shale, silty concretionary shale; brownish grey, fine-grained sandstone and glauconite	19
	<b>Triassic</b> <b>Whitehorse Formation</b> - light grey, dolomitic siltstone and sandstone; red, green and buff mudstone and siltstone; limestone and dolomite breccia; gypsum	18
	<b>Sulphur Mountain Formation</b> - dark grey, thin-bedded siltstone and silty mudstone	17
<b>Palaeozoic</b>	<b>Permian/Pennsylvanian</b> <b>Rocky Mountain Formation</b> - massive chert and cherty, light grey sandstone	16
	<b>Mississippian</b> <b>Rundle Group</b> Formation D - dense, cherty dolomite and argillaceous dolomite Formation C - grey-brown, crystalline, thick-bedded, porous dolomite, with relicts of organic calcarenite	15
	Formation B - dark grey, argillaceous, fine-grained limestone and dolostomite; interbeds of shale, collapse breccia and oolitic limestone Formation A - light grey, massive organic calcarenite	14
	<b>Banff Formation</b> - dark grey, fine-grained, argillaceous, thin-bedded, nodular limestone; brownish grey, thin-bedded to fissile, calcareous shale; interbeds of argillaceous organic calcarenite	13
	<b>Exshaw Formation</b> - black, cherty, fissile shale; brown, fine-grained, quartz sandstone	12
	<b>Devonian</b> <b>Palliser Formation</b> - dark grey, crypto- to fine-crystalline, massive, mottled dolomitic limestone; calcarenite; argillaceous calcarenite	11
	<b>Alexo or Sassenach Formation</b> - yellowish grey, calcareous siltstone; crypto-crystalline limestone; breccia; dolomite	10
	<b>Fairholme Group</b> <b>Mount Hawk Formation</b> - dark grey, argillaceous, thin-bedded, fine-crystalline limestone; calcareous shale,	9
	<b>Southesk Formation</b> - massive, light grey, crypto- to fine-crystalline	
	(continued...)	

	limestone, in part calcarenitic; dolomite	8
	<b>Perdrix Formation</b> - dark grey to brown, fissile shale; calcareous mudstone; thin-bedded argillaceous limestone,	7
	<b>Cairn Formation</b> - massive, brown, fine- to medium-crystalline, cherty dolomitic limestone and calcareous dolomite with <i>Amphiopora</i> and stromatoporoids - part of Perdrix Fm.	6
	<b>Maligne Formation</b> - dark grey, fine-crystalline, thin-bedded limestone	} 5
	<b>Flue Formation</b> - dark grey to brown, fine- to medium-crystalline, cherty dolomitic limestone with <i>Amphiopora</i> and stromatoporoids	
	<b>Ordovician</b>	
	<b>Cushina Formation</b> - greenish grey, argillaceous limestone; calcareous shale; intraformational conglomerate	} 4
	<b>Cambrian</b>	
	<b>Upper Cambrian Lynx Formation</b> - medium to thin-bedded, light grey, fine-grained, laminated, silty carbonates and argillaceous carbonates, siltstone and intraformational conglomerate	
	<b>Middle and/or Upper Cambrian Arctomys Formation</b> - thin-bedded, cross-bedded, orange to yellowish grey dolomitic siltstone and sandstone; lower part - thin-bedded, pale green and maroon mudstone; green argillaceous dolomite; with salt crystal pseudomorphs	3
	<b>Middle Cambrian Pika Formation</b> - thin-bedded, grey calcareous shale and argillaceous limestone; intraformational conglomerate	---
	<b>Titkana Formation</b> - resistant, grey, crypto-crystalline dolomitic mottled limestone	2
	<b>Unnamed Formation</b> - greenish grey shales with interbeds of resistant, grey, micro-crystalline limestone; grey calcareous mudstone	1

Pocahontas Mine during a prolonged strike in 1910 (Mussieux and Nelson, 2000). Soon afterwards, rumors began that drinking and bathing in the Miette Hot Spring water could cure rheumatism and other serious ailments. Dowling's (1911) discovery that the spring water was not radioactive (as most spring waters with rumoured curative properties are), and that its only medicinal benefit could be that its richness in "sulphate of lime... and magnesia..." might render the water "...slightly laxative in its effect on the system", did nothing to deter people from visiting the spring site. Unfortunately, there was no established roadway to the springs, nor were there accommodations once there, and the exertions involved in visiting the springs resulted in the death of a number of people who were physically unfit for the rough conditions. Acting in response to these deaths and complaints, the government furnished the Miette Hot Springs site with a bathhouse, several sweatshouses, a swimming pool, a log bunkhouse, and several tents in October of 1919 (van Everdingen, 1972). Conditions at the springs have continued to improve with the construction of a road in 1932, an Aquacourt in 1938, and a new pool house in the 1980's.

Previous investigations at the springs have been limited to the collection of physical and chemical data. The first data were reported by Dowling (1911), and was followed by a more detailed analysis conducted by Elworthy (1926). Seasonal and annual variation in the chemistry, isotopic composition, temperature, and flow rate of the springs was investigated by van Everdingen between 1967 and 1980, and most recently, chemical and isotopic data were reported by Grasby *et al.* (2000a).

The Miette spring waters are slightly supersaturated with both  $\text{CaCO}_3$  and  $\text{CaSO}_4$  (van Everdingen, 1980b) but are forming few modern precipitates. Diversion of spring waters to the Miette bathhouses and dilution of discharged spring water with fresh water from Sulphur Creek limit the development of mineral deposits. There is, however, substantial exposure of fossil tufa along the west wall of Sulphur Creek Valley, indicating that the activity of the springs was greater in the past. The fossil tufa is vertically and laterally extensive, reaching over 30 m above the level of Sulphur Creek, and extending along the west valley wall for nearly 500 m. It has never been subject to examination and is rarely mentioned in previous publications about the Miette Hot Springs. Dowling

(1911) describes the tufa as “great boulders”, having apparently not investigated the hill slope sufficiently to notice a 400 m long tufa ledge.

#### *1.4 Project Objectives*

A major objective of this project is to describe and characterize both the recent precipitates and the fossil tufa deposits at Miette Hot Springs.

Specifically,

- The fossil tufa is described in a site-specific facies model.
- The physical parameters of the fossil spring and morphology of the tufa are reconstructed.
- The ecology of the modern and fossil spring systems are described.
- Differences in the temperature, outflow volume and velocity, and chemistry of the modern and fossil spring systems are evaluated.
- The driving forces for precipitation are examined in the modern and fossil spring deposits to determine whether microbial biomineralization is/was important.
- The age range of the fossil tufa accumulations is estimated in order to establish the persistence of the springs.
- The context of the fossil spring system in the regional Holocene palaeoenvironment is described with reference to literature.
- The descriptions of the modern and fossil spring systems are synthesized to develop an overall picture of spring history at the Miette site.

#### *1.5 Methods*

##### *1.5a Field Methods*

Fieldwork was conducted during four visits to Miette Hot Springs between May and October, 2001. During the first of these trips, June 12-14<sup>th</sup>, the pH, temperature, salinity, and conductivity of the waters issuing from springs 3, 3a and 3b were measured using an Orion Low Maintenance Triode pH electrode, model 9170WP. Water samples were collected through a 0.45 µm pore size, 47 mm diameter, FisherBrand water-testing membrane filter, and stored in sterile 250 ml Nalgene containers for isotopic and elemental analysis. Precipitates forming near the spring vents, and in the discharge path



of spring 3a, were also collected. Samples of microbial communities inhabiting the immediate spring environments were collected on September 19<sup>th</sup>, and preserved in glass jars containing a 6:3:1 solution of water, 95% alcohol and formalin with 5 ml of glycerol added per 100 ml of the solution.

The extent, and gross morphology, of the fossil tufa deposit was assessed by mapping the west side of the Sulphur Creek Valley. Various tufa morphotypes and facies were identified and sixty-two rock samples were collected, representing the range of variation observed within and between tufa outcrops. Three samples of a bone found embedded in tufa was also collected.

### *1.5b Laboratory Methods*

Samples of the modern spring precipitates were examined by dissecting microscope, scanning electron microscope (SEM), and X-ray analysis. Organic components were removed from subsamples of the modern spring precipitates using household bleach. The bleached material was then flushed with distilled water and dried with acetone. Stable carbon and oxygen isotopes were measured for each sample. Isotope extraction was accomplished by reaction with 100% H<sub>3</sub>PO<sub>4</sub> and  $\delta^{13}\text{C}$  and  $\delta^{18}\text{O}$  determined using a Finnigan Mat 252 mass spectrometer. Fractured samples were thinly coated with gold and examined on a JOEL 6301F field emission SEM with an accelerating voltage of 1.5 - 2.5 kv. The elemental content of the samples was determined using an energy dispersive X-ray analyzer attached to the SEM. Both bleached and unbleached samples were examined by SEM so that the effects of bleaching would be known, and the association between the organic and inorganic portions of the samples could be elucidated.

Samples of microbial communities were dissected, described, and examined by light microscopy. Where possible, genera were identified with reference existing literature, Prescott (1970), Rippka *et al.* (1979), Simonsen, (1987), Canter-Lund and Lund (1995), the Cyanosite Website hosted by the Department of Biological Sciences at Purdue University (<http://www-cyanosite.bio.purdue.edu/>), and expert advice (Appendix 1).

Water samples collected from springs 3, 3a and 3b were sent to the University of Alberta Limnology Laboratory for measurement of elemental constituents, dissolved inorganic carbon (DIC), and total dissolved solids (TDS), and to the University of Waterloo Isotope Laboratory for stable isotope analysis. The University of Alberta Limnology Laboratory uses a flame atomic absorption spectrometer with a low sensitivity to Al (10 mg/L detection limit) and slightly higher sensitivity to Cu and Zn.

Samples of the fossil tufa were examined through hand sample analysis, thin section petrography, SEM analysis, and stable isotope analysis. Thin sections were prepared from representative samples of each facies. These were used to identify intrafacies variation, and specific textures were subsampled for SEM analysis. Samples for SEM analysis were fractured, mounted on stubs, gold coated, and examined at 0.5-2.0 kV. Many of the tufa samples have a cyclic laminar fabric. Subsamples from individual laminae were extracted from four samples in which the laminae were well defined using a hand drill. The subsamples were immersed in bleach, flushed with distilled water, dried with acetone, and stable carbon and oxygen values were measured to examine differences between adjacent laminae. Stable carbon and oxygen values were also measured for a series of samples that span a vertical transect of the fossil tufa, to identify any changes occurring down slope from the fossil spring vent.

Three of the samples examined by SEM (two modern spring precipitates and one from fossil tufa) contained diatom tests. Pieces from these samples and seven others chosen at random were dissolved in 10% HCl, and washed with household bleach, to extract siliceous components. The resulting powder was then examined by SEM and light microscopy in order to identify the diatom species present. Several of the samples examined by SEM also contained ostracode valves. Pieces from these samples and three others chosen at random were subjected to frost wedging to dislodge the fossils. The samples were placed in plastic containers, immersed in boiling water with a teaspoon of Glauber's salt ( $\text{Na}_2\text{SO}_4 \cdot 10\text{H}_2\text{O}$ ), left to cool to room temperature, frozen, removed from the plastic containers, and thawed on glass beneath warm air from a heat gun. Fine material broken away from the samples was collected and the process repeated until thawing resulted little yield of fine material (method after Forester, pers. comm.). The fine material and water was washed through a sieve with 45  $\mu\text{m}$  pores to remove clay

material. The residual material was dried and examined by SEM and light microscopy and images and samples were sent to Dr. Rick Forester with the USGS in Denver, Colorado for identification.

The samples of bone were examined by Dr. Michael Caldwell in the Department of Earth and Atmospheric Sciences, University of Alberta, and by Dr. Jack Brink at the Provincial Museum of Alberta before being sent to the IsoTrace Radiocarbon Laboratory at the University of Toronto where collagen from one bone sample was extracted and purified to allow two separate  $^{14}\text{C}$  analyses (with normal precision).

## **2 The Modern Miette Hot Springs**

### *2.1 General Description*

The Miette springs are the hottest in the Canadian Rockies with a mean temperature of 51.2°C (Borneuf, 1983). They occur as a series of fracture springs and minor seeps that issue from jointed and fractured carbonate rocks a few feet above Sulphur Creek (Fig. 2.1). The lowest spring, spring 1, is situated beneath the Aquacourt at an elevation of 1391.5m above sea level (van Everdingen, 1980a). Also issuing from beneath the Aquacourt is a warm spring with an average water temperature of 15.8°C. These two springs have a combined flow of 2.3 L/s (van Everdingen, 1980a). The two larger hot springs (with flow rates of 3.3 and 7.5 L/s for springs 2 and 3, respectively) are located approximately 120 m upstream of the Aquacourt at slightly higher elevations (van Everdingen, 1980a). The spring waters are piped into a bathhouse and drained into Sulphur Creek after use.

The Miette spring system exhibits a delicate interplay of biological and physical influences. Where uncovered, the spring and seep orifices are brightly coloured by mineral precipitates and microbial communities. The microbes that inhabit the spring discharge channels are calibrated to life at the temperatures and chemistry of the spring water, and influence the precipitates formed from it.

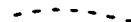



### *2.2 Water Chemistry*

The chemistry of the Miette hot spring waters has been well established through numerous analyses over the last 90 years (Table 2.1). Minor ion concentrations show little fluctuation between analyses, but some of the major ions have pronounced variation. Sodium has varied by 40 ppm, peaking at 50 ppm in 1926 and measuring  $10 \pm 2$  ppm before and since; magnesium is consistently between 60 and 70 ppm but dropped to 21.8 ppm in 1926; sulphate has ranged from 840 to 1138 ppm; calcium has varied within a range of 100 ppm; and bicarbonate within 150 ppm.

Water analyses conducted in June, 2001, and those conducted by van Everdingen (1972; 1980c) show that ionic concentrations vary between the different spring and seep vents. Thus, some of the variation between analyses likely arose because researchers

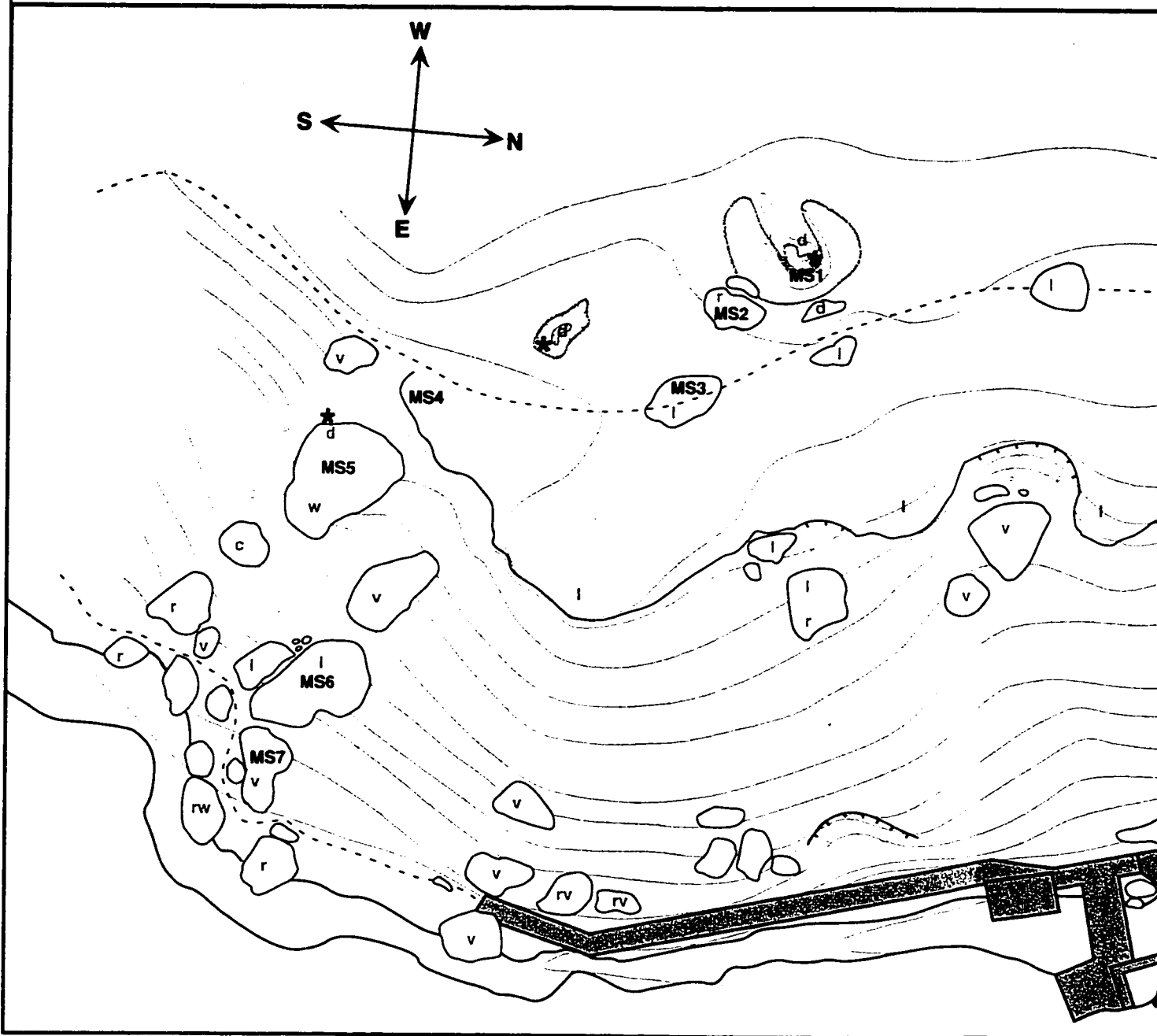
**MAP OF THE MODERN MIETTE HOT SPRING VENTS AND THE DISTRIBUTION OF FOSSIL TUFA IN SULPHUR CREEK VALLEY**

**LEGEND:**

-  Foot Path
-  Boardwalk
-  Wire Cable
-  Fresh Land

mapped by: S. Bonny, K. Kaleta, Z.Parr, August 2001.

**Figure 2.1**





**LEGEND:**



Foot Path



Boardwalk



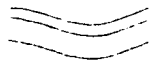
Wire Cable



Fresh Landslide Debris



Elevation marker (m above sea level)



Contour Lines

Densely forested area  
(may contain scattered tufa blocks)



Scarp

3



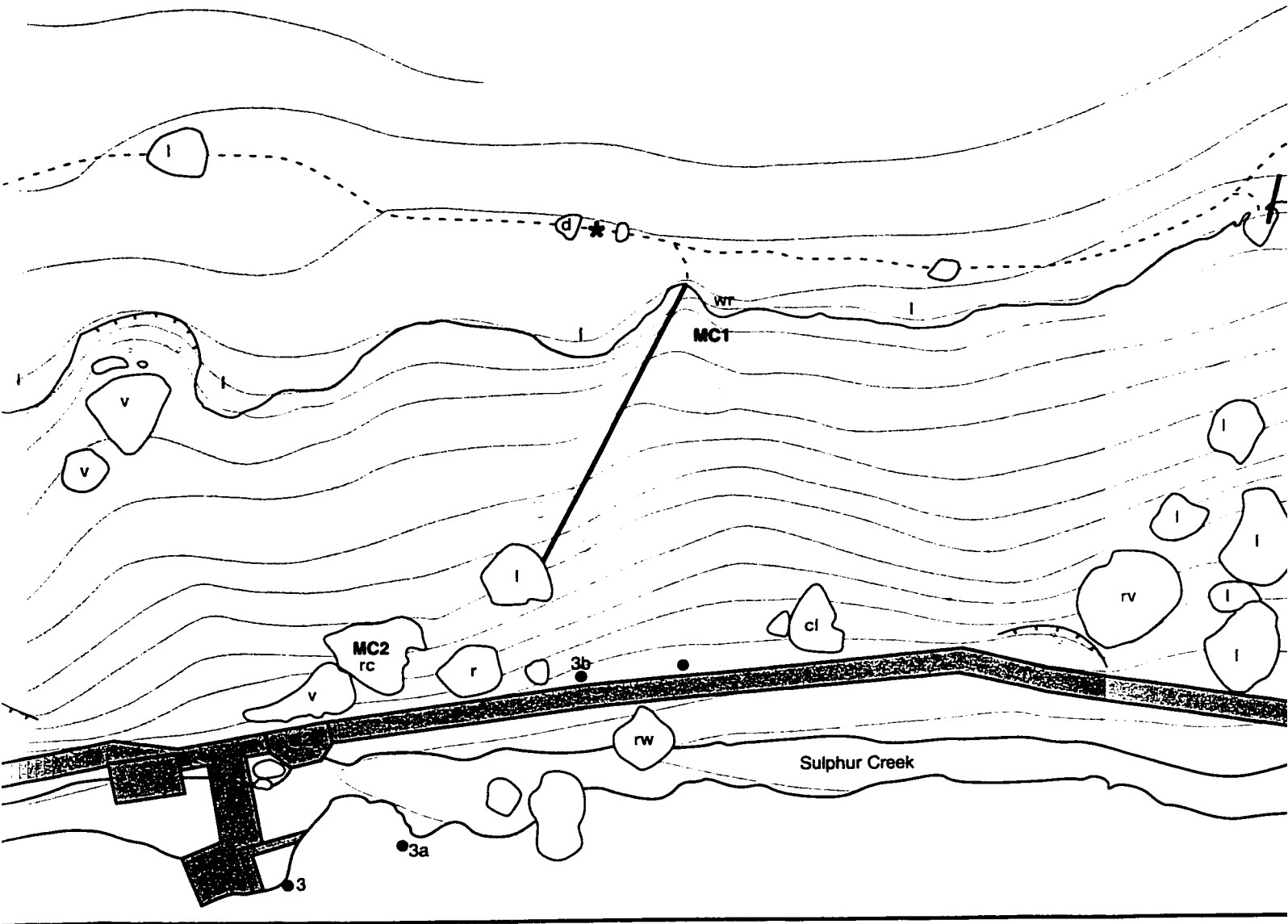
Spring or seep vent



Location of fossil site

MS1

Sample location







above sea level)



Scarp



Edge of continuous tufa ridge

3



Spring or seep vent



Tufa outcrop - tufa morphotype is indicated by a letter

l = flat-banded tufa

v = vertical tufa

r = roll-over tufa

m = mossy bed tufa

d = domal tufa

w = wedge-shaped tufa

c = tufa/allochthonous lithoclast congl

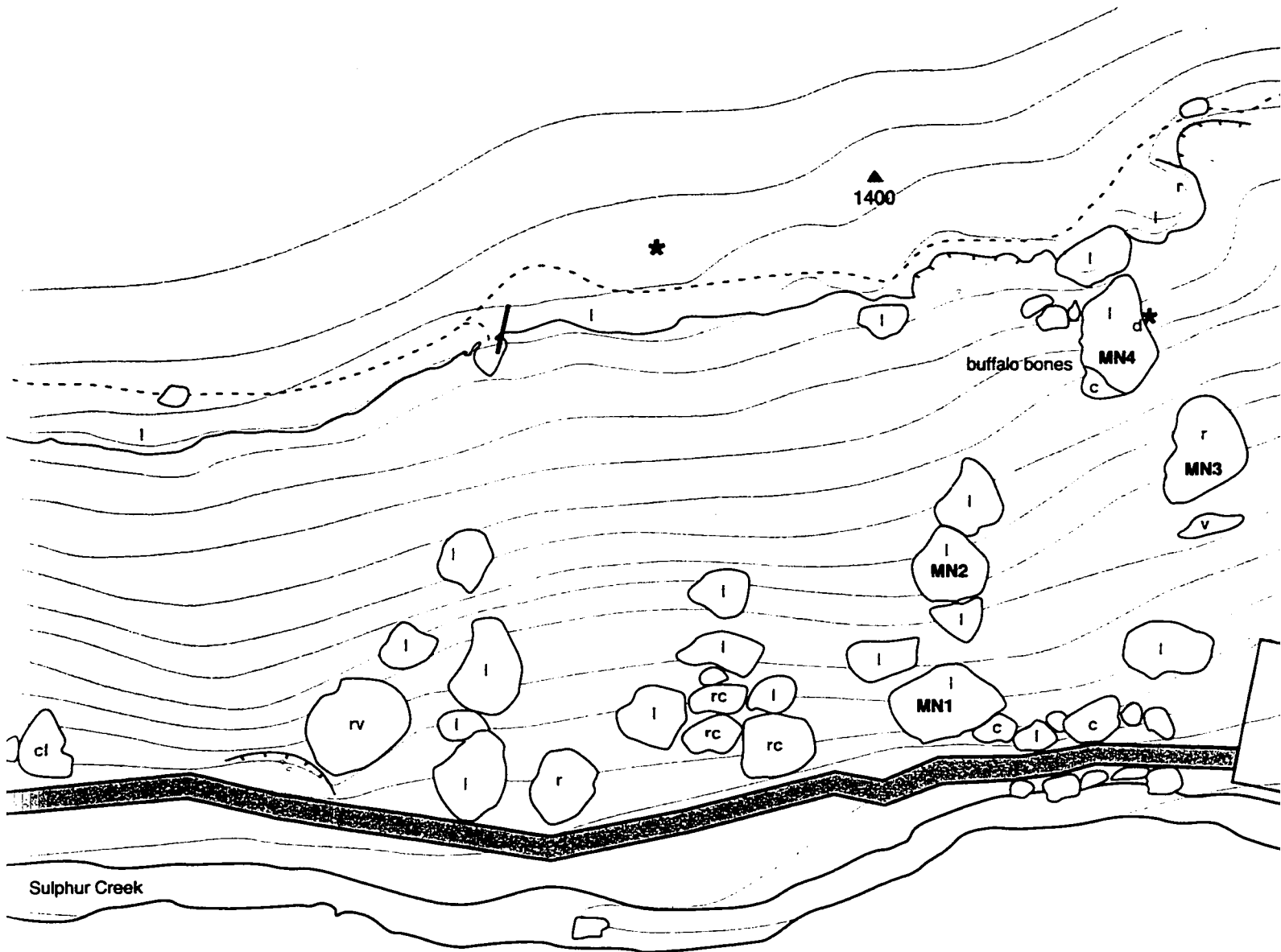


Location of fossil spring vent

tufa blocks)

MS1

Sample location





- lufa ridge
- lufamorphotype is indicated by a letter
- lat-banded tufa
- vertical tufa
- spill-over tufa
- mossy bed tufa
- columnar tufa
- wedge-shaped tufa
- tufa/allochthonous lithoclast conglomerate

Scale: 0  50  
 m

Contour Interval: 2m for heavy lines  
 1m for alternating light and heavy lines

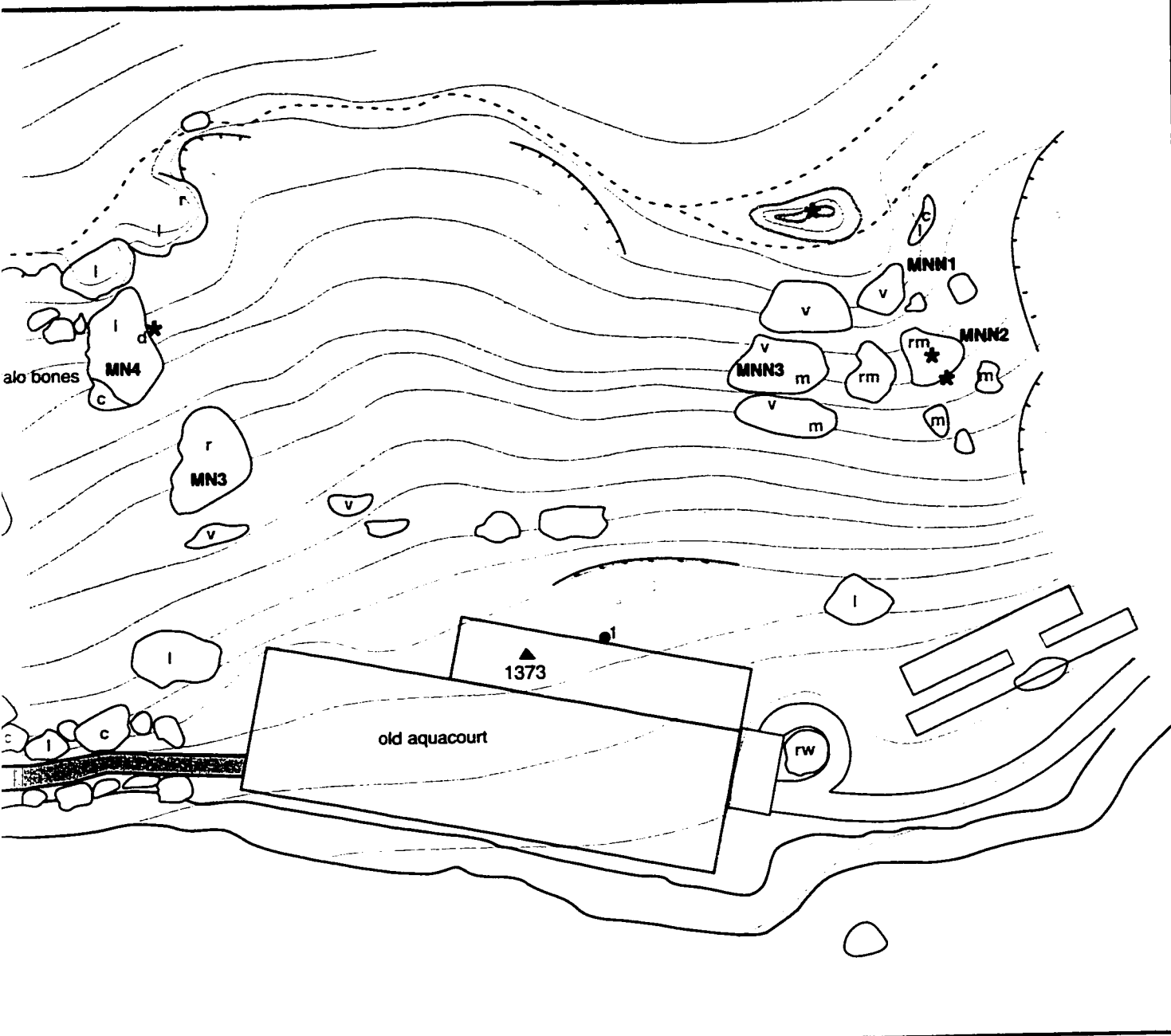




Table 2.1 Miette Hot Spring water chemistry at various dates.

Solute (ppm)	date measured: and/or source:										3a e							
	?	?	1	2	3	1	2	3	1	2	3	?	3	3	3	3a	3b	
Ca	299	85.9	366	403	365.0	407.0	389.0	383.0	330.0	390	358	375	390.0	408.0	383.1	391.3	392.3	386.2
Sr		trace			11.1	13.8	14.7	15.2	58.0	68.0	66.0	12.5	12.4	13.0				
Mg	65.2	21.8	59.6	62.4	65.0	56.0	70.0	73.0				64.5	66.9	66.3	64.9	66.9	67.9	66.9
Fe			0.050	0.116	0.40							0.043	<0.003	0.012	-5	-5	0.41	-5
Mn			0.02	0.03	0.08								<0.01	0.0108	-5	-5	-5	-5
Al			0.32	0.36	0.06								<0.2	0.060				
FeO, Al <sub>2</sub> O <sub>3</sub>	trace	7.3																
Cu			0.002	0.023	0.020							0.011	<0.001	<0.001	-5	-5	-5	-5
Zn			0.025	0.023	0.010							0.004	<0.002	<0.001				
Pb			<0.005	<0.005									<0.02	<0.002				
Na	12.6	50	9.3	10.3	10.3	10.5	10.9	10.0	8.0	9.4	8.7	9.8	9.9	10.2	9.12	9.21	9.53	9.05
K	17.3	trace	13.8	14.6	14.7	14.2	15.0	14.5	12.0	14.0	13.0	14.8	14.0	14.1	15.1	15	14.8	14.7
Li					0.076	0.095	0.098	0.094										
HCO <sub>3</sub>			280.6	129.0	117.0	128.0	117.0	118.0	148.0	124.0	140.0	127.0	134	139				
SO <sub>4</sub>	1068	114.8	1085.0	1176.0	1015.0	1130.0	1160.0	1130.0	840.0	1060.0	980.0	1168.0	1220.0	1150.0	1137.4	1135.7	1138.5	1128
Cl	7	45	3.9	4.3	3.3	4.2	4.2	4.1	3.5	4.1	3.7	4.0	8.0	9.3	4.6	4.62	26.21	4.53
I			0.009	0.010	0.007													
Br			<0.1	<0.1	<0.1													
F			3.5	4.0	3.5				0.55	0.45	0.47							
PO <sub>4</sub>			0.36	0.40	0.11													
NO <sub>3</sub>			0.1	0.1	<0.1	<0.1	<0.1	<0.1				<1.0	<0.1	<0.004				
SiO <sub>2</sub>	45	8.9	58.4	65.2	47.0	48.0	51.0	49.0	56.0	57.0	51.0	1.0	24.6	29.2	25.23	25.77	26.21	25.06
H <sub>2</sub> S						6.0	7.0	7.0					14.5					
CO <sub>2</sub>	116				35.0	40.0	40.0	40.0										
O <sub>2</sub>			0.0	0.0	0.0													
DIC																		
TDS	1740.0	614.3	1664.0	1798.0	1599.0	1740.0	1767.0	1731.0	1456.0	1727.0	1621.0	1828.0		1680	1829	1862	1878	1838

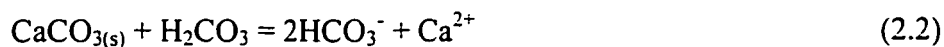
? = author did not indicate the source spring vent

analysed different vent waters. Some variation may also be attributable to errors introduced by the use of different sampling and analytical techniques. For example, calcium concentrations may appear artificially low if samples are not acidified at the time of collection and  $\text{CaCO}_3$  is allowed to precipitate from the waters prior to analysis. Bicarbonate concentrations will also vary depending on whether they were measured in the field or the laboratory: laboratory results will be lower due to the diffusion of  $\text{CO}_2$  from solution, and through precipitation of  $\text{CaCO}_3$  (Gulley, 1993). The aberrant chemistries measured by Elworthy (1926) are probably due to the use of different analytical techniques.

Changes in the  $\text{pCO}_2$  of the spring water can also affect ion concentrations. The introduction of  $\text{CO}_2$  to groundwater produces an acidic solution by the equation:



The solution is able to dissolve solid carbonate:



When the spring water emerges from the ground, loss of  $\text{CO}_{2(\text{g})}$  to the atmosphere drives both equations to the left, promoting calcite precipitation. If the spring water has higher  $\text{pCO}_2$ , there will be more free  $\text{Ca}^{2+}$  in the system, and less  $\text{H}_2\text{CO}_3$  (Gulley, 1993). Thus, analyses measuring higher bicarbonate concentrations might represent the spring water chemistry in years with higher spring water  $\text{pCO}_2$ .

Measurements taken at monthly intervals in 1984 and 1985 show that seasonal variations do occur: spring water temperature varied by as much as  $20^\circ\text{C}$ , and pH and Eh varied by 0.3 and 20 units, respectively (van Everdingen, 1986). These variations are due to differential dilution with surface water between seasons, with the highest volume of flow and lowest temperatures taking place in spring when snowmelt is at its peak. Naturally, meltwaters will dilute ion concentrations. Aperiodic “dirty water” events at the springs also take place when atypically large rainfall or sudden snowmelt carry surficial sedimentary and organic material into the spring channels (van Everdingen, 1983). Thus, variations in the data between years can also arise from differences in the proportion of meteoric water in the spring outflow.

Given the numerous sources of variation, the chemistry of the Miette spring water has been remarkably consistent in the long and short terms. This indicates that the spring

water is probably exchanging in equilibrium with the host rock in the subsurface (cf. Grasby *et al.*, 2000a). Analyses of the stable isotopes  $^3\text{H}$  and  $^{18}\text{O}$  show that the Miette spring waters were derived from local meteoric waters, and the low  $^3\text{H}$  values ( $\sim -8\text{‰}$ ) indicate a residence time in excess of 25 years (van Everdingen, 1986). The high temperature of the spring waters indicates that they circulated to a significant depth. If one assumes an average geothermal gradient of  $1^\circ\text{C}/33\text{ m}$  depth, then the Miette spring water circulated to a minimum depth of 1620 m to achieve its surface temperature of  $51^\circ\text{C}$  (Borneuf, 1983). Considering that dilution with shallow meteoric water produces reduced vent temperatures, the depth of spring water circulation likely exceeds the estimated 1620 m.

The Miette springs discharge mineral rich, sulphate-carbonate type waters with conductivities between 1829 and 1950  $\mu\text{S}/\text{cm}$ , and an average TDS of 1,774 mg/L. They have an average pH of 6.9 (for vents 3, 3a, 3b) that is elevated by cooling and evaporation to  $\sim 8$  four metres from the spring vents (Table 2.2). Their introduction to Sulphur Creek is evidenced by a change in its chemistry, and a 25% increase in water volume downstream of the springs (Table 2.3) (van Everdingen, 1972). The most distinctive chemical feature of the spring water is its high sulphur content ( $\sim 7\text{ mg}/\text{L}$ ) which results in a strong and unpleasant smell in the immediate vicinity of the springs, and apparently impairs spring water palatability: "...a peculiarity in connection with the sulphur water is that it cannot be very well mixed with other liquids; particularly does this apply to 'Scotch'" (from an early guidebook to Banff National Park, quoted by van Everdingen, 1972). The high  $\text{H}_2\text{S}$  content of the water indicates that anaerobic conditions prevail to shallow depth, likely facilitated by a high flow-rate that preserves  $\text{H}_2\text{S}$  during its passage through near-surface oxidizing conditions (van Everdingen, 1972). Most of the sulphur is oxidised to  $\text{SO}_4$  at the surface, and it accounts for more than 60% of the TDS of the spring water. Iron is not abundant in the spring water, so the sulphur is not derived from the subsurface oxidation of pyrite, but more likely from evaporite interbeds in the Rundle Group Carbonates.  $\text{CO}_3^-$  and  $\text{Ca}^{2+}$  are the next most abundant components (up to 280 and 407 ppm, respectively), indicating significant dissolution of carbonate. This is the highest calcium concentration known for spring water in the

**Table 2.2** Physical data collected from the Miette Hot Springs, June, 2001.  
 Two temperatures are given; one as measured by the pH probe (T(pH))  
 and one measured by the conductivity probe (T(Cond)).

<b>spring, distance from vent</b>	<b>pH</b>	<b>T (pH) °C</b>	<b>T (Cond) °C</b>	<b>Conductivity mS/cm</b>	<b>Salinity</b>
#3, 0m	6.89	50.6	--	1829	0.8
#3a, 0m	6.96	44.1	46.0	1875	0.8
#3a, 1.8m	7.97	36.6	--	1933	0.8
#3b, 0m	6.95	40.8	41.9	1877	0.8
#3b, 3.5m	7.38	30.0	30.4	1950	0.8



**Table 2.3** Variation in the water chemistry of Sulphur Creek before and after the addition of water from the Miette Hot Springs. All measurements are given in ppm. (after van Everdingen, 1972)

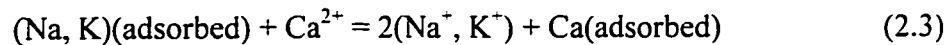
	Ca	Sr	Mg	Fe	Mn	Al	Cu	Zn	Na	K
above springs, 28/12/1966	63.0	0.3	19.5	0.02	0.00	0.05	0.000	0.000	3.6	0.7
below springs, 30/01/1967	163.0	7.4	35.0	0.12	0.00	0.10	0.005	0.000	7.2	5.1

	Li	HCO <sub>3</sub>	SO <sub>4</sub>	Cl	I	Br	F	PO <sub>4</sub>	NO <sub>3</sub>	SiO <sub>2</sub>	TDS
above springs, 28/12/1966	0.002	194.0	82.6	0.5	0.001	0.20	0.09	0.02	0.5	4.2	271
below springs, 30/01/1967	0.020	171.0	397.0	1.9	0.003	0.30	2.00	0.05	0.5	19.0	720

Southern Rocky Mountains, and one of the highest sulphate concentrations (van Everdingen, 1972).

The spring water has relatively high concentrations of Na<sup>+</sup>, K<sup>+</sup>, Cl<sup>-</sup>, and I<sup>-</sup>, which are probably derived from dissolution of interbed shales in the Rundle Group. The Na<sup>+</sup>/K<sup>+</sup> ratio ranges from 0.67 to 0.73, which is significantly lower than the 1:1 ratio found in other Rocky Mountain spring waters (van Everdingen, 1972). The high [K<sup>+</sup>] indicates that the groundwater is undergoing cation exchange with K-rich clays. The exchange reaction that occurs when a solution comes into contact with a clay unit is:



where calcium (or divalent ions) are preferentially held in ion exchange for monovalent ions (Gulley, 1993). The spring water also has an unusually high I<sup>-</sup>/Cl<sup>-</sup> ratio (750 to 900 times that of ordinary seawater). This indicates exchange with marine sediments (shale or fossiliferous limestone) that have high iodine concentrations due to concentration by marine organisms (van Everdingen, 1972).

The most significant trace-metal in the Miette hot spring waters is strontium with a concentration of 11 to 60+ ppm (Table 2.1). The Sr/Ca ratio in the Miette Water Chemistry Report (2000) was 1:553; ratios above 1:300 are found in fossiliferous limestones, so the strontium concentrations are probably also derived from fossiliferous lenses in the Rundle Group Carbonates (cf. Reeder *et al.*, 1972; Hern, 1989).

The emerging waters all have high loads of dissolved inorganic carbon (DIC) (22.16 to 24.86 ppm). The most common sources of groundwater DIC are atmospheric and plant CO<sub>2</sub> dissolved in the water during recharge, and carbon introduced by the dissolution of carbonate rocks along the flow path (Turi, 1986).

### 2.3 Microbial Assemblages

The microbial communities at Miette, colourful and profuse, are the most striking feature of the modern springs (Fig. 2.2-2.4). Unfortunately, the locations of springs 1 and 2 prevent investigation of their microbial assemblages and precipitates, and the remote location of the spring site precludes year-long observation. The summertime microbial assemblages at springs 3 and 3a and seep 3b are dominated by thermotolerant

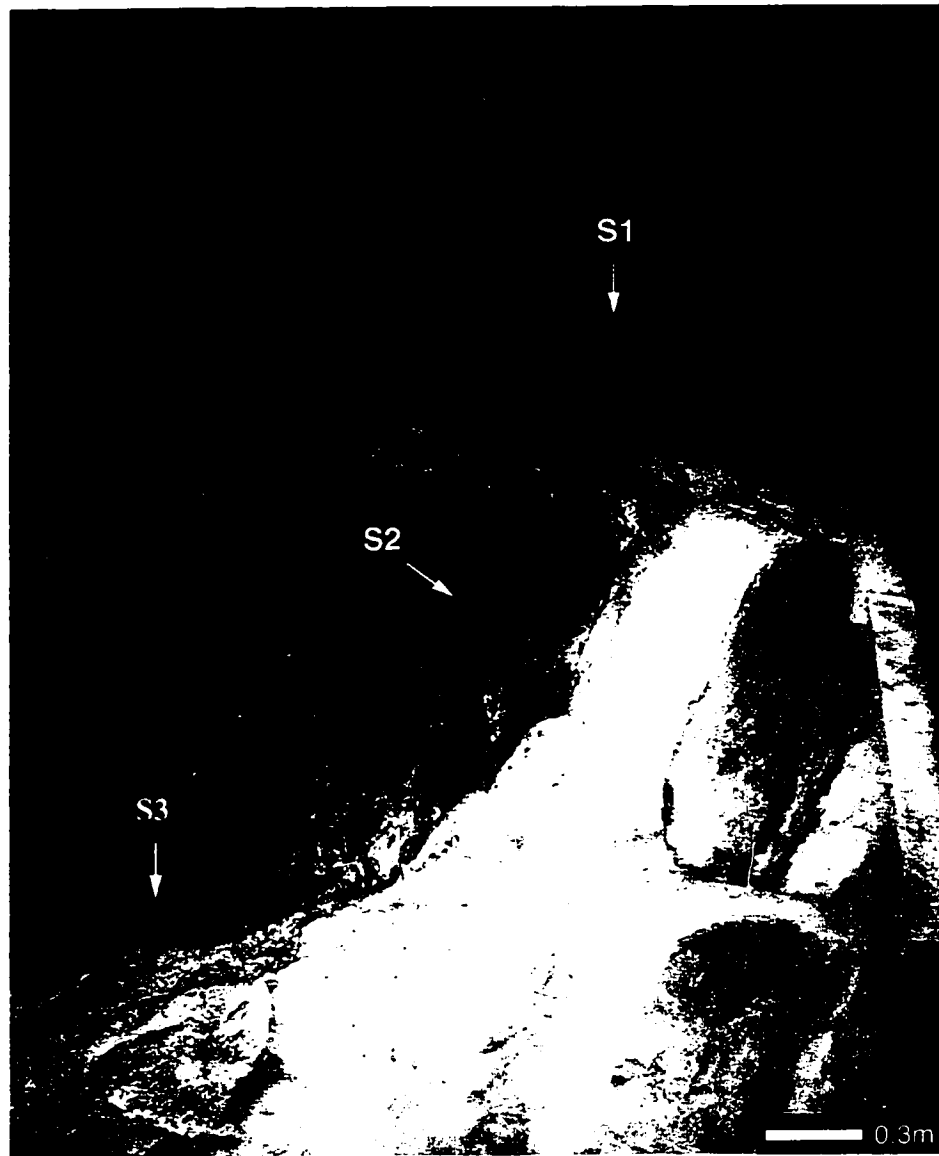


**Figure 2.2**

The orifice of spring 3. Green and orange microbial mats adhere to rocks beside the flow path and sulphur and gypsum precipitate as a white coating beneath the spring water. Arrows indicate locations referred to in the text.

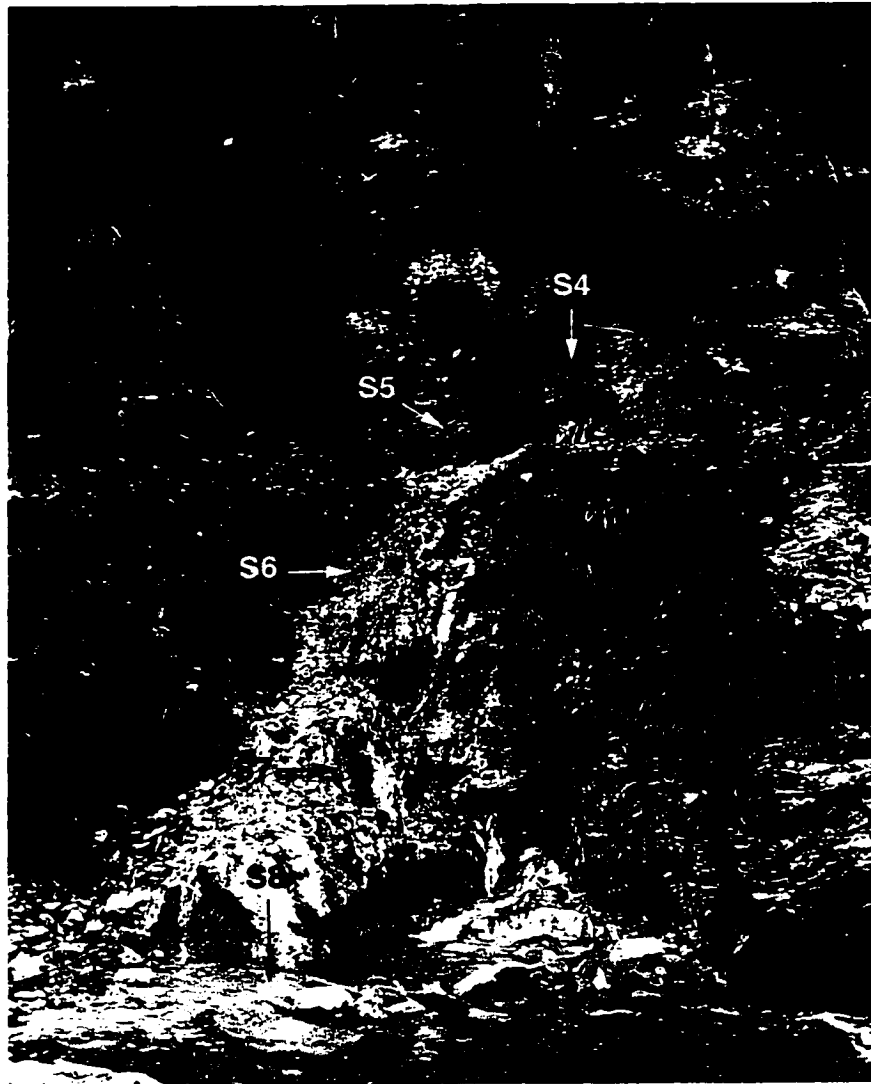


**Figure 2.3**

Microbial colonies in the discharge path beneath spring vent 3a. Gypsum precipitation gives a frosted appearance to microbes growing in the stream and spring water mixing zone. Arrows indicate locations referred to in the text. The vertical distance from point S5 to S7 is approximately 3.5 m.

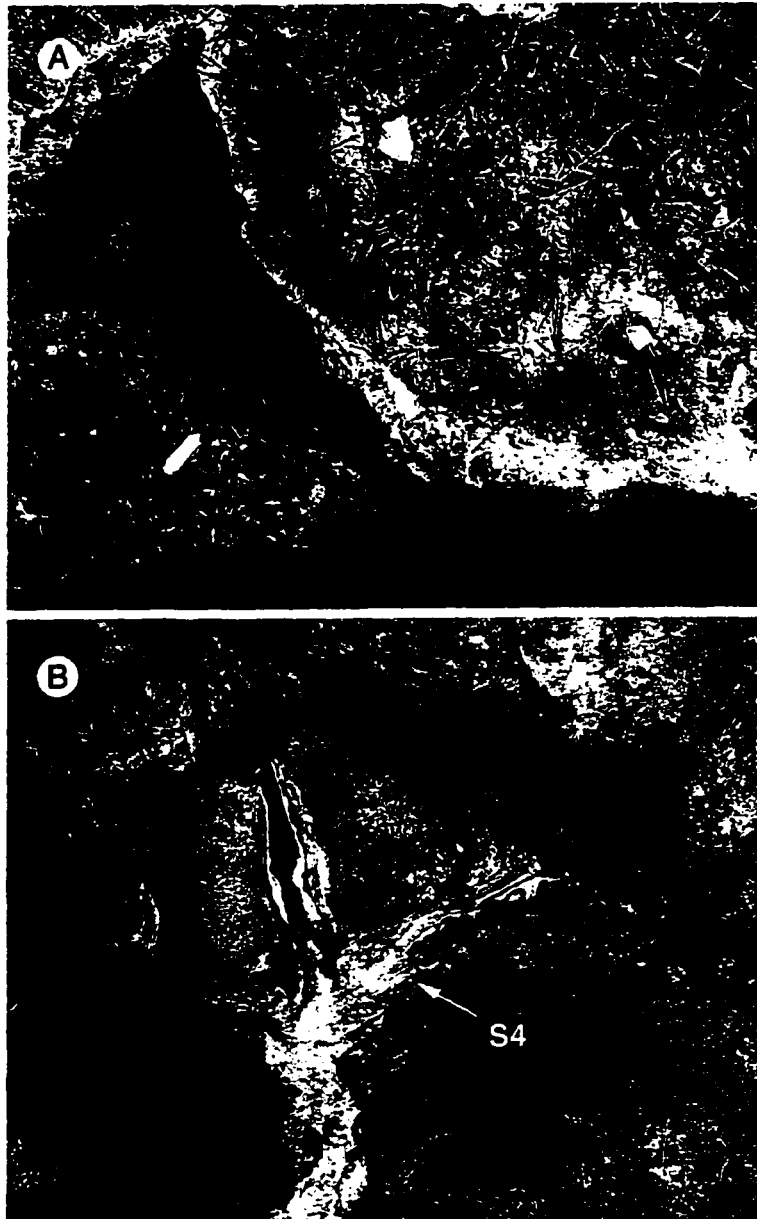


**Figure 2.4**

(A) The orifice of seep 3b, colonised by sulphur and gypsum coated filamentous microbes. The marker is 10 cm long. (B) The orifice of spring 3a. White, green, and red gypsum rinds decorate the rock beside and above the vents and the water hosts profuse microbial growth. The hammer is 25 cm long. Arrows indicate locations referred to in the text.

filamentous cyanobacteria species in the genera *Oscillatoria* and *Phormidium* and diatoms (Appendix 1). *Oscillatoria* is a thermophilic genus known for its sulphur tolerance (Brues, 1927; Cohen *et al.*, 1975; Canter-Lund and Lund, 1995). *Phormidium* is alkalophilic and thermophilic, with some species tolerating temperatures up to 50°C (and slightly beyond if protected by EPS and/or mineral precipitates) and pHs from 6.0 to 8.6 (Rippka *et al.*, 1979; Canter-Lund and Lund, 1995; Jones *et al.*, 2001). *Phormidium* and *Lyngya* are morphologically similar, and the two are difficult to discriminate between by light microscopy for species in the 3-5 µm filament diameter range (Rippka *et al.*, 1979). The microbe at Miette is near the upper size limit for the genus (~5.3 µm diameter - Jones *et al.*, 2002) but has been identified as *Phormidium* based on its ecological preferences, and its precedent to co-exist with *Oscillatoria* in sulphur rich spring water (Castenholz, 1976). There are three types of microbial assemblages in the spring water flow paths: those dominated by cyanobacteria, those dominated by diatoms, and those in which diatoms and cyanobacteria coexist. The colour and character of the microbial assemblages change with location relative to the spring vent, and are influenced by competition between the component species, the temperature of the water, the degree of submersion and the rate and style of precipitation at a site.

In the immediate vent environments of springs 3, 3a and seep 3b, where temperature and flow rate are the highest, white filamentous microbes skirt the flowing water and are bordered by bright green gelatinous mats (Fig. 2.3, 2.4). Light microscopy of samples collected within 0.5 m of spring vents 3 and 3a showed that despite the proximity of the two spring vents, they have different microbial assemblages. The wall of rock between them and the unidirectional flow of the water are effective geographic barriers. At spring 3, the white filamentous community is dominated by aligned filaments of *Phormidium* (5 µm diameter) that are encrusted with sulfur and gypsum crystallites (Fig. 2.5B). The outer 2-3 mm of the mat community is bright green and semi-translucent, with patches of reddish-purple. Under this outer rind, the mats are 1-4 cm thick, non-cohesive, olive green, purple, and gray. The green portions of the mat contain two filamentous cyanobacteria, the *Phormidium* species found in the filamentous portions, and a large diameter *Oscillatoria* (~15 µm diameter) (Fig. 2.5E, F). Unicellular

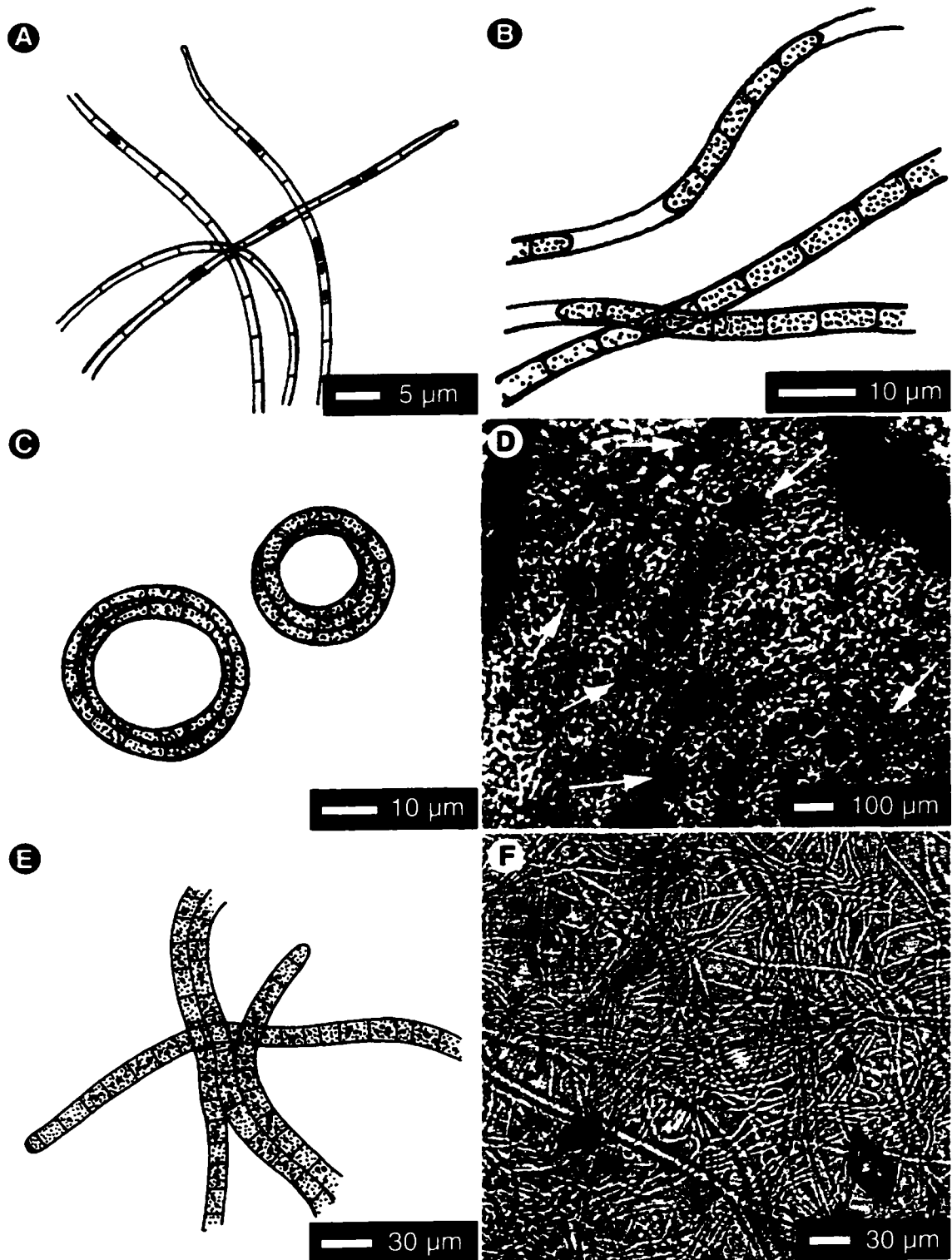


**Figure 2.5**

(A) Drawing of *Oscillatoria limnothrix?* filaments. (B) Drawing of *Phormidium* filaments. (C) Drawing of *Phormidium* filaments coiled into "doughnuts." (D) Photograph of a squash mount of a microbial mat collected from S2. Uncoiled *Phormidium* filaments and mucus surround tightly coiled *Phormidium* doughnuts (arrows). (E) Drawing of the larger diameter *Oscillatoria* species. (F) Photograph of a squash mount of a microbial mat collected from S4 showing large filaments of *Oscillatoria* and smaller *Phormidium* filaments co-habiting in copious mucus.

*Synechococcus* (Fig. 2.6D, E) and spheroidal green algal cells tentatively identified as *Chlorella* (Fig. 2.7A) are found in the mucus rich portions of the green mats along with tightly coiled *Phormidium* “doughnuts” (Fig. 2.6C, D). An unidentified, non-photosynthetic, eukaryotic, sheathed microbe with a 3 µm diameter apically swollen filament and terminal spore clusters is also found amongst the *Phormidium* filaments (Fig. 2.7D). The purple patches of mat are dominated by the thick *Oscillatoria* filaments, *Synechococcus*, and rod-shaped purple sulphate reducing bacteria (SRBs). The patchy purple colouring likely comes from the carotenoid pigments of the SRBs (cf. Pfennig, 1989). The non-cohesive basal layer is composed of decaying organic sludge and mucus, and hosts a dense population of *Synechococcus* and SRB’s (Fig. 2.6). Filaments found in the basal layer are colourless, and colonized by bacteria (Fig. 2.6B, C). The SRBs decompose organic matter from the upper portions of the mat in the basal layer, thus recycling the microbial biomass.

At spring 3a, the mat and filamentous assemblage is dominated by a thin filament cyanobacterial species with large intracellular gas vacuoles tentatively identified as *Oscillatoria. limnothrix(?)* (1.5 µm diameter) (Fig. 2.5A). In filamentous form, the microbes are aligned and coated in gypsum and sulphur crystallites. The mats are striated with an outer bright green gelatinous rind (~2 mm thick), underlain by a leathery orange and purple layer (2-5 mm thick), and a basal layer of non-cohesive purple-gray. The orange/purple and green layers are dominated by densely packed *O. limnothrix(?)* filaments in a mucilaginous matrix. In the green rind, the filaments host pseudo-filamentous epiphytes of the genus *Xenococcus(?)* (Fig. 2.7C). The orange/purple layer contains patches of SRBs, and the basal layer is composed of mucus, decaying filaments, and SRBs.

Rocks bordering and overhanging vents 3 and 3a are encrusted with gypsum crystals kept moist by rising sulphurous steam. The crystals are tinted various colours of green, red, and brown. This colouring originates from the pigmentation of unicellular green and red algae growing in thin films over the crystal surfaces. A pale green mat with a granular or earthy appearance is also found on rocks above the orifice of spring 3. The green rind of the mat, approximately 2 mm thick, is very cohesive and resistant to tearing. It is underlain by a noncohesive rusty brown layer 2 to 5 mm thick that adheres



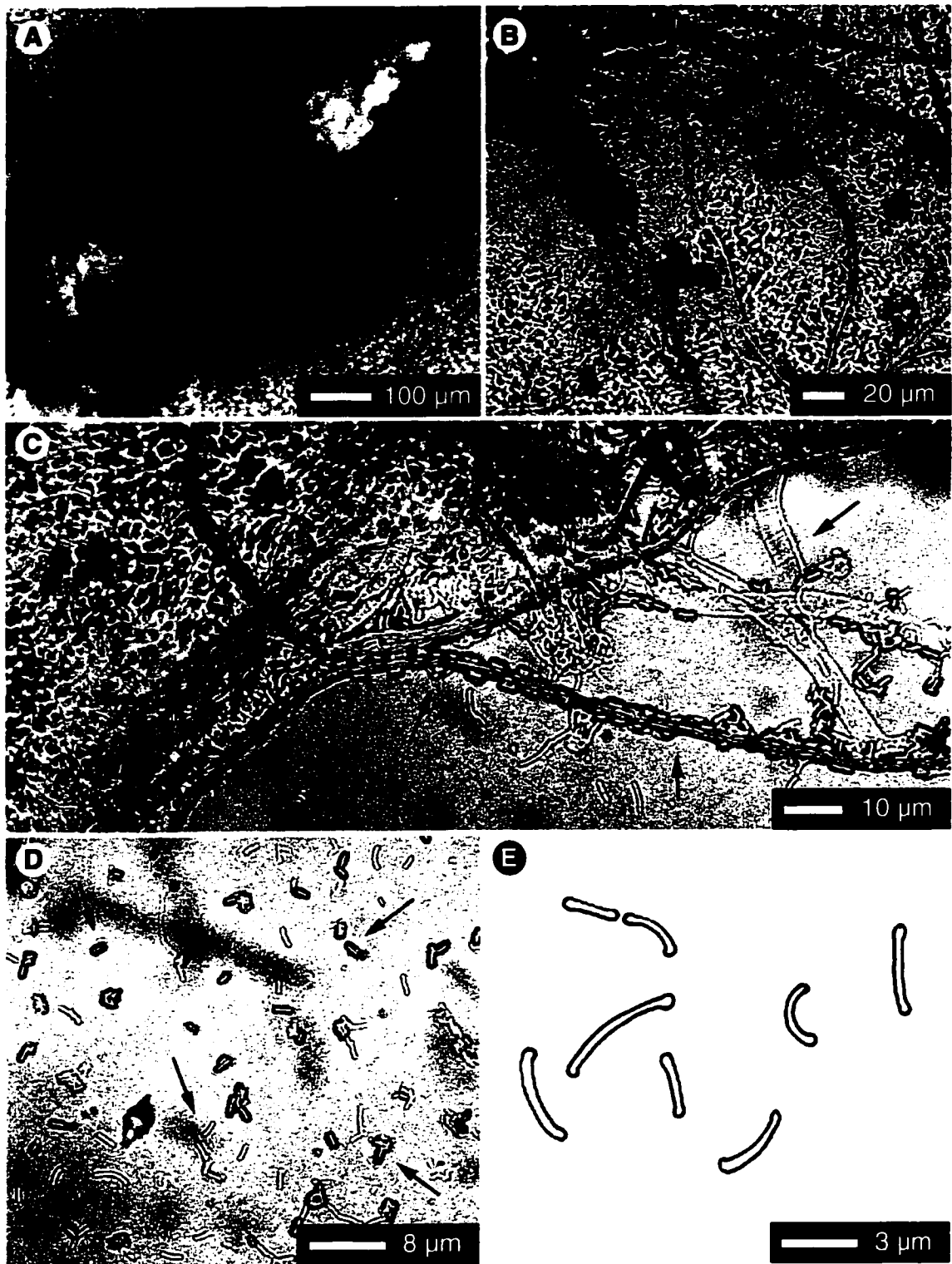


**Figure 2.6**

(A) Photograph of a squash mount of the basal layer of a microbial mat collected from S6. Dark areas contain purple SRBs. (B) Detail of previous showing a dense structureless population of bacteria and *Synechococcus* with a few filamentous microbes. (C) Detail showing bacteria adhering to the surfaces of decaying filaments of *Phormidium*. Note empty sheaths in the top right of the picture (their diameter has been exaggerated by squashing). (D) Detail of bacteria, *Synechococcus* (arrpws), and a gypsum crystallite. (E) Drawing of *Synechococcus*.

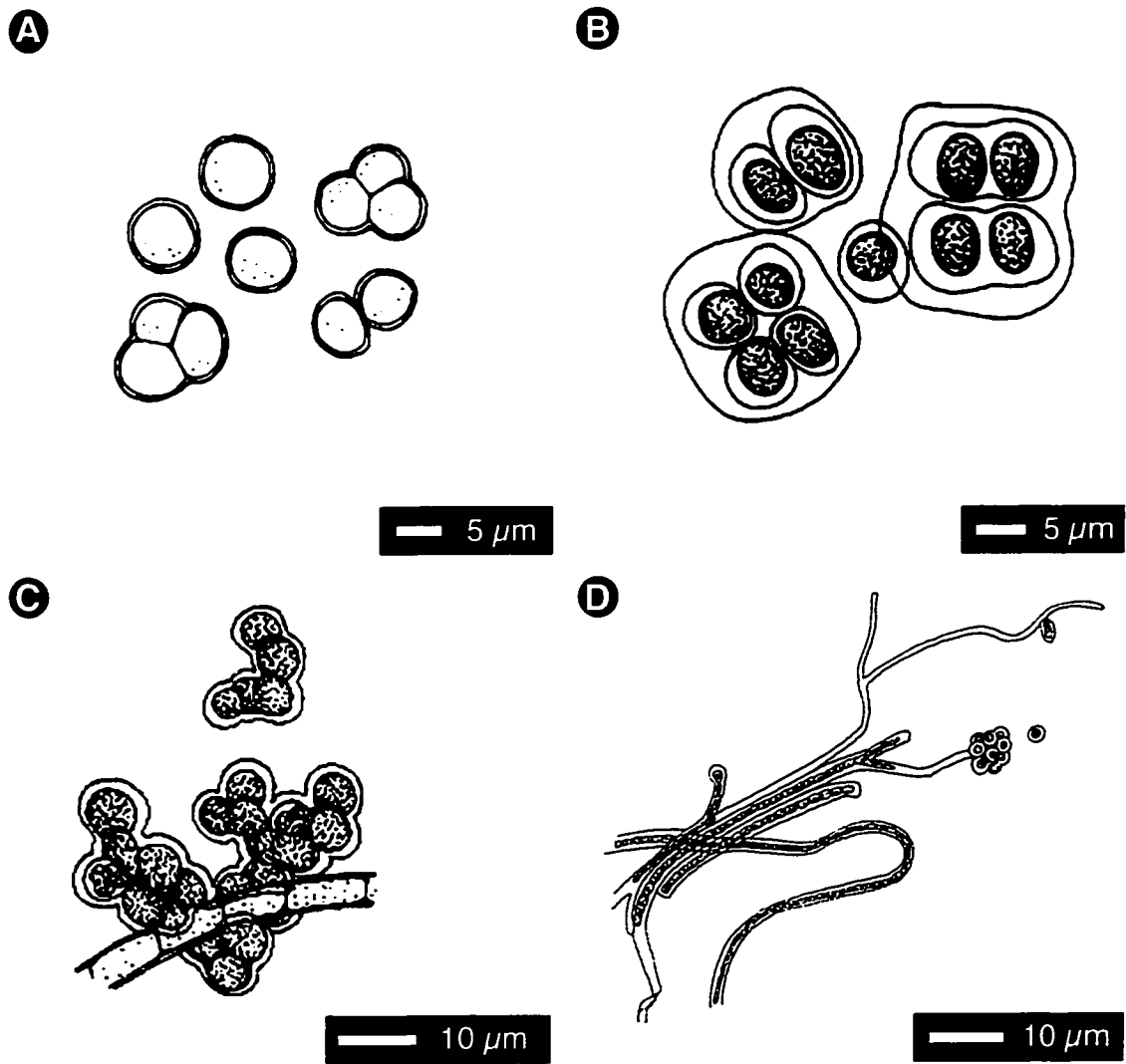


**Figure 2.7**

(A) Drawing of a unicellular algae tentatively identified as *Chlorella* found in microbial mats collected from S1, S2, S7 and S8. (B) Drawing of *Gleocapsa* found in microbial mats from S2, S7 and S8. (C) Drawing of *Xenococcus* found attached to filaments of *Phormidium* and *Oscillatoria* in microbial mats from S4. (D) Unidentified sheathed microbe with spore clusters and some apical swelling found in microbial mats collected from S1.

to the rock. The mat is heavily mineralized with microscopic gypsum crystals, and contains the unicellular *Chlorella*. The fabric-controlling microbe, however, is the thin *Oscillatoria limnothrix(?)*. There is little intercellular mucus in these mats, and mineralisation is concentrated on the surface of filaments. As the water flows away from vents 3 and 3a, the mat communities disappear at locations S5 and S2 (approximately 0.5 m from the vents) and submerged rocks are coated in yellow-white precipitates of sulphur and gypsum made cohesive by mucus secreted by diatoms. At spring 3, the water is collected in a catchment basin. The sides of the basin are ornamented by brightly coloured orange and green mats, and fragments of the mats float in the pooled water, accumulating sulphur and gypsum lime. Below spring 3a, the water flows down a slope into Sulphur Creek and microbial mat communities are re-established in the flow path by location S6 (approximately 2 m from the vent 3a).

The alternation of cyanobacteria and diatom communities at S2 and S5 indicates that the diatoms and cyanobacteria are in competition. This phenomenon has been observed elsewhere, usually with the cyanobacteria out competing the diatom populations due to the better adaptation of prokaryotes to thermal conditions (Brock, 1978; Vinson and Rushforth, 1989). Here it appears that the diatoms out compete the cyanobacteria, albeit in a limited part of the flow path. This interpretation is supported by the fact that the diatom assemblage has higher diversity where microbial mats are not well established. A sample of organics and precipitates collected 1 m from spring vent 3a (where the water temperature is ~ 40°C, approaching the upper limit for diatom viability - Brock, 1978) was dissolved in weak HCl and the residual sample was examined by SEM and light microscopy. This revealed a diverse collection of rheophilic mesohaline diatoms including *Mastigloia elliptica*, *Sellaphora pupula*, *Rhopalodia gibberula*, *Brachysira vitrea*, and species of *Nitzschia*, *Navicula*, *Pinnularia*, and *Cymbella* (possibly *Cymbella ruttneri*, as described by Hutstedt - Simonsen, 1987) (Fig. 2.8-2.10). Near the base of the spring 3a flow path, where the mat communities proliferate, diatom diversity is reduced and the community is dominated by the *Cymbella* species with lesser numbers of *Navicula sp.*, *Brachysira vitrea*, and *Mastigloia elliptica*. There are no nutrient limitations in the Miette spring water, and the heavily silicified tests of the diatoms attest to an abundance of silica. The diatom frustules were mostly articulated,

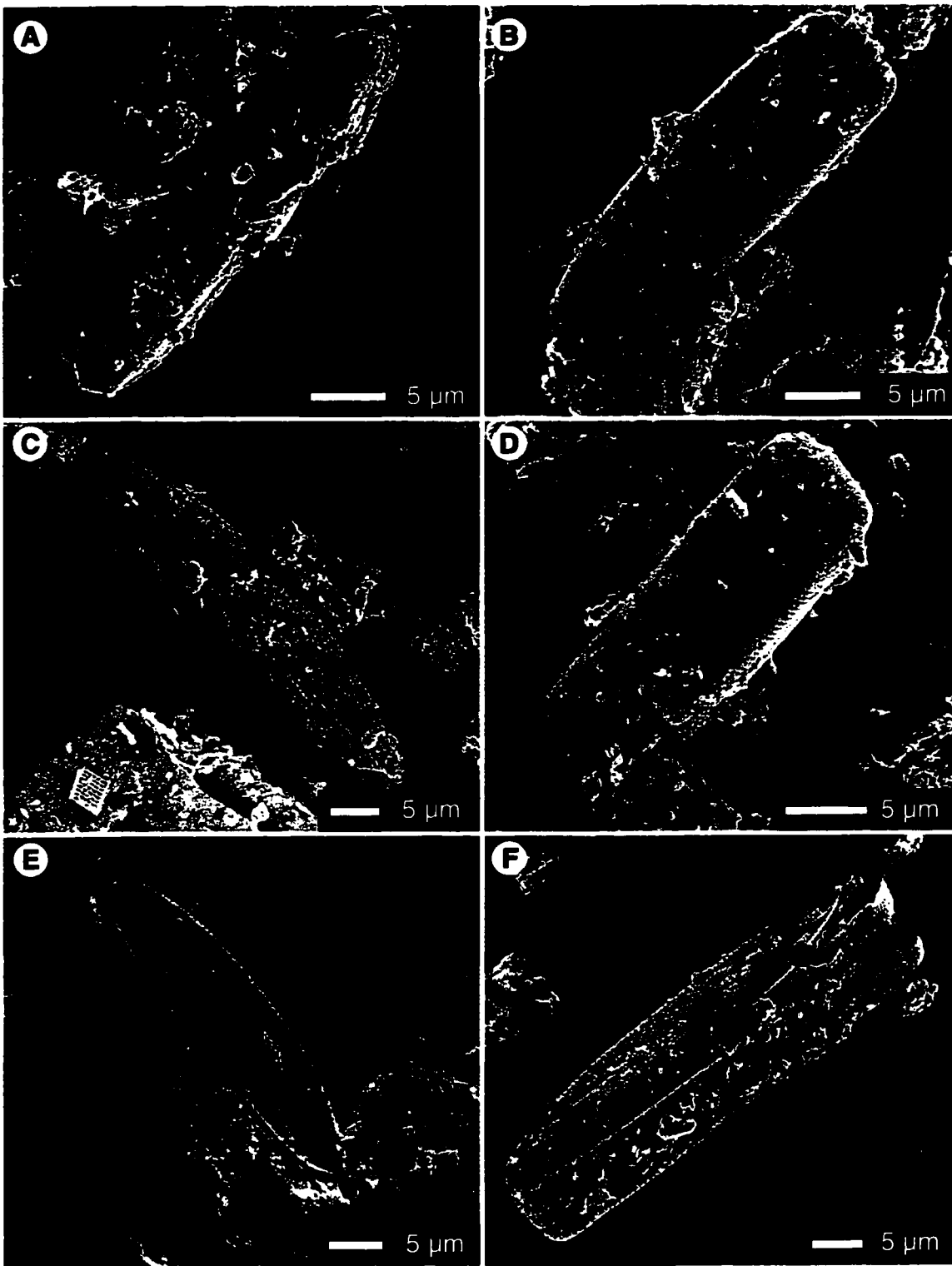


**Figure 2.8**

SEM images of diatom species found at the modern Miette Hot Springs: (A) valve view of *Cymbella rutneri?* (B) girdle view of *C. rutneri?* (C) valve view of *Mastigloia elliptica*, (D) girdle view of *M. elliptica*, (E) inside valve view of *M. elliptica*, (F) intact *M. elliptica* frustrule showing the association of the inner and outer valves.

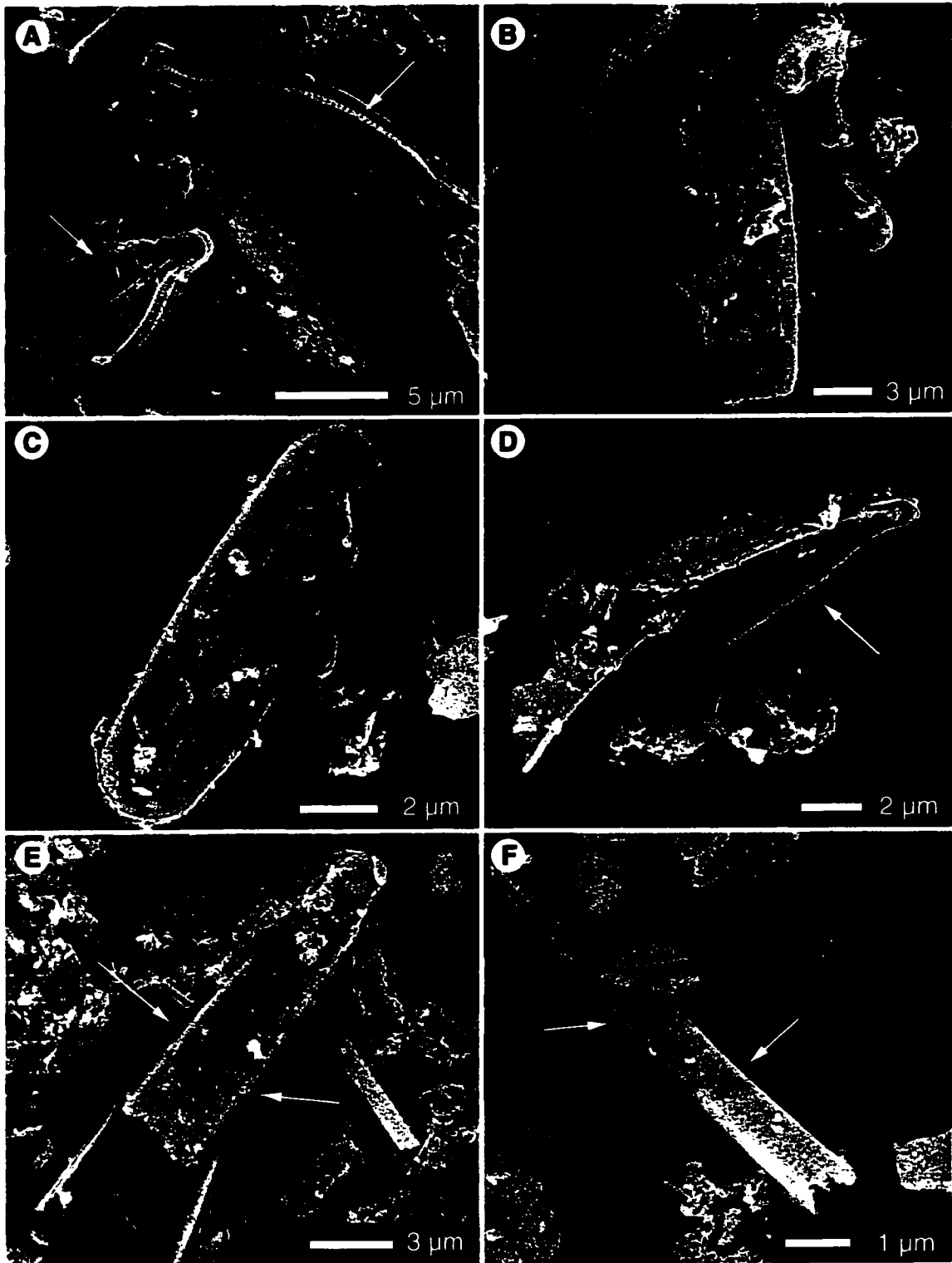


**Figure 2.9**

SEM images of diatom species found at the modern Miette Hot Springs: (A) valve views of *Brachysira vitrea* (arrows), (B) girdle view of *B. vitrea*, (C) valve view of *Sellaphora pupula*, (D) inside valve view of disarticulated *Rhopalodia gibberula*, (E) valve view of disarticulated *Nitzschia sp.*, (F) girdle view of disarticulated *Nitzschia sp.*

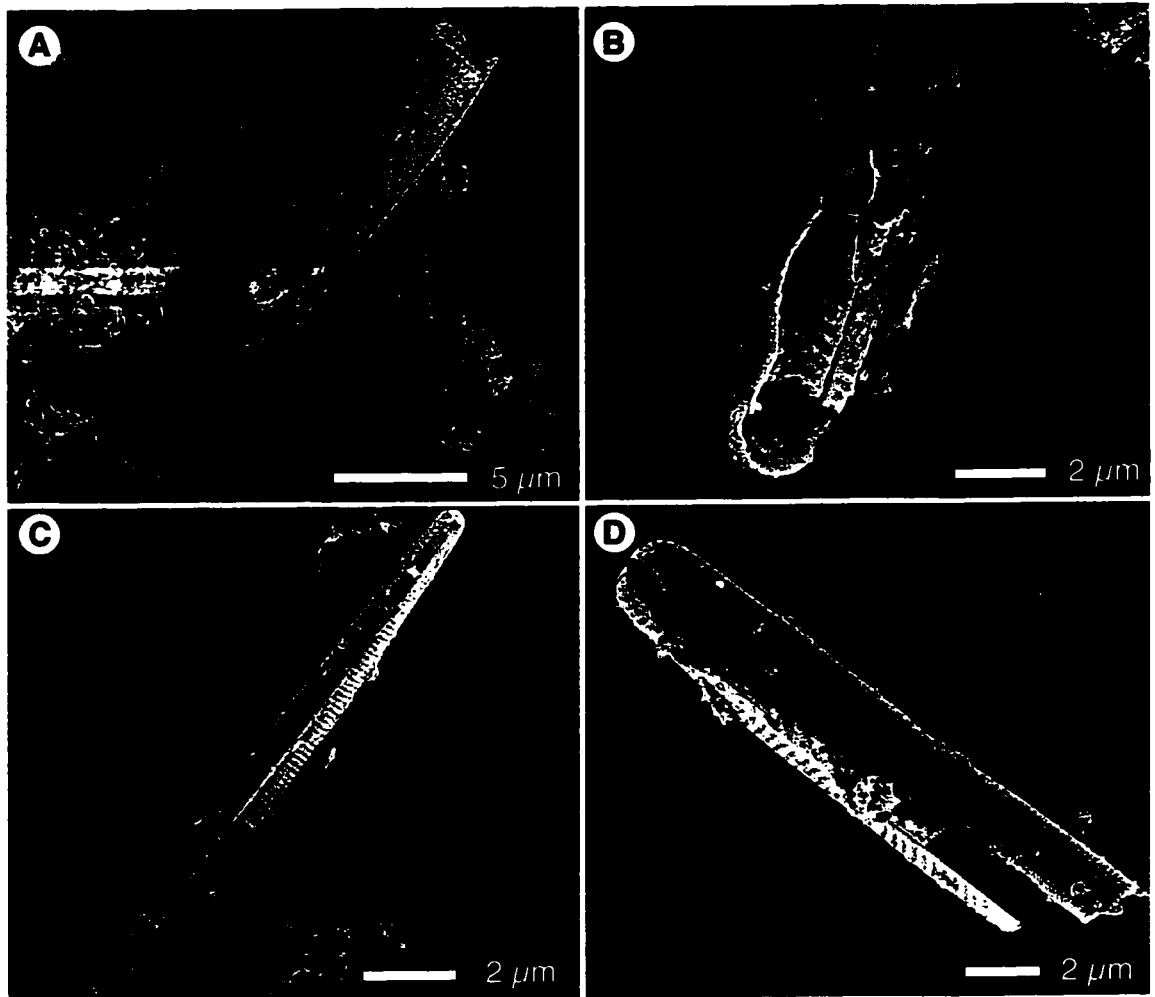


**Figure 2.10**

SEM images of diatom species found at the modern Miette Hot Springs: (A) girdle view of view of *Navicula sp.*, (B) Oblique view of *Pinnularia sp.*, (C,D) Girdle views of unidentified diatoms.

even after processing, with two or more valves connected; they have obviously not undergone significant transport and are endemic to the spring flow path. Other studies have found that species diversity and number of species increase with temperature from 14°C to 25°C, beyond which diversity decreases (Vinson and Rushforth, 1989).

Competition with cyanobacteria seems to override this temperature effect at Miette. The dense precipitation of sulphur in the diatom-rich area could explain this phenomenon: though many diatoms tolerate sulphide up to ~3.9 mg/L (Patrick, 1977), it may prevent cyanobacteria from growing beneath the spring water, permitting the diatoms' success.

The mat communities in the lower discharge path of springs 3 and 3a are best described as metaphyton, wherein substrate-attached microbes, non-attached microbes, and diatoms cohabitate in copious mucus (cf. Round *et al.*, 1990). There is a transitional colour change in the microbes submerged by the spring water. White filamentous forms give way to cohesive gelatinous green and orange mats, and the submerged mats are transitional with episodically submerged olive green or orange/brown mats, and dry rusty brown mats (Fig. 2.4). The mats are cohesive and leathery, but not firmly attached to the rocks beneath them, and can be sloughed off easily. Beneath spring 3a the transition from filamentous (at S7) to mat forming (by S8) communities is concurrent with dispersion of the spring water: as it moves over the slope towards Sulphur Creek, the water abandons tributary flow and falls in thin films. This reduces turbulence at the water/substrate interface, and permits the accumulation of inter-cellular mucus in the microbial colonies. Each mat is composed of a pliable external rind that is underlain by successively less cohesive earthy decomposition layers.

Around the catchment basin of spring 3 (S3, Fig. 2.2), the mats are dominated by thin *Oscillatoria limnothrix*(?); the orange portions of the mat are composed of tightly packed filaments, and the green portions are mucus rich and also contain *Phormidium*, *Gleocapsa*, and *Chlorella* (Fig. 2.7A, B). The olive green and orange/brown partially submerged mats have the same assemblage as the green submerged mats, with the addition of diatoms and SRBs. In the discharge path of spring 3a (S7, S8, Fig. 2.3), the mats are dominated by *Phormidium* and the thick *Oscillatoria* sp. (~15 µm diameter) and contain unicellular *Synechococcus*, *Gleocapsa*, *Chlorella*, SRBs, and diatoms.

In the mixing zone between spring 3a waters and Sulphur Creek, rocks and organic debris are ornamented with white filamentous fringes (S8, Fig. 2.3). The fringes are “fluffy,” 0.5 to 1.5 cm long, and composed of gypsum-coated filamentous cyanobacteria. Larger filaments of *Phormidium* (5 µm diameter) host gypsum crystallites that adhere directly to their sheaths, whereas thin, unsheathed *Oscillatoria limnothrix?* (1.5 µm diameter) filaments form wispy meshworks that trap crystallites and wrap around the *Phormidium* filaments. The unicellular green alga, *Closterium sp.*, was also found among the filaments. *Closterium* is a common inhabitant of nonalkaline epipellic diatom communities (Prescott, 1970) and was probably introduced to the fringe assemblage from populations in Sulphur Creek.

The microbial species found at the Miette Hot Springs are atypical in the regional environment (Gadd, 1999; Lepitzki and Lepitzki, 2001), and species composition may be determined by the concentration of soluble sulfide in the spring water. The distribution of thermophilic species in hot-springs is geographically variable, even in localised thermal regions. Some species, however, have world-wide distribution. *Mastigocladus* (a.k.a. *Fischerella*), for example, is almost ubiquitous in slightly acid to alkaline thermal spring waters with temperatures above 50°C (Castenholz, 1969). *Mastigocladus* is, however, excluded from spring waters with H<sub>2</sub>S concentrations over 0.15 mg/L and 0.25 mg/L at New Zealand and Icelandic spring sites. Sulphur tolerant species of *Oscillatoria* inhabit these spring waters up to 57°C, and are succeeded by species of *Phormidium* in the distal discharge paths of the New Zealand springs (Castenholz, 1976). Thus, the community of *Oscillatoria* and *Phormidium* at Miette has global precedence; it may be a common species association selected by a sulphide-rich water chemistry.

#### 2.4 Precipitates

The Miette spring waters are slightly supersaturated with CaSO<sub>4</sub> and CaCO<sub>3</sub> (van Everdingen, 1980b) and mineral precipitation is facilitated by degassing, evaporation, and cooling. Although Baird (1963) reported the precipitation of calcite and van Everdingen (1972) described “travertine” around the spring vents, gypsum (CaSO<sub>4</sub>) and



elemental sulphur ( $S^0$ ) are the dominant precipitates today. Calcite ( $CaCO_3$ ) and strontianite ( $SrCO_3$ ) are less common.

The precipitation of gypsum is initiated in the proximal vent environment where the oxidation of  $H_2S$  gas in the spring water produces sulphate for the reaction:



$Ca^{2+}$  is derived from the spring water, and may also come from dissolution of limestones overhanging vents 3 and 3a by rising steam and  $H_2S$  gas. Gypsum forms decorative rinds on rocks bordering and overhanging the spring orifices (Fig. 2.4B). These rinds are white but have green or reddish tints where their surfaces are colonized by microbes. The crystals are composite, 0.5 to 3 mm long, and composed of blades of gypsum that are aligned, taking on a macroscopic pseudo-prismatic habit (Fig. 2.11A, B, C). Smaller mineral precipitates of sulphur, calcite, and strontianite are trapped in cavities between the gypsum blades (Fig. 2.11E, F). Similar aggregate gypsum crystals also form on the surfaces of resistant microbial mats in the discharge path of spring 3a. By dissolving the microbial mat with bleach, it was possible to take SEM photomicrographs of the nucleation side of the crystals (Fig. 2.11D). Crystal growth is initially randomly oriented on the mat, and individual gypsum blades become streamlined as competition for space forces the crystals to align. Both the rocks and the microbial mats act as substrates for gypsum nucleation.

Gypsum also precipitates in suspension as microscopic euhedral rhombs that are trapped by sticky extra-polymeric substances (EPS) on the external sheaths of submerged filamentous microbes, giving them a white, frosted appearance (Fig. 2.12). This phenomenon is observed within a two meter radius of spring vents 3, 3a and 3b, and also in the mixing zone of spring and creek water that occurs below spring 3a. The spring water contains some unoxidised  $H_2S$  (Table 2.1) and when it mixes with the well oxidized waters of Sulphur Creek, remaining  $H_2S$  is oxidized to  $SO_4$ , permitting a new wave of gypsum precipitation. The mixing zone at S8 is marked by a cloudy fan of gypsum-frosted filamentous periphyton (Fig. 2.3).

Elemental sulphur is derived from incomplete oxidation of  $H_2S_{(g)}$  and from the reduction of sulphate by SRBs. Sulphur is found trapped in aggregate gypsum crystals close to the spring vents; it is netted by microbial mucus; it accumulates as floating flocs

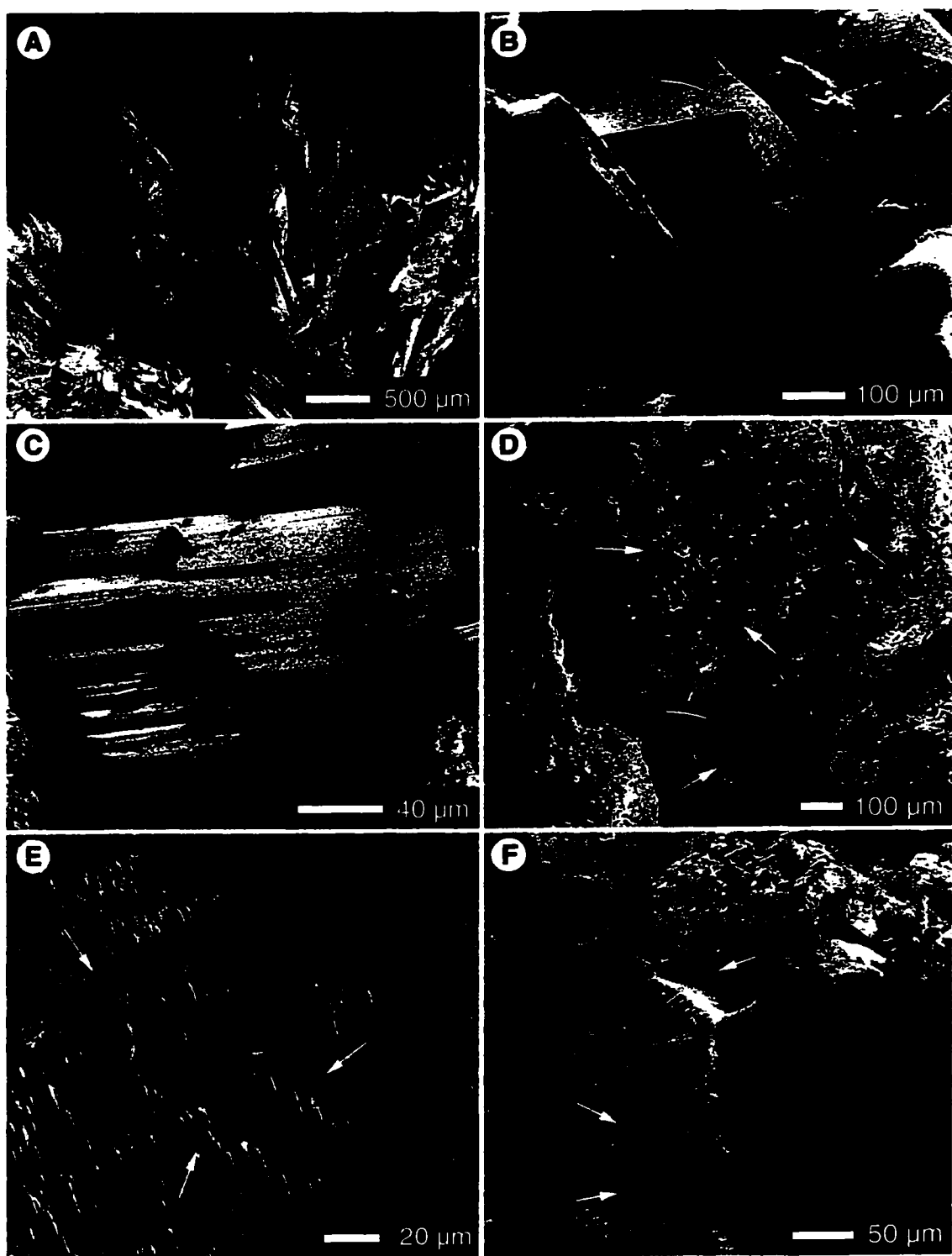


**Figure 2.11**

SEM images of gypsum. (A) Coarse crystals collected above vent 3a (S4). (B) Blocky compound crystals found at the orifice of spring 3 (S1). (C) Detail of blades in a compound crystal from S1. (D) Basal view of randomly aligned gypsum crystals (arrows) found on a microbial mat 0.5 m from vent 3a (S4). (E) Compound gypsum crystal from location S6 with irregular and filament shaped cavities (arrows) containing detritus and calcite and sulphur precipitates. (F) Terminal cavities in gypsum from S1 house calcite crystals (arrows).

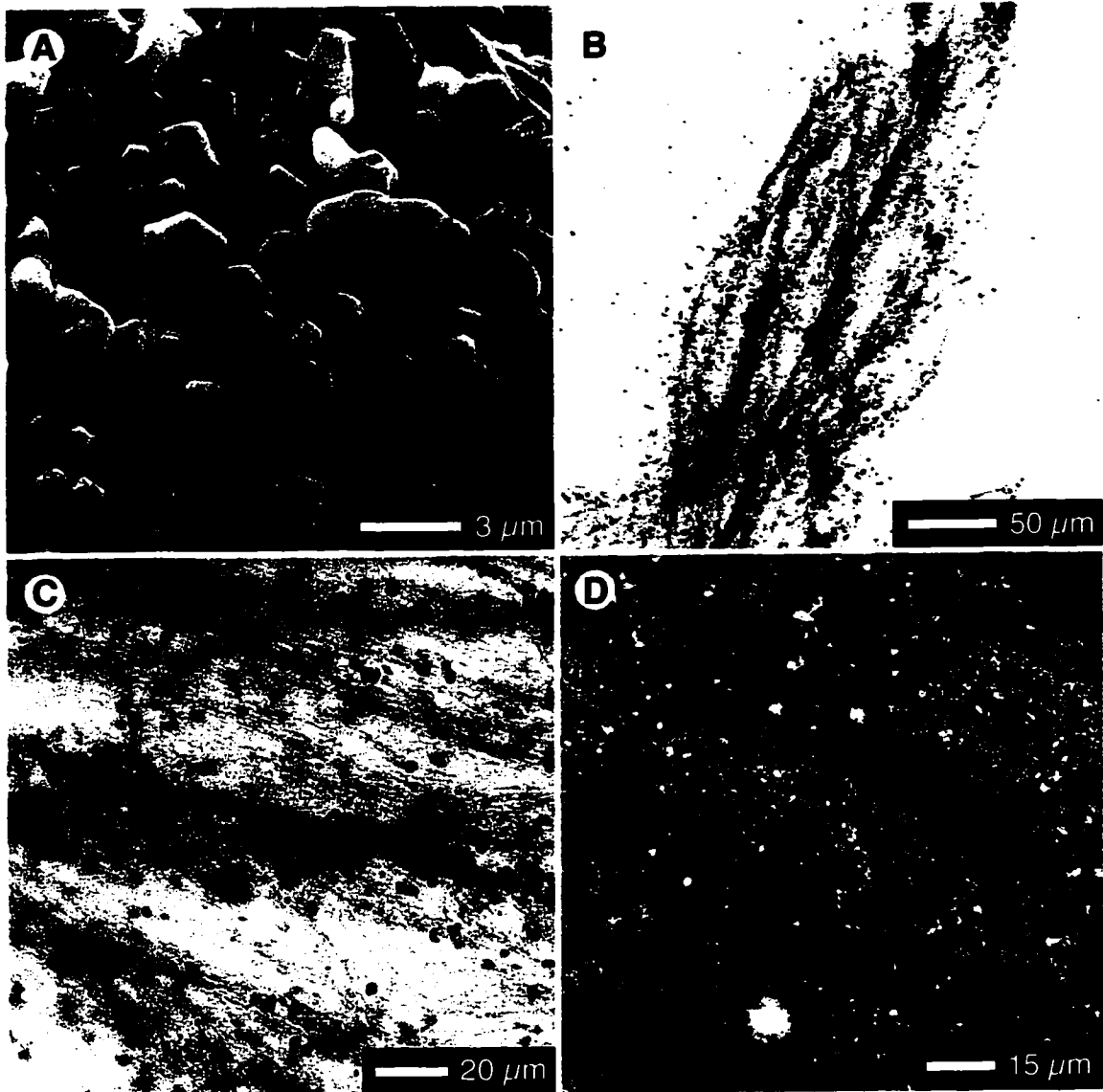


**Figure 2.12**

(A) SEM image of gypsum crystallites found trapped in a microbial mat in the lower discharge path of spring 3a (S7). (B) "Frosted" filamentous microbes collected at S8 in the mixing zone between Sulphur Creek and spring water from spring 3a. Gypsum crystallites adhere to the sheaths of the larger filaments, *Phormidium sp.*, and are caught in meshes of finer filaments, *Oscillatoria limnothix?* (C) Detail of image B showing concentration of gypsum by the larger filaments and filament bundles. (D) Detail of image B showing the random distribution of gypsum crystallites in a meshwork of fine filaments.

where water is pooled (such as the catchment basin beneath spring 3); it adheres to filamentous microbes; and, it forms a yellowish-grey rind on rocks bordering the spring water flow path. The largest accumulations of sulphur are found within a 2 m radius of the vents. Macroscopically, these deposits are massive or granular, but have a microscopic habit as spherical beads and elongate, lumpy rods (Fig. 2.13).

A comparison of ion-activity products with solubility constants show that the Miette spring waters are barely saturated with calcite (van Everdingen, 1972). Precipitation could be initiated by degassing of CO<sub>2</sub> and cooling, but these effects will be offset further from the vent as a rise in pH (concurrent with degassing) decreases the solution's proclivity to precipitation (van Everdingen, 1972). As a further impediment to calcite precipitation, dissolved CO<sub>3</sub><sup>2-</sup> is in competition with the more abundant SO<sub>4</sub><sup>2-</sup> for Ca<sup>2+</sup> ions, limiting the volume of calcite that the spring water can precipitate. Nonetheless, calcite is found as microscopic compound crystals that are trapped in cavities in gypsum crystals, netted by filamentous microbes, and found on and in microbial mats. The crystals take on a variety of morphologies – single cubic and compound spherical (some twinned to form “dumbbells”) and bi-terminal crystals are the most common (Fig. 2.14). Evaporative concentration and photosynthetic withdrawal of CO<sub>2</sub> may be important facilitators of calcite precipitation.

Strontianite is also precipitated in concert with degassing of CO<sub>2</sub>. It is a relatively rare mineral, even in hydrothermal settings – at Zhemchug Hot Springs, Russia, high concentrations of Sr<sup>2+</sup> in the spring water are incorporated into the mineral structure of calcite or aragonite without precipitation of strontianite (Tazaki *et al.*, 2001). At Miette, the sequestration of Ca<sup>2+</sup> in gypsum, which limits calcite precipitation, likely permits the spring water to reach saturation with strontianite. Strontianite forms rosettes that nucleate on the surface of gypsum crystals, and is found as individual blades in cavities in gypsum crystals and in microbial mucus (Fig. 2.15).

The stable oxygen isotopes of a precipitate are sensitive to the composition and temperature of the precipitating fluid. If calcite is precipitating from water in stable isotopic equilibrium, the system can be described by the equation:

$$1000\ln\alpha = 18.3(10^3/T) - 32.42 \quad (2.5)$$

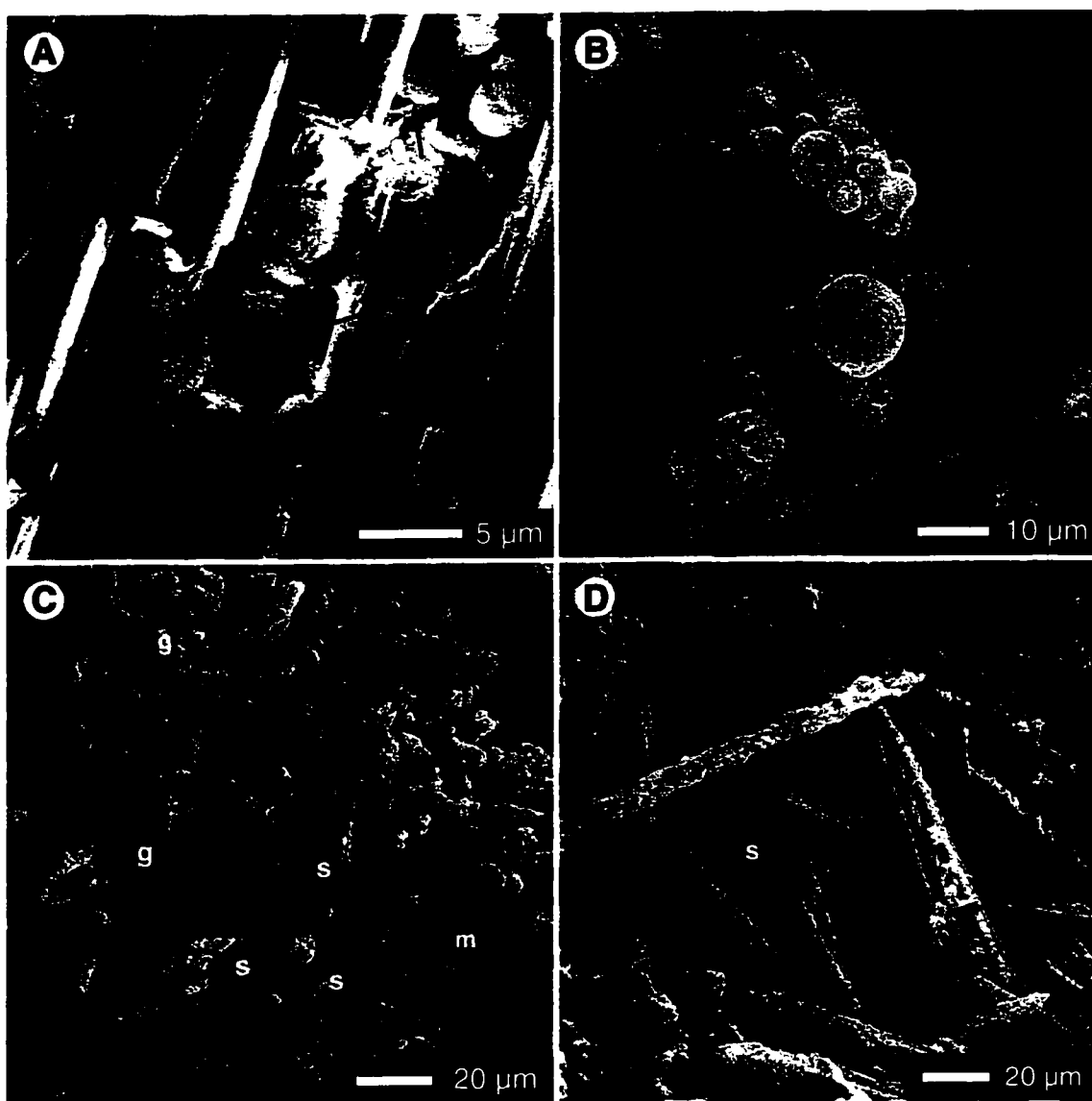


**Figure 2.13**

SEM images of elemental sulphur precipitates. (A) Beads of sulphur (arrows) trapped in a cavity in a large compound gypsum crystal collected from the orifice of spring 3 (S1). (B) Beads and irregular shaped sulphur found coating filamentous microbes at S9 in the discharge path of seep 3b. (C) Rods of sulphur (s) and small rhombs of gypsum (g) bound in diatom mucus (m) found coating rocks in the discharge path of spring 3a (S5). (D) Large rods of sulphur (s) and small gypsum rhombs (g-arrow) that accumulated on floating microbial mats in the catchment basin of spring 3 (S3).

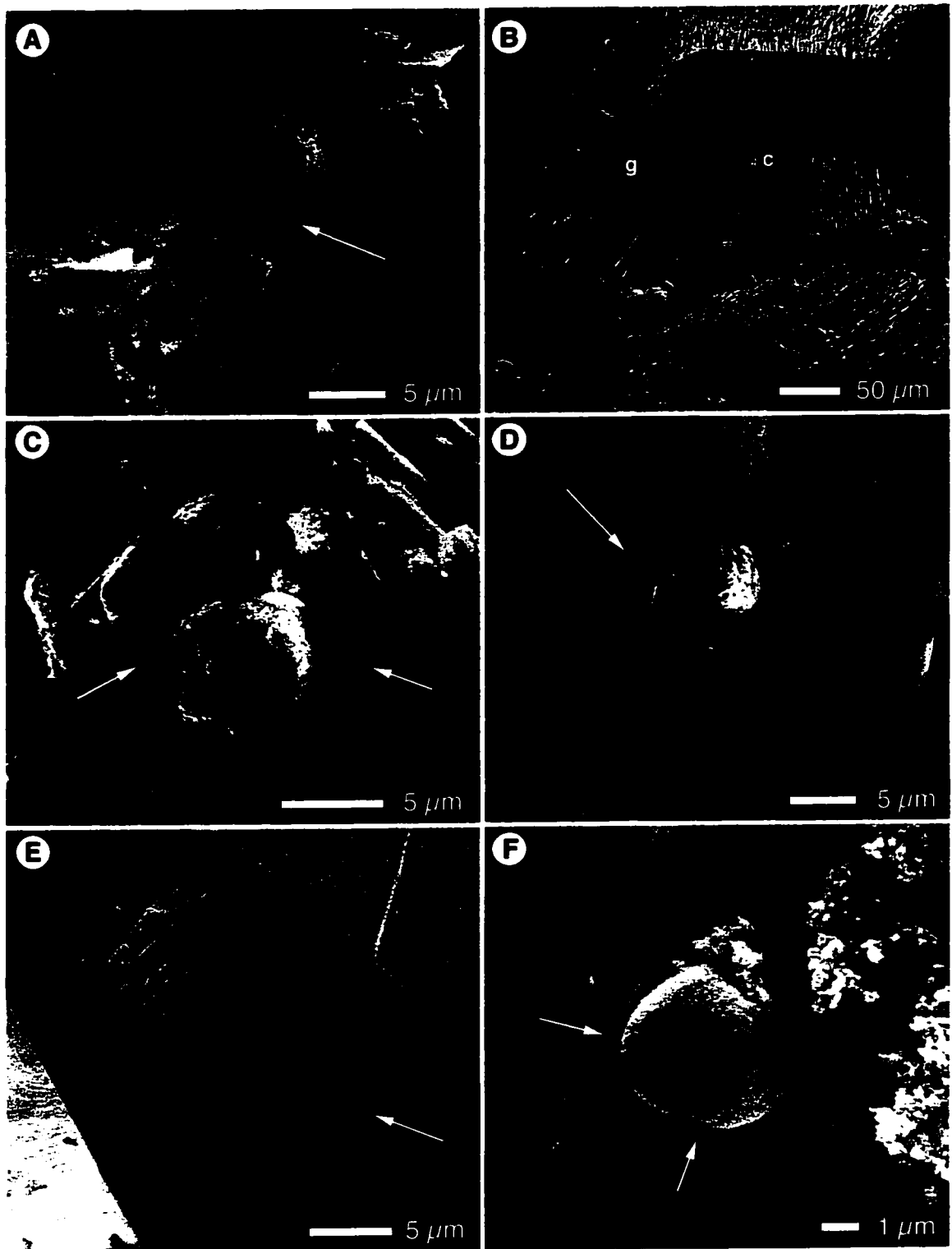


**Figure 2.14**

SEM images of calcite crystals (arrows). (A) Cubic calcite between the blades of a composite gypsum crystal found on rocks beside the office of spring 3a (S4). (B) Calcite rhombs (c) with larger gypsum crystals (g) collected from a crystal rind beside the orifice of spring 3 (S1). (C) Twinned composite calcite spherules trapped in the cavity of a composite gypsum crystal found on a microbial mat at S6. (D) An aggregate of calcite rosettes found adjacent to image C. (E) Composite blocky calcite spherule found trapped between gypsum crystals collected from S1. (F) Composite platy calcite spherule found with clays in a space between gypsum crystals adjacent to those in image E.

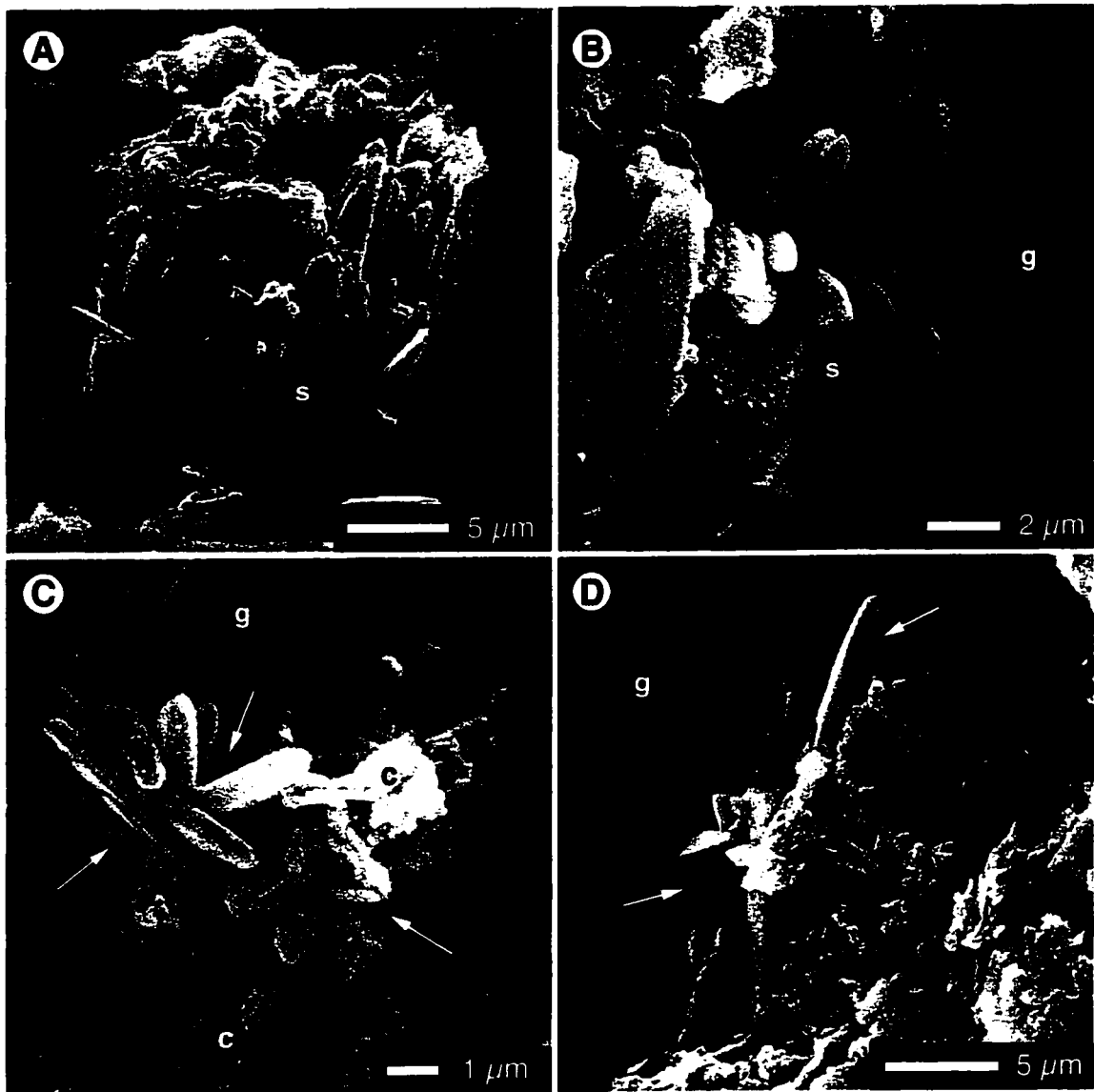


**Figure 2.15**

SEM images of strontianite precipitates. (A, B) Strontianite blade rosettes (s) and detrital clay (c) found on gypsum crystals (g) collected from crystalline rinds above the vent of spring 3a (S4). (C) Intergrown prisms of strontianite (arrows) and detrital clay (c) adjacent to a large gypsum crystal (g) collected from rocks beside spring vent 3a (S4). (D) Blades of strontianite (arrows) lodged with detrital clay (c) in a cavity between two gypsum crystals (g) collected from rocks beside spring vent 3a (S4).

where  $\alpha = (1000 + \delta^{18}\text{O}_{\text{calcite}}) / (1000 + \delta^{18}\text{O}_{\text{water}})$ , T is the water temperature at the precipitation site, and  $\delta^{18}\text{O}_{\text{water}}$  is the value of the spring water measured close to the mineral sample location (Kim and O'Neil, 1997). Five precipitate samples were taken and, since the water temperature was measured at each sample site, and the  $\delta^{18}\text{O}_{\text{water}}$  known, the  $\delta^{18}\text{O}_{\text{mineral}}$  can be used to evaluate if the system is precipitating in isotopic equilibrium. The mineral samples contained gypsum, calcite, sulphur and strontianite, but the carbon and oxygen extracted for analysis were derived solely from  $\text{CO}_3$  in the carbonate minerals.

Applying the  $\delta^{18}\text{O}_{\text{mineral}}$  results to equation 2.3 produced significant discrepancies between the measured water temperature and that predicted by stable isotopic equilibrium precipitation (Table 2.4). Some of the carbonate that was acidified came from strontianite, which has a slightly different fractionation factor than calcite, and the different samples could have contained different proportions of the two carbonate phases. This could explain differences of up to 0.4 ‰ between samples (cf. O'Neil *et al.*, 1969). However, the  $\delta^{18}\text{O}_{\text{water}}$  changed little between sample locations, whereas the  $\delta^{18}\text{O}_{\text{mineral}}$  varied in excess of 0.4 ‰. Energetic degassing at the spring vent and evaporation during its flow path can cause disequilibrium precipitation from spring waters because the lighter  $^{16}\text{O}$  is lost preferentially (Criss and Taylor, 1986). The Miette spring water is hot and the turbulent flow path beneath spring 3a allows efficient evaporation and degassing. Precipitation at the Miette Hot Springs is not proceeding under stable oxygen isotopic equilibrium.

### *2.5 Interplays Between Microbes and Precipitates*

Although precipitation at the modern Miette Hot Springs is not voluminous enough to preserve the microbial communities in tufa, the microbes have important influences on the mineral precipitates.

Their most obvious role is the passive concentration of precipitates; microbial mucus nets and engulfs crystals, and the sticky sheaths of the filamentous cyanobacteria (especially *Phormidium*) trap crystallites forming in solution (Fig. 2.12). The microbial mats also act as nucleation substrates for the growth of the coarse gypsum rinds. Coarse



**Table 2.4** Stable carbon and oxygen isotope measurements for water and precipitates collected from the discharge paths of springs 3, 3a and seep 3b. Fractionation factors ( $\alpha$ ) and temperatures predicted by precipitation under stable isotopic equilibrium (T calculated), were derived from Kim and O'Neil's (1997) fractionation equation for the water-calcite precipitation system. T measured is the water temperature at the sample collection site.

	<b>Sample Description</b>	$\delta^{13}\text{C}_{\text{mineral}}$ (PDB)	$\delta^{18}\text{O}_{\text{mineral}}$ (VSMOW)	$\delta^{18}\text{O}_{\text{H}_2\text{O}}$ (VSMOW)	1000 ln $\alpha$	T (°C) calculated	T (°C) measured
1	ppt. on rock 5m from spring 3a – coarse gypsum crystal rind with accessory strontianite and calcite in gypsum crystal cavities	-5.92	10.32	-20.76	31.25	10.03	36.3
2	ppt. on rock @ orifice of spring 3 – coarse gypsum crystal rind with accessory strontianite and calcite in gypsum crystal cavities	-11.02	10.20	-20.31	30.67	12.65	50.6
3	ppt. on a microbial mat 5m from spring 3a - coarse gypsum crystal crystals with accessory strontianite and calcite in gypsum crystal cavities, and a coating of elemental sulphur	-2.26	10.37	-20.76	31.29	9.83	36.3
4	ppt.s of calcite, strontianite and microcrystalline gypsum found in a white/orange microbial mat 5m from spring 3a	2.56	7.24	-20.76	28.19	24.31	36.3
5	ppt. on rocks near the orifice of spring 3a – granular sulphur, gypsum crystallites, and minor calcite and strontianite bound in diatom mucus	-0.90	18.44	-20.84	39.34	-21.88	44.1-46.0
6	ppt. collected from mineralised filamentous microbes near the orifice of 3b – granular sulphur, crystallites of gypsum, and minor calcite	-1.04	18.29	-20.65	38.99	-20.67	41.9-40.8

crystalline gypsum crystals around and above the spring vents are surrounded and locally colonised by unicellular and filamentous microbes. The subsequent decay of these organisms may be responsible for the creation of cavities in which smaller mineral precipitates are trapped (Fig. 2.11E, F). Mucus secreted by diatoms also affects mineral precipitates; it is associated with etched minerals and probably facilitates the etching and promotes the development of cavities (Fig. 2.16).

The habit of mineral precipitates is also influenced by microbial EPS. Suspension of a nucleated calcite crystallite in gelatinous mucus allows it to grow on all sides (cf. Buczynski and Chafetz, 1991). Thus, bi- or poly-terminal crystals, larger than can be supported by growth in solution, are found in the microbial mats. In the lower, older portion of the mats, crystals are larger, and may be intergrown in star-like clusters (Fig. 2.17). This phenomenon has been described at other spring sites (Weed, 1889) and, if the calcite crystals are allowed to grow for sufficiently long periods, and are concentrated by the decay of the mat, they can accumulate and cement together forming a granular carbonate rock. The intracellular mucus of both *Oscillatoria* and *Phormidium* are known to promote suspended mineral growth (Weed, 1889).

Microbes at the Miette Hot Springs also actively influence mineral precipitation with their metabolic processes and products. The reduction of sulphate, which produces elemental sulphur, is catalysed by the respiration of SRBs. Precipitation of calcite and strontianite is initiated by the withdrawal of CO<sub>2</sub> dissolved in the spring water. This takes place mostly through degassing as the pCO<sub>2</sub> of the water equilibrates with atmospheric pCO<sub>2</sub>, but can also be facilitated photosynthetic CO<sub>2</sub> removal. For example, in the case of crystals growing in mucal mats, the withdrawal of CO<sub>2</sub> from the solutions in the mat by photosynthesis decreases the solubility of carbonate in the solution, promoting the growth of suspended crystallites (Weed, 1889).

At many springs, the relative importance of degassing and photosynthesis to carbonate mineral precipitation changes with distance from the vent (Chafetz and Folk, 1984; Fouke *et al.*, 1997). Close to the vent, efficient degassing is responsible for most CO<sub>2</sub> removal; further from the vent, rates of degassing taper off with cooling and photosynthetic CO<sub>2</sub> withdrawal comprises a larger fraction of the total CO<sub>2</sub> removed. Stable carbon isotopes are not strongly fractionated by either degassing or

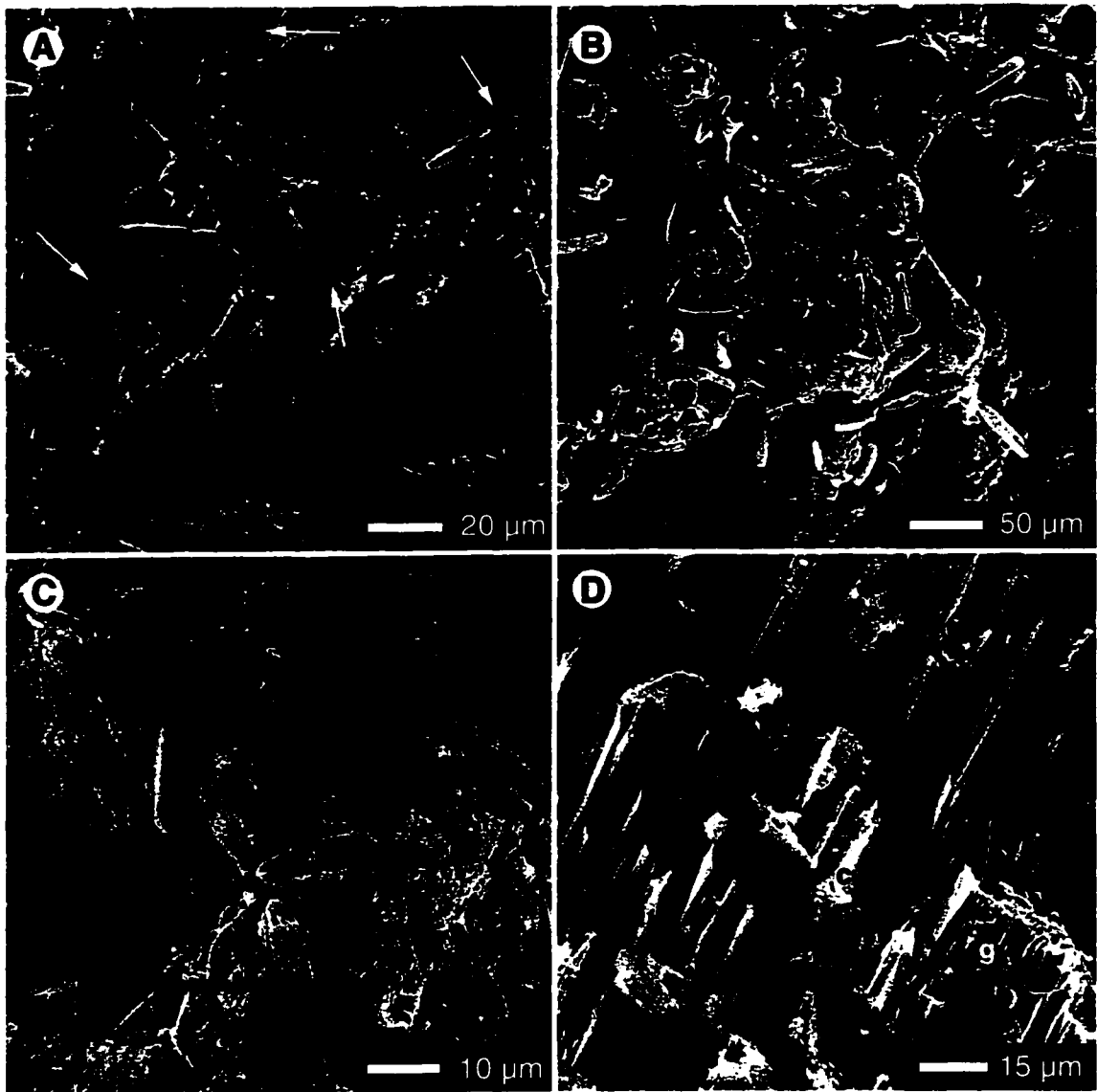


**Figure 2.16**

SEM images. (A) Corroded gypsum crystals and streamers of diatom mucus (arrows), collected from rocks beside the spring water flow path 1 m from spring vent 3a (S5). (B) A dense community of diatoms coating coarse gypsum crystals collected from S5. (C) Bleached sample of the diatom assemblage from image B showing species richness. (D) Bleached sample collected from S5 showing a corroded calcite crystal (c) held in a cavity in a composite gypsum crystal (g).

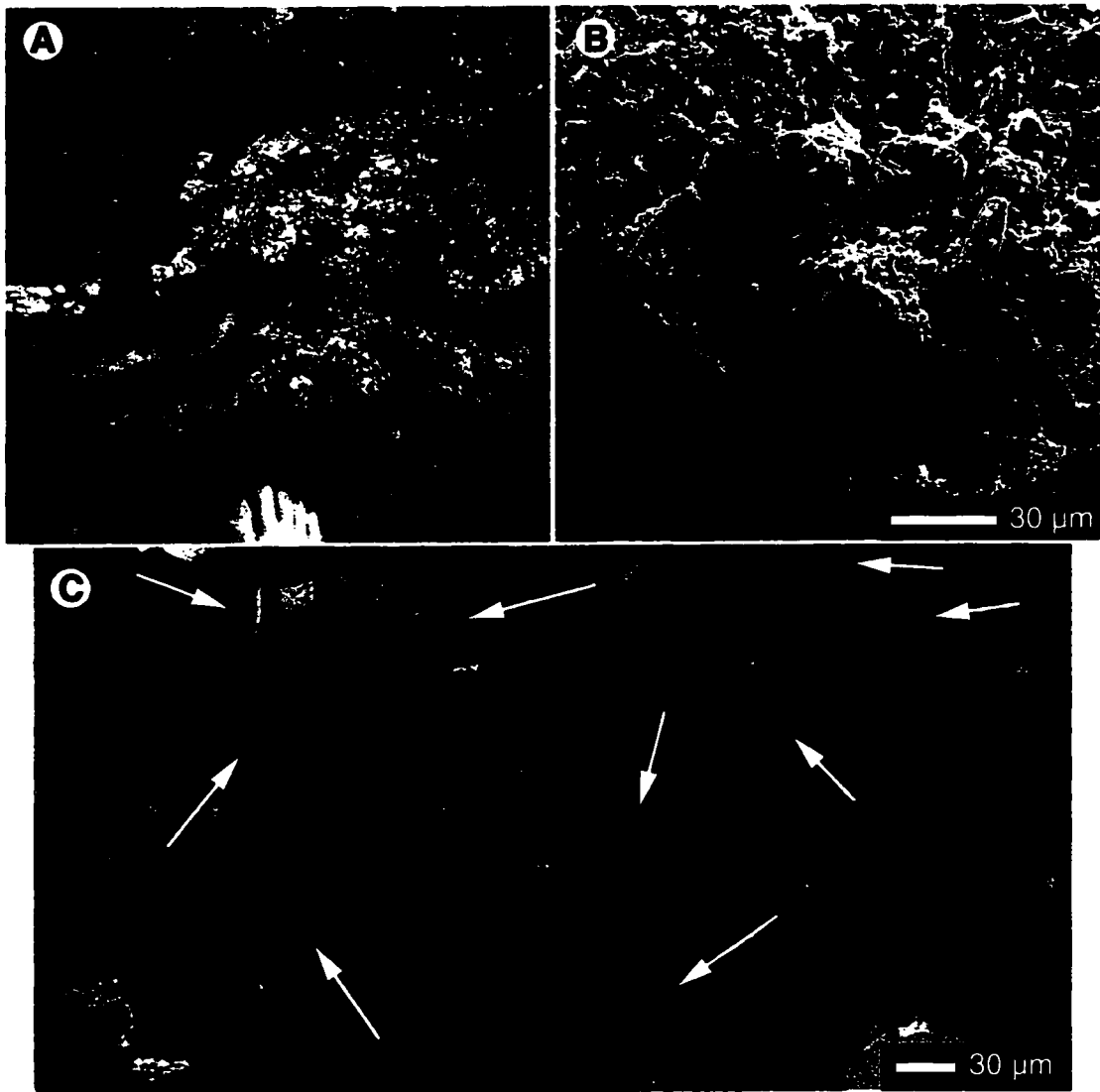


**Figure 2.17**

(A) Photograph of a microbial mat at S6 in the flow path of spring 3a (B) SEM image of the surface of a microbial mat collected from S4 composed of filaments of *Oscillatoria limnothrix*(?), mucus, and diatoms. (C) The residuals left after bleaching a portion of the mat shown in (B). Bi-terminal calcite crystals (arrows) occur singly, and intergrown as rosettes.

cooling over short distances. However, given that photosynthesisers make preferential use of  $^{12}\text{C}$ , they leave a residual pool that is enriched in  $^{13}\text{C}$ , and this may be reflected in the stable isotopic composition of the precipitate (Pentecost and Spiro, 1990). Thus, it is possible to gauge whether photosynthetic removal instigated, or promoted, carbonate mineral precipitation.

At Miette, the diversion of spring waters to the bathhouses and its dilution by the waters of Sulphur Creek confines precipitation to a maximum distance of 7 m from the spring vents. Thus, degassing is the dominant mechanism for  $\text{CO}_2$  withdrawal. The flow paths of the spring water are colonised by microbes, however, many of which are photosynthetic. The stable carbon isotopic signature of carbonate minerals collected at various sites in the discharge paths of springs 3, 3a, and 3b are statistically variable (variations exceed the standard deviation of  $\pm 0.09 \text{‰}$ ), and minerals associated with microbial substrates had enriched  $^{13}\text{C}$  signatures relative to those found attached to inorganic substrates (Table 2.4). Samples 1 and 2, collected from rocks near the orifices of springs 3 and 3a (locations S1, S4), had  $\delta^{13}\text{C}$  values of  $-11.01$  and  $-5.92 \text{‰ PDB}$ , respectively; and sample 3, collected from the top of a dried microbial mat at S6, had a  $\delta^{13}\text{C}$  of  $-2.26 \text{‰ PDB}$ . All of these samples consisted of coarsely crystalline gypsum rinds with minor carbonate minerals. Samples 4 and 5 consisted of mineral coated filamentous microbes collected in the proximal discharge paths of springs 3a and 3b (locations S4, S9). These had  $\delta^{13}\text{C}$ s of  $-0.90$  and  $-1.04 \text{‰ PDB}$ . In these samples, the carbonate minerals were trapped in mucal netting and stuck to the sheaths of the filamentous microbes. Sample 6 was a piece of a microbial mat collected from the base of the discharge path of spring 3a (S8) that contained microscopic polyterminal calcite. It had a  $\delta^{13}\text{C}$  of  $2.56 \text{‰ PDB}$ .

The filamentous and mat forming microbes are photosynthetic and could be responsible for shifting the  $\delta^{13}\text{C}$  of precipitates associated with them. Some species of purple SRBs (*Desulfobacter* and *Desulfubacterium*) also utilise  $\text{CO}_2$  as a carbon source for respiration (Pfenning, 1989) and are cited as taxa responsible for developing local conditions favourable to carbonate mineral precipitation (Chafetz and Folk, 1984). Thus, the SRBs may also have contributed to the  $\delta^{13}\text{C}$  shift. It is not possible to quantify the magnitude of the shift because the  $\delta^{13}\text{C}_{\text{water}}$  is unknown, and because depletion of  $^{12}\text{C}$  by

evaporation may also be occurring between the collection sites.  $\delta^{13}\text{C}_{\text{water}}$  is less sensitive to evaporation and degassing than  $\delta^{18}\text{O}_{\text{water}}$ , however, and the magnitude of the shift in samples 4-6 (greater than 2-3 ‰) indicates that photosynthesis really is promoting the growth of the precipitates (cf. Chafetz *et al.*, 1991b). The effect of photosynthesis on  $\delta^{13}\text{C}_{\text{mineral}}$  is greater in closed environmental settings where non-photosynthetic diffusion of  $\text{CO}_2$  to the atmosphere is limited. The gelatinous mucus of microbial mats can impede diffusion of gasses, allowing the development of an enriched  $^{13}\text{C}$  pool in the mat microenvironment (Pentecost and Spiro, 1990; Chafetz *et al.*, 1991b). Although the filamentous microbes are photosynthesising, precipitates growing attached to their sheaths or in the mucal nets between them will be exposed to  $\text{CO}_2$  in the spring water and air. Thus, one would expect the relative shift of the  $\delta^{13}\text{C}_{\text{mineral}}$  to be greater for minerals grown in a mat than those grown in association with the filamentous microbes, and that is exactly what is observed.

## 2.5 Summary

The modern Miette Hot Springs system displays a complex interplay of biological and chemical influences. The chemistry of the spring water results from dissolution of shale and fossiliferous carbonate units in the Mississippian Rundle Group Carbonates. It is possible that the water moves between these two units, the shale unit acting as a cap for a confined aquifer system.

The heated, mineral rich water supports the growth of cyanobacteria that are atypical of the regional environment (Gadd, 1999; Lepitzki and Lepitzki, 2001). The cyanobacteria, SRBs, and algae found in the Miette spring waters are successful and known to colonise other hot spring sites (Weed, 1889; Brues, 1927; Lepitzki and Lepitzki, 2001). The spring waters also support a diatom assemblage that is so successful that it out competes cyanobacterial communities for part of the spring water flow path. Villeneuve and Pienitz (1998) examined the diatom flora of four thermal springs in Canada, Japan and Iceland, and found that the assemblage at each site was dominated by one or two species. The Miette springs host at least eight diatom species with robust populations and should be considered a unique habitat.

Mineral precipitation is driven by inorganic degassing and cooling but is promoted by the respiration of SRBs and photosynthetic cyanobacteria and diatoms. The intercellular mucilage of the cyanobacteria promotes crystal growth by acting as a nucleation substrate and by permitting suspended crystal growth. Diatom EPS, on the other hand, may be corrosive to the precipitates.

The opportunity for precipitation at the modern springs is restricted by the fact that the waters from the three largest springs are piped off to the bathhouses, and the water from the fourth largest spring (3a) is diluted by Sulphur Creek before cooling significantly. The substantial fossil tufa deposits adjacent to the modern springs indicate that the opportunity for precipitation was much higher in the fossil spring system.

### 3 The Fossil Miette Tufa Deposits

#### 3.1 General Description

The fossil spring precipitates at Miette are composed of calcite (uniformly stained by Alzarin Red dye), most have high porosity, and many contain branch and stem casts and microbial fabrics. Although there are some dense rocks in the fossil deposit, their low porosity is attributable to the presence of void filling cements, rather than to the original structure of the rock. Thus, the rocks meet Ford and Pedley (1996) and Woodsworth's (1997) definition of tufa.

The fossil tufa precipitated from water ejected from a line of perched springs located ~30 m above the floor of Sulphur Creek on the west side of Sulphur Creek Valley. Tufa forms a continuous ledge (accessible by a horse path) at the elevation of the former springs, and appears as boulders and *in situ* outcrops down slope (Fig. 2.1). The slope above and below the ledge is unstable and warped tree trunks, fallen boulders and cobbles, landslide scars, and a boulder of tufa thrown onto the east side of the valley evidence a history of and rockfalls. Indeed, this is the reason that the bathing facilities were relocated in the 1980's. Support structures at the old Aquacourt were compromised as their foundations shifted, and rockfalls made the valley hazardous for bathers (van Everdingen, 1972).

The highest elevation tufa is found at the south end of the exposure (Miette South - MS) on an open slope with little tree cover (Fig. 3.1A). The tufa is well exposed in two caves that mark the location of former spring vent pools (FSVPs) (Fig. 3.1B, C). The FSVPs are found in flat areas (with respect to the surrounding slope) and are encircled by raised tufa mounds. The mounds are transitional with the southernmost end of the upper tufa ledge, and, beneath this, large blocks of *in situ* tufa are skirted by boulders and underlain by a poorly sorted conglomerate.

The upper ledge of tufa is continuous north of MS, first increasing and then decreasing in thickness. Several raised depressions that mark the location of filled FSVPs are found slightly above and behind the ledge. Beneath the ledge, *in situ* and displaced boulders are found amongst dense vegetation (Fig. 3.2A). In the middle of the outcrop (Miette Central - MC) the slope steepens and recent landslide scars punctuate



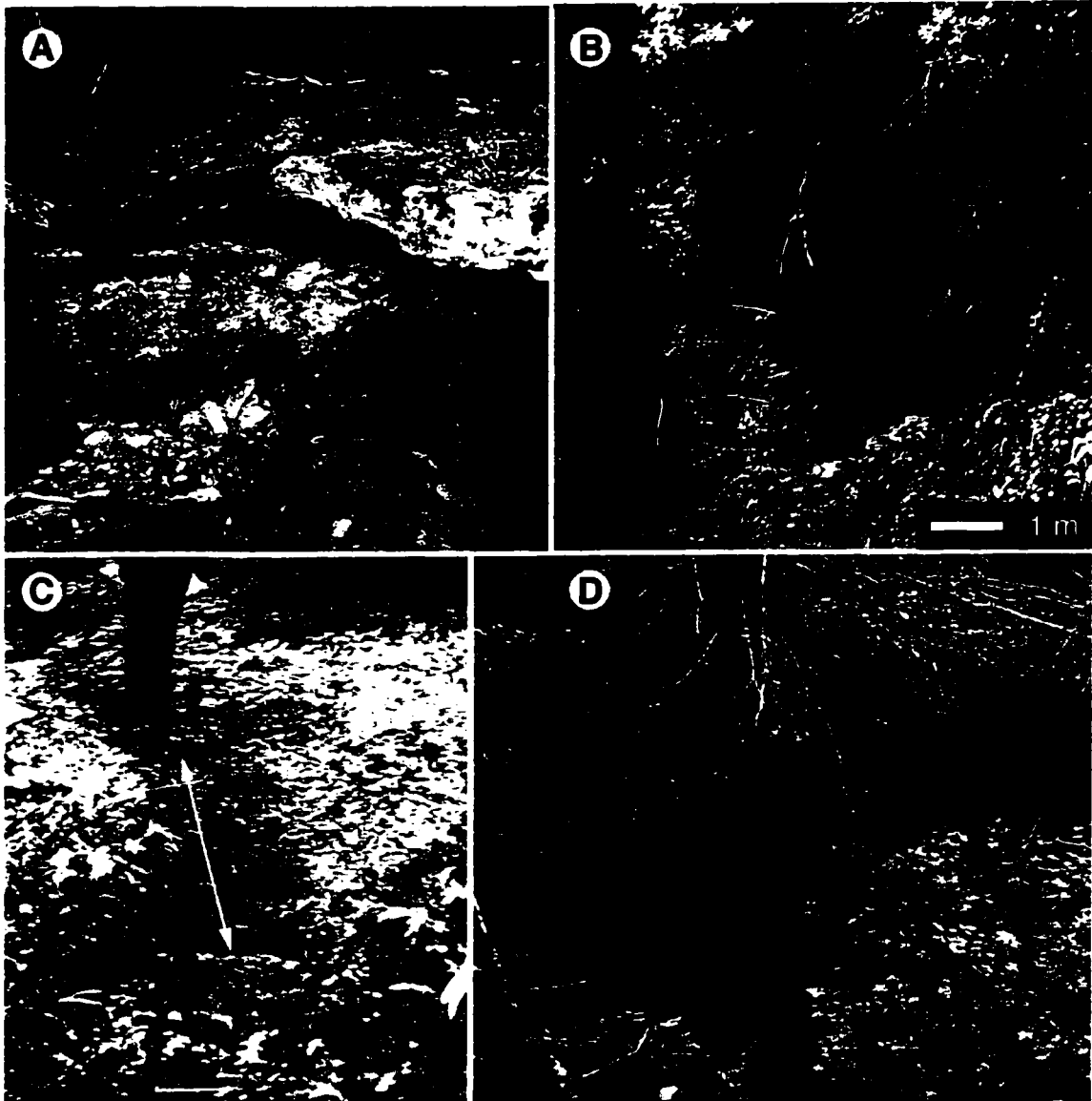


**Figure 3.1**

(A) The southernmost edge of the upper tufa ledge (at MS4). (B) The upper tufa ledge thickens northwards and here, near MC1, intercalated layers of tufa and conglomerate are up to 5 m thick. (C) A raised depression bordered by sloping tufa marks the location of a former spring vent pool (FSVP) along the upper horse path - the arrow spans the width of the central depression, i.e. former pool. (D) At MS1 a former spring vent pool remains as a shallow cave. The tree above the cave has a base diameter of 75 cm.



**Figure 3.2**

(A) General view of the hillslope in the central part of the fossil Miette tufa exposure. Displaced boulders and *in situ* tufa form an unsteady substrate for forest vegetation. (B) The banks of Sulfur Creek are bordered by blocks of tufa that have fallen from the hillslope above. This boulder is approximately 2.5 m high.

vegetation (Fig. 3.2B, C). Several tufa blocks are restrained by metal cables in an attempt to increase slope stability.

The northernmost tufa (Miette North – MN and Miette Far North - MNN) is found on a steep slope behind the old Aquacourt foundations. The tufa forms a steep *in situ* deposit that is the only exposure in which the upper ledge and lower elevation deposits are still continuous (Fig. 3.2D).

### 3.2 Tufa Morphotypes

The fossil tufa displays considerable morphological variation arising from deposition on divergent topography (Pedley, 1990). Although a common terminology for spring deposit morphotypes has not been established, similar morphotypes are found at other modern and fossil spring sites (i.e. Chafetz and Folk, 1984; Pedley, 1990; Guo and Riding, 1998). The morphotypes observed at Miette are descriptively named; they are called domal tufa, roll-over tufa, vertical tufa, flat banded tufa, wedge-shaped tufa, and mossy bed tufa.

The *domal tufa* morphotype is found in FSVPs and where spring water issued from pre-deposited tufa (Fig. 3.3A, B). It is defined by the presence of concave laminae and unique erosional features. Accumulating tufa may form a raised mound around the spring vent in which laminae are curved and conform to the shape of the spring mound (Chafetz and Folk, 1984; Pedley, 1990). As the spring mound grows, older basal tufa may be dissolved by rising steam, contact with sitting water, or currents within an active vent pool. These processes produce distinctively rounded erosional features that cross cut depositional laminae. If a spring vent migrates away from the spring mound, similar features may be evident in tufa that overhangs the new spring vent (i.e. Fall Creek Springs, Alberta, personal observation).

The *roll-over* morphotype describes tufa with downwards curving depositional laminae (Fig. 3.3C, D). It is generated where carbonate rich waters flow over sharp lips or structural barricades and rapid degassing prompts mineral precipitation (cf. Pedley, 1990). Log casts are common in roll-over tufa at Miette but, due to the rapid rate of precipitation, these disturb laminae for relatively short vertical distances. Laminae thin

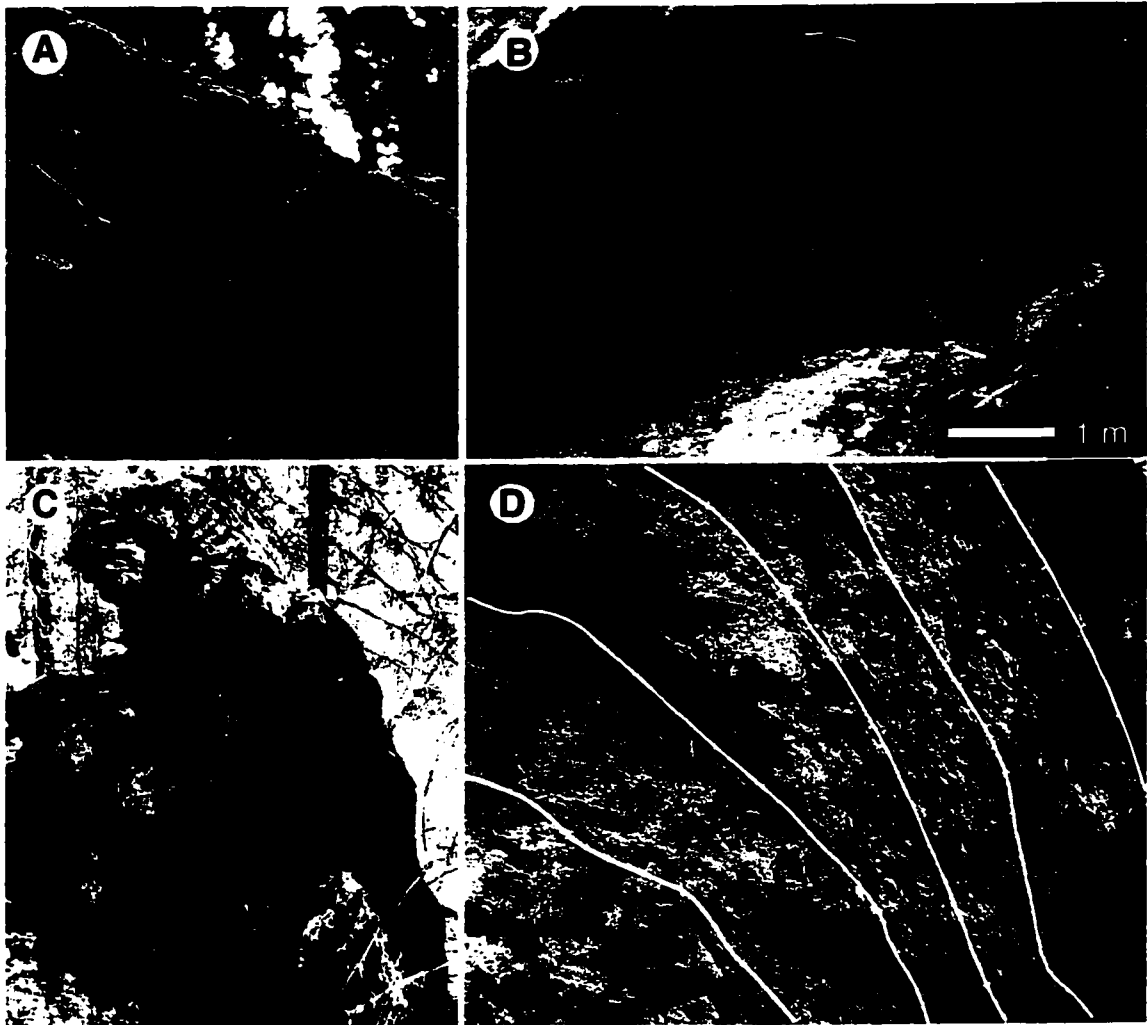


**Figure 3.3**

(A,B) Domal tufa morphologies at MNN and MN3. Tufa forms domes with erosional concavities that cross-cut original laminations in the tufa (arrows in B). (C) Roll over structure at MN4. (D) Closer view of the roll-over morphology at MC1 - texturally distinct packages (outlined by white lines) narrow moving towards the break in slope. A quarter (2.4 cm diameter) is shown for scale. The rock hammer in images A and C is 25 cm long.

towards the roll-over structure, and are usually transitional with laminae in vertical tufa.

*Vertical tufa*, is composed of very thin laminae that form vertical sheets (Fig. 3.4A). It is generated by precipitation from falling or steeply inclined flowing waters. Where the slope of the sheets exceeds 90°, the laminae become convoluted and form folded draperies (Fig. 3.4B) that are similar to the cascade draperies described by Chafetz and Folk (1984) and Pedley (1990).

The *flat banded tufa* morphotype describes outcrops in which vertical successions of tufa contain laminae or texturally distinct units that maintain relatively constant thickness down slope (Fig. 3.4C, D). This morphotype is generated by precipitation along a gentle slope, beneath moving or shallowly ponded water (cf. Walter, 1976; Guo and Riding, 1998; Jones *et al.*, 1998; Chafetz and Guirdy, 1999).

*Wedge-shaped tufa* contains texturally distinct laminar units that change thickness down slope (Fig. 3.5A, B). Generally, lower laminae show the greatest change in thickness, expanding rapidly down slope, whereas upper units may show very little change in thickness. The component textural facies of wedge-shaped tufa are akin to those in flat-laminar tufa, and the two morphotypes are laterally and vertically conformable. Wedge-shaped tufa is thought to form where there is a break in slope that is not steep enough to generate the vertical tufa facies. Such breaks might be found where rotational slumping has taken place, where rockfalls have altered topography, or where spring water has collected in shallow pools beneath overhanging rock. Deposition beneath the slope break gradually reduces slope angle until upper units conform to the flat banded morphotype.

*Mossy bed tufa* is fan shaped in plan view, has a bumpy surface texture, indistinct or irregular depositional laminae, and is dominantly composed of calcified mosses. This morphotype, generated by the calcification of hummocky moss beds (cf. Pedley, 1990; Janssens, 1990), is only found at the far north end of the Miette fossil tufa exposures (Fig. 3.5C, D). Elsewhere, small bryophyte hummocks (hemispherical colonies several feet wide) are found in flat banded and wedge-shaped tufa morphotypes.

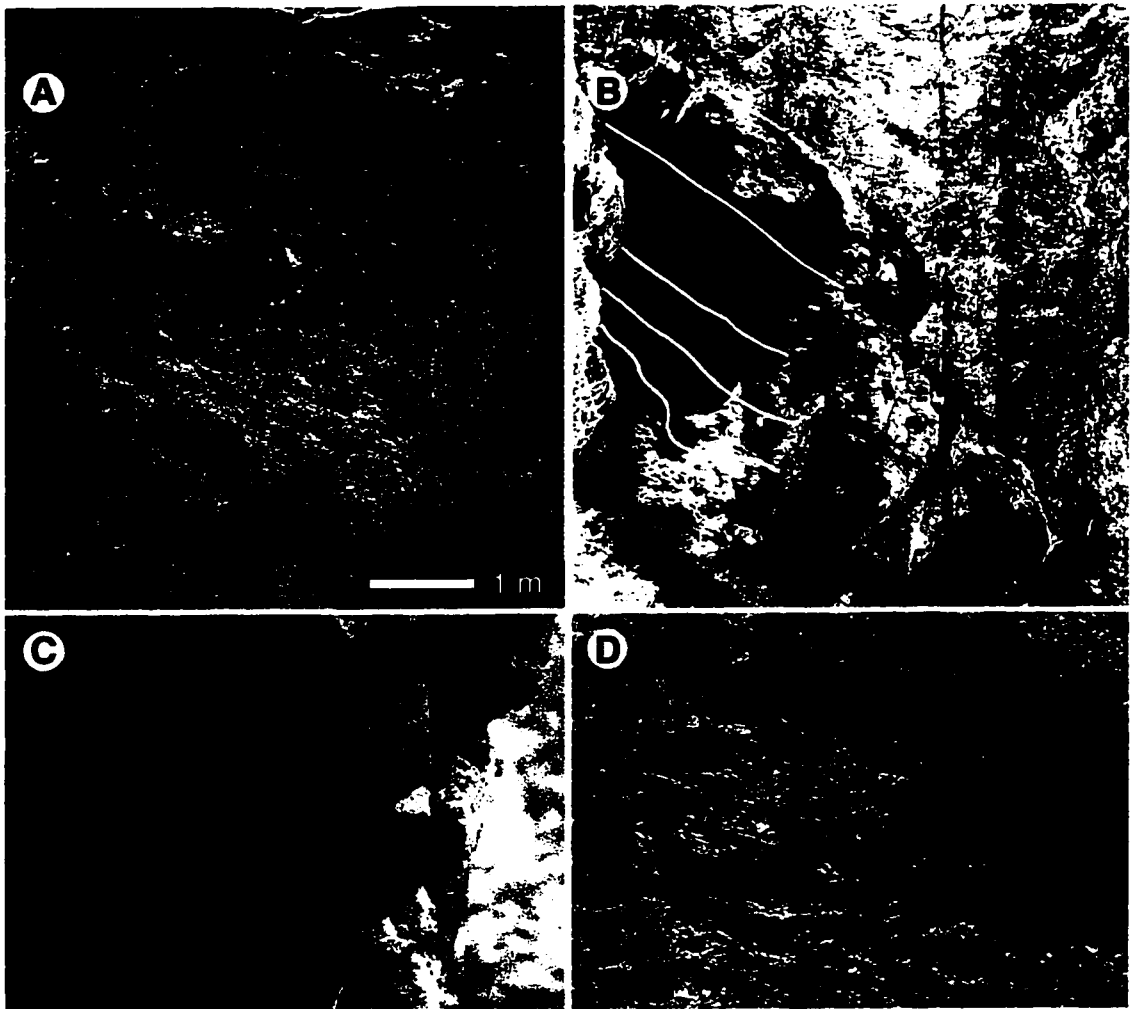


**Figure 3.4**

(A,C) Photographs of vertical tufa consisting of inclined sheets at MN1 (A) that form convoluted draperies at MC1 when inclined beyond vertical (C) (a pencil is shown for scale). (B) Flat banded tufa at MN4. White lines delineate texturally homogeneous packages that maintain regular thickness down-dip (with the exception of the lowest layer that overlies an irregular conglomerate layer). Image D shows a texturally homogeneous package with internal laminae (a pen is shown for scale).

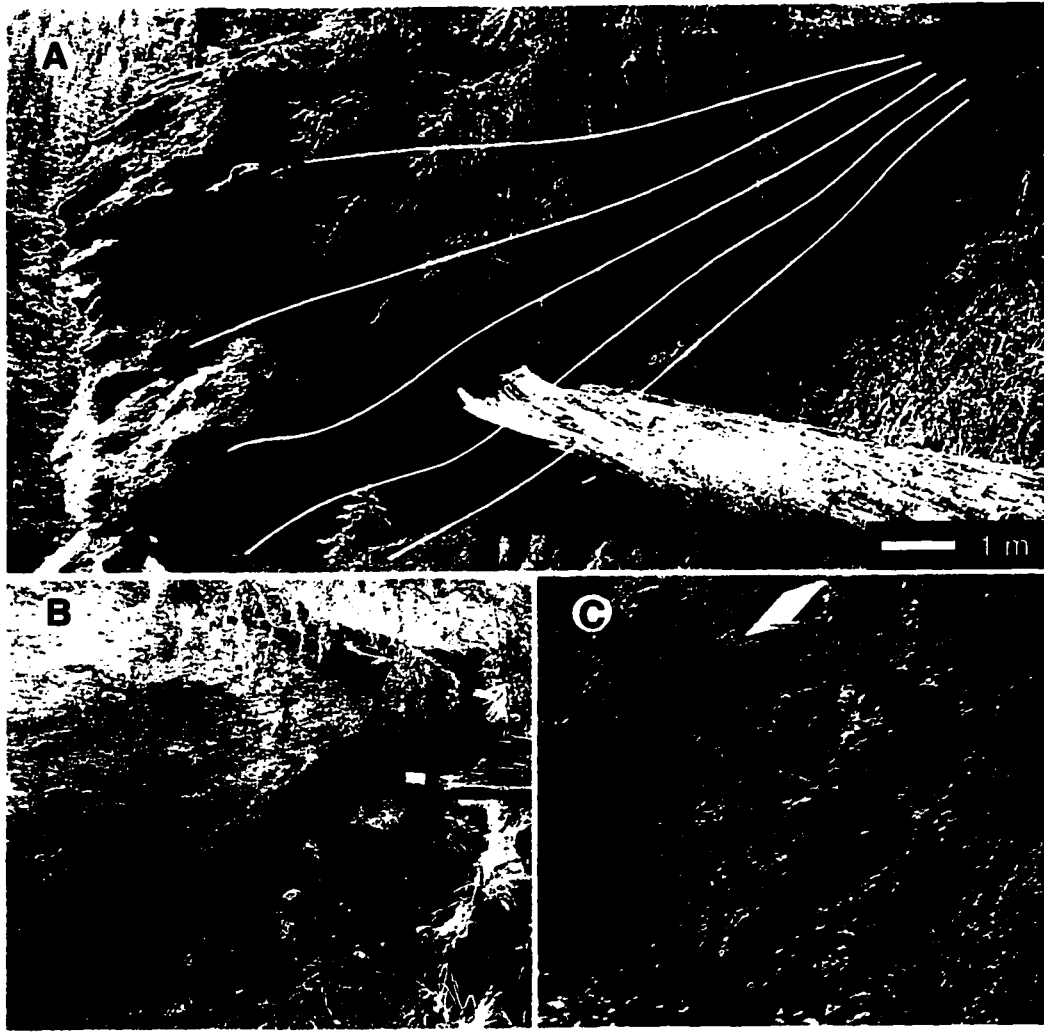


**Figure 3.5**

(A) Wedge-shaped tufa at MS4. Texturally distinct units (marked by white lines) increase in thickness downdip. Lower units expand more than upper units. (B) Upslope end of the wedge-shaped tufa block shown in image A. (C) Irregular surface of mossy bed tufa at MNN. The field notebook shown for scale in images B and C is 10 cm wide.

### *3.3 Tufa facies*

Differences in the type of vegetation, the water temperature, the water flow rate, and the input of clastic or organic debris between depositional niches in the spring water flow path produced numerous textural facies in the fossil Miette tufa. These facies are distinguishable in the field, and their descriptions have been further refined by thin section and SEM analysis. Much of the fossil tufa formed in the presence of filamentous microbes. These were preserved through encrustation or impregnation of their sheaths and are found as cylindrical molds and body fossils. Unfortunately, coatings of calcite have obscured many surface features of the filaments, and it is impossible to determine their length because they are rarely found in long section. Though the internal and external filament diameter, the presence or absence of a sheath, and the overall morphology of the microbes are evident in some specimens, insufficient information exists to allow confident taxonomic assignment. Species names are suggested based on filament diameter and the presence or absence of a preserved sheath. A number of siliceous and calcareous microfossils are also found in the fossil tufa – their distributions are discussed in Chapter 5, and they are mentioned in the following facies descriptions only if they are especially characteristic of a facies.

#### *3.3a Tufa/Allochthonous Lithoclast Conglomerate Facies*

Poorly sorted, sub- to well-rounded lithoclasts are welded together with calcite cement (20-40%) forming thick beds of conglomerate that grade upwards into tufaceous deposits. The lithoclasts include sandstone, limestone, ferromagnesian rocks, and quartz grains. This basal facies commonly underlies thick accumulations of tufa, but is also found as pockets and lenses in tufaceous strata (Fig. 3.6A), where it contains both allochthonous lithoclasts and angular tufa clasts. In thin section, multiple generations of isopachous calcite cement line void spaces, attesting to high porosity in the original conglomerate, which permitted fluid flow (3.6B, C). Microbial structures are found between lithoclasts near the top of conglomerate layers, signaling the transition to overlying tufa facies (Fig. 3.6D). Shards of mineralized wood (at MC2 and MNN2) and animal bones (at MN4) were locally incorporated into the conglomerate.



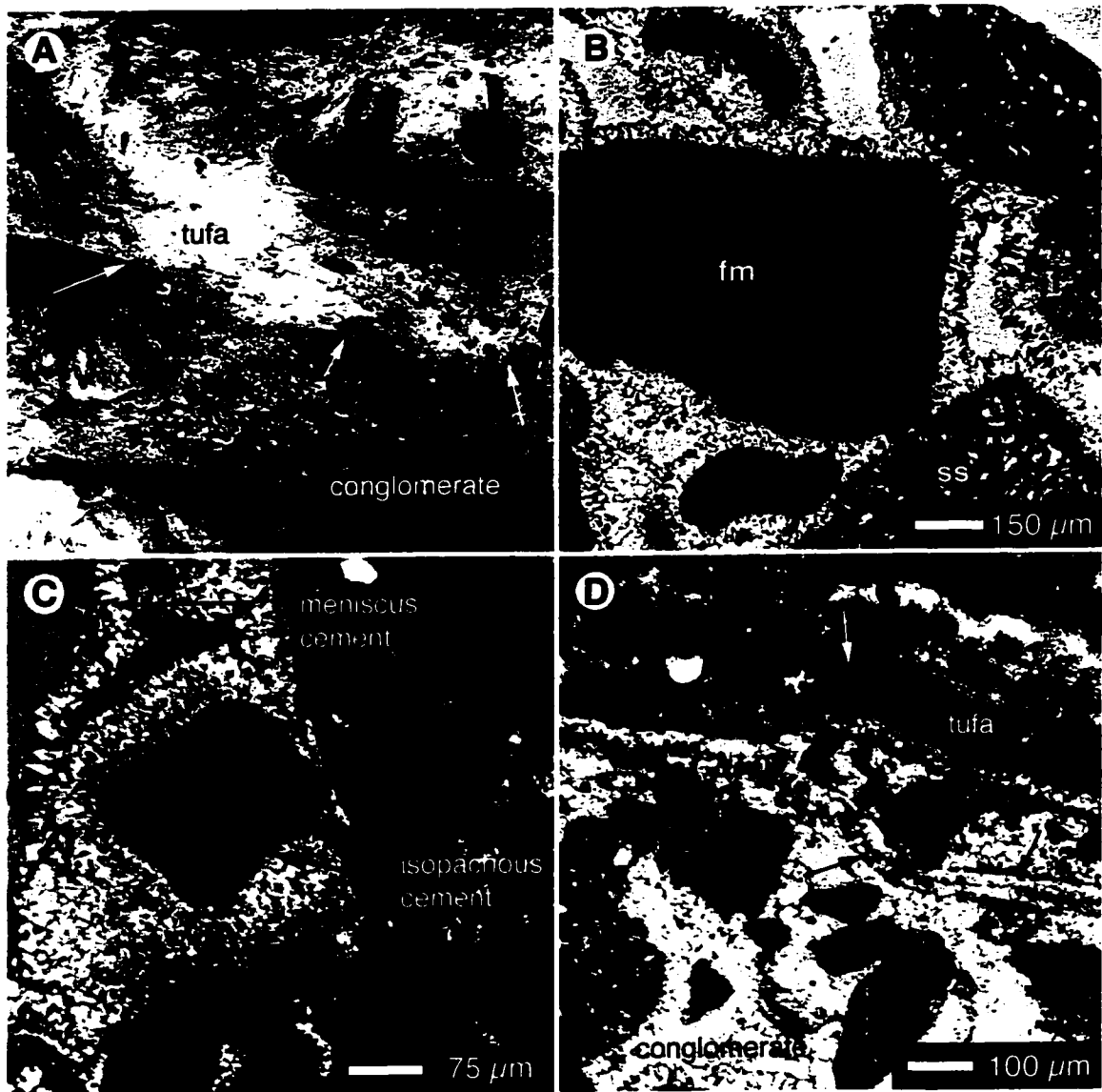


**Figure 3.6**

(A) The tufa/allochthonous lithoclast conglomerate facies at MN1. Note the poor sorting - clasts range from boulder to sand sized. The conglomerate is basal to massive tufa and the transition between facies (indicated by arrows) is sharp. The rock hammer is 25 cm long. (B) Thin section of sample M30 collected from MC1 showing angular to subrounded clasts with variable mineralogy (ss=sand stone, qtz=quartz, f=feldspar, fm=ferromagnesian mineral) cemented by isopachous sparry calcite. (C) Thin section of handsample M33 collected from MC1 showing multiple generations of cement. Note that earlier cements are isopachous while meniscus cements developed at a later stage. (D) Thin section of handsample M26 collected near MS6 showing the transition from conglomerate to dense laminar tufa with filamentous microbial structures defined by rims of micrite (arrows).

### *Interpretation*

Percolation of carbonate precipitating spring water through landslide and rockfall debris generated this facies. The component lithoclasts of the conglomerate were derived from rockfalls on the unstable slope. The lithoclasts are mineralogically similar to a large till exposure further down the Fiddle Creek Valley, and their poor sorting and variable lithology support a till derived origin. Air photos also show a slope break roughly 40 m upslope from the horse path that may represent the upper extent of a moraine or glacial terrace that underlies the tufa and forest vegetation. The angular tufa lithoclasts were generated from fragmentation of pre-existing tufa during rockfalls.

#### *3.3b Stromatolitic Tufa Facies*

Much of the fossil Miette tufa formed by precipitation on and about filamentous microbial communities and it contains textures controlled by the growth of the component microbes. This tufa contains laminations defined by colour and/or density contrasts in which preserved microbial structures alternate between horizontal and vertical orientations in successive laminae. As rocks with “organized structure that accreted as a result of a benthic community... forming the locus of mineral precipitation” that have “fine, approximately planar internal laminations” these rocks meet the definition of stromatolites (Jones *et al.*, 1998). There are three distinct stromatolitic facies in the fossil Miette tufa: streamer facies, porous laminar facies, and dense laminar facies. Though distinct, these facies are transitional, and represent end members of a textural continuum.

#### *3.3bi Streamer Facies*

This facies is comprised of thin wavy laminae that are 2 (common) to 8 (rare) mm thick) separated by dense laminae <1.5 mm thick. The laminae contain inclined or prostrate filament structures, and have “streamer” textures (elongate filamentous patterns oriented parallel to the bedding) on their upper surfaces (Fig.3.7A). The streamer facies forms a capping layer on many tufa blocks in the south and central fossil tufa exposure. The thin, dense laminae contain aggregates of bi-terminal calcite crystals (~15 µm long and 5 µm wide) that have micritised cores (Fig. 3.7B). The thicker

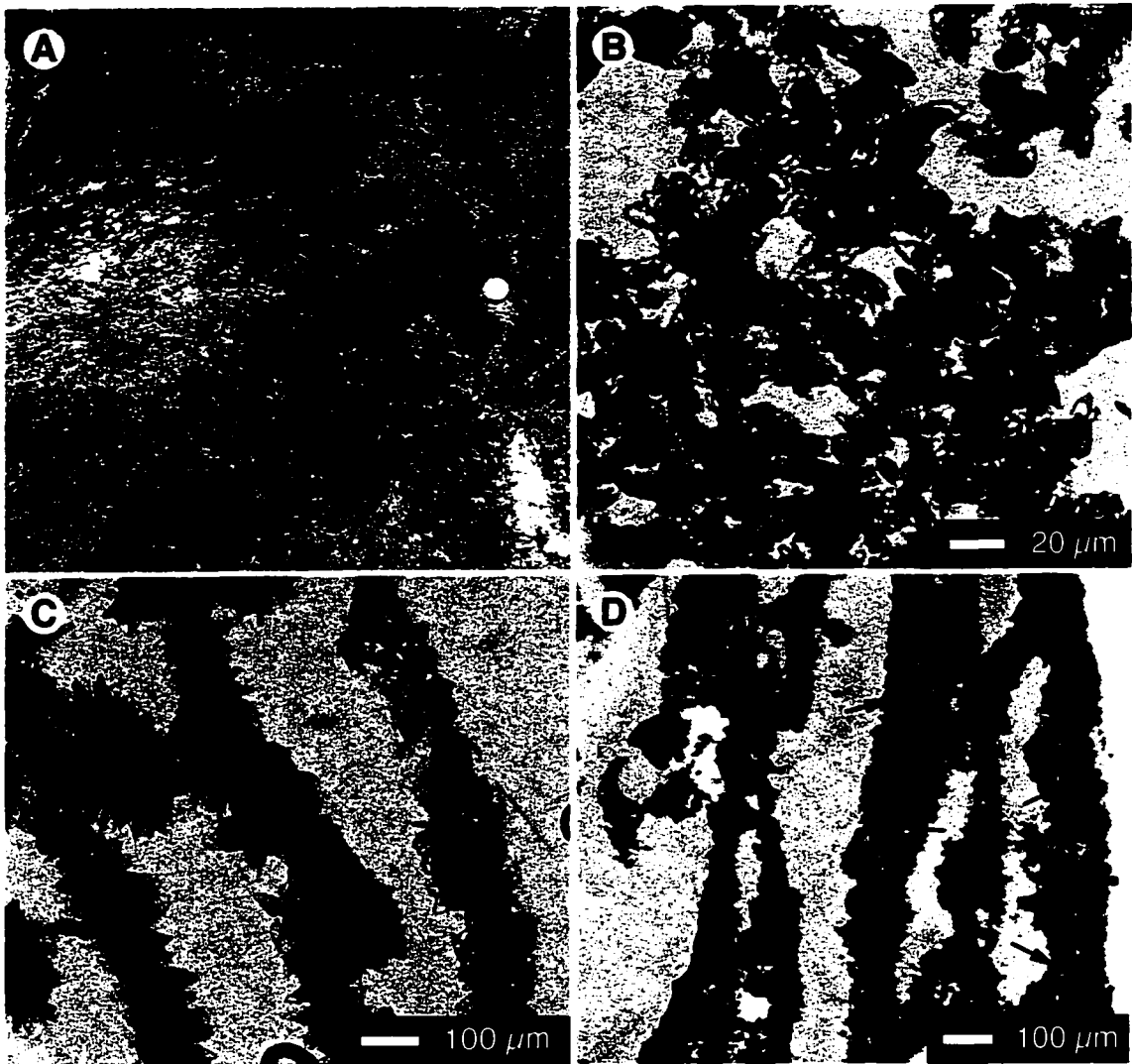


**Figure 3.7**

(A) Photograph of streamer textures exposed at MS6 with a quarter (2.4 cm diameter) for scale. (B) Thin section of bi-terminal crystals in a pocket in streamer facies handsample M42 from MC1. (C) Thin section cut vertically through sample M42 showing inclined spar coated columns. (D) Thin section cut horizontally through sample M42 showing current aligned filamentous structures coated in spar. The external diameter of the filaments or filament bundles is defined by a dark micrite rim (arrows).

laminae are composed of spar encrusted filament structures 30 to 200  $\mu\text{m}$  in diameter (Fig. 3.7C). Filament structures consist of sinuous bands of finely crystalline calcite that are outlined by micrite rims 10 to 25  $\mu\text{m}$  thick (Fig. 3.7D). In some instances, the finely crystalline calcite encloses layers of micrite, indicating that the filament structures formed around multiple microbial filaments; hence, the diameter of the component microbial filaments cannot be resolved.

### *Interpretation*

This facies is similar to “streamermats” in palaeosinters from Queensland (Walter *et al.*, 1996), “streamers” in sinters from Ohaaki Pool, New Zealand (Jones *et al.*, 1998; Fig. 2A, 2B - Jones *et al.*, 2001) and to actively precipitating siliceous and calcareous mats in Yellowstone National Park (Walter *et al.*, 1996). It is formed by mineral encrustation of flow-oriented filamentous microbes growing beneath thermal waters (<73°C) with strong, unidirectional currents (cf. Guo and Riding, 1998). The encrusted microbe could not be identified in the streamer facies because smaller diameter filaments formed streamer bundles in which the diameter of individual filaments could not be determined. Cyanobacteria known to form “streamer” textures, however, include *Calothrix* (a sheathed, tapering, non-branching filament up to 35  $\mu\text{m}$  diameter), *Oscillatoria* (a non-sheathed, non-tapering, non-branching filament with diameters ranging from 1.5  $\mu\text{m}$  to 40  $\mu\text{m}$ ) and *Phormidium* (a sheathed, non-tapering, non-branching filament with diameters ranging from 0.2 to ~5.3  $\mu\text{m}$ ) (Weed, 1889; Walter, 1976; Canter-Lund and Lund, 1995; Walter *et al.*, 1996; Jones *et al.*, 1998).

The bi-terminal crystals probably grew in mucus rich portions of the filamentous microbe communities. Their size (up to 15  $\mu\text{m}$  long) precludes their growth in suspension, and intergrowth features indicate rapid growth with space limitations. They are nearly identical to smaller bi- and poly-terminal crystals isolated from microbial mats at the modern Miette hot springs, and to similar-sized bi-terminal crystals precipitated within a gelatinous secretion of bacteria and algae from the Bahamas (Fig.3H - Buczynski and Chafetz, 1991). Higher ion delivery rates, and a longer growth period, may have allowed bi-terminal crystals in the streamer facies to exceed the size of the bi-terminal crystals forming in the modern springs.

### *3.3bii Porous Laminar Facies (PLF)*

The porous laminar facies (PLF) is found in flat banded and wedge-shaped tufa, and is most abundant midway down slope at MS and MN. It is a porous stratiform stromatolite consisting of intercalated thick (0.5-2.5 cm) porous laminae and thin (maximum 0.7 cm) dense laminae. The porous laminae have millimetric features oriented perpendicular to the laminae, and are generally lighter in colour than the dense laminae. Laminae are swaly and rarely constant in thickness for more than several centimeters (Fig. 3.8A).

There are four morphological textures in the two types of laminae. The first, restricted to the thick porous laminae, is composed of widely spaced vertical columns that are up to 200  $\mu\text{m}$  in diameter and curve, or locally branch, but maintain a vertical to subvertical orientation (Fig. 3.8B, C). They are encrusted by radiating trigonal sparry calcite (Fig. 3.9B) with internal laminations and/or hollow or micritised cores (Fig. 3.8F). The centers of the columns are composed of solid (Fig. 3.8D) or corroded calcite (Fig. 3.8E, F) and many host calcified microbial filaments or filament casts (Fig. 3.9A). Generally, the degree of crystal corrosion increases, and filament casts are found, towards the center of the columns. A 10  $\mu\text{m}$  diameter filamentous microbe is preserved as cylindrical casts, and the external sheaths ( $\sim 0.2$   $\mu\text{m}$  thick) and (rarely) internal sheaths of a  $\sim 1.5$   $\mu\text{m}$  diameter filamentous microbe are preserved within cylindrical casts (Fig. 3.9B, F).

The second texture, restricted to thin dense laminae, is composed of closely spaced and heavily mineralized flat-lying structures that are alike in all but orientation to the vertical columns (Fig. 3.10A). Indeed, individual columns change orientation as they pass from the porous to the dense lamina (Fig. 3.10B), so the same microbial community probably produced the two laminar types.

Composite bi-terminal crystals comprise the third texture, forming dense lenses or laminae. The crystals are uniform in size and shape (20-30  $\mu\text{m}$  wide, 75-90  $\mu\text{m}$  long), show complex intergrowths, and are not associated with a growth substrate (Fig. 3.10C-E). Although these crystals appear pristine in SEM when intact, they commonly have hollow or micritised cores, or contain concentric void spaces (Fig. 3.10E, F).

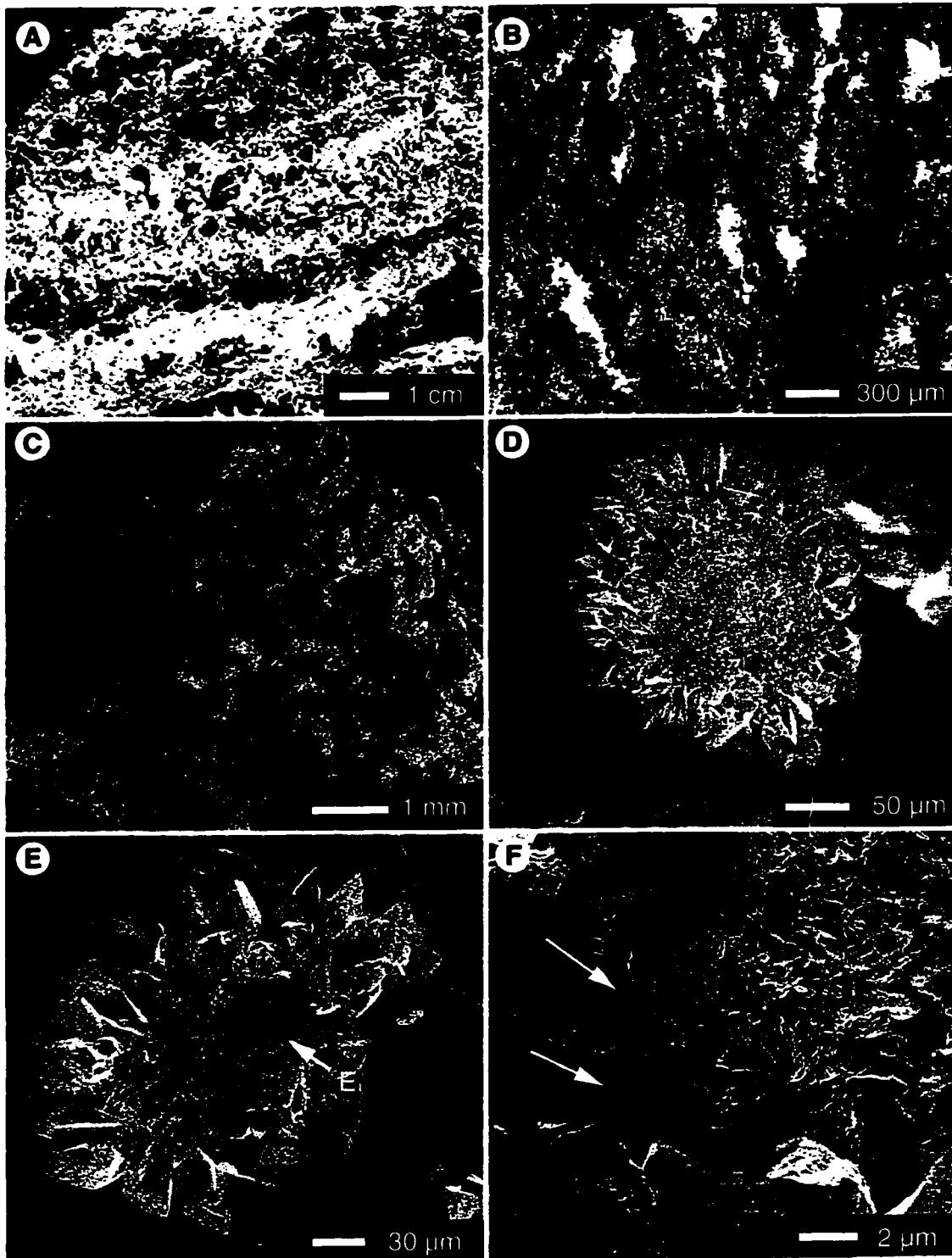


**Figure 3.8**

(A) Photograph of PLF sample M22 collected from MS6. (B) Thin section of a porous lamina in sample MS9 showing upright filament structures. (C-F) SEM images of PLF sample M18 from MS5 showing upright filament structures. (D) Cross section through an upright column with a solid calcite core surrounded sparry calcite. (E) Cross section through an upright column with a corroded calcite core surrounded by sparry calcite. (F) Detail of E showing corroded calcite crystals and remnants of crystal junction planes at a triple junction (arrows).

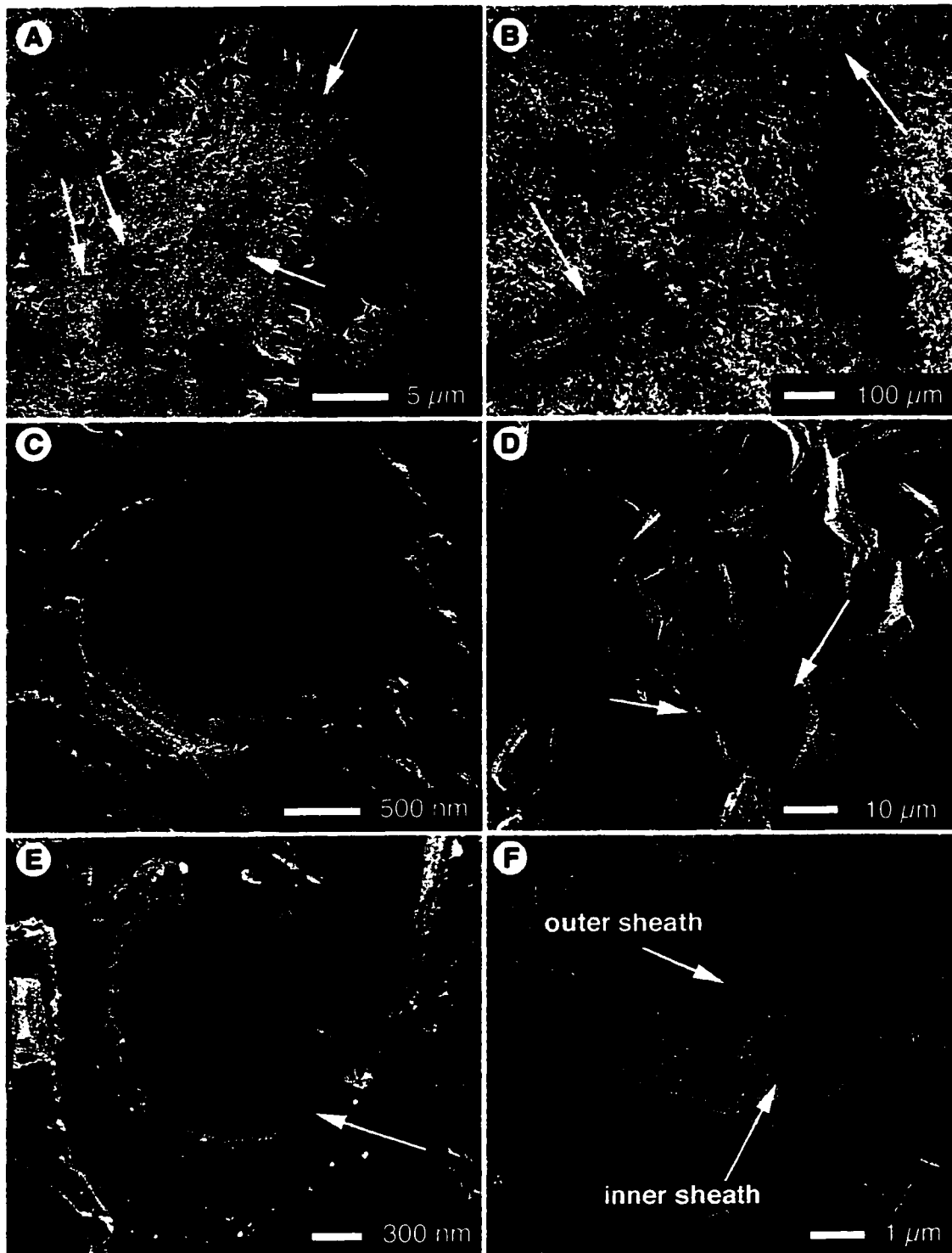


**Figure 3.9**

(A) Cross section through a vertical column from a porous lamina in PLF sample M53 collected from MN2 showing filament casts (arrows). (B) Detail of A showing plant root material and a long filament cast (arrows). (C-F) Different modes of filament preservation in sample M53: (C) a small diameter filament cast through a solid calcite crystal; (D) a larger diameter filament cast bordered by blocky calcite; (E) a small diameter filament preserved through impregnation of its sheath; (F) a small diameter filament with preserved inner and outer sheaths.

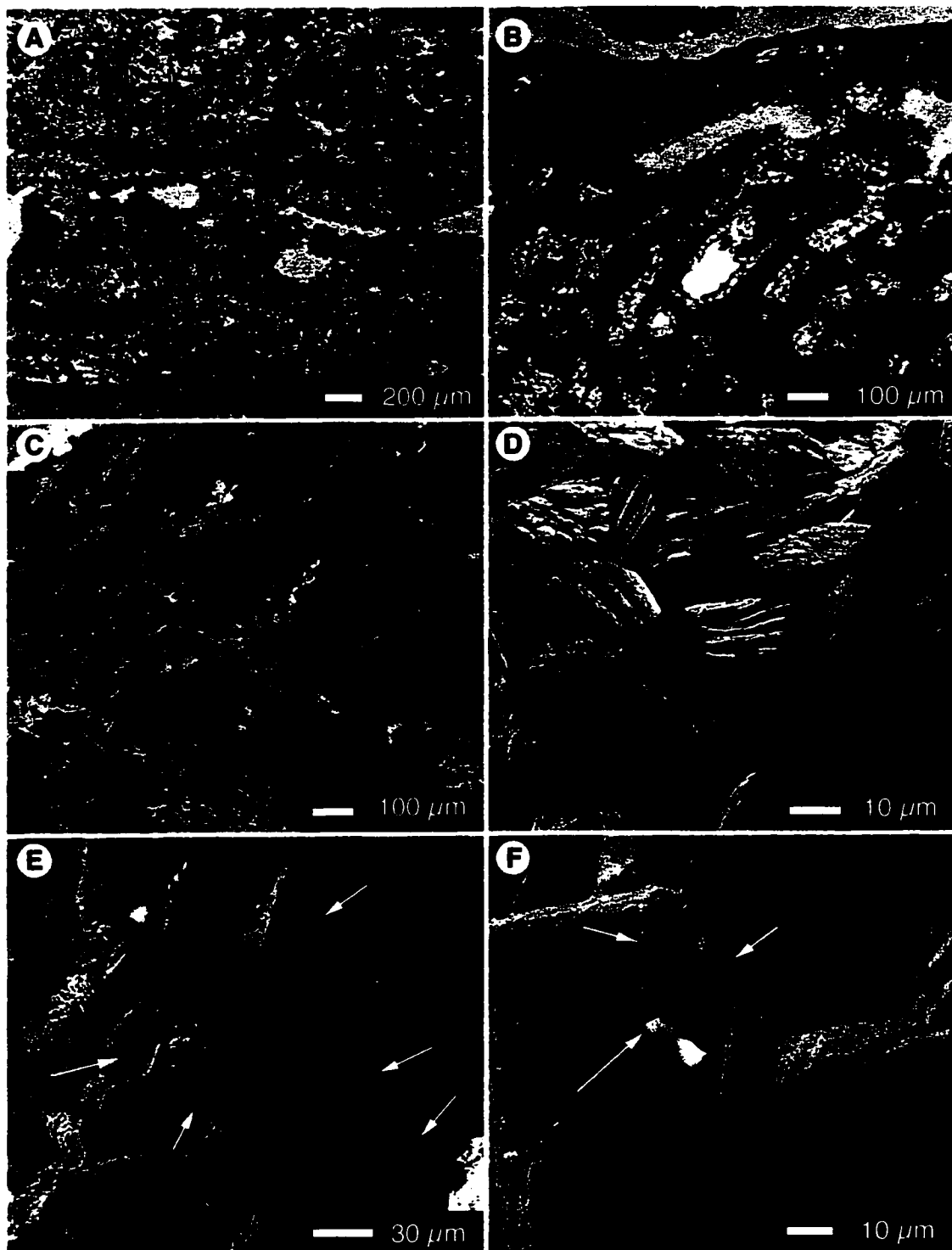


**Figure 3.10**

(A) Thin section from PLF sample M20 collected at MS5 showing flat-lying filament structures in a dense lamina. (B) Individual filament structures bend and merge as they pass from a porous lamina to a dense lamina. (C) A clump of bi-terminal crystals found within a dense lamina in porous laminar tufa sample M42 from MC1. (D) Intergrown bi-terminal crystals in sample M9 from MS4. (E) Detail of D showing intergrowth features, the composite crystal structure of the bi-terminal crystal ends, and the appearance of concentric void spaces in cross section. (F) Detail of D showing a crystal which has been internally corroded leaving a hollow shell.



The fourth texture in the PLF, found in the thick porous laminae, is defined by an alignment of upright sheets (Fig. 3.11A, B). The sheets have spar covered sides and crystalline cores (Fig. 3.11C). The crystals in the center of the sheets are euhedral, abutting adjacent crystals at triple-junctions, and commonly contain concentric void spaces (Fig. 3.11D, E) or have micritised cores (Fig. 3.11F).

Fossilised organics are also found in this facies. Siliceous auxospores, and calcified plant roots, fungal rhizomorphs, and spore bundles are common (Fig. 3.12A-E). The siliceous plates of the testate protozoan *Quadrullella* are abundant, and some retain the shape of the original organism (Fig. 3.12F). Although not found in SEM analysis, light microscopy of residue produced by immersion of tufa (samples M24 from MS5 and M36 from MC1) in dilute HCl revealed the presence of diatom tests. Only the heavily silicified central raphe structure of the tests remained, identifiable as a species of *Cymbella*.

#### *Interpretation*

The size and morphology of the vertical and prostrate columnar structures in this facies indicate that they formed by the encrustation of microbial filaments or filament bundles. Similar textures have been described as a fabric controlled by the morphology of component filamentous microbes growing beneath shallow flowing water (Walter, 1976; Casanova and Renaut, 1987; Chafetz *et al.*, 1991b; Jones *et al.*, 1998; Renaut *et al.*, 1998; Konhauser *et al.*, 2001). The alternation of erect and prostrate filament orientations is probably seasonally controlled, with erect filament growth in the summer and prostrate filament growth in the winter (cf. Chafetz *et al.*, 1991b; Konhauser *et al.*, 2001), but proof of this is enigmatic (Chapter 4). The higher density of the prostrate filament layers may be explained by a concentration of mineralization on a smaller microbial population during a period of reduced growth (i.e. during winter).

Species of the cyanobacteria *Calothrix*, *Phormidium*, *Oscillatoria* and *Mastigocladus* (a branching, tapering, non-sheathed genus with ~5 µm diameter filaments), and the flexibacterium *Chloroflexus* (a non-branching, sheathed filament <1 µm diameter) are known to produce laminated hot spring stromatolites, commonly in association with the unicellular cyanobacteria *Synechococcus* (Castenholz, 1969; Walter *et al.*, 1976; Jones *et al.*, 1998; Jones *et al.*, 2002). The porous laminar facies was

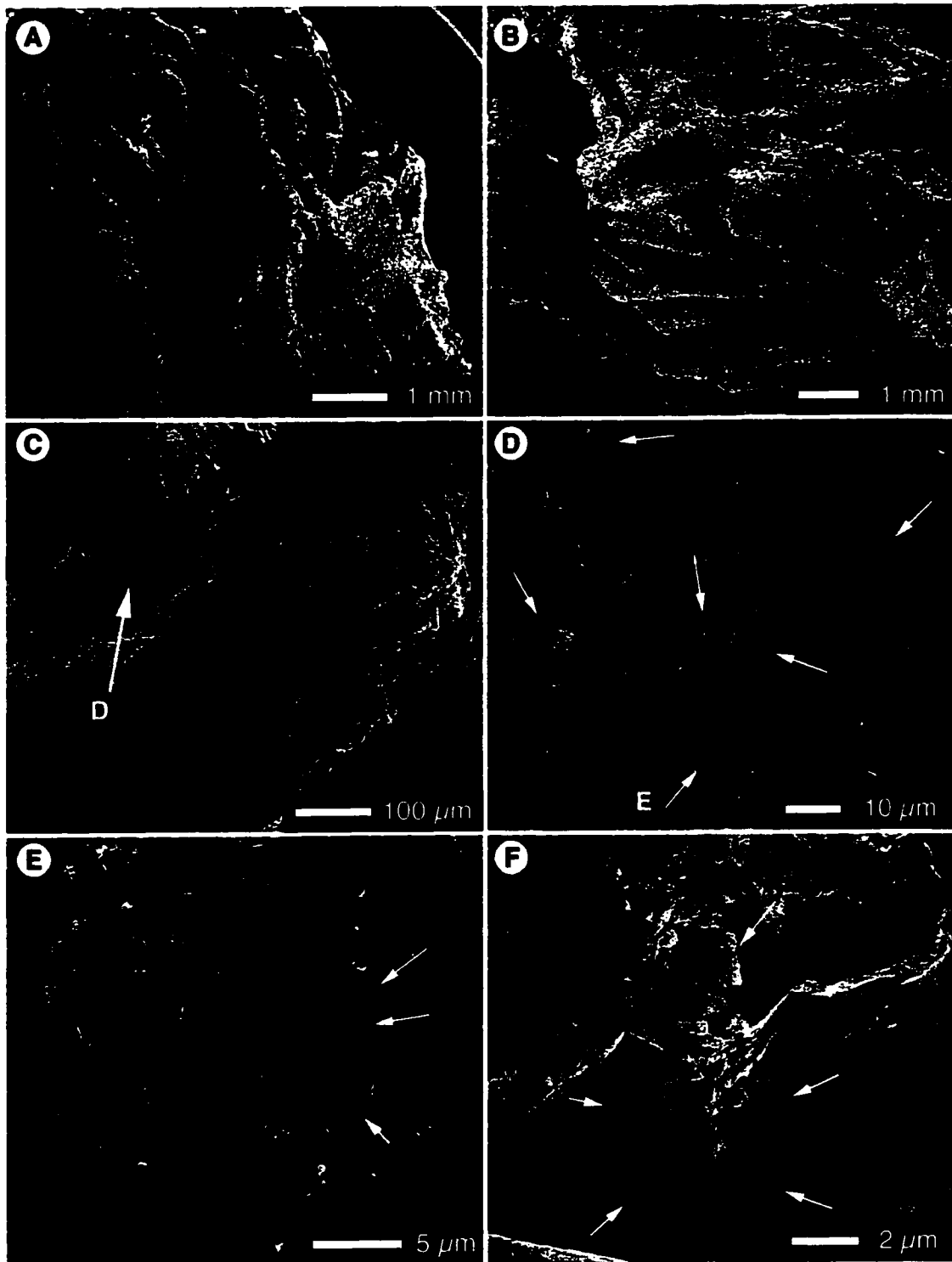


**Figure 3.11**

SEM images of a vertical sheet lamina in PLF sample M42 collected at MC1. (A) End view of vertical sheets. (B) Side view of vertical sheets. (C) Detail showing a cross-section through two vertical sheets. (D) Detail of image C. Note the void spaces surrounding the crystals that form the core of the sheet. (E) Detail of concentric void spaces in a crystal from the centre of the sheet. (F) A long view of a crystal from the centre of the sheet. The void spaces are confined to the centre of the crystal which is truncated against adjacent crystals.

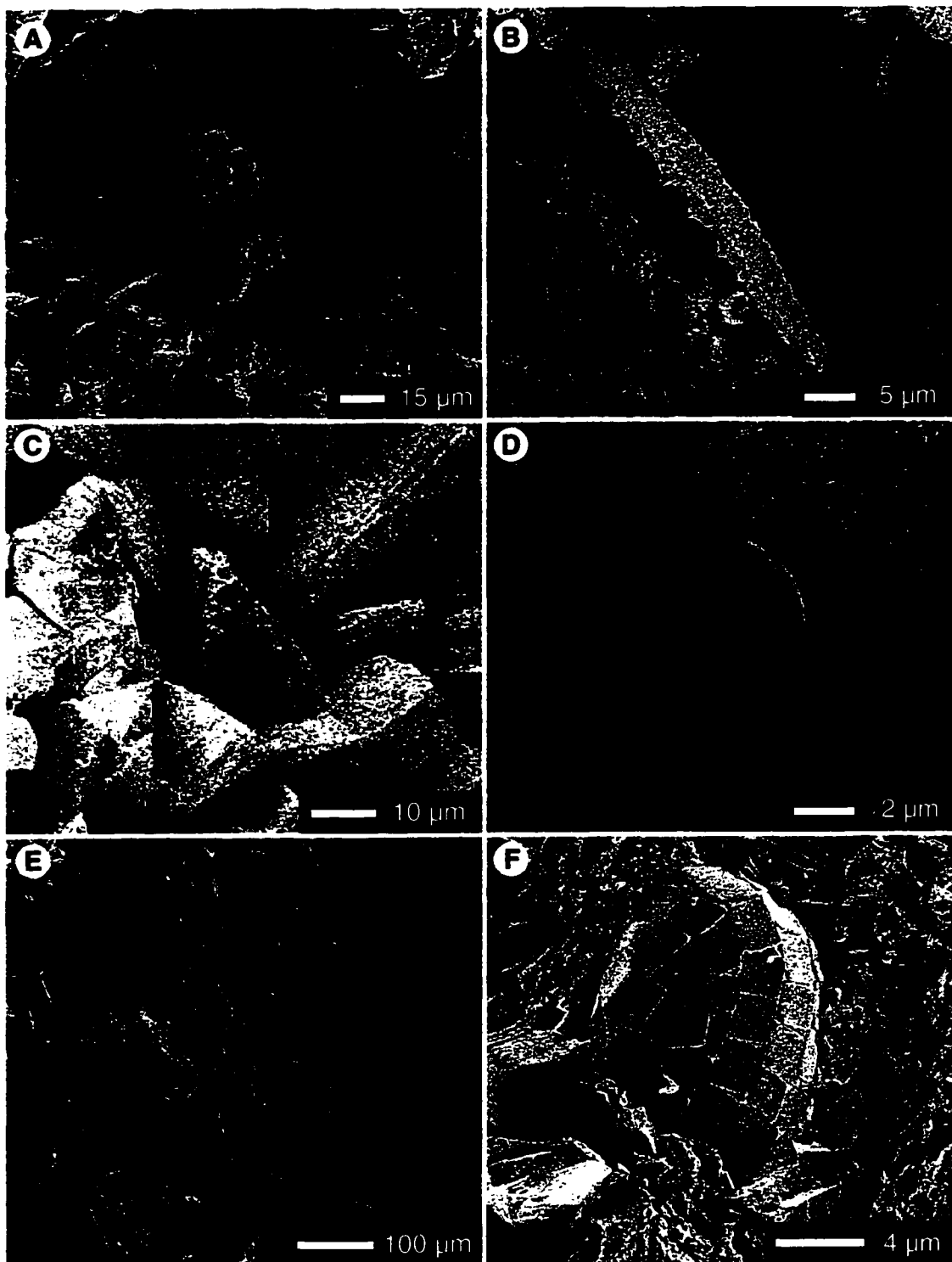


**Figure 3.12**

SEM images of mineralized organics found in the PLF: (A) calcified spore bundle from sample M42, (B, C) siliceous phytoliths found throughout sample M53, (D) pollen grain from sample M9, (E) calcified fungal rizomorph found throughout sample M42, (F) siliceous plates of the testate protozoan *Quadrulella* from sample M9.

formed by two dominant microbial species. The small diameter thinly sheathed, non-branching filaments are tentatively assigned to the genus *Phormidium*. The preserved sheaths are commonly smaller than the cylindrical casts they are found in. This may indicate that the small diameter microbes were first encrusted with calcite, and their sheaths shrunk (through desiccation or cell death) before they were mineralized. The larger diameter filaments, which do not have preserved sheaths and lack evidence for branching or tapering, may belong to a larger diameter species of *Oscillatoria* (such as that found at the modern Miette hot springs).

The bi-terminal crystals probably grew suspended in microbial mucus. They are larger than those in the streamer facies, indicating that the growth period was longer. Many of the bi-terminal crystals, and the trigonal sparry calcite crystals that coat the filament structures, exhibit corrosion, micritization, or contain internal void spaces. The void spaces in the crystals could arise from the dissolution of less stable phases - the crystals are low magnesian calcite and the void spaces may represent high magnesian calcite or aragonite layers that succumbed to dissolution during diagenesis. Alternately, the hollow trigonal sparry calcite crystals may have formed as skeletal crystals that were filled with less organized precipitates. Similar skeletal trigonal calcite crystals are reported from Kenyan and New Zealand hot springs, forming under “disequilibrium conditions that are unrelated to a specific environmental or diagenetic setting” that may be established through rapid degassing of CO<sub>2</sub> from thin water films (Jones and Renaut, 1996a). Hot spring stromatolites form beneath thin sheets of flowing water (cf. Guo and Riding, 1998) and CO<sub>2</sub> loss can be rapid during sheet flow because of the high surface area of water exposed to the atmosphere, so disequilibrium precipitation could have prevailed. It is difficult, however, to conceive of skeletal growth of composite bi-terminal crystals. The internal corrosion of the bi-terminal crystals may have arisen from dissolution and/or recrystallization of the high energy composite crystals during diagenesis (cf. Buczynski and Chafetz, 1991).

The upright sheet texture that forms thick porous laminae has been found in calcareous precipitates at various New Zealand hot springs (Jones, pers. comm.). It is probably formed by mineralization of netted current aligned mucal sheets. The microbes responsible for producing these mucal sheets are unknown, but sheet forming algae like

*Hydrodictyon* are common inhabitants of cold mineral springs (Canter-Lund and Lund, 1995), and may have a thermophilic relative. A comparison of Figures 3.10E and 3.11E, F indicates that the crystals making up the vertical sheets are related to the bi-terminal crystals. Though smaller, the crystals in the vertical sheets are nearly identical to the bi-terminal crystals in cross section and, like the bi-terminal crystals, they are internally vacuous. One explanation could be that upright vertical sheets trapped calcite crystallites that continued to grow in the mucus, much like the bi-terminal crystals, until the space restriction of the narrow mucus sheet caused them to truncate against one another.

In summary, PLF tufa formed through encrustation and replacement of a filamentous microbial community growing in shallow flowing water. Where turbulence was low, intercellular mucus accumulated and supported the growth of suspended bi-terminal crystals. A profusion of mucus may also explain the abundance of detrital organic fossils in this facies; low flow rates and sticky mucal traps allowed detrital material to accumulate. Locally, populations of *Quadrulella* and *Cymbella* lived amongst the filamentous microbial community, and a mucal sheet forming non-filamentous microbe produced upright sheets that were calcified.

### 3.3biii Dense Laminar Facies (DLF)

The dense laminar facies (DLF) is a stratiform stromatolite found in flat banded and wedge-shaped tufa, especially in upper ledge at MS and MC. It has lower porosity than PLF, and is characterized by alternations of light and dark coloured laminae, 0.5-1.5 cm thick, which are bounded by relatively flat parallel planes (Fig.3.13A). The light coloured laminae contain vertical and upwards branching columnar structures (Fig. 3.13B), whereas the dark coloured laminae contain flat lying sub-parallel filament structures (Fig. 3.14A). The columns are coated by sparry calcite and most have filament casts in their centers (Fig. 3.13C-F). The filament casts are cylindrical voids (~ 2 µm in diameter) that are bordered by radiating calcite (Fig. 3.13E). In some specimens the apparent diameter of the filament cast has been increased, and made irregular, by dissolution along the filament cast cavity (Fig. 3.13F). Some columns

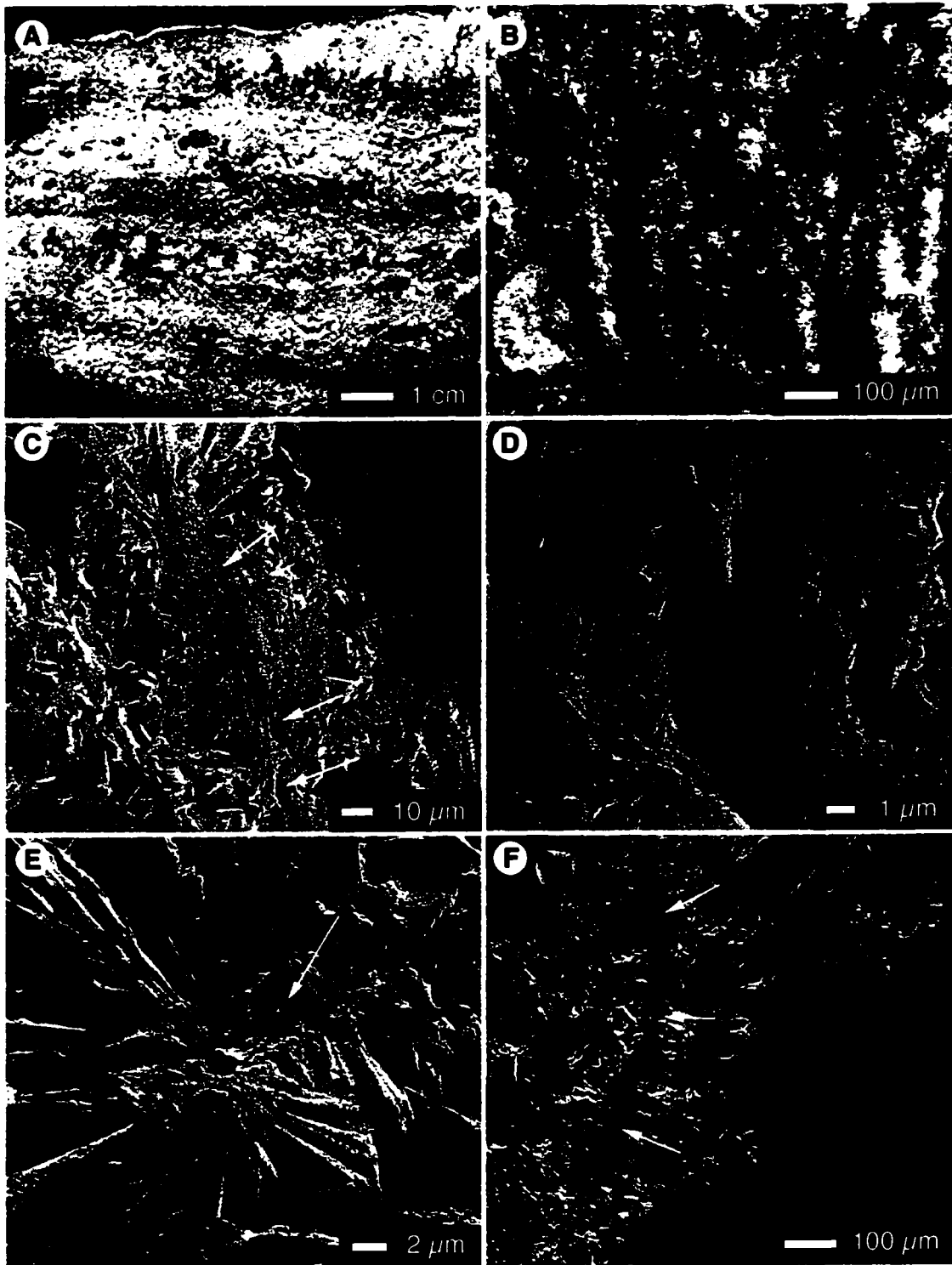


**Figure 3.13**

(A) Photograph of DLF sample M24 from MS6. (B) Thin section photograph of a light coloured lamina in M24 showing vertical and upwards branching columnar features. (C) SEM image of a long section through a vertical column in sample M24 with a filament cast at its core (arrow). (D) Detail of the filament cast shown in image C. (E) Cross section through a vertical column with a partially preserved filament in the centre of the column bordered by radiating sparry calcite. (F) Long section view of a vertical column whose centre has experienced dissolution along a filament cast.

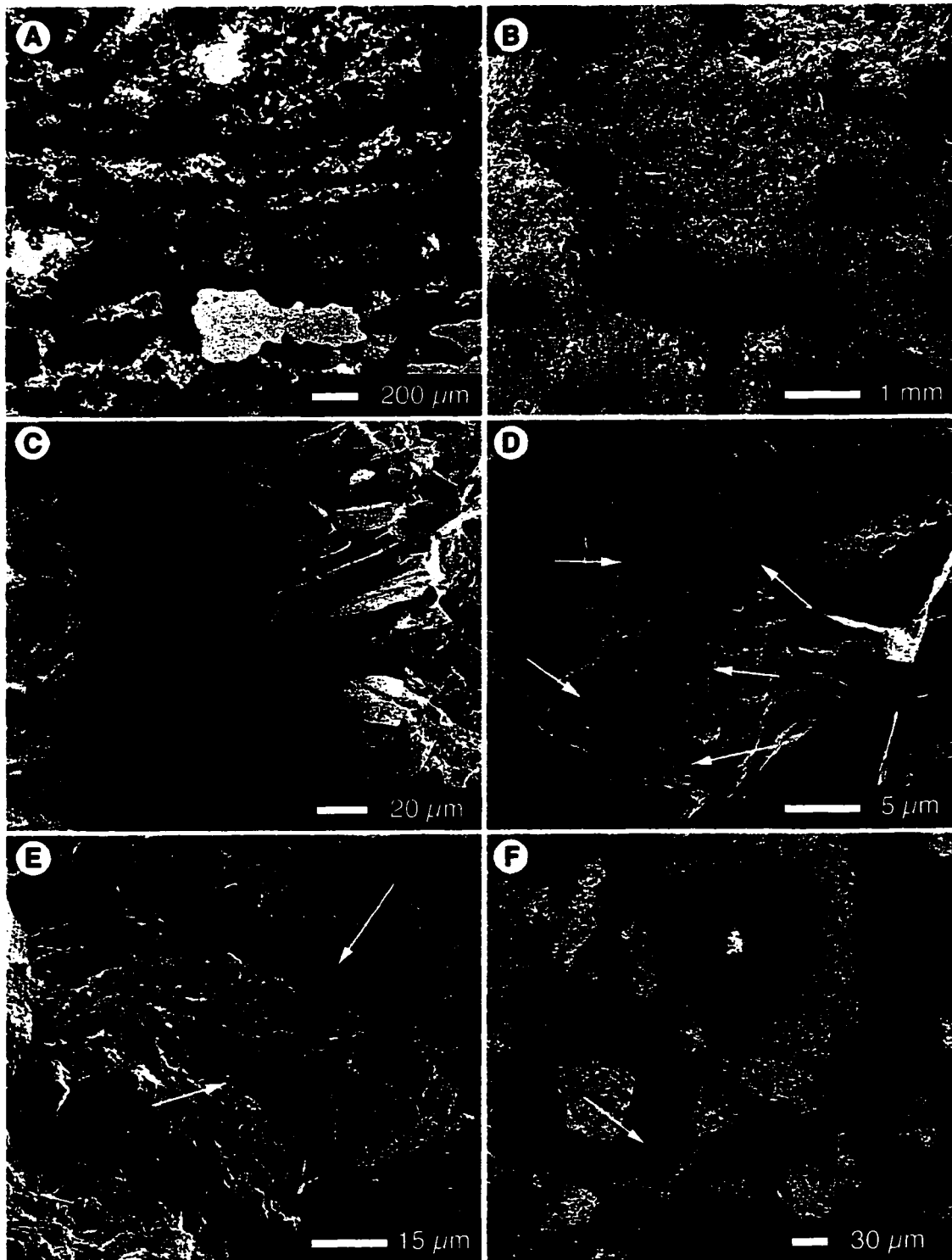


**Figure 3.14**

(A) Thin section of a dark coloured lamina in dense laminar facies sample M24 from MS6. (B) SEM image of a dark coloured lamina from M24 showing flat-lying filament structures composed of solid calcite and fringed by sparry calcite. (C) Detail of sparry calcite that coats filament structures. (D) Long section through a flat-lying filament structure showing preserved filaments in its centre (arrows). (E) Cross-section view shows a filament with a preserved and infilled sheath. (F) Flat-lying filament structures bend upwards and merge to form vertical columns as they pass from dark to light laminae.

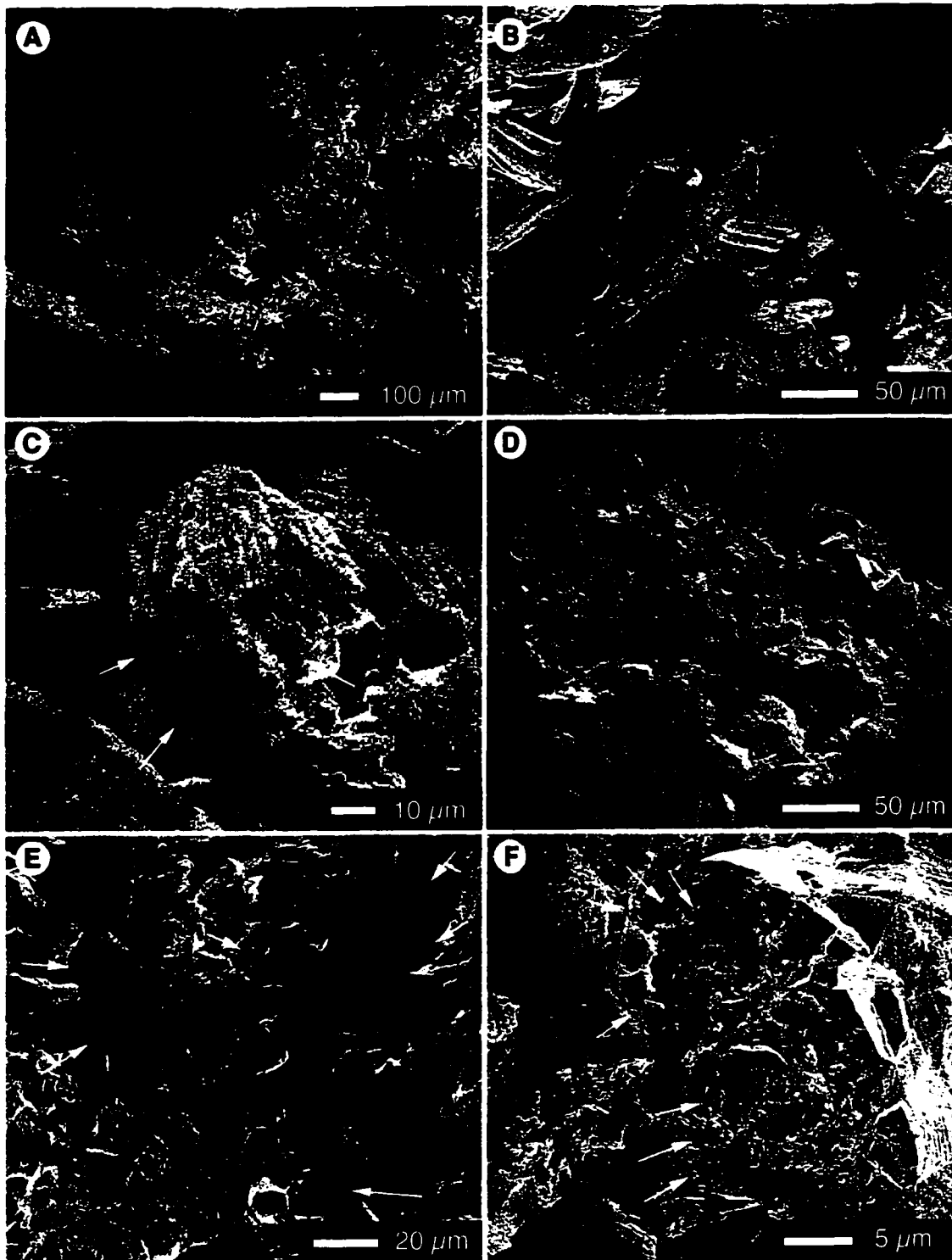


**Figure 3.15**

(A) SEM image of a pocket of bi-terminal crystals found within a dark coloured lamina in dense laminae facies sample M24. (B) Detail of bi-terminal crystals shown in A. The crystals are composite and show complex intergrowths (arrows). (C) End view of a bi-terminal crystal showing that the composite crystals are trigonal prisms. (D) Cross section through a vertical column in a light coloured lamina from M24. Solid blocky calcite surrounds a core of corroded crystals. (E) Detail of the centre of the column shown in image D. (F) Detail of corroded crystals shown in E. They have concentric hexagonal shaped void spaces and are truncated against other each other in flat planes.



also contain calcite crystals with concentric hexagonal void spaces, or hollow cores (Fig. 3.15D-F). Pockets of intergrown bi-terminal calcite crystals (up to 130  $\mu\text{m}$  long and 40  $\mu\text{m}$  wide) composed of numerous trigonal prismatic calcite crystals are locally distributed in and between the dark and light coloured laminae (Fig. 3.15A-C).

The flat-lying filamentous structures in the dark coloured laminae are coated in calcite spar, but have more solid cores than the upright filament structures. Filaments are preserved as body fossils with heavily mineralized sheaths. Despite the difference in filament preservation between the dark and light coloured laminae, individual filament structures change orientation between laminae (Fig. 3.14F), indicating that the same microbial community formed the both laminar types. In one sample of dense laminar tufa, etching exposed preserved filaments in great detail (Fig. 3.16A, B). Filaments preserved by encrustation and sheath mineralization have external filament diameters of 1, 3, and 10  $\mu\text{m}$  (Fig. 3.16C-F). The 10  $\mu\text{m}$  diameter filament has a preserved sheath, is non-branching, non-tapering, and regularly segmented into 20-25  $\mu\text{m}$  lengths (Fig. 3.16D). The segmentation probably denotes the location of septae in the original filament. In several examples, the 1  $\mu\text{m}$  diameter filament is found wrapped about the larger diameter filaments (Fig. 3.16E).

### *Interpretation*

Like the PLF tufa, this facies formed by mineral encrustation/replacement of a filamentous microbe dominated community, and, where intercellular mucus accumulated, bi-terminal crystal growth was permitted. The microbial community that formed the DLF facies consisted of three filamentous microbes. The taxonomic affinity of the 10  $\mu\text{m}$  diameter filament is unknown. The 3  $\mu\text{m}$  diameter filaments have a thin preserved sheath, and may be a species of *Phormidium* (Jones *et al.*, 2002). The 1  $\mu\text{m}$  diameter filaments that wrap around larger filaments could be another species of *Phormidium*; they are similar to the small diameter *Phormidium* described by Jones *et al.* (2002). Interestingly, the sheaths are better preserved in the dark coloured laminae, whereas evidence of filaments in the light coloured laminae comes from cylindrical void spaces generated by the decomposition of encrusted filaments. The bending of filament structures between

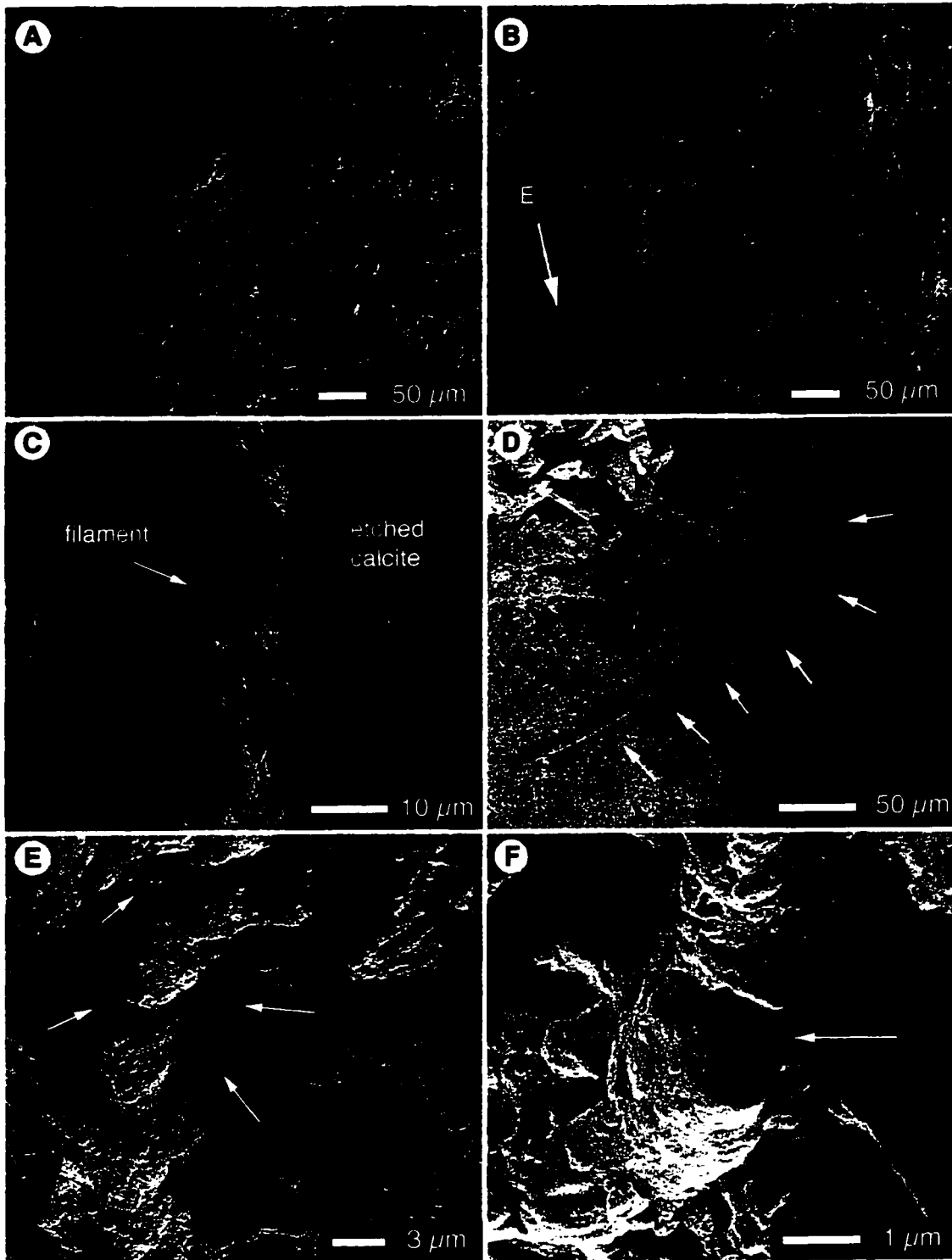


**Figure 3.16**

(A,B) SEM images from a dark coloured lamina in dense laminar facies sample M24. Etching has exposed preserved filaments. (C) Detail of a filament encrusted with blocky calcite (arrow). A badly etched calcite crystal is visible in the background. (D) A segmented filament. (E) Detail of filaments from image B. Two size classes are visible - smaller diameter filaments wrap around the larger diameter filaments. (F) Detail of a segmented smaller diameter filament preserved by calcification of its sheath.

laminae indicates that the same microbial community generated both the light and dark laminae, so the presence or absence of a preserved sheath may be more indicative of the precipitation environment (i.e. summer vs. winter conditions) than of the microbial species present.

The DLF and PLF locally succeed one another vertically, but in general, the DLF is found further upslope, closer to the FSVPs. Many differences between the two facies are attributable to differences in the water temperature, flow rate, and rate of precipitation between the upper and lower spring mound:

- (1) The bi-terminal crystals in the DLF are morphologically different, both in size and habit, from bi-terminal crystals found in other facies and at the modern springs. Buczynski and Chafetz (1991) found, however, that bacterially induced bi-terminal crystal morphology is more strongly influenced by the viscosity of the growth medium than by its composition or the polymorph of calcite being formed. Temperature affects the viscosity of many media, and it is reasonable to assume that mucus masses submerged in warmer water near the spring vents would have different viscosity than mucus masses submerged in cooler water down slope. This may explain the morphological differences between bi-terminal crystals in the DLF and PLF.
- (2) The DLF does not contain the upright sheet texture found in the PLF. If the upright sheets formed by mineralization of mucal sheets produced by a colonial microbe, a temperature restriction in the proximal slope may have inhibited their growth, preventing development of upright sheets in the DLF.
- (3) The variable thickness of porous and dense laminae in the PLF contrasts with the even thickness of dark and light laminae in the DLF and may also be explained by different proximity to the spring vents. At the modern Miette Hot Springs, the warmest waters issue in the winter with temperatures up to 20°C greater than summer values, but cooling is also most efficient in the winter; thus, variations in the ambient air temperature and the vent temperature mitigate one another, reducing the variability of the spring water temperature between seasons near the vent (van Everdingen, 1986). Downslope, however, cooling to ambient air temperature could generate a strong seasonal disparity in water temperature. On the distal slope, where the PLF formed, summer water temperatures optimized the growth of the filamentous microbes (such that the resultant

porous laminae were up to 2.5 cm thick) and permitted the growth of the algae responsible for the generating upright mucal sheets. Cooler temperatures in winter inhibited microbial growth, resulting in the thin (<0.7 cm) dense layers in the PLF. The DLF formed upslope, where more consistent water temperatures allowed stable microbial growth, resulting in the development of similar sized dark and light, i.e. summer and winter, laminae.

Precipitation rates in the distal flow path may also have been slower in winter: because the solubility of CO<sub>2</sub> increases with decreasing temperature, degassing is retarded in winter as the water moves away from the vent and cools. At Rabbitkettle Hot Springs, Yukon Territory, this results in a 50% reduction in the rate of precipitation by the time the spring water has reached a distance of 40 m from the spring vent; differences are less pronounced in the proximal flow path where waters have not cooled as much (Gulley, 1993). So, if proximal precipitation coated relatively stable microbial communities with relatively consistent rates of precipitation, summer and winter laminae would be similar in thickness - as are found in the DLF; in the distal flow path, compromised microbial growth in winter and lower winter precipitation rates would result in thin winter laminae and thick summer laminae - as are found in the PLF.

(4) Filaments are generally better preserved in the DLF compared to the PLF. Rates of precipitation are highest in the proximal vent environment at thermal springs because of rapid degassing (Chafetz *et al.*, 1991a; Folk, 1994). High rates of precipitation yield the best preservation of microbial communities (Renaut *et al.*, 1998). Thus, the better preservation of filaments in the DLF also supports the conjecture that it is an upslope facies.

(5) There may also have been a difference in flow rate between the proximal and distal slope wash environments. The PLF is more porous, has more widely spaced upright filamentous structures in its light coloured laminae, and contains more bi-terminal crystals than the DLF. This suggests that the microbes forming PLF were supported by abundant intercellular mucus. Observation of the modern Miette Hot Springs shows that intercellular mucus accumulates where flow rates and water turbulence are low. If the water at the fossil springs dispersed as it moved downhill, flow rate and water turbulence would both decrease, permitting more mucus to accumulate in down slope microbial

communities. Thus, the DLF is interpreted to be an upslope sheet flow facies, and the PLF its down slope counterpart.

### *3.3c Bedded Facies*

This facies is only found in the domal tufa morphotype associated with the FSVPs and it is commonly obscured by speleothems. Indeed, it is usually coated by a soft layer of lime, or “moon-milk”, in the field and the true structure of the facies was revealed only after hand samples were cut (Fig. 3.17A). The rock has irregular cm-scale colour banding and contains sinuous subparallel features defined by concentric mineralization around thick micrite bordered strands. In thin section, the strands are revealed to be calcite replaced microbial filaments (Fig. 3.17B-D). The preservation of the filaments is very good, especially compared to thin section images of the stromatolitic tufa facies (Figs. 3.7, 3.8, 3.10, 3.13, 3.14). The centers of the strands contain finely crystalline calcite, and the external filament diameter (~30  $\mu\text{m}$ ) is outlined by a dark micritic rim (Fig. 3.17B), which is basal to multiple generations of thick calcite cement (Fig. 3.17C-D). The bedded tufa facies has low porosity relative to the other fossil tufa facies, and filament structures are separated coarsely crystalline calcite. Although a distinctive feature of the facies, the sinuous microbial strands do not organize the macroscopic texture of this mostly crystalline facies.

#### *Interpretation*

Found solely at the location of former spring vents, this facies obviously formed in the immediate vent environment. Rapid cooling and degassing resulted in rapid mineralization (and excellent preservation) of microbes growing on the spring mound and spring pool rims. Precipitation in this environment was almost certainly inorganic, induced by degassing, but, where present, microbial surfaces provided a nucleation site for the precipitation. The lack of stromatolitic structure suggests that the microbial species did not control the morphology of the precipitate. The irregular colour banding is not defined by a change in the orientation of the microbes, but may reflect changes in the spring water chemistry or flow rate. High flow rates in the immediate vent environment may have precluded the accumulation of intercellular mucus to support vertical filament growth and growth of bi-terminal crystals. The component microbe had an external

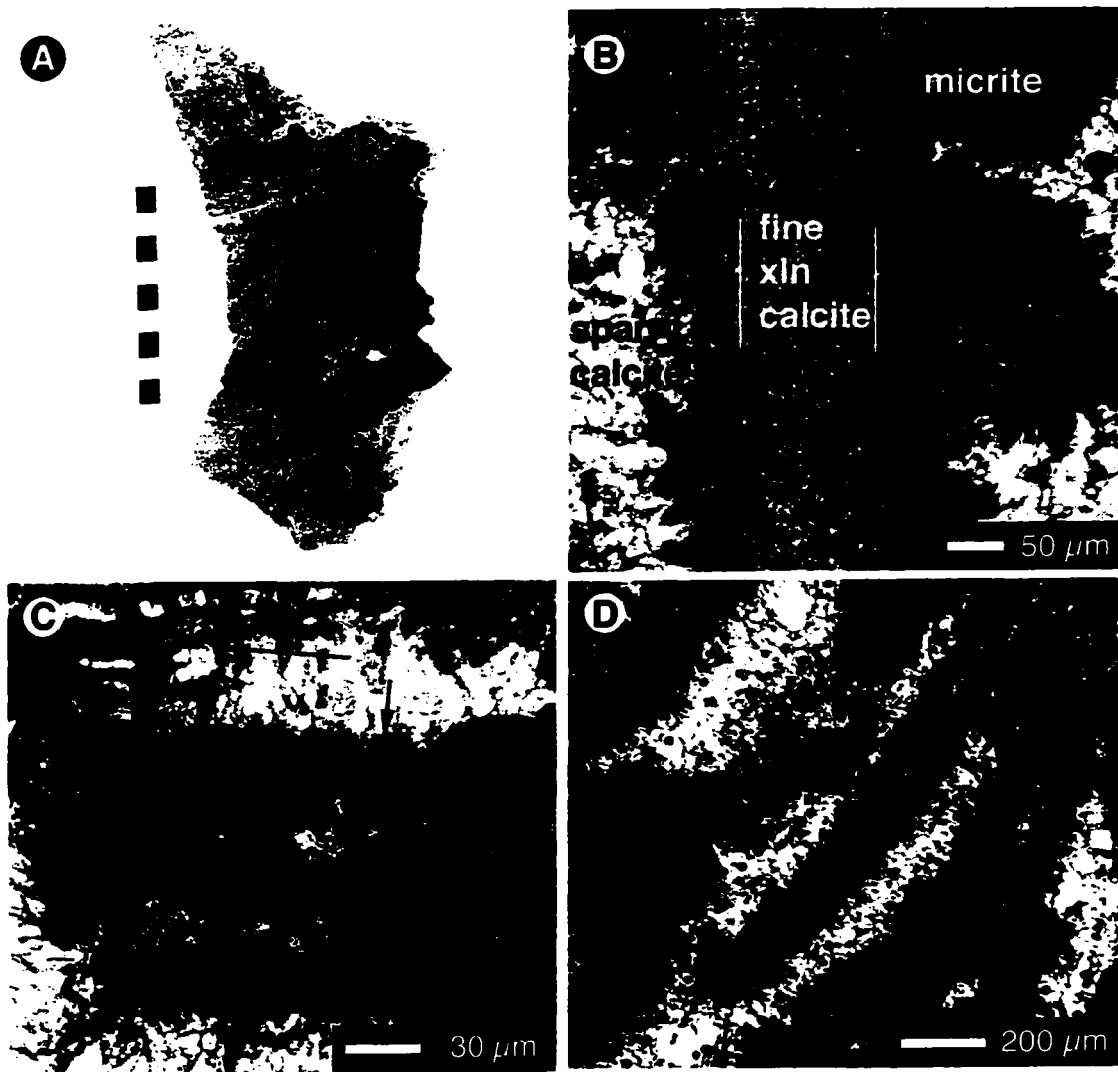


**Figure 3.17**

(A) Photograph of bedded facies sample M2 collected within a former spring vent pool at MS1. (B) Thin section of sample MS1 showing a microbial filament structure filled with fine crystalline calcite bordered a rim of micrite and surrounded by coarse calcite spar. (C) Detail of the end of the filament structure in image B. Banding in the sparry calcite (arrow) indicates precipitation from waters with changing chemistry. (D) Thin section overview of the bedded facies in thin section - sinuous filamentous structures are surrounded by solid sparry calcite.

filament diameter of ~30  $\mu\text{m}$ . Non-tapering filaments this large could belong to a large diameter *Oscillatoria* species.

### 3.3d *Crenulated Facies*

This facies consists of thin crenulated sheets (17-22 sheets per 10 cm) separated by elongate pore spaces. It is found in wedge-shaped tufa at MC1 and MS5, and in laterally adjacent flat banded tufa at MS6. The sheets, horizontally continuous for up to a meter, are irregularly contorted, and may or may not conform to laminae immediately above or below (Fig. 3.18A). Void spaces are commonly filled with gypsum and amorphous K-rich salt (Fig. 3.18B). There are three types of crenulated sheets: (1) sheets 100 - 150  $\mu\text{m}$  thick composed of solid calcite and bordered by blocky calcite spar (Fig. 3.18D), (2) sheets 50 - 100  $\mu\text{m}$  thick composed of, or covered by, fans of platy calcite crystals (Fig. 3.18E, F), and (3) sheets ~100  $\mu\text{m}$  thick composed of badly corroded, intergrown, non-composite bi-terminal calcite crystals that are locally adorned with blades and rosettes of strontianite (Fig. 3.19A-E). Coatings of gypsum and K-rich salt prevented more comprehensive investigation of the three sheet types (Fig. 3.19F).

#### *Interpretation*

The presence of this facies in wedge shaped tufa indicates that it formed in ponded water below breaks. A possible petrogenic scenario is that the crenulated facies formed as an overbank deposit in stagnant water that experienced periodic flooding and desiccation. The crenulated sheets could be calcified remains of mucal sheets that became convoluted and rigid through desiccation and shrinking, and were strengthened and thickened by encrustation with calcite spar during later immersion events. The bi-terminal calcite sheets may have developed through desiccation concentration, and subsequent cementation, of bi-terminal calcite crystals grown suspended microbial mucus (cf. Weed, 1889). The internal corrosion of the bi-terminal crystals indicates that they may have incorporated an unstable mineral phase, such as high-Mg calcite, that succumbed to diagenesis. Evaporative concentration of Mg in stagnant water could have facilitated the precipitation of the less stable calcite polymorph, and periodic wetting and drying due to episodic flooding of the pool bed would allow the development of successive, non-conformable laminar sheets.

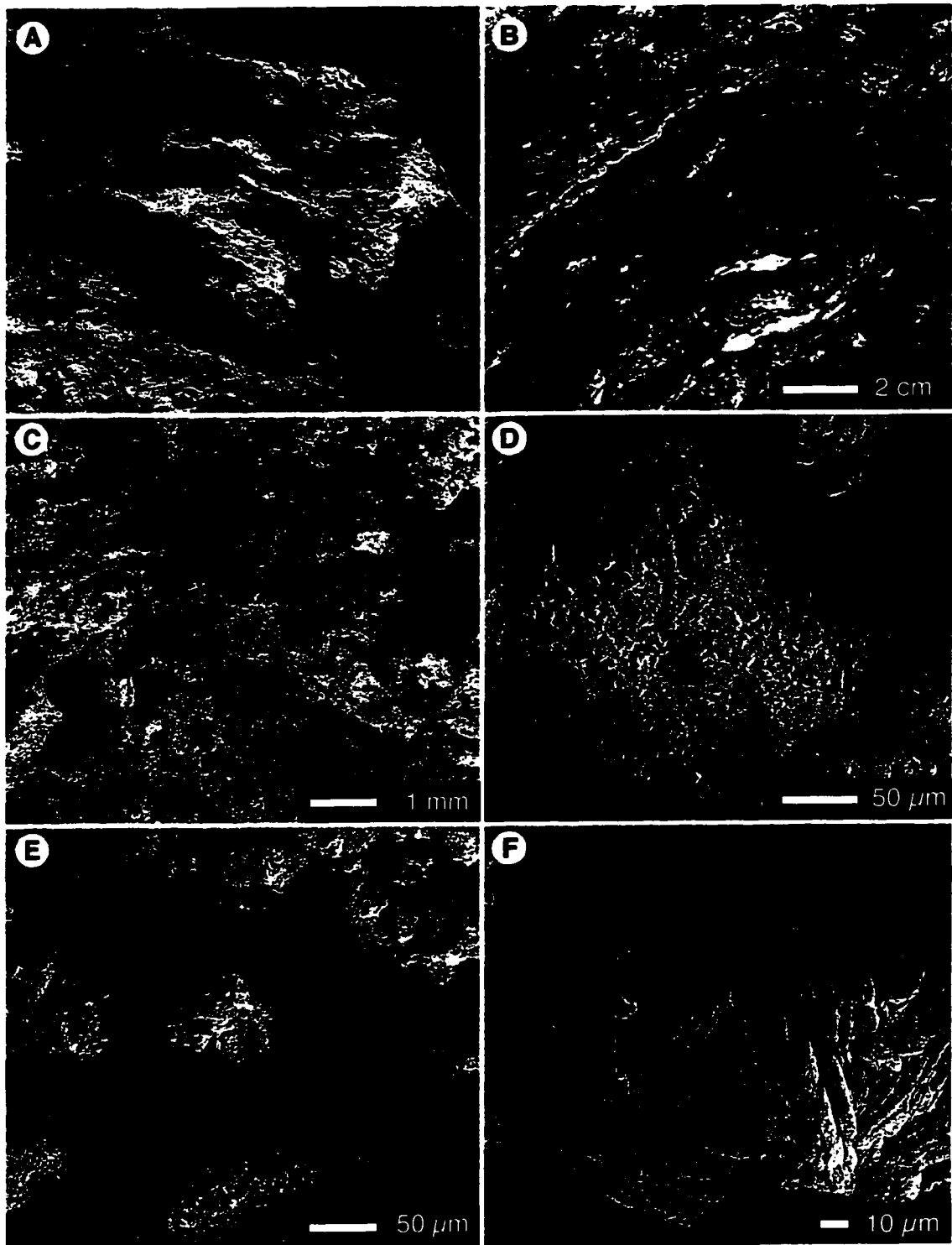


**Figure 3.18**

(A) Photograph of the crenulated facies exposed at MS6. A quarter (2.4 cm diameter) is shown for scale. (B) Crenulated tufa from MS5 in which the void spaces between sheets have been filled with white precipitates. (C) SEM image overview of sample M16 from MS5 showing the ends of crenulated sheets on a larger scale. (D) Cross-section through a crenulated sheet from M16. The interior of the sheet is solid calcite and the edges are bordered with calcite spar. (E) Crenulated sheets from M16 covered in platy calcite fans (arrows). (F) Detail of platy calcite fans.



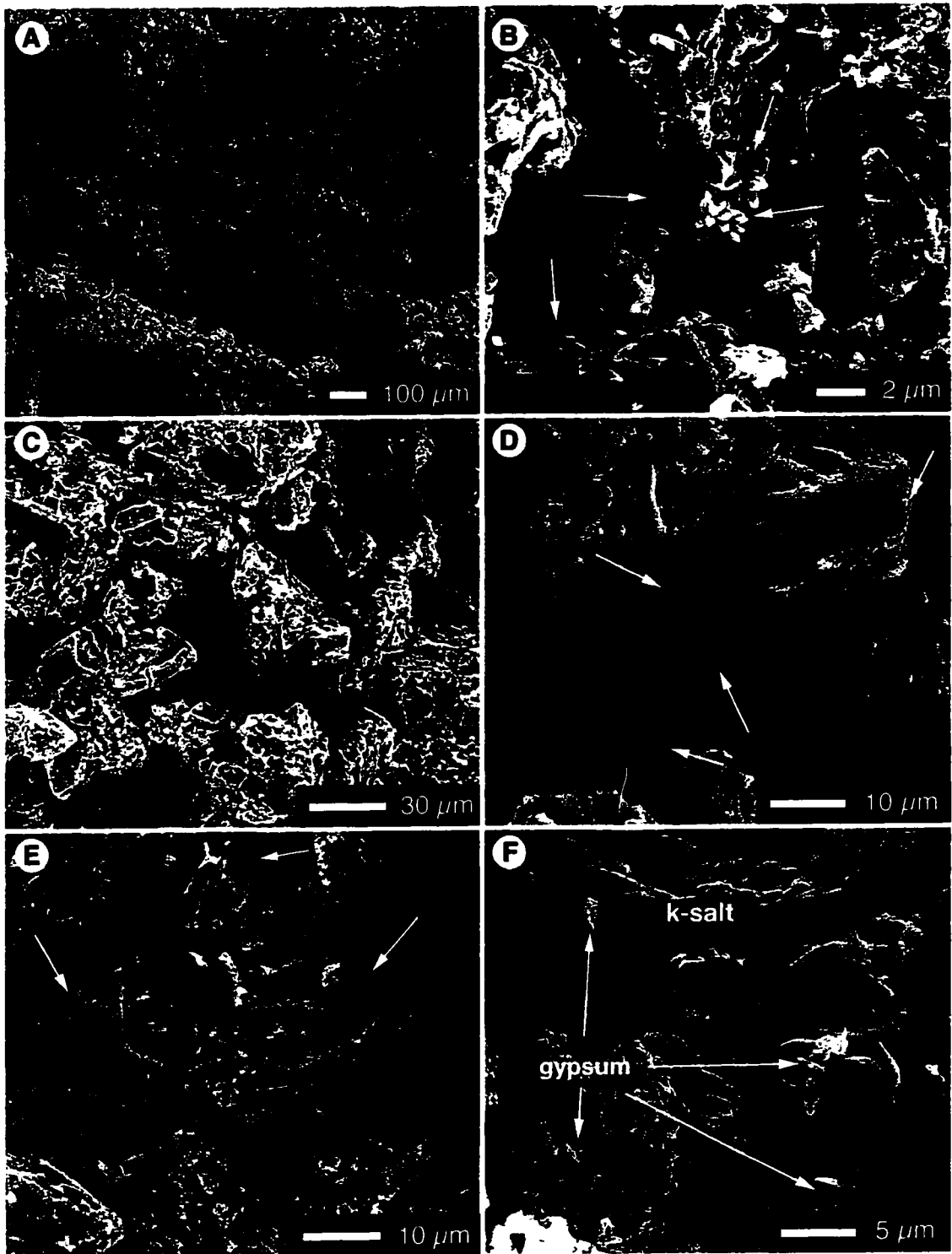


**Figure 3.19**

(A) SEM image of crenulated sheets composed of biterminal calcite crystals in sample M16 from MS5. (B) Blades and rosettes of strontianite (arrows) are found between calcite crystals. (C) Detail of bi-terminal calcite crystals. Many are internally corroded. (D, E) Details of internally corroded bi-terminal calcite with remnants of the external crystal planes (arrows). (F) K-rich salts and blades of gypsum obscure details of the underlying calcite in much of the crenulated tufa facies.

The origin of the platy calcite sheets is enigmatic. It is not clear if the sheets are actually composed of platy calcite, or merely coated in platy calcite. Platy calcite crystals, with their *c* axes much shorter than their *a* and *b* axes, have commonly been ascribed to precipitation from boiling waters. Jones and Renaut (1998), however, showed that platy calcite can form at temperatures below boiling if rapid CO<sub>2</sub> degassing results in a high CO<sub>3</sub>:Ca ratio in the precipitating fluid. Since a viable microbial community was preserved in fossil Miette vent precipitates (the bedded tufa facies), the spring water cannot have been boiling; nor is there evidence for especially rapid loss of CO<sub>2</sub>. Indeed, CO<sub>2</sub> loss is greatest from fast flowing, turbulent water and all other evidence suggests that the crenulated tufa facies formed in stagnant water. If the “platy calcite sheets” are composed of, rather than covered by, platy calcite, this suggests that evaporative concentration is a third generative mechanism. Alternately, the platy calcite could have precipitated as a coating from spring waters moving through pre-existing crenulated facies tufa.

Gypsum, strontianite, and potassium salts are not prevalent in most of the fossil Miette tufa, and they are found in this facies as void fill. They probably precipitated from waters that moved through pre-deposited tufa. Gypsum and strontianite are typical precipitates of the modern spring deposits and there is evidence (a domal tufa morphotype) that a spring vent emerged through tufa just uphill of the largest crenulated tufa outcrop (at MS5).

### 3.3e *Sheet Facies*

This facies is found in roll-over and vertical tufa throughout the fossil Miette tufa exposure. It is a crystalline crust deposit composed of steeply inclined sheets of sparry calcite. Where sheets are inclined beyond 90°, they are convoluted and form draperies (Fig. 3.20A-C). The sheets have finely crystalline interiors that are transitional with coatings of coarse trigonal calcite spar. Most of the calcite spar crystals have solid external faces but micritised, or hollow cores (Fig. 3.20E, F). Cross-sections through externally intact crystals reveal concentric triangular void spaces within the crystal cores (Fig. 3.21A, B). The sparry crusts are punctuated by filament and root casts with common flow-orientation. Microbial filaments (~1.5 µm diameter) with preserved

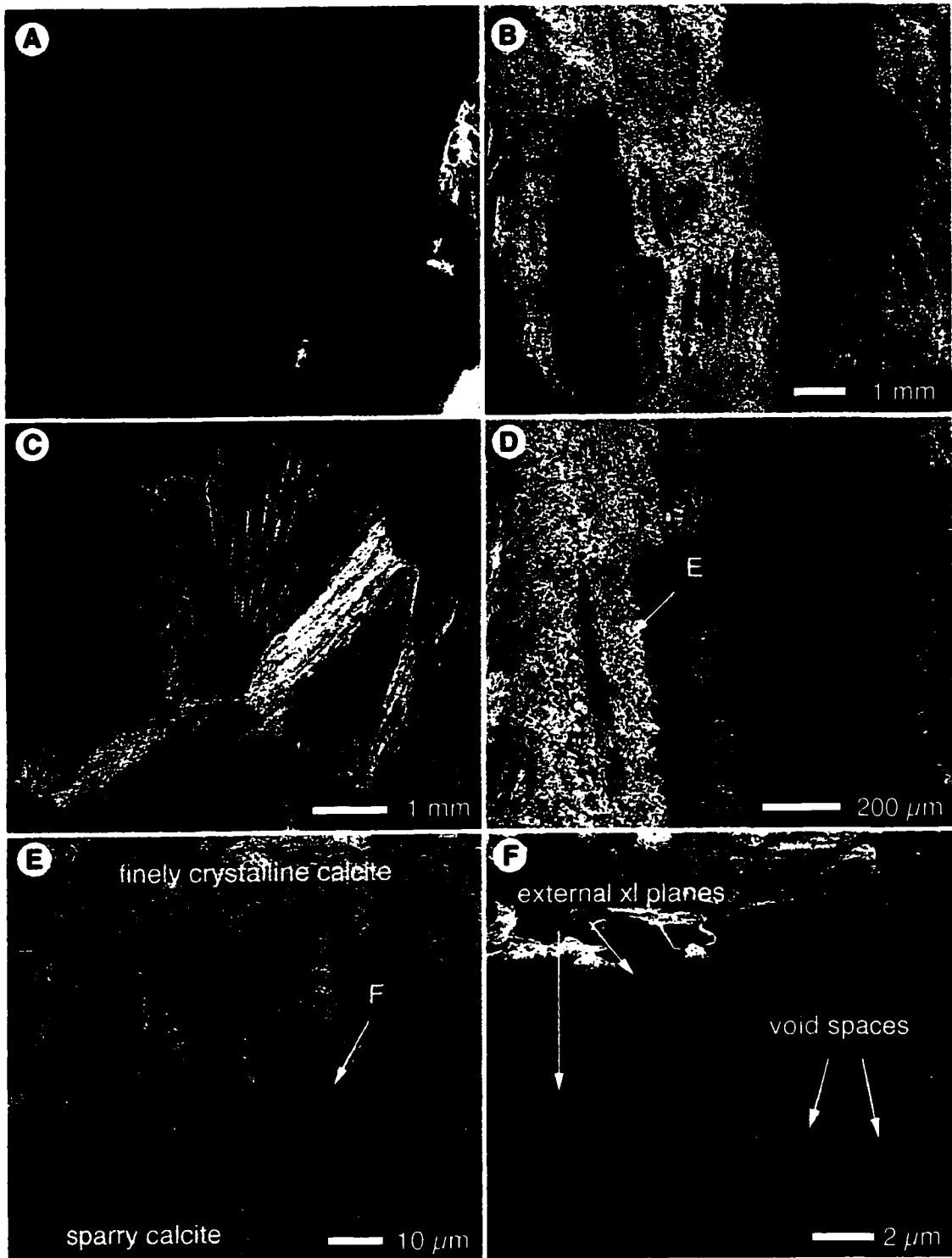


**Figure 3.20**

(A) Photograph of sheet facies from the front of a vertical tufa drapery at MC1, a pencil is shown for scale. (B) SEM overview of sheet tufa sample M32 from MC1. Note concentric sheets of sparry calcite. (C) Calcite fan found on the outer edge of sample M32. (D) Detail of concentric sparry sheets in M32. (E) Detail of image D showing a cross-section through a crystalline sheet - the interior of the sheets are finely crystalline to micritic and the outside of the sheets consist of coarse trigonal calcite spar. (F) Detail of calcite spar in image E. Many of the crystals have hollow cores and/or internal void spaces. The external crystal planes are well preserved.

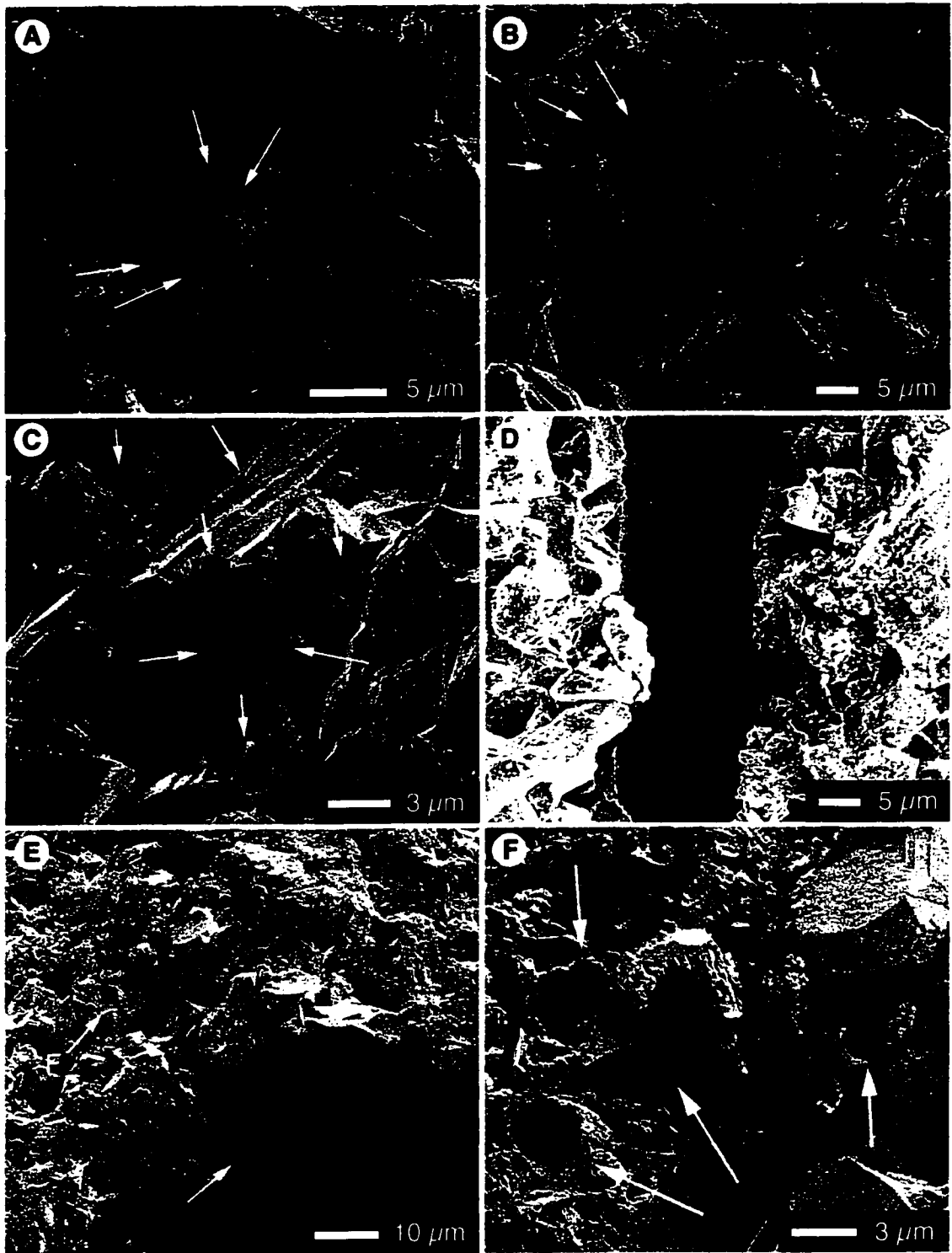


**Figure 3.21**

(A,B) SEM images of cross-sections through sparry calcite crystals found in sheet facies sample M32 that contain concentric void spaces (arrows). (C) Small filament casts with like orientation and preserved sheaths (arrows) in the centre of solid calcite crystals whose growth faces meet in triple junctions (arrows) are found towards the centre of crystalline sheets. (D) Large diameter filament cast in long section with the nucleation faces of calcite crystals visible filament cast. (E) Large filament or root cast with bundle of small filament casts. (F) Detail of small filaments with preserved sheaths from image E.

shrunk sheaths in oversized cylindrical voids are found in the center of solid calcite crystals (Fig. 3.21C); 10  $\mu\text{m}$  diameter cylindrical filament casts are bordered by sparry calcite (Fig. 3.21D); and 3  $\mu\text{m}$  diameter filamentous microbes with preserved sheaths are found in bundles of 4 to 10 filaments (Fig. 3.21E, F).

### *Interpretation*

This facies is found in tufa that formed from steeply flowing water. Inorganic degassing is efficient where water flows over slope breaks, and promotes rapid inorganic precipitation (Pedley, 1990). The smooth crystalline sheets formed on smooth substrates, and where microbial filaments grew, or were strung out, beneath flowing water, precipitates coated them, preserving microbial filament casts and structures. The presence of filament casts in the center of solid calcite crystals (Fig. 3.21C) indicates that the filaments acted as the nucleus of precipitation in sheet tufa inclined past  $90^\circ$  (cf. Emeis *et al.*, 1987; Janssen *et al.*, 1999). The small sheathed filaments might belong to *Phormidium*, and the larger, unsheathed filaments to *Oscillatoria*; other taxa were probably also incorporated into the sheet tufa facies given that it formed at different elevations and water temperatures across the spring mound.

### 3.3f *Granular Facies*

This facies is named for its appearance in outcrop. It looks like a grainstone with well-sorted clasts that range in size from 1 to 2 mm and is found at two locations near MS4. The rock contains no visible laminae, and cementation is irregular, making the rock variably hard or friable (Fig. 3.22A). On the SEM, much of the calcitic structure is obscured by precipitates of gypsum and strontianite (Fig. 3.22B). Gypsum is found as tabular crystals that form rosettes and fans (Fig. 3.22bB, C, F) and strontianite is found as rosettes and bi-terminal crystals that grow on and between gypsum blades (Fig. 3.22D, E). Where calcite is visible amongst these precipitates, it is etched and/or hollow (Fig. 3.22F). A SEM image overview of a gypsum and strontianite free portion of the granular tufa facies shows the rock's bumpy, irregular fabric (Fig. 3.23A). Round protrusions are coated in corroded trigonal sparry calcite (Fig. 3.23B, C, E) or non-corroded sparry calcite with faceted crystal ends (Fig. 3.23D). Bacterial mucus and rod-shaped micrite are associated with the corroded spar, whereas non-corroded spar is

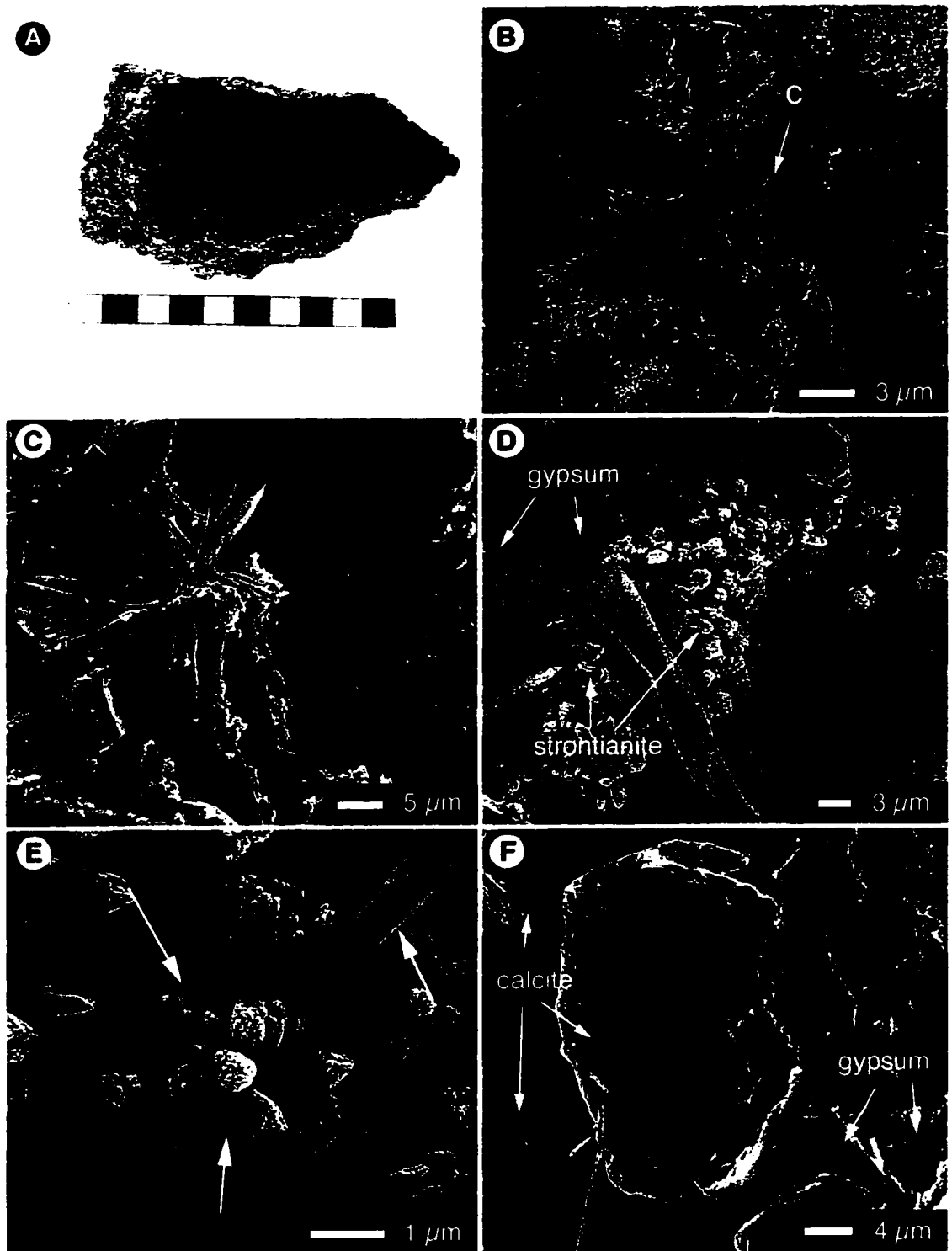


**Figure 3.22**

(A) Photograph of granular facies sample M12 collected from MS4. (B) SEM image overview of a gypsum dominated portion of handsample M12. (C) Detail of gypsum blades and fans from image B. (D) Strontianite rosettes found associated with gypsum blades. (E) Detail of strontianite rosettes and a bi-terminal strontianite crystal (arrows). (F) Where gypsum occurs amongst calcite crystals in handsample M12, the calcite is etched (background) and/or hollow (foreground).

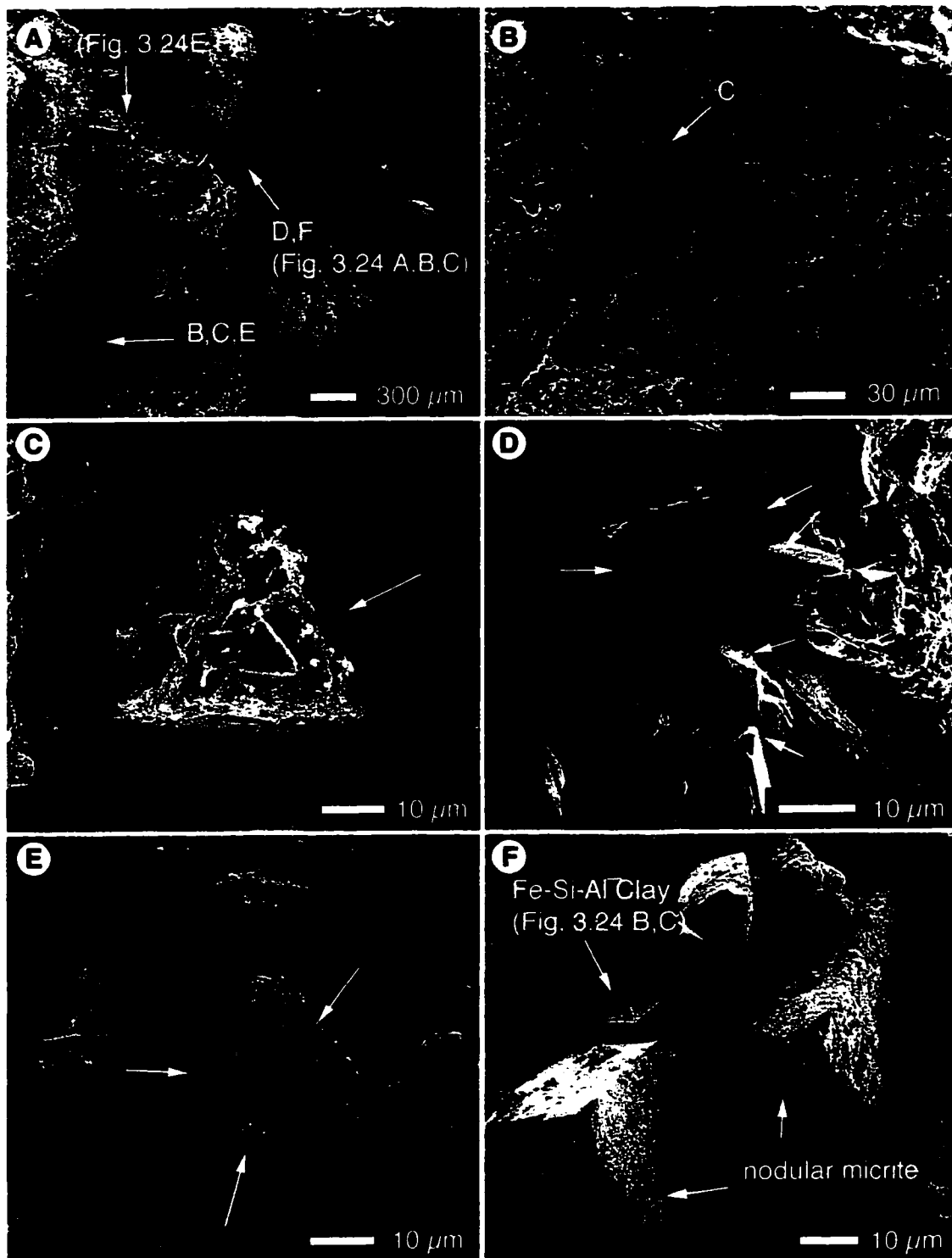


**Figure 3.23**

(A) SEM image overview of a calcite dominated portion of the granular facies sample M12. (B) Pocket of trigonal sparry calcite with corroded exteriors and internal void spaces. (C) Detail of corroded trigonal sparry calcite crystal from image B. (D) Non-corroded sparry calcite with faceted ends (arrows) found in a pocket adjacent to the corroded calcite in images B,C and E. (E) Bacterial mucus, and fibre micrite (arrows) are found in association with corroded sparry calcite crystals. (F) Detail of the faceted ends of non-corroded trigonal sparry calcite. Patches of nodular micrite and an Fe-Si-Al clay are found on the crystal faces.

patchily covered with nodular micrite and a reticulate Fe-Si-Al clay (Fig. 3.23F). The clay is found in cavities and niches between crystals (Fig. 3.24A) and also forms a bumpy, nodular coating in association with mucus on crystal faces (Fig. 3.24B, C). Areas lacking spar have irregular surface textures and contain preserved microbial filaments. 10  $\mu\text{m}$  diameter and 1.5  $\mu\text{m}$  diameter filaments were preserved through encrustation of their sheaths (Fig. 3.24D). Encrustation of one filament increased its apparent diameter three-fold (Fig. 3.24E, F). The calcite hosting the microbial fossils is nondescript, and has probably experienced some dissolution with diagenesis.

### *Interpretation*

The origin of this facies is enigmatic. Similar granular tufa textures are described by Janssen *et al.* (1999) in which the clasts were small pieces of detrital tufa or encrusted plants and branches that were deposited in pools. The granular tufa facies could be the diagenetic remains of a detrital tufa deposit, but it is not truncated at its sides or base, as one might expect a pool deposit to be.

A second possibility is that the granular tufa facies was developed through *in situ* decomposition of tufa in the upper ledge catalyzed by through flow of spring water with a different chemistry, which precipitated the gypsum and strontianite. The gypsum and strontianite are typical precipitates at the modern springs, and a shift in the spring water chemistry of a vent above the upper ledge could have resulted in the flow of calcite poor, gypsum and strontianite rich water through portions of the upper ledge tufa. If this spring water actively dissolved the tufa along paths of existing porosity, the tufa would lose its original texture, and might experience local collapse, generating a grain-stone like rock. Gypsum has been described as a “notorious source of stone decay” because of its tendency to recrystallize through periods of wet-to-dry cycling (Lewin and Charola, 1981), so its presence may also explain the lack of structure in the surrounding calcite. Differential flow of water through more or less porous parts of the rock could generate the variable hardness of the granular tufa facies.

The nodular clay coating found around calcite spar is similar to a reticulate clay coating described from boiling springs in Kenya and New Zealand (Fig. 2f-1 Jones and Renault, 1996b). Bacterial mucus is known to adsorb Si, Mg, Al and Fe from spring water, and the nodular clumps of clay are similar in size to bacterial bodies, so it has been



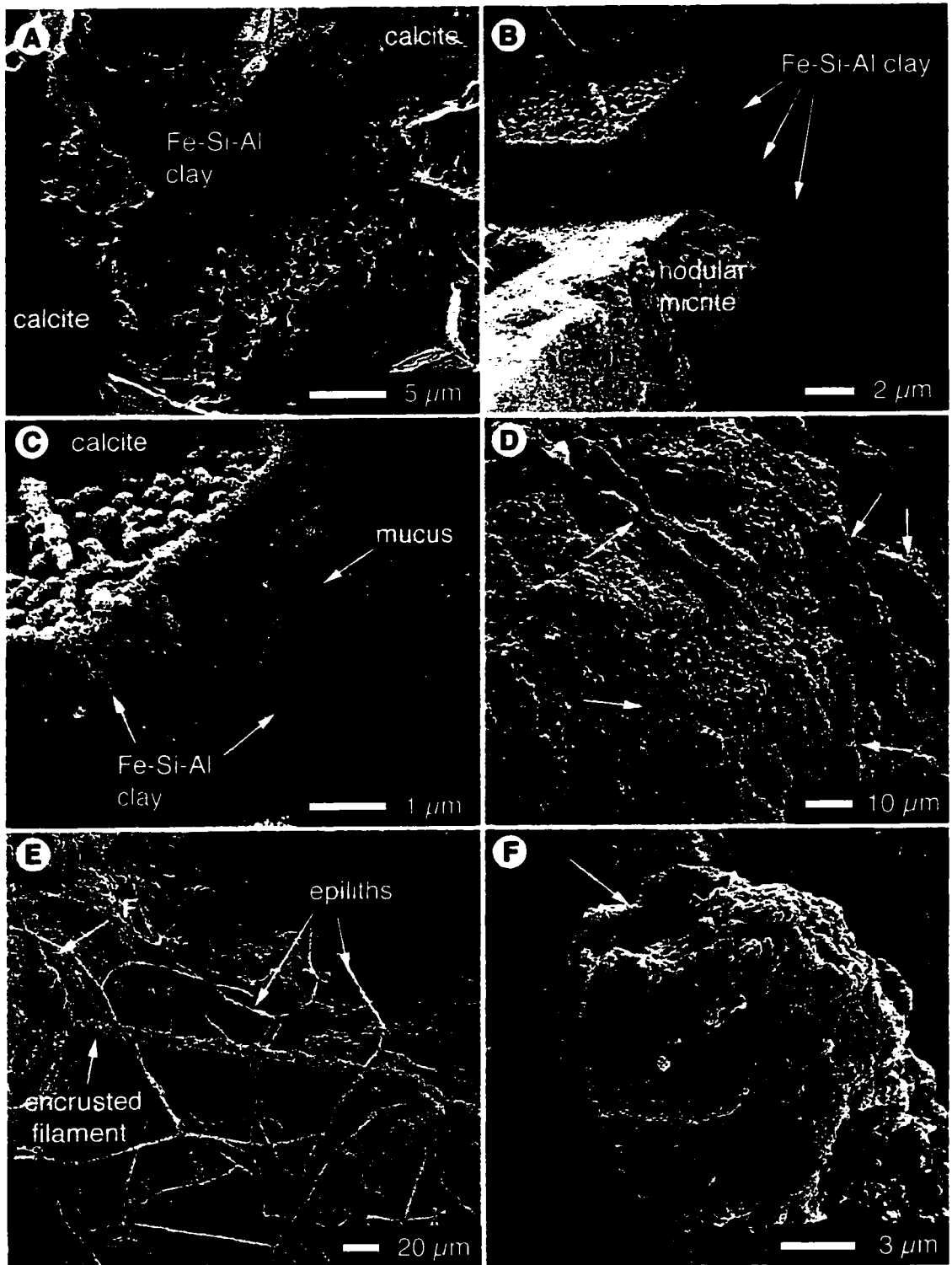


**Figure 3.24**

(A-F) SEM image of ganular facies sample M12 from MS4. (A) Fe-Si-Al clay filling a pocket between calcite crystals. (B) Bumpy coating of clay on a faceted calcite crystal with nodular micrite in the foreground. (C) Detail of image B. (D, E) Details of image 3.23A showing preserved filaments. The smaller filaments in image E are modern epiliths, the larger filament has been preserved through encrustation. (F) Detail of the end of the filament in image E - encrustation increased the filament diameter (arrow) three-fold.

suggested that precipitation of the clays is initiated by a concentration of elements in and about thermophilic bacteria and their exudates (Casanova and Renaut, 1987; Defarge *et al.*, 1994; Jones and Renaut, 1996b). Recent observations of Kenyan hot springs and geyser basins, however, suggest that the reticulate clay coatings may form as inorganic precipitates (Jones, pers. comm.). The occurrence of the clay coating in the Miette springs indicates that it is not restricted to boiling spring environments. Unfortunately, the clay coatings are not helpful for resolving the petrographic origin of the granular tufa; the facies has obviously been affected by diagenesis, and possibly been subject to through-flow of secondary spring waters.

### 3.3g *Bryophyte Facies (and Mineralised Wood)*

This facies is porous but hard and displays macroscopic features of the bryophytes that formed its organic substrate. It is found as lenses in flat-banded tufa, and comprises large mossy bed tufa deposits at MNN. Found as lenses, the bryophyte facies is heavily cemented and forms hummocks several feet in diameter and 15-45 cm high (Fig. 3.25A). The bryophyte facies lenses are composed of solid and sparry calcite that is punctuated by stem casts (Fig. 3.25B, C), arcuate void spaces left by the decomposition of moss leaves, and ostracode carapaces (Fig. 3.25D). The arcuate void spaces are bordered by crystalline crusts of blocky calcite spar, platy calcite, and “spiky” calcite (Fig. 3.25E, 3.26A, B). Unique crystalline precipitates (similar to those called “comb” or “brush” calcite (Buczynski and Chafetz, 1991)), wherein branching bristles of calcite stem from a rhombic calcite plate, are found in association with the crystalline crusts (Fig. 3.25F). In other instances, precipitation has taken place on both sides of a moss leaf or stem, generating a “sandwich” in which large calcite crystals radiate outwards from a central void space (Fig. 3.26C). The central void is partially filled with rhombohedral calcite plates (Fig. 2.36D), or filled or partially filled with blocky calcite (Fig. 3.26E), and blocks of solid calcite, composed of twinned calcite plates or blades, are commonly found above arcuate void spaces (Fig. 3.26F).

The bryophyte facies at MNN is less heavily cemented than bryophyte facies to its south, and details of the bryophyte morphology are apparent in hand sample. In SEM, arcuate and cylindrical voids generated by decomposition of bryophyte stems and leaves

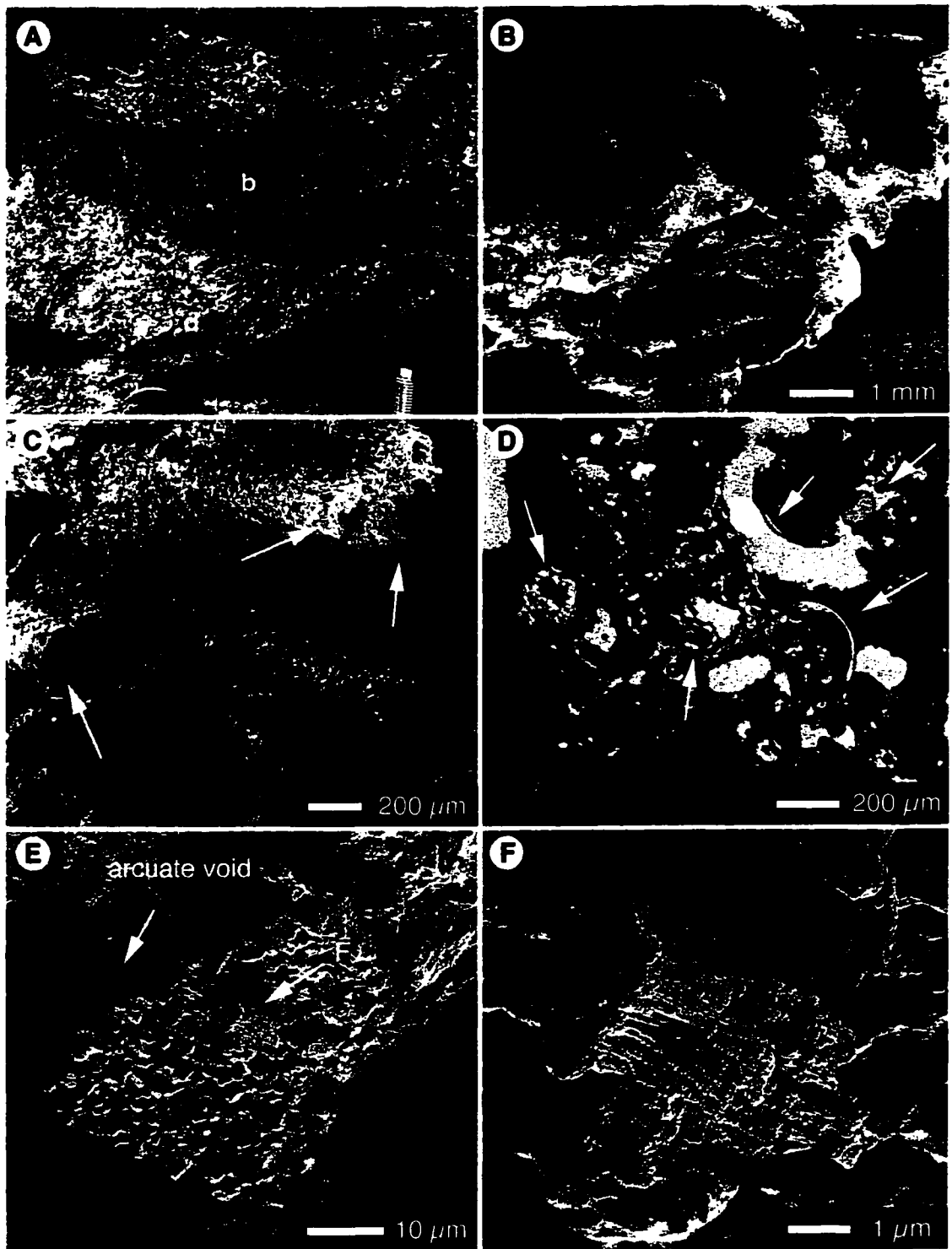


**Figure 3.25**

(A) Bryophyte hummock (b) sandwiched between crenulated facies (c) and dense laminar facies (d) in outcrop MS5. (B) SEM image overview of the bryophyte facies in sample M38 from MC1. (C) Bryophyte stem casts preserved in sample M38. (D) Thin section of sample M38 - arcuate forms are leaf casts infilled with calcite and cross-sections through ostracode shells. (E) SEM image of blocky calcite found above an arcuate void created by the decomposition of a bryophyte leaf. (F) Unique crystals are associated with the calcite that borders leaf casts. Buczynski and Chafetz (1991) describe a similar crystal habit as "comb" calcite.

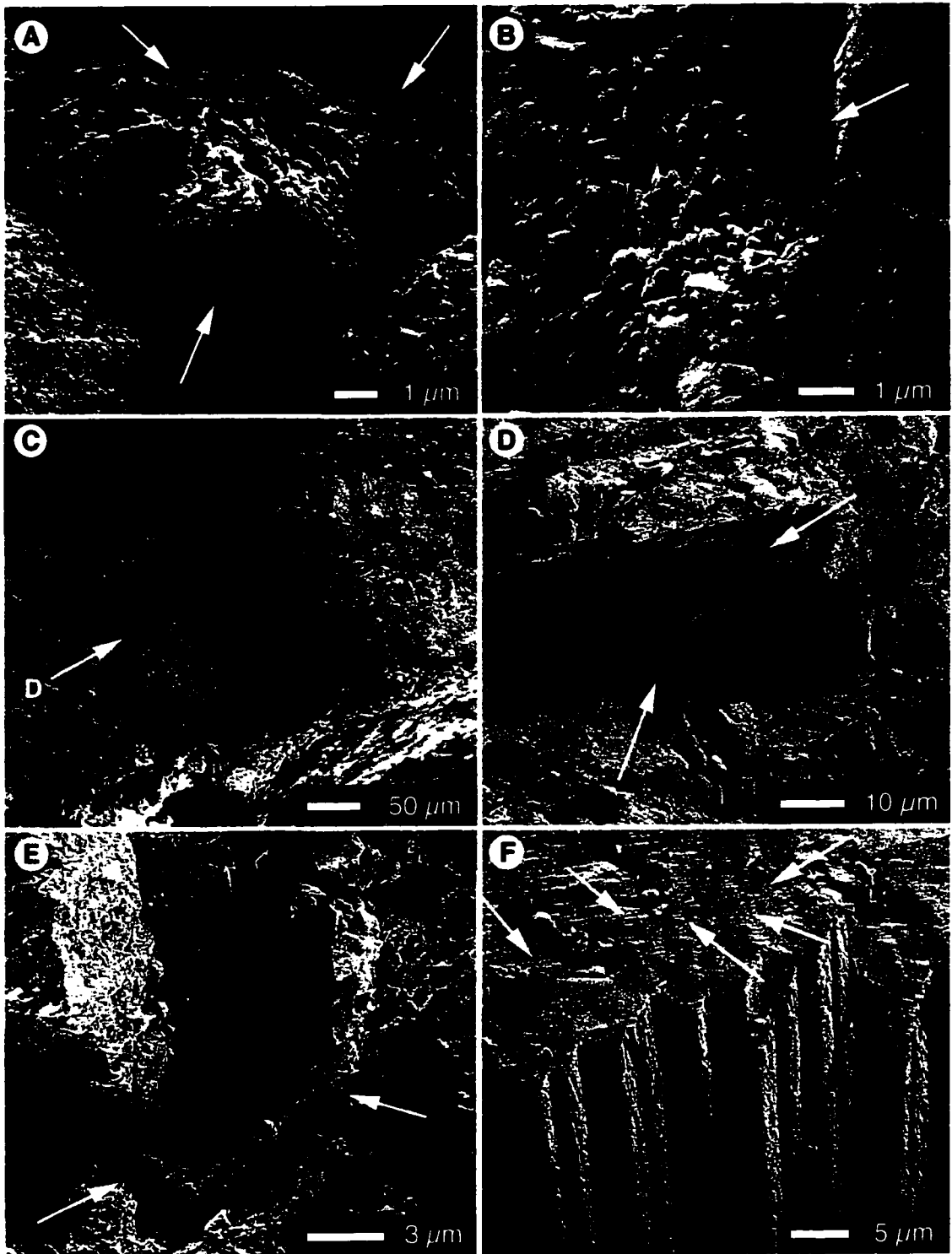


**Figure 3.26**

(A-F) SEM images of crystal habits found in association with replaced moss leaves and stems in bryophyte facies sample M38 collected from MCI. (A) "Snake" of platy calcite found filling an arcuate void left by decomposition of a moss leaf. (B) "Spiky" calcite crystals growing from a leaf surface. (C) Cross-section through a replaced moss leaf. The interior is porous and hosts rhombohedral calcite plates. (D) Detail of rhombohedral calcite plates from image C. (E) Solid blocky calcite fills an arcuate void left by decomposition of a moss leaf. (F) Blocks of solid calcite composed of twin calcite plates (arrows show crystal boundaries) are often found above arcuate voids.

are rarely filled with cements (Fig. 3.27A, E, F) though, locally, leaves were replaced by solid calcite (Fig. 3.27B) and individual plant cells were mineralized, preserving fine cellular details (Fig. 3.28A, B). The moss leaves acted as a nucleation substrate for solid calcite that grew upwards around filamentous microbes (with external diameters  $\sim 5\mu\text{m}$ ) whose preserved sheaths are found in cylindrical voids (3.27F, 3.28C-E).

Siliceous auxospores are abundant in the bryophyte facies at MNN (Fig. 3.28F), as are tests of the diatom *Orthoseira roseana* (Fig. 3.29), and ostracode carapaces with varying degrees of mineralization (Fig 3.30). Mineralised wood is also associated with the mossy bed tufa at MNN. The cellular structure of the wood is preserved in patches surrounded by solid and sparry calcite (Fig. 3.31A). Fine details like ray cells and pit connections were preserved (Fig. 3.31B, C) through replacement of the cellular material with microcrystalline trigonal or rhombohedral calcite (Fig. 3.31D). As with the preservation of bryophyte cells, only select wood cells are preserved; in some cases only the outer layer of cells is preserved, while elsewhere multiple layers of cells were mineralized (Fig. 3.31E, F).

Concave cavities are found in both the bryophyte tufa and the associated mineralized wood. These empty “bubbles” are defined simply by the truncation of surrounding crystals and lack any interior lining (Fig. 3.32).

### *Interpretation*

This facies is generated by encrustation of bryophyte colonies. Post-mineralization decomposition of plant material generated arcuate and cylindrical voids, some of which were filled with calcite cements producing the arcuate calcite observed in thin section. The unique crystal habits found in bryophyte facies occurring as lenses in other facies probably formed under the influence of bacterial communities living amongst the bryophytes. Buczynski and Chafetz (1991) demonstrated that formation of “comb” calcite is bacterially induced, and the “snakes” of platy calcite and sheets of “spiky” calcite may be similarly formed.

Bryophytes are subaerial, preferring moist but non-submerged substrates, and are not thermophilic; though some species have lethal temperature thresholds as high as  $50^{\circ}\text{C}$ , temperatures below  $30^{\circ}\text{C}$  are preferred for optimal growth (Kallio and Karenlampi, 1975; Proctor, 2000). Hummock forming communities are generally located above

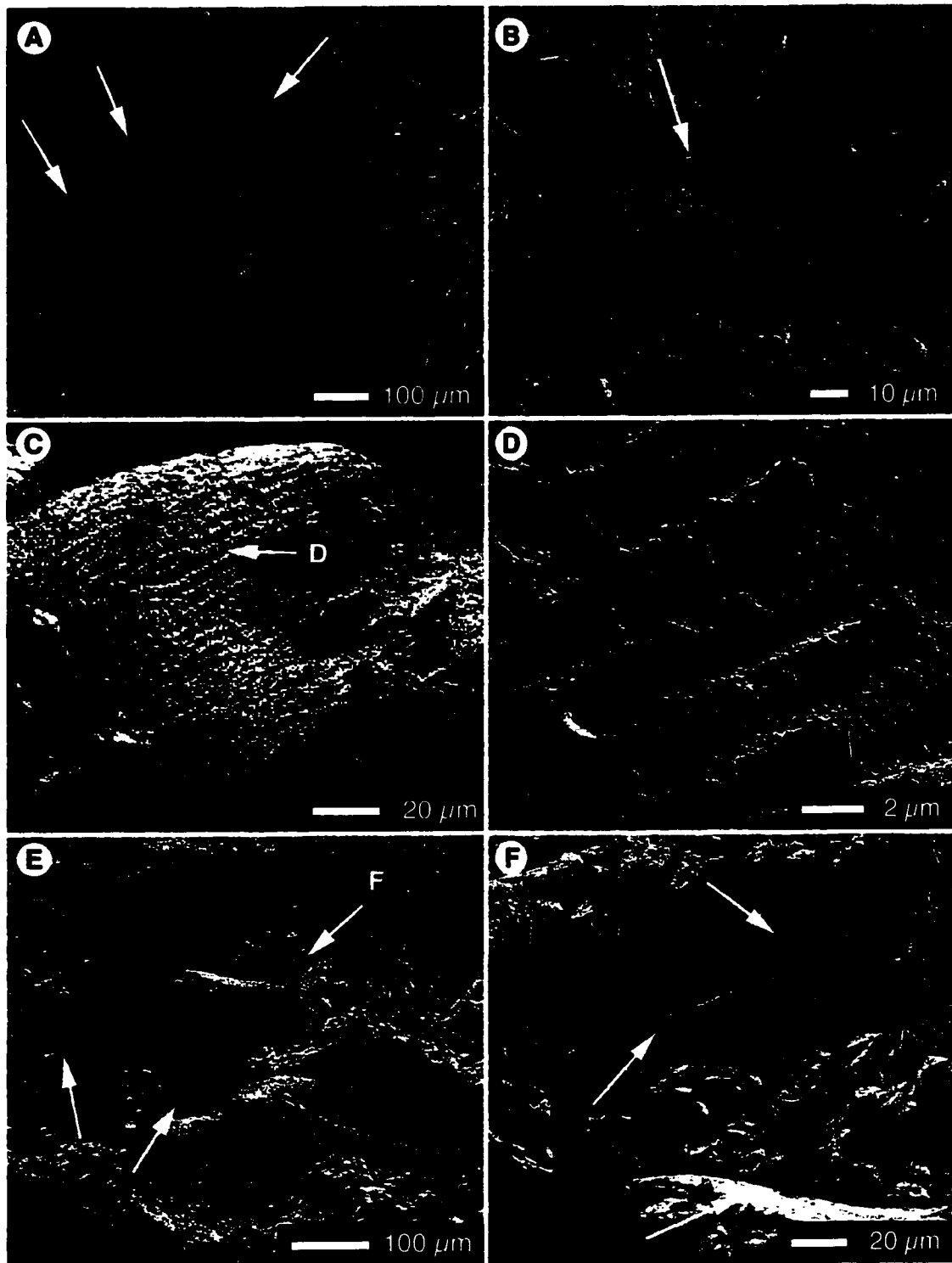


**Figure 3.27**

SEM images of bryophyte facies sample M59 collected from MNN1. (A) Decomposition of moss leaves and the stem they branched from generated arcuate void spaces in the calcite that surrounded them. (B) In this instance the void space was filled with calcite. (C) Cast of a leaf showing its cellular structure. (D) Detail of cell structure preserved on the surface of a leaf from image C. (E) Stem cast and casts of leaves that branched off from it. (F) A void space separates the cast of a leaf from calcite crystals that nucleated on the leaf. Microbial filament casts and body fossils punctuate the calcite above the leaf cast.

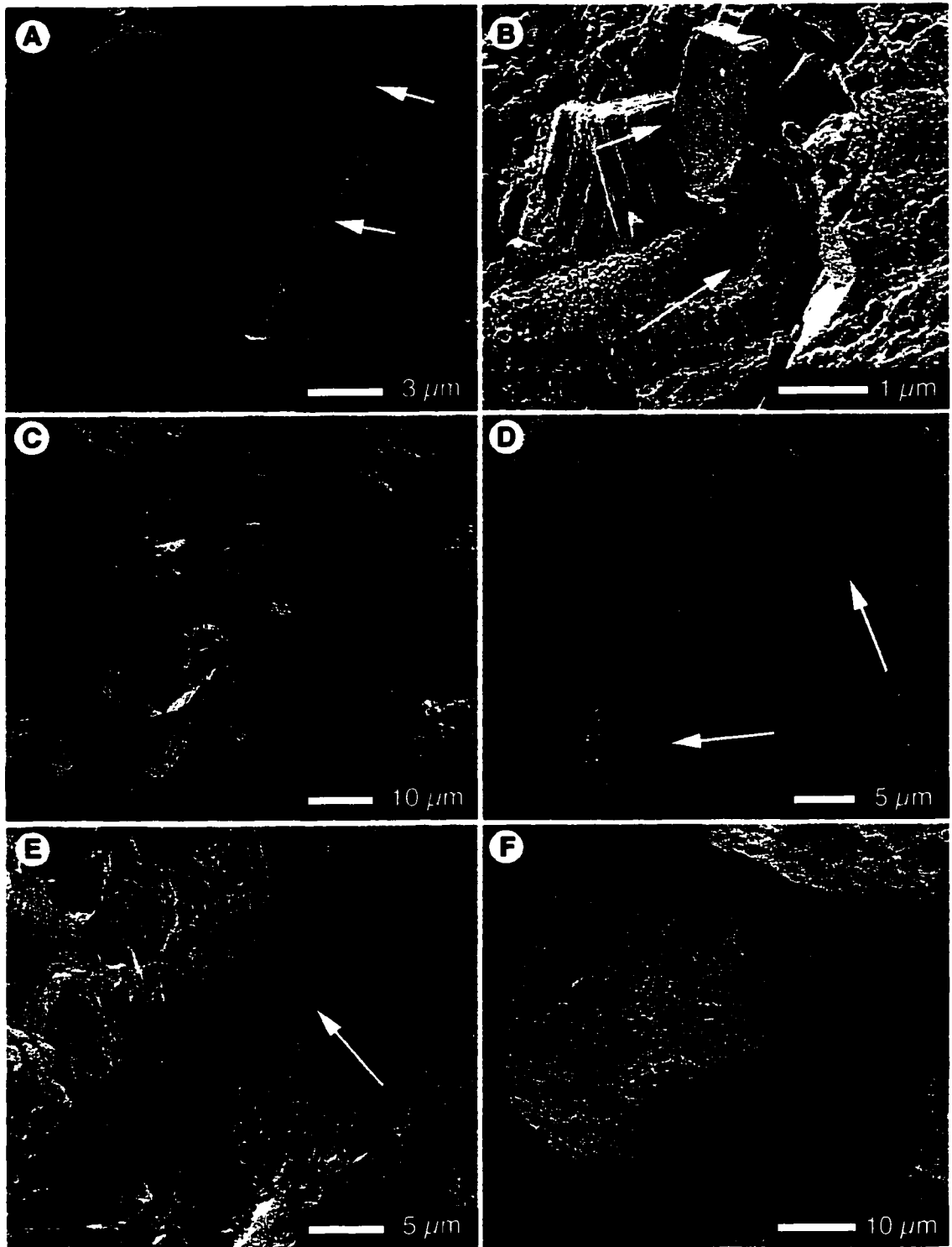


**Figure 3.28**

SEM images of bryophyte facies sample M59 collected from MNN1. (A) Calcified moss cells preserved at the edge of a leaf cast. (B) Detail of calcified moss cells showing a pit connection, and hexagonal cell walls. (C) Microbial filaments found in sparry calcite above a moss leaf cast. (D) Detail of microbial filament casts with collapsed and calcified sheaths. (E) Cylindrical cast left by decomposition of a microbial filament whose sheath was not preserved. (F) Siliceous algal auxospores such as this are found throughout sample M59.

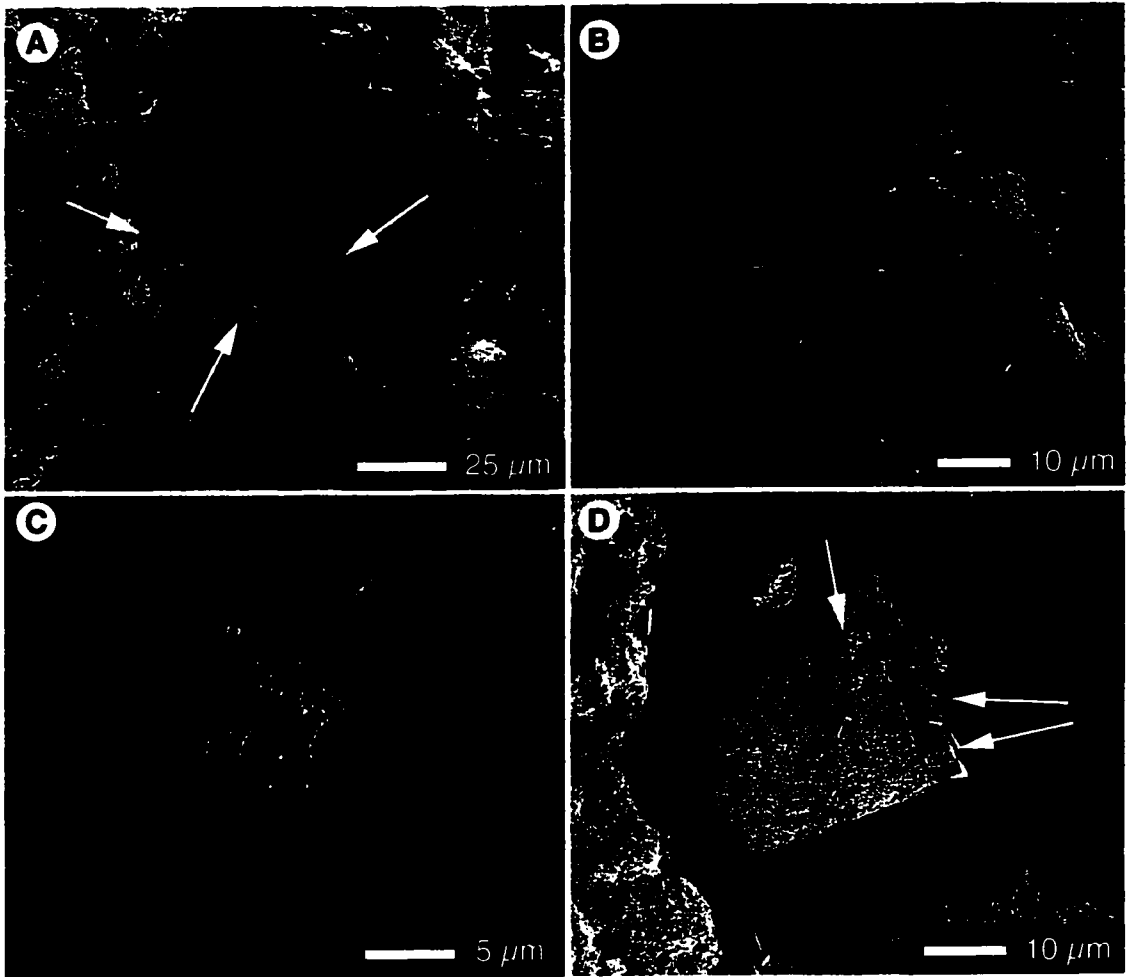


**Figure 3.29**

SEM images of the diatom *Orthoseira roseana* found in bryophyte facies sample M59 collected from MNN1. (A) Several specimens found amongst calcite spar and micrite. (B) Detail showing chained specimens of *O. roseana* in girdle view. (C) Valve view of *O. roseana*. (D) Girdle view of *O. roseana* with calcium oxalate crystals (arrows).



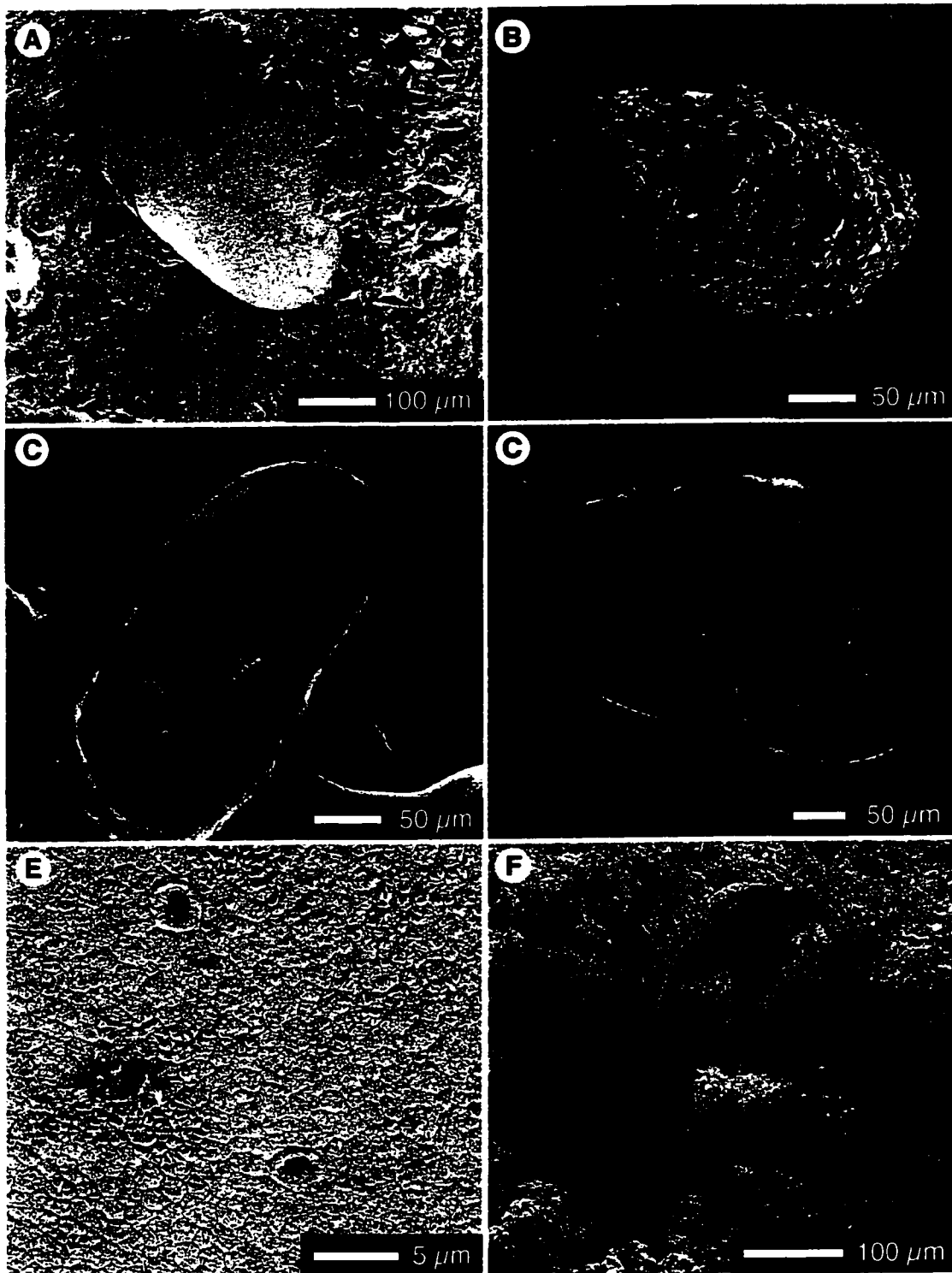


**Figure 3.30**

(A-F) SEM images of ostracodes. (A) External view of a carapace in bryophyte facies sample M38 from MC1. (B-D) Carapaces extracted from bryophyte facies sample M59 from MNN1 showing differing degrees of mineralisation: (B) shows paired valves with external mineralisation, (C) an internal valve view showing little mineralisation of a carapace that contains detrital pollen grains, (D) an internal view of a spar-lined valve. (E) Detail of the exterior of a well-preserved carapace found in sample M38. (F) Paired valves found in sample M38 that enclose sparry calcite but are not externally coated.

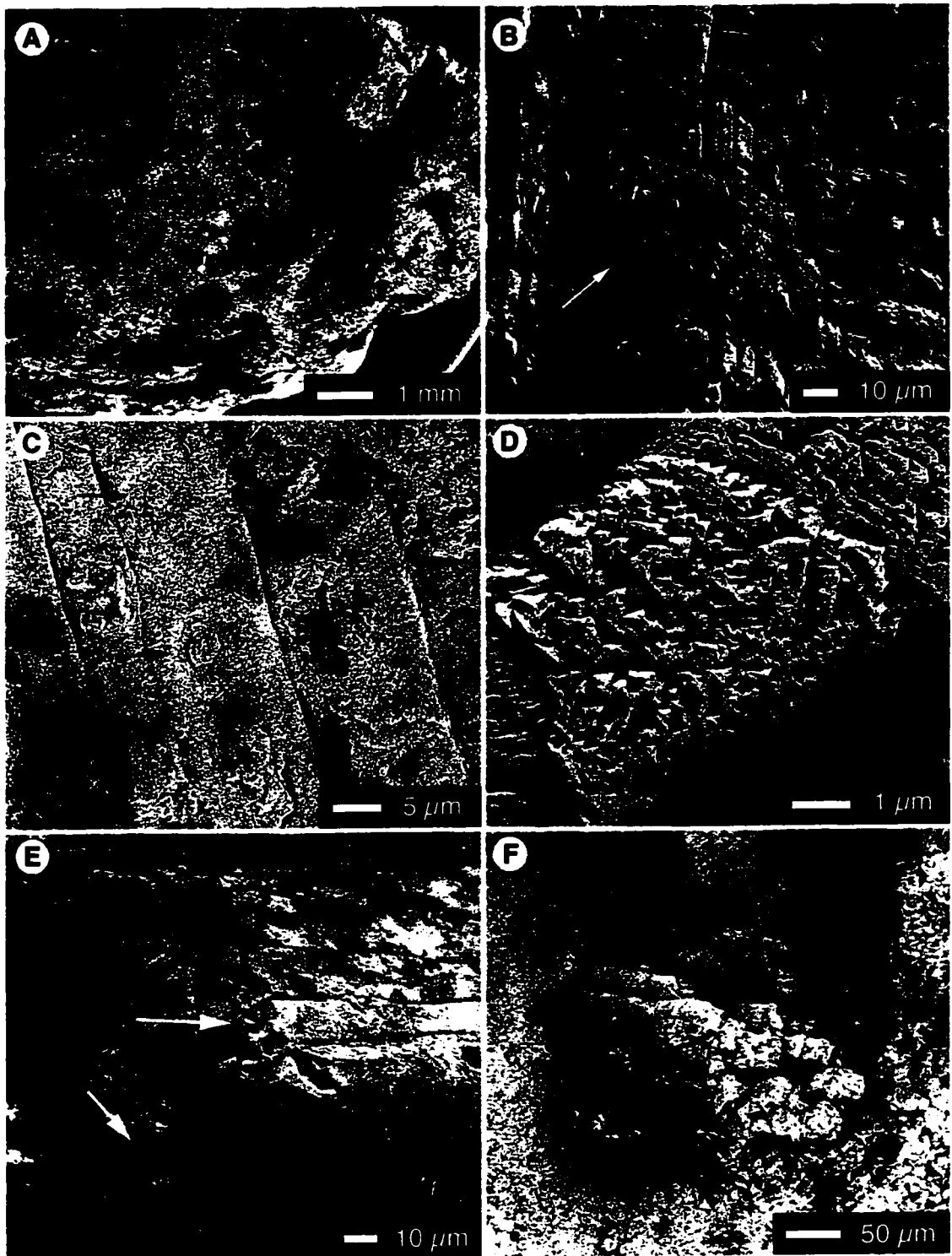


**Figure 3.31**

(A) SEM image overview of a piece of mineralised wood, M60, found at MNN2. Cellular structure (arrows) is preserved in patches surrounded by solid and sparry calcite. Fine details like ray cells (B) and pit connections (C) are preserved. (D) Detail of the surface of cells in image C; cellular material is replaced by trigonal and rhombohedral calcite. In some cases, only the outer layer of cells is preserved (D) while multiple layers of cells are preserved elsewhere (F).

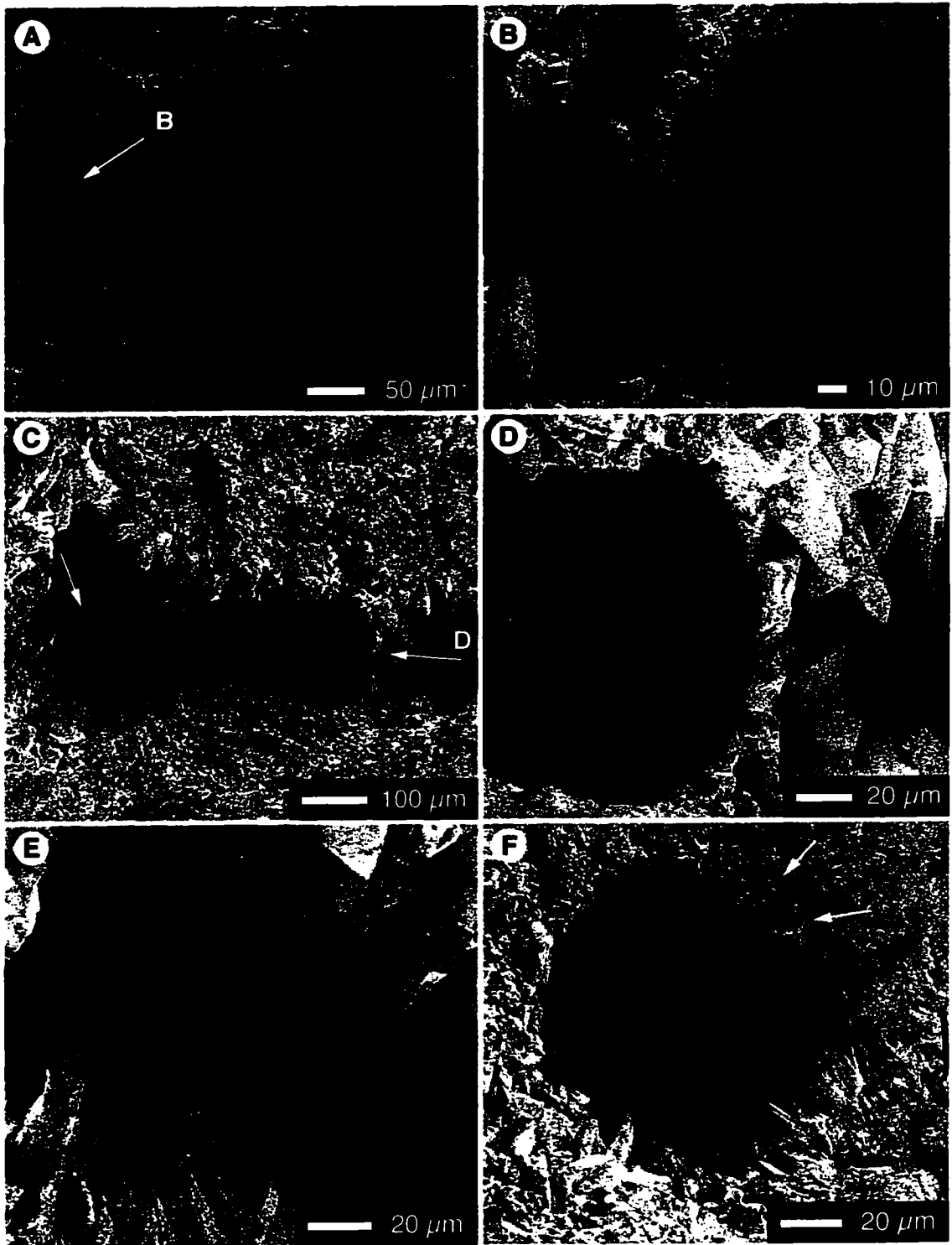


**Figure 3.32**

(A) SEM image of a "bubble" found in mineralised wood sample M60 collected from MNN2. (B) Detail of the previous image showing the interior of the bubble. It is defined by truncated crystals and is unlined. (C) A squashed bubble structure. (D) Detail of the right hand side of the bubble in image C. (E) Detail of the left hand side of the bubble in image C. (F) Another bubble which is surrounded by radiating calcite crystals (arrows).

maximum water levels (Janssens, 1990) and the lens generating bryophyte facies hummocks probably developed on dry areas of the spring mound where mineralization was facilitated by splashing spring water, rather than inundation. Bryophyte hummocks are favoured resting and breeding locations for animals grazing on surrounding vegetation (i.e. microbial mats)(Janssens, 1990), which explains the abundance of ostracode carapaces preserved in the bryophyte tufa.

At MNN, bryophytes were able to colonize the spring water flow path within 10m of the spring vent, forming mossy beds whose mineralization preserved details of the bryophyte community. *Orthoseira roseana* is a subaerial diatom known to colonize moss leaf niches, and ostracodes graze on plant material in damp environments (Spaulding and Kociolek, 1998). The siliceous auxospores and mineralized wood represent a detrital contribution from the surrounding forest. The excellent preservation of cellular details from the bryophytes and the wood require that the plant material be replaced by calcite before decay, and that it be submerged in water to facilitate diffusion of calcium and carbonate ions through the wood. This processes is poorly understood and infrequently reported from spring deposits. At Rabbitkettle Hot Springs, Yukon Territory, a high discharge rate, and thus delivery of ions to the wood, has been held responsible for wood calcification (Gulley, 1993).

The round “bubbles” found in the bryophyte facies are unusual. They could be concavities left behind when round objects (like ostracode carapaces or spores) were dislodged from them. However, some of the bubbles are squashed or distorted (Fig. 3.32c-e). They may be “coated bubble” structures. Coated bubbles with smooth interiors are formed by rapid calcification of gas bubbles (Chafetz *et al.*, 1991a), in this case probably methane generated by microbial mineralization of the bryophyte or wood tissue. The formation and preservation of these delicate features require that gas be trapped in stagnant or near stagnant water with rapid precipitation rates (Chafetz and Folk, 1984; Chafetz *et al.*, 1991a; Guo and Riding 1998). However, coated bubbles usually have a micritic lining basal to larger crystal growth (Guo and Riding, 1998) and/or a three-layered structure consisting of inner stellate crystals, a middle layer of radiating needle crystals, and an external layer of radiating spar crystals (Chafetz *et al.*, 1991a). If the

bubbles in the MNN bryophyte tufa are coated bubbles, either the micritic envelope has been lost, or layering is not a true architectural requirement for bubble mineralization.

### 3.3h *Massive Facies*

The massive tufa facies is found throughout the fossil Miette tufa exposure from MS to MNN and is commonly capped by thin beds of streamer tufa. It is a dense, featureless, carbonate rock (Fig. 3.33A). SEM analysis revealed very little porosity, and no distinguishing textural features (Fig. 3.33B). In thin section, large radiating calcite crystals abut one another (Fig. 3.33C), and some vestigial textures – such as a cross section through a vertical column from stromatolitic tufa – are visible (Fig. 3.33D).

#### *Interpretation*

This facies is diagenetic and originated through recrystallization and cementation of more porous tufa facies.

### 3.4 *Original Deposit Morphology and Depositional Context of the Facies*

By coupling the interpreted depositional environment for each textural facies with the morphotypes in which it is found, it is possible to reconstruct a profile of the fossil spring system during its activity. The MNN mossy bed tufa deposits are markedly different from the rest of the fossil tufa and are described by a separate profile.

At MS, MC and MN (Figure 3.34), the waters of several springs emerged in vent pools that were surrounded by spring mounds. The spring precipitates prograded down slope, and merged to form a ledge at the elevation of the springs. Beneath this, spring water flowed steeply down slope to Sulphur Creek. The spring water flow path was colonized by filamentous microbes (including species of *Phormidium*, *Oscillatoria* and possibly *Calothrix*) that were incidentally preserved in some precipitates and organized the structure of others. The bedded facies was deposited around the spring vents, streamer facies formed where filamentous microbes colonized tributaries of swiftly flowing water, and the dense laminar facies formed on microbial communities growing beneath thin sheets of flowing water in the proximal spring flow path, whereas the porous laminar facies formed down slope. Landslide debris was stabilized by calcite cements

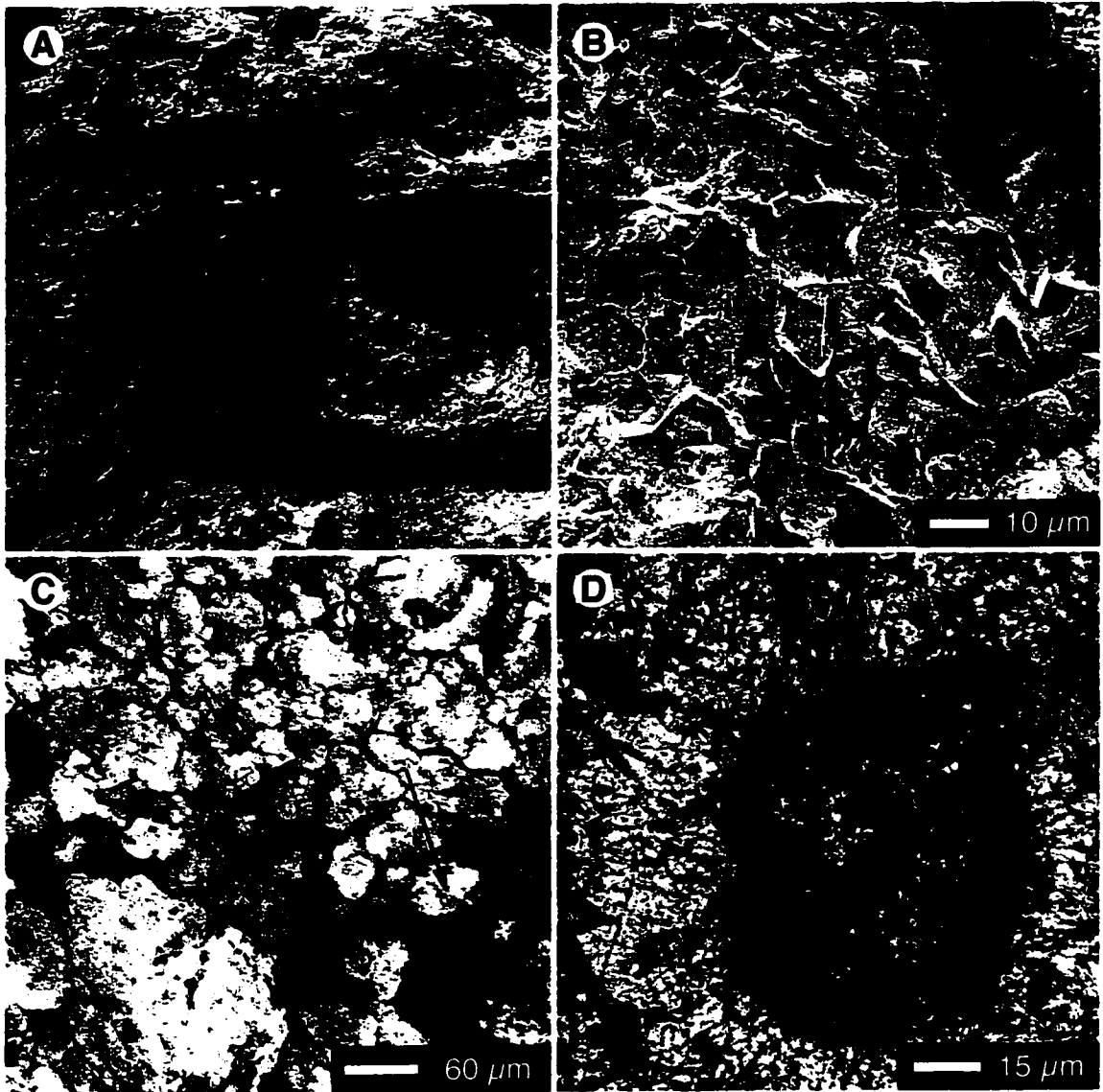


**Figure 3.33**

(A) Photograph of the massive facies in outcrop near MN1, a pencil is shown for scale. (B) SEM image of a subsample of M44 (from MN1) showing the low porosity of this facies. (C) Thin section of M44 showing large recrystallised calcite crystals and smaller splaying calcite mosaic spars (arrow) in pore spaces. (D) Thin section of M44 showing a cross-section through a columnar structure with a micritic core surrounded by radiating sparry calcite crystals.

**Tufa Morphotypes:**  
 D - domal tufa                      V - vertical tufa  
 R - roll over tufa                  F - flat banded tufa  
 W - wedge shaped tufa          M - mossy bed tufa

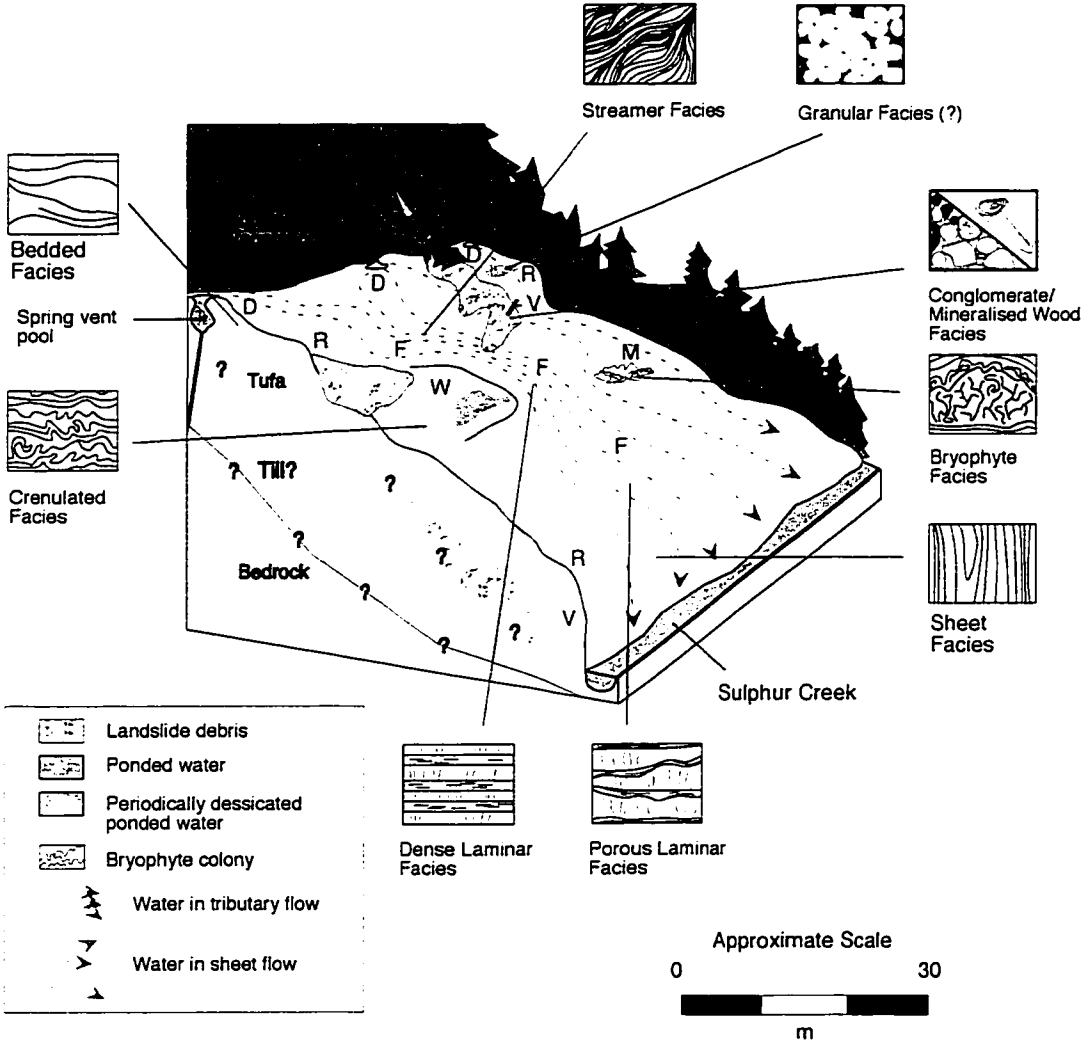


**Figure 3.34**

Idealised profile of an actively precipitating spring slope showing the hypothesized depositional environments and associated tufa facies and morphotypes found in the MS, MC, and MN fossil tufa deposits at Miette Hot Springs.

and eventually colonized by microbial communities generating the tufa/allochthonous lithoclast conglomerate facies; the sheet facies precipitated where water flowed down steep inclines; periodically hydrated depressions generated the crenulated facies and were gradually filled with precipitates producing wedge-shaped tufa morphologies; and, bryophyte colonies exploited raised parts of the mound, whose re-hydration resulted in the incorporation of bryophyte hummocks in other facies.

At MNN (Figure 3.35), the deposit is dominated by sheet and bryophyte tufa. The bedded tufa facies was deposited around the spring vent, which emerged from a shallow pool, and streamer facies are found between the FSVP and the upper ledge, where the spring water flow rate was high. Beneath the upper ledge, the water flowed over a succession of sharp drops and small bryophyte colonized ledges generating a down slope alternation of sheet and bryophyte tufa. Woody debris that fell into the spring water flow path was selectively mineralized. At the base of the deposit, a broad ledge colonized by bryophytes was preserved, generating the mossy bed tufa morphology. There may have been more precipitation down slope from this, but these precipitates were cleared to build the Aquacourt facility, so their nature cannot be known. Most likely, bryophyte colonies extended down to the level of the creek, forming a large mossy bed tufa fan.

The two profiles shown in figures 3.34 and 3.35 are idealised for the sake of clarity. The Miette tufa was episodically rearranged by landslides during its growth, locally vegetated by grasses and other plants, and the spring vents migrated down slope several times, emerging through and altering pre-deposited tufa. The actual morphology of the spring deposits at a given point in time is impossible to reconstruct - it was complex and facies alternations occurred in response to both gradual and episodic changes in depositional conditions.

### *3.5 Facies Alternations*

Facies alternations in the Miette fossil tufa take place over short vertical and lateral distances juxtaposing facies generated in contrasting depositional conditions. These alternations can be explained by:

- (1) Progradation of the tufa mound



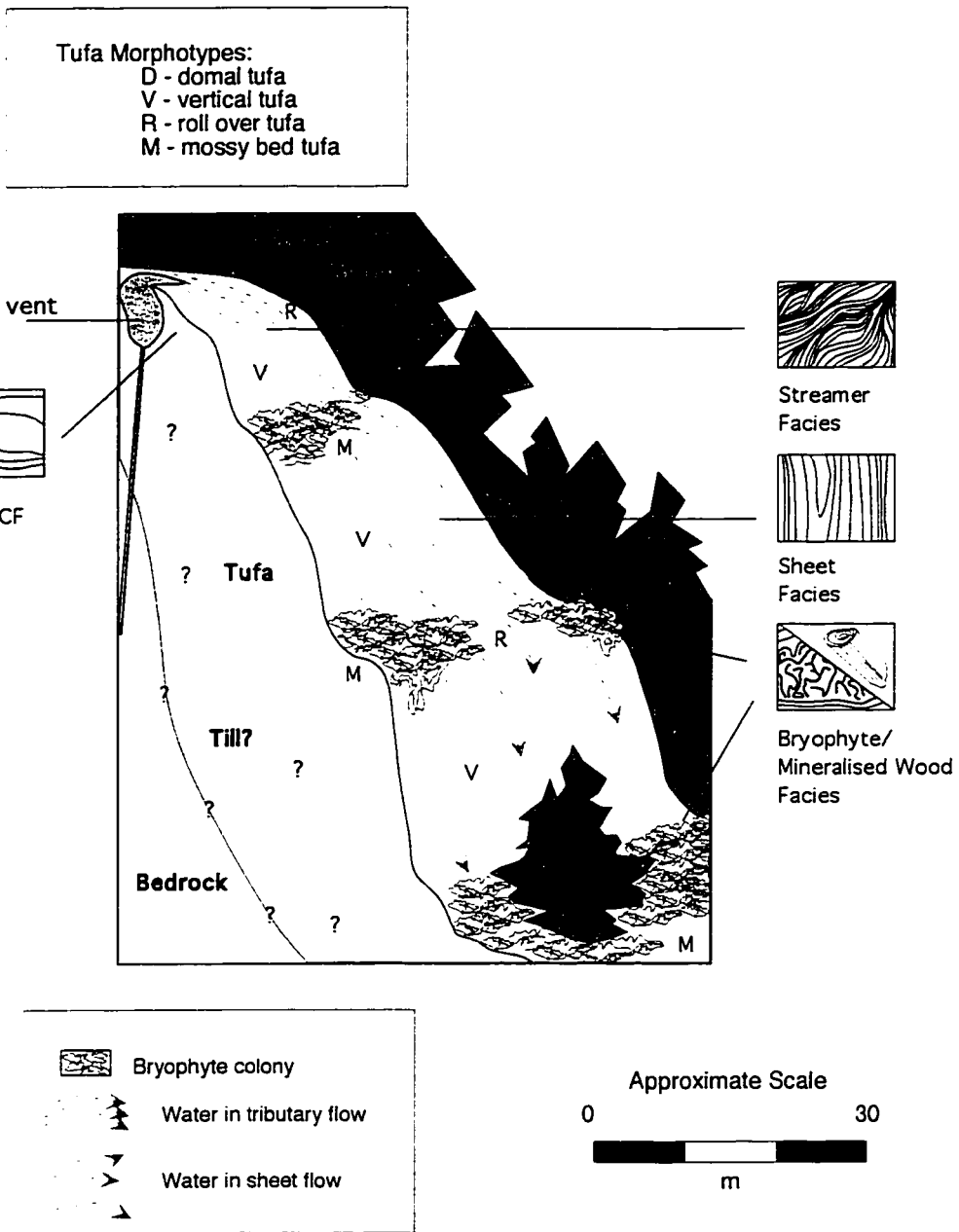


**Figure 3.35**

Idealised profile of an actively precipitating spring slope showing the depositional environments and associated tufa facies and morphotypes found at the far north end of the fossil Miette Hot Spring tufa deposit.

As the spring mound progrades, depositional environments will change accordingly. For example, an increase in the size of the spring mound will generate more proximal slope wash deposits.

(2) Relocation of spring water discharge

Flow paths relocate as tufa growth blocks old routes or makes new ones more favourable. This may leave stagnant water where there were once high flow rates, or inundate a dry surface; thus, the crenulated facies might succeed a stromatolitic facies, and a bryophyte facies hummock might be engulfed by a facies formed in flowing water. At MS5 and MS6 tree stumps are rooted in massive tufa and covered over by streamer tufa. A hiatus in spring water flow to that area allowed saplings to grow to significant size (the stumps have base diameters of 10 and 18 cm).

(3) Fluctuations in the flow rate of the spring water

Higher flow rates will result in stronger currents, allowing warmer water to travel farther before cooling, increasing the range of high temperature facies. In contrast, a decrease in the flow rate of the spring would restrict high temperature facies to the proximal vent area. Intercalated dense and porous laminar facies deposits, and the streamer facies tufa that coats many flat-banded tufa blocks, record waxes and wanes in the spring water flow rate.

(4) Fluctuations in the temperature or rate of cooling of the spring water

Hotter waters promote the growth of filamentous microbes and generate microbially controlled facies, whereas cooler waters are more inviting to higher taxa and generate bryophyte facies tufa. At MNN, the abundance of bryophyte facies tufa indicates that these deposits precipitated from cooler water.

(5) Relocation of the spring vent

There is evidence that the spring vents at Miette migrated downhill several times. Facies relocated concurrently, juxtaposing proximal and distal

facies, and later stage spring waters may have facilitated degradation of pre-deposited tufa they emerged through.

(6) Periodic reorganization of the tufa mound by landslides and rockfalls

The Miette tufa sat on an unstable slope affected by landslides and rockfalls. Huge blocks of tufa were broken off, rolled down slope, and then coated by new precipitates. This resulted in the juxtaposition of non-conformable facies with discordant depositional laminae. The landslides also brought material down from the slope above the springs, introducing clastic debris that was cemented together to form the tufa/allochthonous lithoclast conglomerate facies.

### 3.6 *Summary*

The fossil tufa deposits at the Miette Hot springs precipitated from the effluent of a line of perched springs. The morphology of the precipitates changed with distance from the vent, and was controlled underlying topography. Variations in the vegetation, amount of allochthonous debris, slope angle, and in the temperature, and flow rate of the spring water resulted in the development of nine facies: the streamer facies, porous laminar facies, and dense laminar facies contain stromatolitic layering; the bedded facies, crenulated facies, and bryophyte facies are non-stromatolitic but have biologically controlled textures; the tufa/allochthonous lithoclast conglomerate is a detrital facies; the origin of the granular facies is enigmatic; and the massive facies was generated by diagenetic recrystallization and cement growth. Each facies formed in a unique depositional environment, and reorganization of these environments resulted in juxtaposition of non-conformable

## 4 Stable Isotope Study of the Stromatolitic Tufa

### 4.1 Introduction

Stromatolitic layering is one of the most common features of both calcareous and siliceous spring precipitates. In calcareous deposits, the stromatolites generally display couplets of light and dark laminae in a cyclic, varve-like pattern (e.g., Chafetz *et al.*, 1991b). The alternation of light and dark laminae may be due to seasonal changes in the spring system, with each laminar couplet recording a year of precipitation. Pentecost and Riding (1986) found that the lighter coloured laminae commonly represent summer precipitation and darker laminae are generated by winter precipitation. In different localities, laminar alternations have been attributed to seasonally controlled differences in the rate of biological processes and to the growth of different microbial taxa during different seasons (Pentecost and Riding, 1986; Chafetz *et al.*, 1991b).

Stromatolitic laminae defined by an alternation of upright and flat-lying microbial structures are reported from both siliceous and calcareous spring deposits (Pentecost and Riding, 1986; Jones *et al.*, 1998; Konhauser *et al.*, 2001). Chafetz *et al.* (1991b) used stable oxygen isotope analysis to examine successive laminae in travertine stromatolites from the Arbuckle Mountains in Oklahoma and from the Eocene Palm Park Formation in south-central New Mexico. They demonstrated that a seasonal difference in microbial growth controlled the fabric of the stromatolitic travertine: at both localities, laminae containing sparry calcite and upright biogenic structures have  $\delta^{18}\text{O}$  signatures typical of spring-summer precipitation temperatures, whereas the  $\delta^{18}\text{O}$  of laminae composed of micritic calcite and flat-lying biogenic structures corresponded to fall-winter conditions (Chafetz *et al.*, 1991b). Alternating microbial filament orientations are not always seasonally controlled, however; some are attributable to the activity of phototactic microbes that change orientation in response to light variations. One example is *Phormidium hendersonii*, a common species in shallow marine stromatolites, whose trichomes turn upwards toward incident sunlight by day and lie prostrate at night (Monty, 1976). Conversely, the filamentous bacterium *Chloroflexus* migrates vertically at night, due to positive aerotaxis, responding to reduced  $\text{O}_2$  levels induced by respiration (Doemel and Brock, 1977). At geothermal springs in Yellowstone National Park, the orientation

of microbial filaments in siliceous stromatolites has been attributed to phototactic behaviour in resident microbial populations and, hence, each laminar couplet represents a day of growth (Walter *et al.*, 1976). Seasonal inconsistency in the growth of the microbial populations complicates matters, however; only 70% of summer days were recorded by laminar couplets and even fewer couplets formed in the winter. Thus, a seasonal control is also enforced, and may overprint diurnal controls (Hinman and Lindstrom, 1996).

The factors that control laminae alternation in hot spring stromatolites are easiest to identify if the system is still actively precipitating. A change in the dominant microbial taxa, for example, could be identified by sampling. Other investigative methods have involved collecting precipitates known to have formed in a particular season, comparing their  $\delta^{18}\text{O}$  values with those of discrete laminae (Chafetz *et al.*, 1991b; Guo *et al.*, 1996; Janssen *et al.*, 1999), and experimenting with the stromatolite-forming microbes to observe physiological responses to environmental stimuli (Monty, 1976; Doemel and Brock, 1977). If the system has ceased precipitation, none of these investigative routes is feasible.

Seasonal, or temperature dependent, controls can be investigated through stable isotope analysis of relict precipitates. Temperature changes in the spring water may be reflected in the stable isotopic composition of the spring precipitates, providing they were precipitated in isotopic equilibrium (Andrews *et al.*, 1997). Thermal spring waters cool as they achieve greater distances from the spring source; thus, the temperature calculated from a measured stable isotopic ratio may not be the maximum temperature of the waters at the spring orifice. Spring waters will not cool below the ambient temperature of the environment. Thus, seasonal variation in ambient air temperature can be recorded in the oxygen isotopic signature of precipitates at any point in the spring outflow path. Stable isotopes of carbon do not show strong fractionation with temperature, but photosynthesis preferentially takes up  $^{12}\text{C}$ , leaving the remaining pool enriched in  $^{13}\text{C}$ . Photosynthesis is usually more efficient in summer than winter because the climate is more conducive to growth, and light intensities are higher and longer. Thus, precipitates formed in the summer are expected to have heavier stable carbon isotopic signatures. These stable

isotopic effects can allow investigation of seasonal effects on mineral precipitation and spring ecology (Chafetz *et al.*, 1991b).

#### 4.2 *Stromatolitic Layering in the Fossil Miette Tufa*

Both the porous laminar facies (PLF) and dense laminar facies (DLF) found in the fossil tufa at Miette contain stromatolitic layering. In the PLF, laminae are defined by a thickness and density contrast between layers and by an alternation in the orientation of the component microbial filaments. In the DLF, laminae are defined by a colour contrast and an alternation of filament structure orientation.

The cause of the alternation of laminations in both facies is unknown. It is difficult to determine because precipitation has ceased, the amount of time represented by individual laminae is unknown, and the laminar stacking may not be temporally continuous. Vertical sequences of laminar growth may be locally truncated by periods of reduced precipitation and, at Miette, the emplacement of landslide debris and the growth of the tufa mound changed the topography of the hill slope and rerouted the discharging spring water repeatedly. Since precipitation occurs only in hydrated areas, successive stromatolitic laminae may not be temporally conformable.

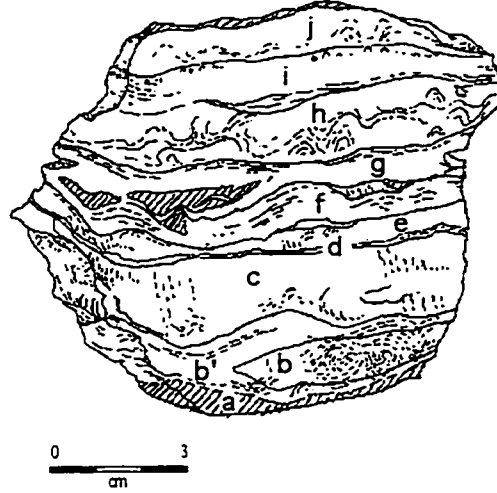
The two stromatolitic facies contain preserved cyanobacterial filament sheaths, filament casts, and filament structures generated by mineralization around microbial filaments. In many instances, filament structures are continuous, bending between vertical and horizontal orientations between laminae. These facies, however, embrace a number of different sized filaments. Arp *et al.* (1999) examined biomarker compositions in tufa from Pyramid Lake, Nevada and demonstrated that the primary cyanobacterial populations were subject to significant temporal changes in their species distribution during the growth of macroscopically homogeneous stromatolitic tufa. Thus, they concluded that the species composition of the cyanobacterial community may not be critical to the development of laminar textures in microbial carbonates. The homogeneity of the dense and laminar tufa facies across the Miette fossil tufa outcrop, which no doubt had different cyanobacterial populations across its breadth, indicates the same. Thus, the laminar alternations are not attributed to changes in the cyanobacterial species.

The thickness of the laminae in the fossil Miette tufa is too great to have accumulated during twenty-four hour periods – precipitation rates of 0.5-2 cm/day are unheard of, even in large spring systems (Gulley, 1993). Thus, it is unlikely that diurnal changes in light intensity were responsible for the alternation between upright and flat-lying microbial structures in either facies. Given that a diurnal control is improbable, a seasonal control was hypothesized and tested through stable isotope analysis of successive laminae in four representative hand samples. Samples M22 and M9 are representatives of the PLF, and M24 represents the DLF. Sample M13 represents a transitional texture between the PLF and DLF (Fig. 4.1-4.4). Bulk stable carbon and oxygen isotopes from laminated and non-laminated samples collected from a vertical transect at the north end of the Miette tufa exposures were also analysed to assess whether down-slope cooling of the spring water was reflected in the isotopic composition of the precipitates.

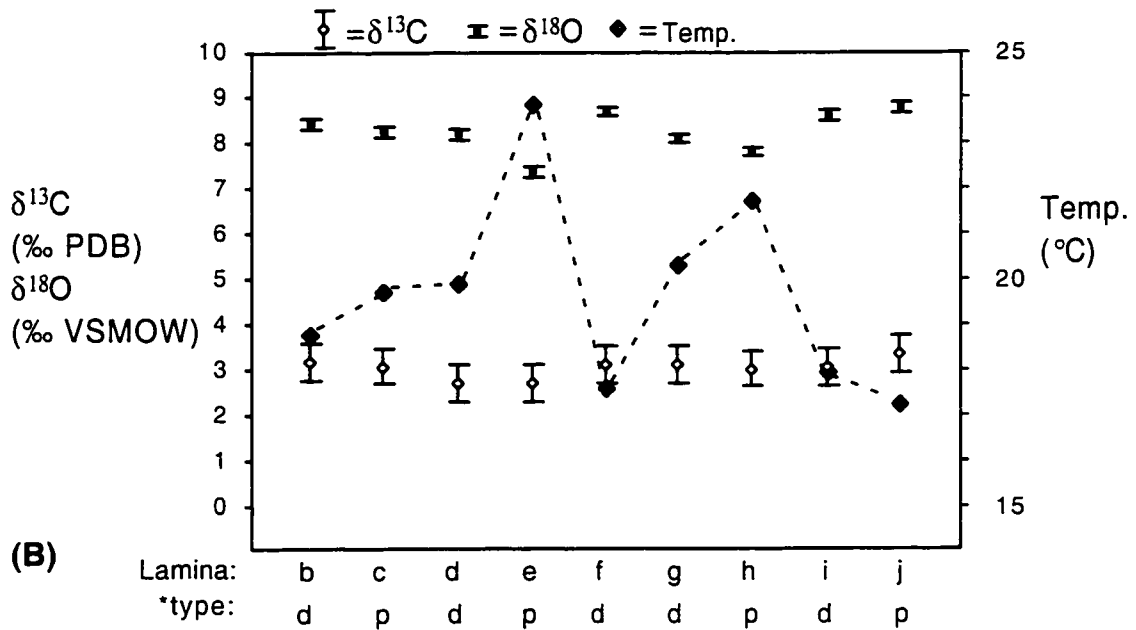
#### 4.3 *Results and Interpretation*

NBS-18 and NBS-19 standards run with the samples yielded results within their standard deviations, so all results may be referenced to the VSMOW and PDB scales. The average standard deviation between repeated samples is 0.11 ‰ for the  $\delta^{18}\text{O}$  values, and 0.41 ‰ for the  $\delta^{13}\text{C}$  values. These values are quite high (standard deviations in Chafetz *et al.*'s (1991b) study were an order of magnitude smaller) and indicate that stable isotope values are not homogeneous within individual laminae. Results are compiled in Appendix 1.

Samples from the PLF showed no distinct trend in either the stable carbon or oxygen isotopic signature between dense and porous laminae (Fig. 4.1, 4.2). Sample M9 had  $\delta^{13}\text{C}$  values ranging from 0.88 to 2.61 ‰ PDB, but there is no difference between the average values of laminae with upright and flat lying microbial structures (2.10 and 2.12 ‰ PDB, respectively). The  $\delta^{18}\text{O}$  values range from 5.77 to 7.10 ‰ VSMOW, but the greatest difference observed between successive laminae is only 0.7 ‰. Sample M22 had  $\delta^{13}\text{C}$  values ranging from 2.75 to 3.40 ‰ PDB and  $\delta^{18}\text{O}$  values ranging from 7.43 to 8.82 ‰ VSMOW. Again, differences between adjacent laminae are not significant.



(A)



(B)

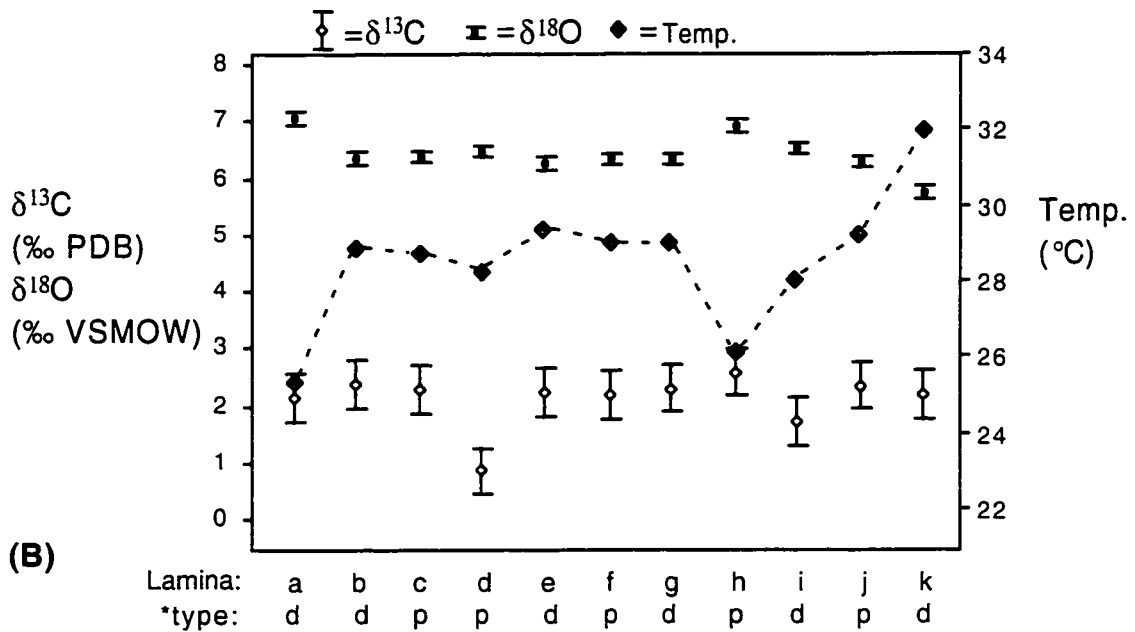
**Figure 4.1**

(A) Drawing of porous laminar facies sample M22 showing individual laminae sampled. (B) Stable carbon and oxygen isotope values measured for successive laminae and the estimated precipitation temperature calculated by Kim and O'Neil's (1997) equation for the precipitation of calcite from water under isotopic equilibrium - \* d = dark coloured lamina with flat-lying microbial structures, p = light coloured lamina with upright microbial structures.





(A)



(B)

**Figure 4.2**

(A) Drawing of porous laminar facies sample M9 showing individual laminae sampled. (B) Stable carbon and oxygen isotope values measured for successive laminae and the estimated precipitation temperature calculated by Kim and O'Neil's (1997) equation for the precipitation of calcite from water under isotopic equilibrium - \* d = dark coloured lamina with flat-lying microbial structures, p = light coloured lamina with upright microbial structures.

Sample M13 – a transitional facies – had  $\delta^{13}\text{C}$  values ranging from 1.87 to 2.13 ‰ PDB and  $\delta^{18}\text{O}$  values ranging from 6.90 to 9.64 ‰ VSMOW (Fig. 4.3). There is no significant distinction between the stable isotopic signatures of the laminae with flat lying and upright structures.

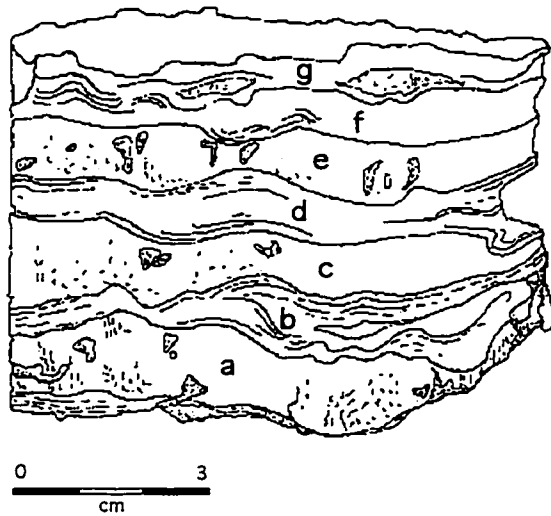
Sample M24 belongs to the DLF. It has  $\delta^{13}\text{C}$  values ranging between 2.76 and 4.02 ‰ PDB and  $\delta^{18}\text{O}$  values ranging from 6.97 to 8.70 ‰ VSMOW (Fig. 4.4). In this sample, both  $\delta^{18}\text{O}$  and  $\delta^{13}\text{C}$  are highest in the darker laminae that contain flat-lying microbial structures.

The samples collected along the down slope transect showed no clear trend (Fig. 4.5).  $\delta^{13}\text{C}$  values ranged from 2.04 to 3.35 ‰ PDB, and  $\delta^{18}\text{O}$  values from 5.56 to 8.79 ‰ VSMOW, but neither proceeded regularly down slope. Samples from which multiple textures were subsampled showed internal variation of up to 0.6 ‰ PDB for  $\delta^{13}\text{C}$  and up to 1.0 ‰ VSMOW for  $\delta^{18}\text{O}$ .

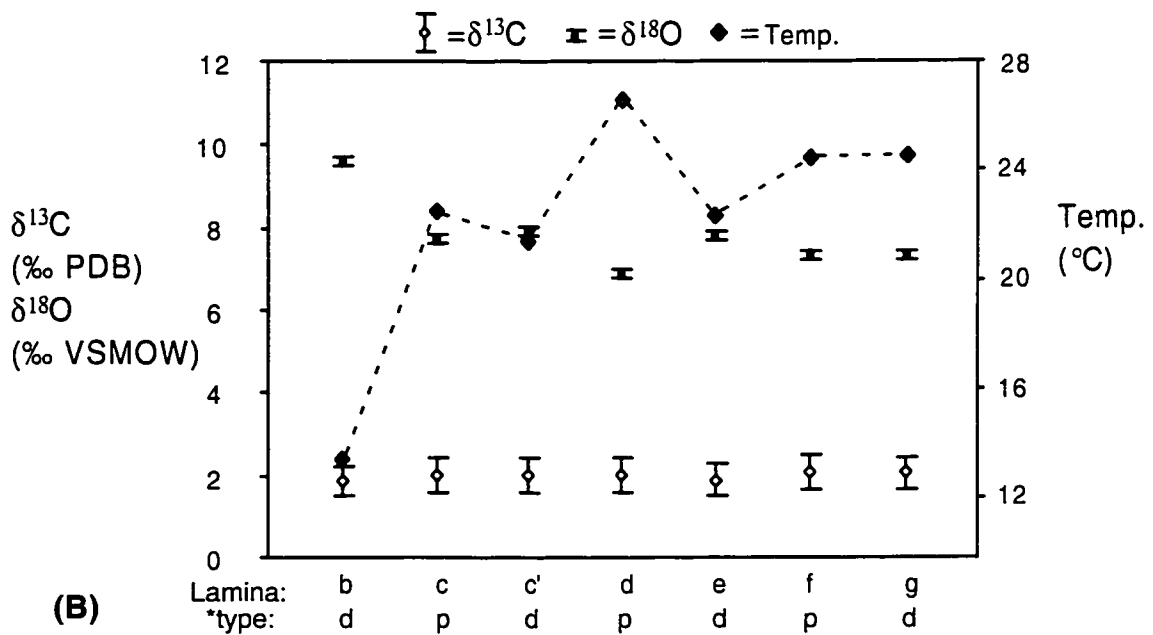
#### 4.4 Discussion

The lack of a down slope precession of stable isotope values is not surprising. The samples were selected based on their position on the hill slope, not on their position in the tufa stratigraphy (the latter is denied by the fragmented nature of the deposit). There is no way to assess if the samples were deposited from the same water, or from different waters in different years or seasons. Even those samples collected down slope from one another within individual textural units (i.e. samples M17, 18, 19 and M27, 28, 29) may have been deposited under different conditions. Thus, no cooling rate can be elucidated. If the  $\delta^{13}\text{C}$  and  $\delta^{18}\text{O}$  values are accurate, the most that can be said from the results of the down slope investigation is that water temperature, degassing rates, and photosynthetic influences were variable during the fossil system's depositional history.

The  $\delta^{13}\text{C}$  values in all four of the laminated samples failed to show a seasonal trend. Even in sample M24, where there was a statistical difference in  $\delta^{13}\text{C}$  between layers e-g (Fig. 4.4), the trend may not be large enough to permit the interpretation that it was caused by seasonal differences in rates of photosynthesis. Chafetz *et al.* (1991b) suggested that a difference of 2 to 3 ‰ between successive layers is evidence for a seasonal photosynthetic effect – the maximum difference measured for the Miette



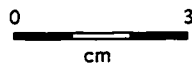
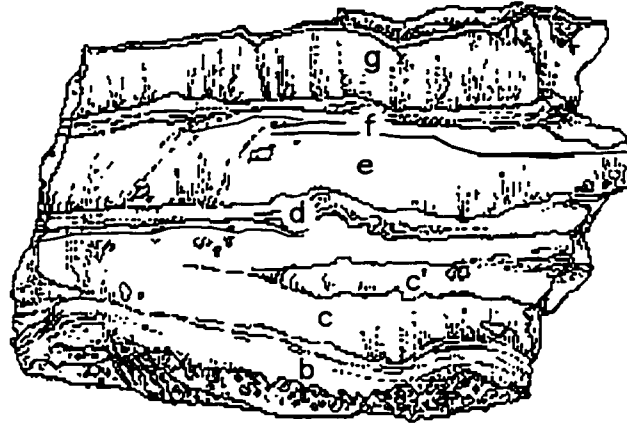
(A)



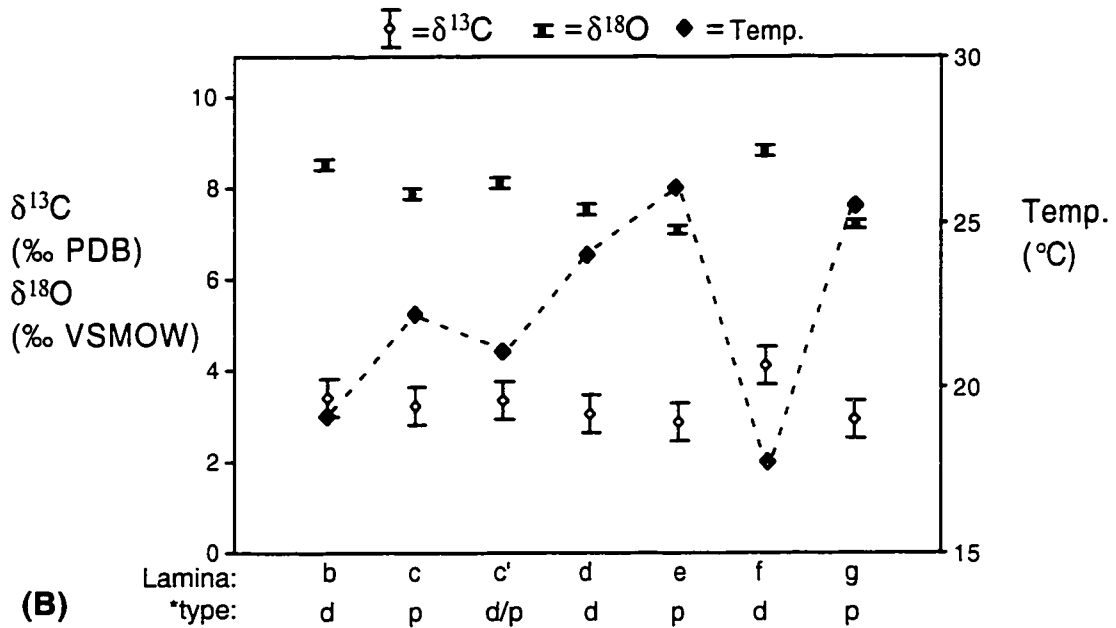
(B)

**Figure 4.3**

(A) Drawing of transitional laminar facies sample M13 showing individual laminae sampled.  
 (B) Stable carbon and oxygen isotope values measured for successive laminae and the estimated precipitation temperature calculated by Kim and O'Neil's (1997) equation for the precipitation of calcite from water under isotopic equilibrium - \*d = dark coloured lamina with flat-lying microbial structures, p = light coloured lamina with upright microbial structures.



(A)



(B)

**Figure 4.4**

(A) Drawing of dense laminar facies sample M24 showing individual laminae sampled. (B) Stable carbon and oxygen isotope values measured for successive laminae and the estimated precipitation temperature calculated by Kim and O'Neil's (1997) equation for the precipitation of calcite from water under isotopic equilibrium - \*d = dark coloured lamina with flat-lying microbial structures, p = light coloured lamina with upright microbial structures, d/p = a pocket of dark coloured tufa with flat-lying microbial structures contained within a light coloured lamina with upright microbial structures.

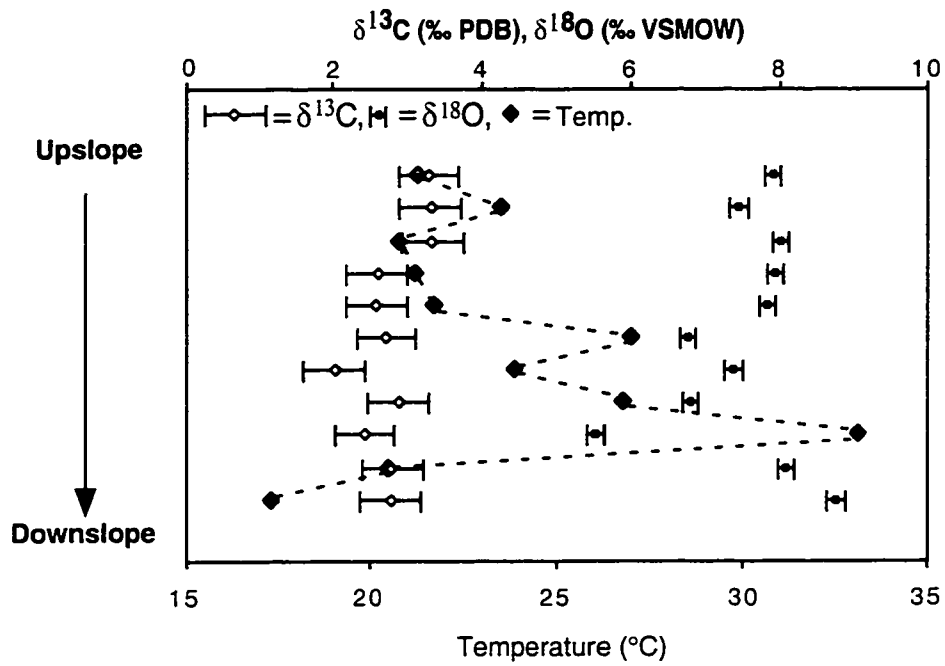


**Figure 4.5**

Stable carbon and oxygen isotopes from bulk tufa samples collected along a downslope transect from MS1 to MS7 and estimated precipitation temperature calculated by Kim and O'Neil's (1997) equation for the precipitation of calcite from water under isotopic equilibrium.

samples was 1.3 ‰. Additionally, if the  $\delta^{13}\text{C}$  values were seasonally controlled, they show a trend opposite to the hypothesis. That is, the heavier, enriched  $\delta^{13}\text{C}$  values in sample M24 are found in the darker layers with flat-lying microbial structures, whereas lighter  $\delta^{13}\text{C}$  values are found in the lighter layers with upright microbial structures. In all previous studies, the lighter, upright layers have been identified as summer precipitates (Pentecost and Riding, 1986; Chafetz *et al.*, 1991b; Andrews *et al.*, 1997); here, the  $\delta^{13}\text{C}$  values would indicate that they formed in the winter. A possible explanation for this effect could be that the  $\delta^{13}\text{C}$  values are affected more strongly by the loss of  $^{12}\text{C}$  to outgassing than by photosynthesis (cf. Fouke *et al.*, 1997). Photosynthetic effects are strongest for precipitates formed in closed environments but the DLF is thought to have formed from flowing water. The rate of outgassing of flowing water is controlled by the  $\text{pCO}_2$  gradient between the water and the air, and by the water turbulence. At the modern Miette Hot Springs, flow rates are highest in the summer and lowest in the winter, and a similar situation may have existed at the fossil springs. If less water is flowing, a higher proportion of that water will have surface area exposed to the atmosphere, and outgassing will be more efficient. Thus, if significantly more outgassing occurs in the winter than summer, we would expect to see the enriched  $\delta^{13}\text{C}$  values in the winter precipitates, which is consistent with the values measured for sample M24.

It is also possible that the  $\delta^{13}\text{C}$  values in these stromatolites no longer reflect their depositional environment. Thin section and SEM analyses show that growth of secondary cements and micrite, has taken place (Chapter 6). These processes, and exchange with isotopically heavier meteoric and ground waters moving through pre-deposited tufa, may have overprinted the original  $\delta^{13}\text{C}$  signature of the precipitates (cf. Janssen *et al.*, 1999). Additionally, many of the samples examined by SEM contained rock inhabiting microbes and organic detritus. These organic components may not have been fully removed by immersion in bleach, and may have contaminated the  $\delta^{13}\text{C}$  measurements.

$\delta^{18}\text{O}$  values in sample M24 also vary significantly between successive laminae. In M24, lighter  $\delta^{18}\text{O}$  values are associated with light coloured laminae, and dark laminae are enriched in  $^{18}\text{O}$ . Back-calculation of the temperature of the precipitating fluid supports the hypothesis that laminar alternation was seasonally controlled. The oxygen

isotope fractionation factor of the water-calcite precipitation is determined by the formula:

$$\alpha = (1000 + \delta^{18}\text{O}_{\text{calcite}}) / (1000 + \delta^{18}\text{O}_{\text{water}}) \quad (4.1)$$

The average of the values measured from the modern spring water (-20.86 ‰) was used because the  $\delta^{18}\text{O}_{\text{water}}$  of the fossil spring water is unknown. Estimates of the temperature at which the calcite in each layer precipitated are calculated using Kim and O'Neil's (1997) experimentally derived equation for the precipitation of calcite from water under isotopic equilibrium:

$$1000 \ln \alpha = 18.3(10^3/T) - 32.42 \quad (4.2)$$

Inserting the  $\delta^{18}\text{O}$  values for laminae from sample M24 yields precipitation temperatures of 17.7 to 24.0°C for the dark laminae, and 22.2 to 26.1°C for the light laminae (Fig. 4.4). These values are somewhat cooler than the spring water temperatures indicated by the ecology of the fossil spring mound (Chapter 5) – but this may be attributable to the use of the standard  $\delta^{18}\text{O}_{\text{water}}$  value in calculations. There is no reason that the fossil spring water should have had the same  $\delta^{18}\text{O}_{\text{water}}$  value as the modern springs; thus, the calculated temperatures are valuable to show relative, rather than absolute, changes in the temperature of the fossil spring water.

As spring waters flow away from the vent, they cool to equilibrium with ambient air temperature. The modern climate at the spring site has a maximum seasonal variation of 70°C and varies regularly by about 40°C between seasons (Gadd, 1999). Because the modern spring waters are diluted by shallow meteoric water, the warmest waters issue in the winter when precipitation and snowmelt are reduced. The winter waters may be up to 20°C warmer than summer waters at the vent (van Everdingen, 1986). The ambient air temperature and the dilution of the spring water mitigate one another, reducing the variability of the spring water temperature between seasons. Assuming similar controls on water temperature at the fossil springs, a point in the flow path where significant cooling had occurred (15-30 m down slope from the vent) might have a maximum difference between summer and winter water temperatures of 10 to 20°C. Less extreme variation would be found in upslope precipitates.

The fossil spring waters probably issued in a similar environmental setting to that of the modern springs (see Chapter 5). They evidently had a higher carbonate mineral

load than the modern springs, but may also have been diluted by meteoric waters. Thus, the differences of  $\sim 4^\circ\text{C}$  indicated by the  $\delta^{18}\text{O}$  values between the laminae in sample M24 could reasonably be interpreted to reflect an upslope seasonal change in precipitation temperature for a thermal spring that was seasonally diluted with meteoric water.

The PLF and transitional laminar facies samples lacked regular or cyclic variation in the  $\delta^{18}\text{O}$  between successive laminae, and temperature calculations produce suspect values (Fig. 4.1-4.3). As with the  $\delta^{13}\text{C}$ , the  $\delta^{18}\text{O}$  values may also have been affected by exchange with diagenetic fluids and cement growth. These processes would have less effect on the DLF tufa (i.e. sample M24) whose lower porosity restricts fluid flow. Several other processes could also explain the lack of seasonal stable isotopic changes between laminae in the PLF samples:

- (1) The original system may have been precipitating in isotopic disequilibrium (Although the presence of cyclic variations in  $\delta^{18}\text{O}$  values in M24 indicates otherwise).
- (2) There may not have been a distinct seasonal change in the temperature of the water, due to the mitigating effects of changing ambient temperature and dilution with fresh meteoric water.
- (3) Equilibrium precipitation from summer waters with slow rates of cooling and from winter waters with increased  $\text{CO}_2$  degassing and evaporation may have produced homogeneous stable isotopic signatures between seasons.

#### 4.5 Conclusion

Stable isotope analysis of the fossil Miette tufa did not yield evidence for a seasonal control on laminar alternation in its stratiform stromatolites. Investigations at other springs sites have shown that dense, darker laminae with flat-lying component microbial structures are the products of winter precipitation while more porous, lighter laminae with upright structures form in the summer (Pannella, 1976; Chafetz *et al.*, 1991b; Jones *et al.*, 1998; Konhauser *et al.*, 2001). This is supported for the Miette fossil tufa by  $\delta^{18}\text{O}$  values in DLF tufa sample M24, but  $\delta^{13}\text{C}$  values in the same sample did not lend clear support, and PLF tufa samples and a transitional facies sample did not show consistent stable isotopic variation between laminae. This is probably because diagenetic



processes can equilibrate isotopic differences between laminae (Janssen *et al.*, 1999), obliterating primary seasonal signatures. It is also possible that the original precipitates did not have strong seasonal isotopic variation. The original spring system was complex, and spring waters may have been seasonally diluted by meteoric waters. As the factors that controlled the water temperature of the fossil springs are unknown, it is difficult to interpret a stable isotope effect from the fossil Miette tufa. Stable carbon and oxygen isotopes may not be viable investigative tools for examining fossil tufa deposits in the Rocky Mountains.

## **5 The Fossil Miette Springs: Physiochemistry, Length of Activity and Palaeoenvironmental Context**

### *5.1 Introduction*

Observation of modern spring sites has revealed that the controls on texture and mineralogy of spring deposits are complex, and commonly site specific. Thus, if facies descriptions of spring deposited rocks are to have interpretive value (i.e. as analogues for ancient fossil spring deposits and stromatolites), it is important to investigate the physiochemical environments in which they were deposited. The differences in precipitation between the modern and fossil Miette springs are obvious, and indicate physical or chemical differences between the two spring systems, denying the assumption that a modern spring can be used as an analogue for a fossil spring, even if they are at the same site. Fortunately, information provided by the fossilization of organisms in the fossil Miette tufa offers insight into the physiochemistry of the fossil springs, providing a petrographic context for the facies described in Chapter 3.

A spring is never isolated, but emerges into an ambient environment, which can influence developing facies as much as intrinsic factors like spring water temperature and chemistry (Pedley *et al.*, 1996). Thus, the palaeo-environmental context of the fossil Miette springs, and the controls on activity at the spring site, are also discussed.

### *5.2 Physiochemistry of the Fossil Miette Springs*

Plants and animals inhabit preferred chemical and physical environments, thus, the presence of identifiable fossils in tufa can be used to bracket the physiochemical conditions of the fossil springs (i.e. Forester, 1991; Pritchard *et al.*, 1991; Griffiths *et al.*, 1996). The facies assemblages at MNN are discordant with those found elsewhere in the fossil tufa mound so the MNN fossil spring will be discussed independently.

#### *5.2a Miette South-North*

Taxa present in tufa from MS, MC, and MN (Fig. 2.1) include: the diatom *Cymbella* and the testate protozoan *Quadrullella* (found in tufa collected in and beneath the upper ledge), and cyanobacteria tentatively identified as *Phormidium*, *Oscillatoria*

and *Calothrix(?)* (found above and beneath the upper ledge). These taxa probably lived beneath the spring water and on subaerial substrates bordering the flow path (cf. Jones *et al.*, 1997; Pentecost *et al.*, 1997). All of these taxa have upper temperature limits that qualify them as thermo-tolerant, and all prefer near neutral pH (Table 5.1). Ostracodes identified as *Darwinula sp.*, *Heterocypris sp(?)*, *Candona sp(?)*, *Cyclocypris sp(?)*, and *Potamocypris sp(?)* were also found in the fossil tufa. Most of the ostracodes were found in bryophyte facies hummocks – the raised hummocks probably provided a necessary refuge from the currents and temperatures found in the flow path. Ostracodes have permanent upper temperature limits around 50°C, but they are found at higher temperatures, because they embark on temporary forays into inhospitable temperatures (Castenholz, 1973). All of the ostracode genera found are common to spring flow paths and wetlands, and some specimens may have been living in semi-terrestrial niches on the borders of the flow path. *Heterocypris* and *Darwinula*, however, are active microbial mat grazers and probably fed on cyanobacterial mats beneath the spring water (cf. Wickstrom and Castenholz, 1985). These two taxa have been found at temperatures up to 55-56°C, and prefer neutral pH (Wickstrom and Castenholz, 1985; Gandolfi *et al.*, 2001; Forester, pers. comm.).

This list of organisms is not diverse, and the abundance of fossils, excepting bryophytes and cyanobacteria, is low. In contrast, the modern springs host eight species of diatoms, at least four filamentous microbes, as well as unicellular microbes. At Pamukkle Travertine, Turkey, there are 17 species of cyanobacteria, 16 species of diatoms, and 5 species of Chlorophyceae (Pentecost *et al.*, 1997). There are two explanations for the low fossil abundance and diversity in the fossil Miette tufa: either the physiochemistry of the fossil spring mound was restrictive, or the fossils were not well preserved. There is some evidence for both of these interpretations. At MSS, the diatom *Cymbella* was found in several samples. Specimens had experienced dissolution and only the heavily silicified central raphes remained, so there is evidence that preservation of the tests was poor. The turbulent flow of the spring water as it descended to Sulphur Creek probably destroyed many tests. However, tests of species found with *Cymbella* at the modern springs, *Mastagloia elliptica* and *Navicula sp.* have better preservation potential than tests of *Cymbella* (Ryves *et al.*, 2001) but are not found in the fossil tufa.

**Table 5.1** Upper temperature limits and preferred pH of organisms found fossilized within the fossil Miette tufa. Where information about specific species or genera could not be found, upper temperature limits are given as the maximum temperature known for a species in the group – the actual temperature limit of the genera or species may be lower. (Castenholz, 1969; Kallio and Karenlampi, 1975; Brock, 1978; Wickstrom and Castenholz, 1985; Vinson and Rushforth, 1989; Jones *et al.*, 1998; Proctor, 2000; Gandolfi *et al.*, 2001; Forester, pers. comm.)

<b>Group</b> <i>Genera or Species</i>	<b>Upper Temperature Limit (°C) Found in Springs</b>	<b>Preferred pH</b>	<b>Other:</b>
<b>Diatoms</b> (i.d. by Dr. Alex Wolfe)			
<i>Cymbella sp.</i>	max. 50	>6	
* <i>Orthoseira roseana</i>	~40	~7	
<b>Protozoa</b>			
<i>Quadrullella sp.</i>	max. 56	~7	
<b>Ostracodes</b> (i.d. by Dr. Rick Forester)			
* <i>Scottia spp.</i>	max. 40	~7	semi-terrestrial, probably lived on margins of the spring flow path
<i>Candona sp.</i>	max. 40	~7	
* <i>Darwinula sp.</i>	55-56	>7	benthic microbialite grazers that probably grazed microbial mats growing in the spring flow path
* <i>Heterocypris sp. (?)</i>	~55	~7	
* <i>Potamocypris sp. (?)</i>	~51	~7	
<b>Cyanobacteria</b>			
<i>Phormidium</i>	~50	>5	
<i>Oscillatoria</i>	60+	>5	
<i>Calothrix (?)</i>	35-40	>5	
<b>Bryophytes</b>			
Boreal Moss	30-35		assemblage of several species tolerating ranging pH conditions

\* found only in tufa collected from MNN  
 • found only in tufa south of MNN

This may indicate that the other diatom species were not viable on the spring mound. Diatoms are common inhabitants of spring mounds and the remains of successful populations can accumulate as thick diatomite layers that are interbedded with spring precipitates (Weed, 1889). Diatom abundance is, however, reduced at many spring sites because of competition with cyanobacteria (i.e. at Yellowstone, Wyoming: Weed, 1889; Walter et al., 1976). At the modern Miette Hot Springs, *Cymbella* co-habitates with cyanobacteria more successfully than the other diatom species. *Cymbella* may have dominated the diatom population on the fossil spring mound much as it does in the lower flow path of the modern springs.

Chemical restrictions may have controlled the distribution of ostracodes on the fossil spring mound – they were only extracted from tufa samples collected beneath the upper ledge. Many ostracodes have low tolerance to reduced sulphur, whose presence requires negligible concentrations of dissolved oxygen, and the limited ostracode distribution may indicate the presence of H<sub>2</sub>S in water at the fossil spring vent (Forester, pers. comm.). The microbe found in the bedded tufa facies has been tentatively identified as a species of *Oscillatoria*, a genus known for its sulphur tolerance (Cohen *et al.*, 1975). Oxidation of H<sub>2</sub>S to SO<sub>4</sub> as the spring water flowed downslope may have made the distal slope mound more favourable to ostracode species. In addition to this chemical restriction, the filaments of larger species of *Oscillatoria* are not easily grazed by ostracodes (Castenholz, 1973), and the smaller diameter cyanobacterial filaments found downslope may have provided a more favourable grazing ground.

A lack of siliceous microfossils in tufa collected around the spring mounds indicates that vent conditions were hostile to diatoms and *Quadrullella* whose maximum terminal temperatures are <50°C and ~56°C, respectively (Castenholz, 1969; Brock, 1978). The cyanobacteria *Oscillatoria* identified in bedded tufa, however, has a maximum terminal temperature above 60°C (Castenholz, 1969; Walter, 1976). Some cyanobacteria are found around springs and geysers at temperatures above their thermal limits, but these survive in protected habitats on the spring mound or are protected by rapidly precipitated mineral coats (Jones *et al.*, 1998; Jones, 2002). The excellent preservation of filaments in the bedded tufa facies indicates that microbes were

mineralized quickly around the fossil spring vents, but the presence of streamer facies above the upper ledge indicates that the upper ledge surface was inundated with rapidly flowing water - microbial populations were expansive, not restricted to protected habitats. Thus, the upper limit of the vent temperature of the spring water is taken to be 65°C, slightly above the reported terminal temperature for *Oscillatoria*. The springs waters cooled flowing downslope, but bryophyte growth (which is compromised at temperatures > 30°C - Kallio and Karenlampi, 1975) was restricted to raised hummocks, indicating that temperatures did not fall below ~30°C before waters entered Sulphur Creek.

The chemistry of the fossil springs may have been similar to that of the modern springs: sulphur and carbonate rich. The spring water was evidently Ca<sup>2+</sup> and CO<sub>3</sub><sup>2-</sup> rich, and supersaturated with a carbonate mineral phase. The pH of the emerging spring water was neutral to alkaline, permitting precipitation of calcite, and probably increased downslope as CO<sub>2(g)</sub> was lost by degassing. Near neutral pH conditions are confirmed by the excellent preservation *Quadrulella*'s silica plates (because silica forms complexes in basic conditions that would obscure fossils - Round *et al.*, 1990) and the calcareous ostracode carapaces (which dissolve in acid conditions).

### **5.2b Miette Far North End**

A difference in spring water physiochemistry between the fossil spring vents at MNN and those to the south is indicated by its discordant facies assemblage, and confirmed by differences in its fossil ecology. Although the tufa at MNN does contain some preserved filamentous microbes around its former spring vent pool, it is dominated by bryophyte facies tufa beds that were established within 10 m of the spring vent. The testate protozoan genus *Quadrulella*, the diatom *Othoseira roseana*, and an ostracode species belonging to the genus *Scottia* were found in the bryophyte tufa. Both *O. roseana* and *Scottia* are common inhabitants of bryophyte leaf niches and are found on wet forest floors and on mosses and grasses near spring flow paths (Spaulding and Kociolek, 1998).

Few bryophyte species have optimal growth temperatures above 30°C, and most prefer cooler waters (Kallio and Karenlampi, 1975; Proctor, 2000). Thus, the spring water that generated the tufa at MNN clearly had a lower emerging temperature than the

springs to it is south. It probably had a lower flow rate as well. Bryophytes, which typically inhabit cool and warm thermal spring flow paths (Ford and Pedley, 1996), are typically found where water moves in thin sheets, baffled by the plant roots, or trickles around the plant bases (Janssens, 1990). Near neutral pH conditions are also inferred for the fossil spring at MNN based on the excellent preservation of both calcareous and siliceous micro-fossils (Fig. 3.29, 3.30).

### 5.3 *Precipitation at the Fossil Springs*

CaCO<sub>3</sub> precipitates from spring water only when it is thermodynamically favourable, which requires a critical degree of supersaturation 5 to 10 times higher than saturation concentration (Gulley, 1993; Merz-Preiß and Riding, 1999). This supersaturation is achieved by withdrawal of CO<sub>2</sub> from the spring water by inorganic degassing and/or cooling, and by biological photosynthesis. The relative importance of these two processes differs between cool and thermal springs, and results in a difference in the gross morphology of the spring deposit. In thermal springs, CO<sub>2</sub> degasses rapidly at the spring vent. Consequently, precipitation is concentrated around the spring orifice (Folk, 1994; Chafetz *et al.*, 1991a). The high temperature precludes the growth of macrophytes in the tufa, and high rates of precipitation in the immediate vent environment can block spring water discharge channels so that they are episodically re-routed (Guo and Riding, 1998). Cool spring waters degas CO<sub>2</sub> more slowly than their thermal counterparts, and precipitation usually commences a short distance away from the spring vent (Guo and Riding, 1998). As a result, the spring flow path usually remains unblocked and spring vent and discharge channel positions are relatively stable (Guo and Riding, 1998). Cooler spring waters are less disparate in temperature and chemistry from ambient environmental conditions than thermal springs, and cool spring basins may be suitable localities for the growth of higher plants. Even very close to the spring orifice, photosynthetic CO<sub>2</sub> withdrawal may be important to carbonate mineral precipitation (Ford and Pedley, 1996).

Of these two broad macrofacies, the southern fossil tufa exposures at Miette best fit the thermal spring model. Tufa is concentrated near the vents raising them into mounds, contains few macrophytic textures, and contains rapid vertical facies alternations that

attest to repeated re-routing of the spring water flow path. The fossil Miette springs had similar chemistries to the modern Miette springs, and can be classified as a hot thermal mineral spring (cf. van Everdingen, 1991). To generate the volume of tufa that they did, the fossil springs obviously had a much faster flow rate, probably driven by a higher hydrologic head, and may have had a slightly higher emerging temperature than the modern springs. All of these factors could lead to increased CO<sub>2</sub> loss in the vent environment, which would lead to rapid supersaturation with CaCO<sub>3</sub> and may explain the increased carbonate mineral precipitation at the fossil springs. Phytoliths and plant debris were also found in the fossil tufa (Fig. 3.12), indicating that plants inhabited the slope surrounding the spring mound, and may have colonized dry portions of the mound. Tree trunks and grasses can provide a nucleation site for carbonate mineralization if spring waters are re-routed to flow through their growth site, and can create zones of turbulence that locally enhance rates of precipitation (Gulley, 1993).

Although photosynthetic microbes inhabited the southern spring mound, and provided templates for textures in the stromatolitic facies, mineralization of the filaments seems to have been controlled by abiotic factors. For example, filaments are better preserved in the bedded and sheet tufa facies that formed around the spring vents and beneath slope breaks where rapid precipitation was driven by rapid CO<sub>2</sub> loss via cooling and degassing, than on gentle slopes where photosynthetic processes may have been more important (compare Fig. 3.14A showing indistinct preservation of filament structures in the dense laminar tufa facies with Fig. 3.17A-C showing preserved filaments with distinct borders and micritic rims in the bedded tufa facies). Further, in some dense laminar facies samples, filaments have preserved sheaths in dark (winter) laminae but are preserved only as cylindrical casts in light (summer) laminae. The calcification of cyanobacterial sheaths requires a suitable sheath structure and composition, supersaturation of the spring water with calcium carbonate (Riding, 1991; Merz, 1992) and that photosynthetic utilization of bicarbonate and release of OH<sup>-</sup> create a pH microgradient within the cyanobacterial sheath to induce CaCO<sub>3</sub> impregnation (Pentecost and Bauld, 1988; Merz-Preiß and Riding, 1999; Arp *et al.*, 2001). If the water the microbes inhabit has high dissolved inorganic carbon (DIC), above ~10 mmol/L, photosynthesis will not be able to produce this gradient and, though precipitation may



proceed in intercellular mucus, the sheath will not be preserved (Merz, 1992). Further conditions required for sheath impregnation include near equilibrium between the water and atmospheric  $p\text{CO}_2$ , low DIC, and high concentrations of  $\text{Ca}^{2+}$  (Arp *et al.*, 2001). If photosynthesis was driving withdrawal of  $\text{CO}_2$ , one would expect to find preserved sheaths in summer laminae that formed when photosynthesis was maximized (cf. Merz-Preiß and Riding, 1999), but the opposite is observed in the dense laminar facies. At the modern Miette Hot Springs, water temperature and dissolved ion concentrations are lowest in summer due to dilution by rain and snowmelt (van Everdingen, 1986). Ionic concentrations are higher in winter, and rates of  $\text{CO}_2$  degassing are maximized by a stronger temperature difference between the spring water and ambient air – i.e. relatively lower DIC and higher  $[\text{Ca}^{2+}]$  are found in winter. If similar hydrology prevailed at the fossil Miette springs, changes in the rate of inorganic degassing between summer and winter may have determined if photosynthesis was able to facilitate sheath impregnation.

The deposits at MNN were precipitated from the waters of a warm thermal mineral spring, and the tufa is intermediary between Guo and Riding's (1998) broad macrofacies: although the tufa is concentrated around the fossil spring vent, it is thickest midway downslope, and the flow path was colonized by bryophytes. With lower flow rates and lower emerging vent temperatures at the MNN fossil spring,  $\text{CO}_2$  loss by degassing would not be as great as for the other fossil springs. Turbulence generated by the flow of water around plant stems can enhance  $\text{CO}_2$  loss (Gulley, 1993) and withdrawal of  $\text{CO}_2$  from the spring water due to bryophyte photosynthesis may also have encouraged mineral precipitation on the bryophyte colonies.

Interestingly, the Miette tufa mound lacked the terraced pools that distinguish many thermal spring deposits. In hot spring deposits, surface irregularities drive increased loss of  $\text{CO}_2$  and cause localized precipitation of calcite that forms barriers or rims (Chafetz and Guidry, 1999). This commonly results in the development of step-like successions of dammed pools with raised rims, or rim pools, on the spring mound. The appearance of the rim pools is a function of the gradient of the deposit, which determines the rate at which  $\text{CO}_2$  is lost: gentle slopes develop long, shallow basins, and steep slopes develop deep pools and large rim dams (Chafetz and Folk, 1984; Gulley, 1993; Kerr and Turner, 1996). With the possible exception of the granular tufa facies, there is no

evidence of a pool facies in the Miette tufa, and roll-over structures lack the raised rims distinctive of thermal spring mound rim pool dams. The high gradient of the slope beneath the fossil Miette springs may not have been favourable to rim pool development and the landslide activity that plagued the spring mound was certainly unfavourable. Raised rim pools develop over years of precipitation and are stable features of many spring mounds (i.e. Angel Terrace at Yellowstone, Wyoming, or the Pink Terraces at Tarawhera, New Zealand - Kerr and Turner, 1996) – the repeated reorganization of topography at Miette by landslides and rockfalls may have been a critical impediment to the evolution of rim pool terraces.

The mineralogy of  $\text{CaCO}_3$  precipitates is controlled by a complex set of interactive variables including water temperature and chemistry, rate of  $\text{CO}_2$  loss, ion delivery rate, and biological influences (Buczynski and Chafetz, 1991; Guo and Riding, 1998; Folk, 1994; Jones *et al.*, 1996; Renaut and Jones, 1997). In general, however, cold spring precipitates are dominated by low-Mg calcite, and aragonite and high-Mg calcite are more prevalent in thermal springs with vent temperatures  $>40^\circ\text{C}$  (Folk, 1994). The fossil Miette precipitates are composed of low-Mg calcite, but may have originally contained unstable phases of high-Mg calcite or aragonite. The ubiquitous occurrence of skeletal and/or hollow crystals, and of solid crystals with internal (commonly concentric) void spaces, indicates either disequilibrium precipitation conditions (cf. Jones and Renaut, 1996a), or the dissolution of unstable primary phases.

#### 5.4 *The Growth Rate and Age of the Fossil Miette Tufa*

It is difficult to pinpoint when and for how long the fossil springs were actively depositing tufa, but “back of the envelope” calculations indicate that the fossil hot thermal spring system that generated tufa from MS-MN was long lived. First, if one assumes that the laminations in the stromatolitic facies are seasonally generated, an annual rate of tufa growth can be estimated. With an average laminar thickness of 1.5 cm in the porous laminar facies, this yields a maximum tufa growth rate of 3 cm/year. The thickest vertically continuous tufa outcrop at Miette is ~ 7 m high and, at a maximum growth rate of 3 cm/year, represents a minimum 233 years of continuous precipitation. Non-stromatolitic facies, in which the precipitates are not supported by microbial growth,

would have much slower vertical growth rates. At Rabbitkettle Hot Springs in Nahanni National Park, N.W.T., tufa mounds build outwards at a maximum measured rate as low as 3.9 mm/year (Gulley, 1993). At this rate, the 7 m exposure at Miette would require nearly 1800 years of continuous tufa growth. Considering that both stromatolitic and non-stromatolitic facies are found throughout the mound, that all parts of the mound were not hydrated continuously, and that parts of the spring mound were displaced by landslides as it grew, the formation of the fossil Miette tufa probably required ~ 2000 years.

The remains of a bison were found in tufa at MN4 (Fig. 5.1A). It was only possible to extract the tip of the left tibia and several vertebrae of the bison from the tufa, but these proved to be informative. First Nations peoples are known to have inhabited the Athabasca Valley, and there is anecdotal evidence that they made use of hot springs for bathing (Mussieux and Nelson, 2000). The discovery of the bison bones led to speculation that these people might have brought the remains of a bison killed in the Athabasca Valley up to the fossil Miette Hot Springs for a barbeque. Jack Brink at the Provincial Museum of Alberta examined the bones and concluded that the bison met a natural end. Had it been butchered, the tibia of the bison would have borne knife marks, and the First Nation peoples would most likely have saved the bone to extract its marrow. So there is no evidence for a barbeque at the springs. Instead, it appears that the bison came to the springs on its own accord, probably using it as a watering ground. The bison bones are found at the top of a lens of tufa breccia/conglomerate and the bison may have been killed by the rockfall that generated the lens.  $^{14}\text{C}$  dating of the bison's bones yielded a date of  $3,770 \pm 60 \text{ C}^{14}$  years, which corresponds to 2350-2025 sidereal years BC (with 95% confidence). It is impossible to know at what stage in the growth of the overall deposit the outcrop at MN4 formed, but the bones were found in the bottom third of the outcrop. If one estimates that the bison died during the first third of the tufa growth, and that tufa was actively forming for ~2000 years, then spring flow would have been initiated ~ 4,500 years BP and continued until ~ 2,500 years BP.

The age and longevity of the warm thermal spring tufa deposits at MNN is uncertain. The MNN tufa may have been precipitating concurrently with the hot thermal

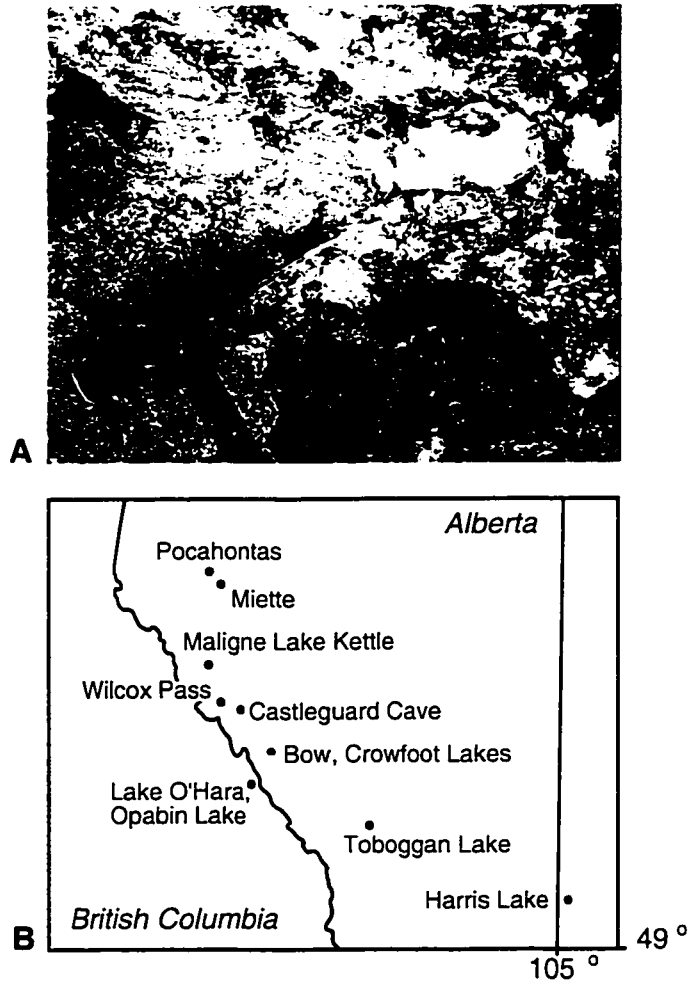


**Figure 5.1**

(A) Photograph of the bison bone found in tufa outcrop MN4. (B) Location map showing sites mentioned in Fig. 5.2.

spring tufa, or may postdate it. A warm spring issues in association with spring 1 at the modern Miette hot springs, so there is precedent for warm and thermal spring systems to operate in tandem in Sulphur Creek Valley. The excellent preservation of detail in the bryophyte facies at MNN, however, indicates that they have not undergone extensive diagenetic change; the tufa at MNN is likely younger than tufa to its south.

### 5.5 *Palaeoenvironmental Context*

The carbon dates place peak activity at the fossil hot springs during the Neoglacial period, which followed the Wisconsin glaciation (Fig. 5.1B, 5.2). At the height of the Wisconsin Glaciation the Miette springs site was buried by glaciers that extended down through the Athabasca Valley. Deglaciation began ~13 ka BP and glacial retreat was complete by 10 ka BP (Heusser, 1956). A  $^{14}\text{C}$  date extracted from gastropod shells indicates that Pocahontas, a site near the Miette springs, was ice free by  $11,900 \pm 120$  years BP (Levson and Rutter, 1985; Osborn and Luckman, 1988), and glaciers retreating up Fiddle Creek Valley left till deposits in their wake. Deglaciation was followed by a period of rapid warming that culminated in the Hypsithermal, a multi-phased warm period between ~9000 to ~5000 years BP. Limnological and palaeoecological evidence indicate that, during this period, the climate was warmer and dryer than average, with mean annual temperatures 0.5 to 1.5°C above modern (Kearney and Luckman, 1987; Vance *et al.*, 1995). A shift towards cooler and moister conditions began in the Rockies around 5000-4500 years BP, resulting in small glacial advances and readjustment of vegetation boundaries, and heralding the beginning of the Neoglacial (Osborn and Luckman, 1988; Vance *et al.*, 1995; Sauchyn and Beaudoin, 1998).

The fossil Miette springs emerged through glacial till that formed an unstable substrate for growing mineral deposits. The large volumes of tufa at Miette required a voluminous water source, and this may have been supplied by regionally higher water tables. Data collected from pollen cores, plant fossils, limnology and peats all indicate increased humidity and precipitation on the western plains, the Foothills and the Rockies during the Neoglacial (Sauchyn and Beaudoin, 1998; MacDonald and Case, 2000). This cooling, moistening trend is temporally correlated to climatic changes in South America

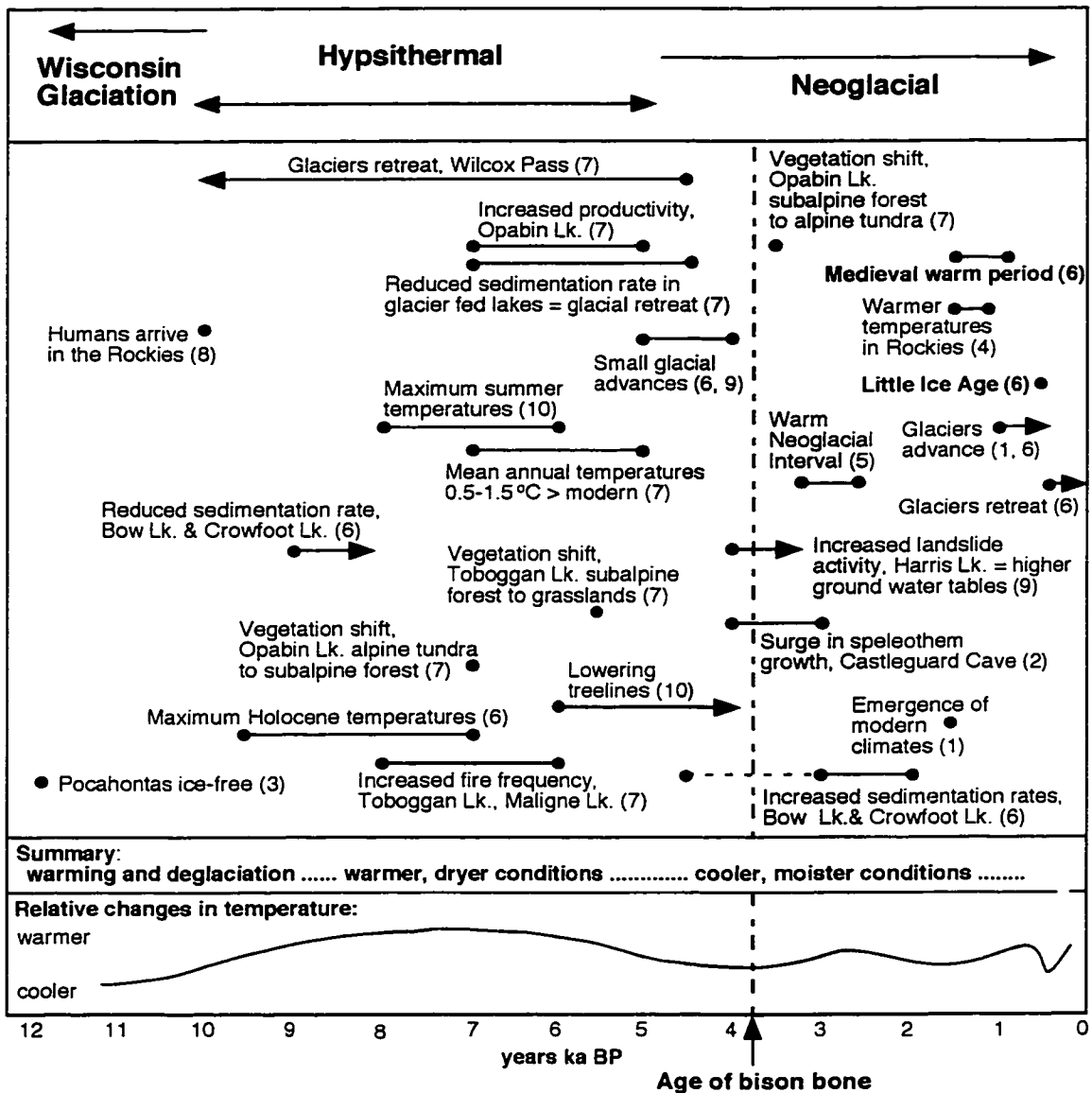


**Figure 5.2**

Summary of palaeoenvironmental change in the southern Canadian Rocky Mountains. The age of the bison bone (Fig. 5.1A) extracted from tufa outcrop MN4 is indicated by a dashed vertical line and the shaded region represents the probable span of activity at the fossil Miette Hot Springs. See Fig. 5.1B for the location of sites named in this figure. (Sources: 1- Heusser (1956), 2- Henning *et al.* (1983), 3- Levson and Rutter (1985), 4- Luckman (1986), 5- Kearney and Luckman (1987), 6- Osborn and Luckman (1988), 7- Vance *et al.* (1995), 8- Beaudoin *et al.* (1996), 9- Sauchyn and Beaudoin (1998), 10- MacDonald and Case (2000)).

and may have resulted from changes in ocean circulation and North Pacific sea surface temperatures (MacDonald and Case, 2000; Haug *et al.*, 2001).

Whatever its cause, the moistening trend appears to have been widespread in the Rockies and Foothills. The increased carbonate precipitation at Miette between 4,500 and 2,500 years BP is coincident with surges in speleothem growth in Castleguard Cave (Banff National Park, Alberta) between 4,000 and 3,000 years BP (Henning *et al.*, 1983), and with increased landslide activity due to rising groundwater tables as far east as Harris Lake, Saskatchewan (Sauchyn and Beaudoin, 1998). There are other fossil tufa deposits in the Southern Rocky Mountains and Foothills (Woodsworth, 1997) but these have not been dated. Small volume springs still emerge at many of the sites, flowing over the fossil tufa deposits of larger fossil spring systems. It is possible that the fossil tufa deposits record the same moist climate event that generated the fossil Miette tufa and mid-Holocene speleothem growth in Castleguard Cave.

Although modern climates did not emerge in the Rockies until ~ 1500 years BP (Heusser, 1956), the environmental setting of the fossil Miette Hot Springs was probably similar to modern, characterized by subalpine forest. Detrital phytoliths and plant fossils in the fossil tufa show that the hill slope was vegetated by mosses, grasses, and trees (including pine and spruce), and animals like bison (and probably other ruminants and rodents) frequented the spring mound. Seasonal variations in ambient temperature and solar incidence were large enough to influence microbial populations and precipitation on the spring mound (thus influencing laminar alternations in the stromatolitic tufa facies).

van Everdingen (1972) envisioned very high water tables during the initiation of precipitation at the Miette Springs site. The fossil tufa deposits reach elevations well above the bed of Sulphur Creek, and van Everdingen (1972) suggested that erosion of bedrock by Sulphur Creek, and concurrent downwards migration of the creek bed, provided the springs with progressively lower outlets resulting in re-location of the spring vents. Although Sulphur Creek was no doubt higher in the past, van Everdingen's (1972) explanation does not agree with outcrop observation. Relocated spring vents are found within pre-deposited tufa, so Sulphur Creek must have been well below the tufa deposits, and vent relocation cannot be explained by erosive excavation of spring channels. Rather, the downslope migration of the fossil spring vents probably occurred in response

to a waning hydrologic head and/or as a physical response to growth of the spring mound: rapid deposition of precipitates in slope deposits can lead to re-orientation of the spring vent because the hydrostatic pressure at the base of a slope deposit may become so great that a new vent will form lower on the slope (Harrington, 1948, cited in Chafetz and Folk, 1984).

The peak growth phase of the fossil tufa probably ended around 2500 years BP. The presence of gypsum and strontianite in pore spaces in the crenulated facies at MS5 indicates a shift in the style of precipitation at the Miette springs. The high hydrologic head at the fossil springs brought hot water to the surface rapidly and in volume, resulting in efficient loss of CO<sub>2</sub> and carbonate mineral precipitation. As the hydrologic head waned, the water may have been cooler at the vents, and CO<sub>2</sub> loss may have been diminished, leading to undersaturation with calcite, and a predominance of gypsum, sulphur, and strontianite precipitates (as are found at the modern springs – Chapter 2). The thermal spring vents began to migrate downslope, eroding and undercutting pre-deposited tufa, until they reached their present elevations.

There is no way to determine if spring water flow was continuous between deposition at the modern and fossil springs. Either the springs continued activity but did not leave a robust mineral deposit, or their channels were blocked and activity at the site ceased. The similarity in the inferred chemistry of the fossil hot thermal springs and the modern springs suggests that the two systems shared a flow path through the Rundle Group Carbonates, but it is possible that the subsurface feeder channel to the springs was occluded or re-routed at some point between deposition of the fossil tufa and initiation of flow at the modern springs.

## 5.6 *Summary*

The fossil Miette hot springs consisted of a number of perched spring vents that issued hot thermal waters (~50-65°C), that were Ca<sup>2+</sup>, CO<sub>3</sub><sup>2-</sup>, and H<sub>2</sub>S rich, had near neutral pH, and supported a community of thermotolerant cyanobacteria, diatoms, testate protozoa, and ostracodes. Precipitation of (probably) low or high-Mg calcite was initiated by inorganic CO<sub>2</sub> loss, and mineral deposits were concentrated around the spring vents, resulting in the development of raised spring mounds. A warm thermal spring with



similar chemistry issued at MNN, and lower water temperatures in its flow path permitted colonization by bryophytes, and bryophyte leaf inhabiting diatoms and ostracodes. Most of the fossil Miette tufa, however, formed from the hot thermal spring water. The volume of fossil tufa at the Miette site indicates that active tufa formation continued for ~2,000 years, and radiocarbon dating of a bison bone embedded in the tufa indicates that the springs were at peak activity during a regional moistening phase in the early Neoglacial. Since that time, the fossil Miette tufa has been disarticulated by landslide activity and obscured by the growth of forest vegetation. Nature has had about 2,500 years to wreak diagenetic havoc and the tufa has been subject to extensive change since deposition.

## 6 Diagenesis in the Fossil Miette Tufa

### 6.1 Introduction

The fossil tufa at Miette is far from pristinely preserved. The original precipitates were deposited on and about microbes, bryophyte colonies, and woody plant debris. After initial lithification of the precipitates, the organic matter decayed, leaving behind a porous carbonate framework in which plant remains were preserved as molds or mineralized body fossils. Since that time, fragmentation, dissolution, cementation, recrystallization, and new crystal formation have altered the rock. These diagenetic changes did not happen in isolation; rather, they were initiated by environmental stresses and influenced by biological communities living on and around the tufa.

### 6.2 Environmental Stress

Subaerially exposed on a hill slope, the fossil tufa has been subject to environmental weathering. Dissolution of carbonate by meteoric water has resulted in a loss of surface texture throughout much of the deposit. Meteoric waters are undersaturated with carbonate mineral phases, and become enriched in CO<sub>2</sub> via percolation through CO<sub>2</sub> rich organic debris and humic soils, further increasing their corrosivity to carbonate (Schneider, 1976).

Temperature variations between summer and winter drive cyclic freezing and thawing of waters that have infiltrated the tufa's porosity. The result is weakening of the rock by frost wedging. In some of the Miette tufa, this effect is enhanced by the presence of soluble salts (gypsum and a potassium chloride salt) in some pore fluids that increase the volume of expansion when the fluids are frozen (cf. Lewin and Charola, 1981). Areas of the tufa that are capped by streamer facies tufa have been strongly affected by frost wedging and thin layers of streamer tufa slough off easily when touched.

Trees took root on the fossil tufa and the penetration of their roots through the rock has weakened it, and opened conduits that allow infiltration of meteoric water. The generally unstable slope beneath the tufa has resulted in shifting of tufa blocks through time, and many of the trees that colonize the tufa have warped or "s" shaped trunks which indicate movement of their substrates (cf. Gadd, 1999). Besides physically

disarticulating the tufa through root wedging, plants colonizing the tufa (grasses, mosses and lichens) also release organic acids that promote dissolution of carbonate (cf. Lewin and Charola, 1981).

Physical stresses imposed by large mammals (mostly mountain sheep and human tourists) have also worn the tufa, and mammalian trails are littered with hand sample sized pieces of tufa that have been broken away from outcrops. Smaller mammals (squirrels, ground squirrels and mice) and insects also frequent the tufa outcrops, nesting and cocooning in large pore spaces and branch and log casts.

### 6.3 *Microbiological Colonization*

In addition to abuses incurred by mammals and insects, the Miette tufa suffers a thriving microbial community. Sheltered areas of the deposit, especially in the former spring vent pool caves, are thinly coated by soft lime or “moon-milk.” Some of these coatings are locally green or brown, revealing the presence of pigmented epilithic microbes (Fig. 6.1A). The epiliths may be crucial to the development of the moon-milk coats: they form surface films in which diurnal cycles of photosynthesis and respiration alternately produce carbonate dissolving acids or promote mineral precipitation, generating soft surface coats on carbonate rocks (Viles, 1987; Castanier *et al.*, 1999).

Microbes, mostly fungi and bacteria, have also taken residence in open pore spaces in the fossil Miette tufa and have recolonized primary filament casts (those produced during precipitation of the tufa) (Fig. 6.1B-E). These chasmoliths can influence carbonate dissolution by altering the chemistry of pore fluids and may release acidic or chelating metabolic by-products that can compromise the structure of the spaces they inhabit. Some chasmolithic microbes can also increase the stability of tufa. If they are photosynthetic, they may deplete CO<sub>2</sub> within pore spaces, promoting reprecipitation of carbonate (Viles, 1987). The chasmoliths may act as the substrate for reprecipitation and, although some chasmoliths in the Miette fossil tufa are free of mineral coats, others are heavily calcified, or host patches of micrite (Fig. 6.1F). If the microbes are calcified, they can act as pore-fill obstructing through-flow of fluids, thus retarding weathering

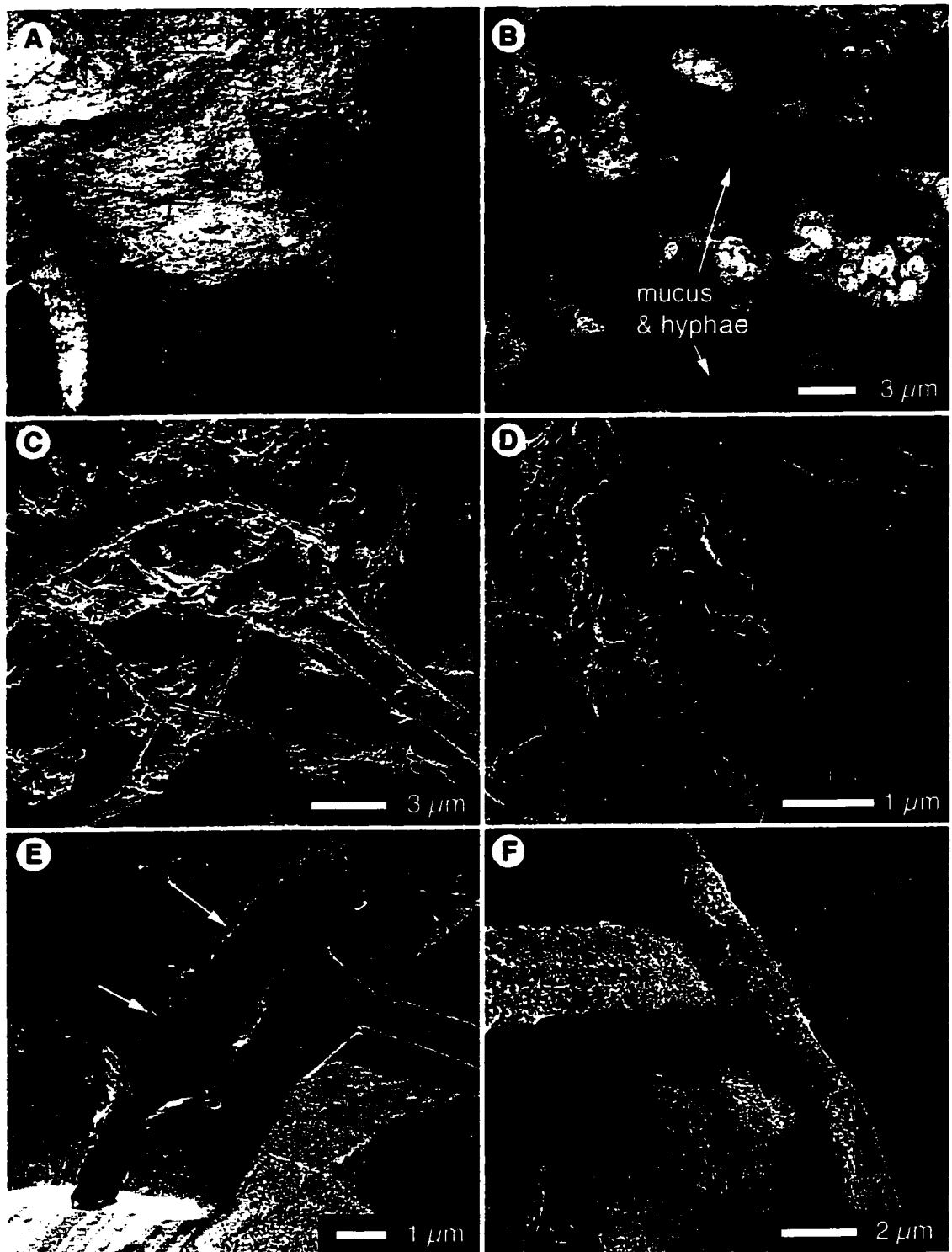


**Figure 6.1**

(A) Photograph of the soft lime coating found in FSVP caves and beneath overhangs. Greenish coloured patches are colonised by epilithic microbes. A rock hammer is shown for scale. (B) Mucus, fungal hyphae and spores found in porous laminar tufa sample M53. (C) Bundles of chasmolithic microbes (probably fungi) found in porous laminar tufa sample M9. (D) Bacteria and mucus coat crystal faces in bryophyte tufa sample MNN1b. (E) Bacteria also line void filament casts in dense laminar tufa sample M24. (F) Chasmolithic microbes in porous laminar tufa sample M53 show varying degrees of mineral encrustation.

(Viles, 1987). Bacteria and bacterial fossils were found on and around chasmolith filaments, and they are surrounded by mucus that also acts as a locus for authigenic mineral growth (Fig. 6.1D).

Endolithic microbes bored tunnels through surficial layers of the fossil tufa, compromising its resilience and providing conduits for the infiltration of meteoric waters that facilitate dissolution and frost-wedging (Fig. 6.2). The boreholes have irregular edges and expose etched calcite (Fig. 6.2B), indicating that boring was facilitated by acid attack (cf. Viles, 1987). Cyanobacterial endoliths have a limited depth of penetration because they require light for photosynthesis, whereas fungal endoliths have no light limitation (Viles, 1987). At Miette, most of the endolithic activity is found in the outer edges of the tufa, penetrating no further than 2-3 cm, so the endolithic community may consist of cyanobacterial borers. The exposed surfaces of many of the massive tufa outcrops at Miette are dark grey – this may be due in part to the presence of decaying organic material in surficial boreholes (cf. Squair, 1988) and to staining by organic rich humic acids.

#### 6.4 *Mineralogical Changes*

The fossil Miette tufa contains a variety of calcite mineral habits including composite bi-terminal crystals, microcrystalline calcite, and sparry calcite. Although locally etched or corroded, the distinctive bi-terminal calcite crystals (Fig. 3.10E, F, 3.15B) have maintained their original form. It is difficult to determine how many of the other crystal habits are primary.

Some less stable mineral phases may have recrystallized. Thin section and SEM investigations showed that filament structures in the stromatolitic facies and void spaces in the other facies were commonly bordered by sparry calcite. Sparry crystalline cements in tufa form (1) as a result of primary precipitation due to inorganic processes, (2) as organically induced precipitates formed around cyanobacterial bushes, or (3) they may be produced diagenetically by recrystallization of initially micritic or sparry calcite phases (Janssen *et al.*, 1999). There is great disparity in the degree of preservation of sparry coats found throughout the fossil Miette tufa: some have pristine crystal faces (Fig. 3.14C, 3.23D), some are badly corroded (Fig. 3.20F, 3.23E), and some host growths of

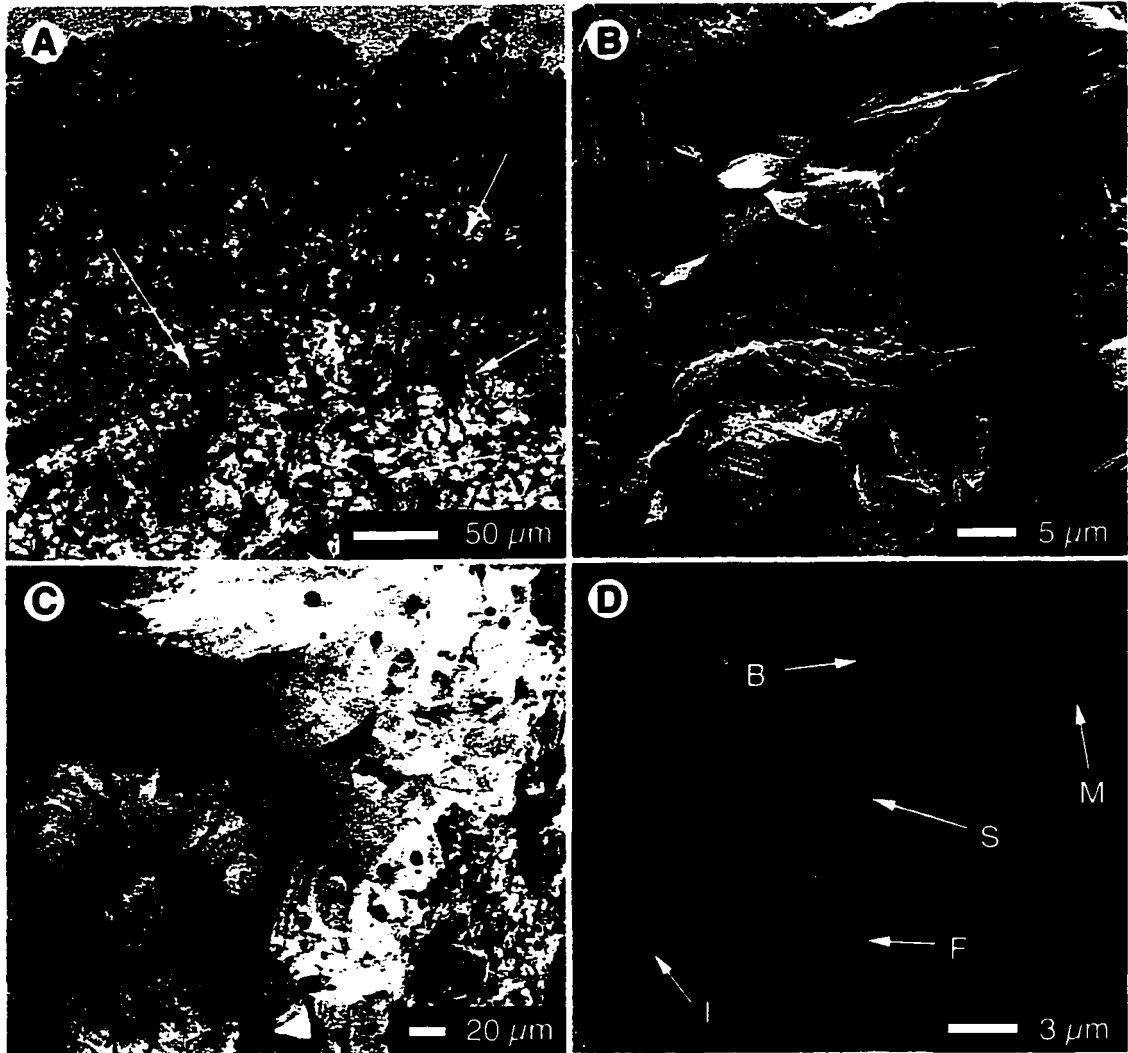


**Figure 6.2**

(A) Thin section photograph of filament shaped boreholes found in the outer rind of massive tufa sample M44 from MN1. (B-D) SEM images from byrophyte facies sample M60 from MNN1. (B) A desiccated branching filamentous microbe in its borehole which is bordered by badly etched calcite. (C) Boreholes punctuate gothic arch mosaic spar in shallow pore spaces (the round object is a siliceous auxospore). (D) Group shot of creatures inhabiting sample M60: a soil mite (I), fungal hyphae (F), a spore bundle (S), and bacterial mucus (B) that has been coated in micro-rod needle fibre micrite (M).

nodular or rod-shaped micrite (Fig. 3.32D, F). The more pristine calcite spar probably formed through recrystallization or as secondary cements. Gothic arch sparry calcite (crystals with triangular faces that converge to a point having a main face and smaller, successive slabs with similar triangular outline), for example, is typical of meteoric phreatic diagenesis (Janssen *et al.*, 1999). Gothic arch crystals found in the fossil Miette tufa (Fig. 6.2C) almost certainly precipitated from calcite saturated pore waters (cf. Janssen *et al.*, 1999).

Pore filling cements are found in all facies, and heavy cementation results in a loss of surface textures, ultimately producing the massive tufa facies. The cements consist of isopachous banded calcite, isopachous and meniscus sparry calcite fringes, and mosaic spar. The isopachous banded calcite is found prevalently in the bedded and bryophyte tufa facies. Rims of cement containing micro-laminations of dark and light coloured calcite border filament and bryophyte structures and terminate in euhedral blades in open pore spaces (Fig. 6.3A, B). The cements are 40 to 130  $\mu\text{m}$  thick and may contain as many as 80 dark/light alternations. Sparry isopachous banded cements form beneath thin, continuously flowing sheets of water (cf. Braithwaite, 1979). The banding likely results from an alternation between precipitation of coarse grained light coloured spar and fine grained dark coloured micrite, which may be controlled by seasonal, chemical, or  $\text{pCO}_2$  differences in the precipitating fluid (cf. Pentecost, 1999). In some isopachous cements in the Miette tufa, dissolution of micritic bands has left sub-aligned void spaces (Fig. 6.3B). The cements in the bedded tufa facies appear to be primary; some stem directly from preserved filaments (Fig. 3.17C) and banding probably reflects changes in the chemistry or temperature of the spring water from which they precipitated.

Isopachous and meniscus sparry calcite fringes formed as primary encrusting precipitates on microbial structures in the stromatolitic tufa facies (Fig. 3.10B) and as later stage cements (Fig. 6.3C). Isopachous calcite fringes form in pore spaces inundated with through flowing water, whereas meniscus calcite fringes form in pore spaces partially filled with flowing water (Pedley, 1992). Cessation and resurgence of water movement through the Miette tufa resulted in multiple generations of sparry calcite fringes in the tufa/allochthonous lithoclast conglomerate (Fig. 3.6C, D).

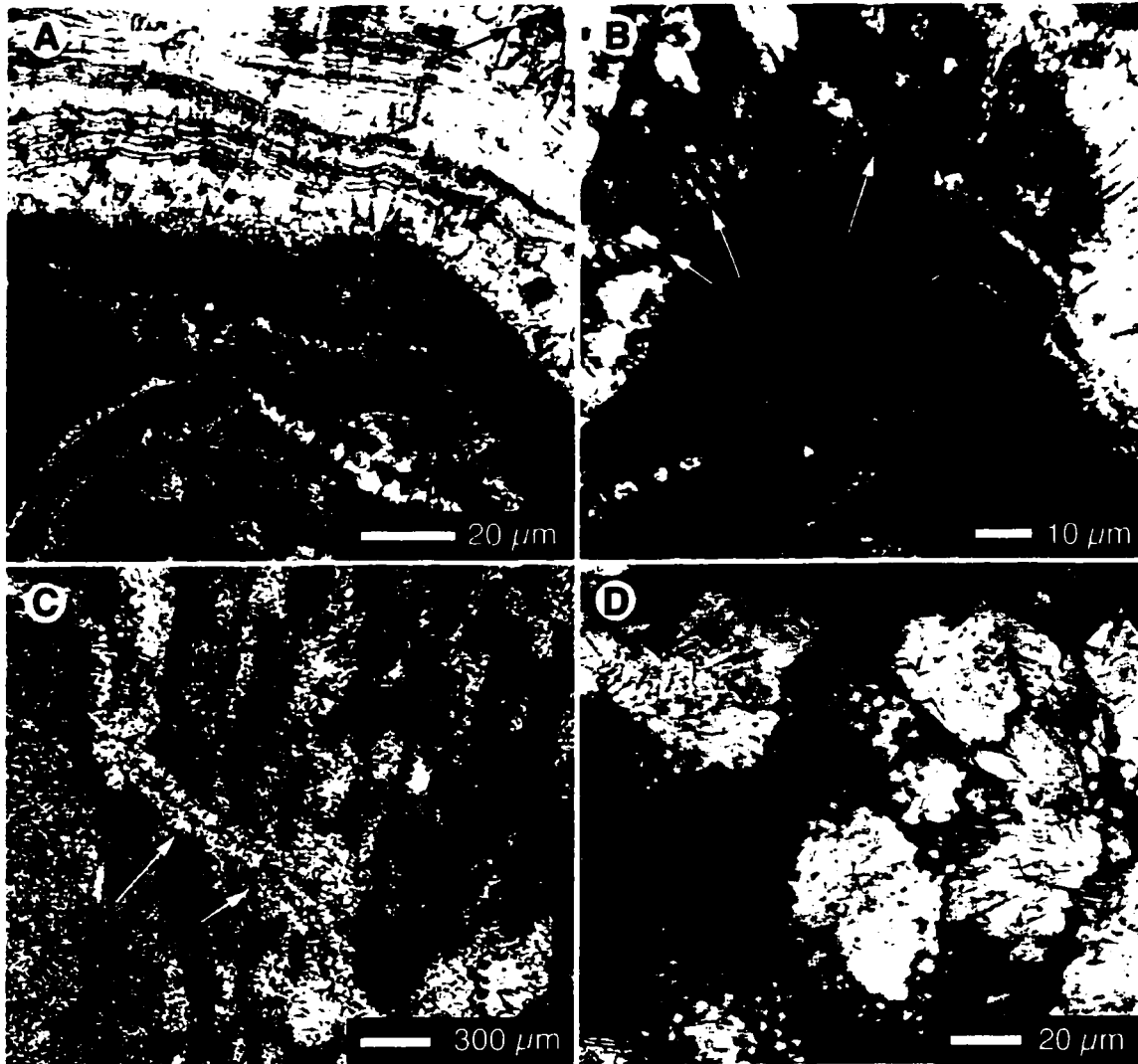


**Figure 6.3**

(A,B) Photographs of a thin section of the bedded facies (sample M2 from MS1) showing banded isopachous calcite cement. The cement rims consist of aligned calcite crystals which have euhedral ends where they terminate in open pore space (arrow in A), and have alternating bands of light coloured macro-crystalline calcite and dark coloured micrite. In some instances, micritic layers have dissolved out, leaving bands of pore space (arrows in B). (C) Photograph of a thin section of PLF tufa (sample M22 from MS6) showing isopachous sparry fringes coating void spaces between microbial structures and along a fracture (arrows). (D) Detail of splaying mosaic calcite cements found in pore spaces in massive facies sample M44 from MN1.



Mosaic cement textures are found in the center of filament structures in the stromatolitic facies, throughout the sheet facies, in sheets in the crenulated facies, and as a later stage cements in the massive facies (Fig. 6.3D). Mosaic cements consist of equant calcite crystals with planar to sub-planar crystal boundaries and have euhedral crystal ends where they terminate in open space (cf. Scholle, 1978). Such cements can form as primary cements around organic structures (cf. Pentecost, 1978; Emeis, 1987; Love and Chafetz, 1988). The presence of filament casts in the center of well-formed mosaic calcite crystals in the sheet tufa facies (Fig. 3.21C), and in the center of microbial columns in the stromatolitic facies (Fig. 3.31E, F), implies that the cement was a primary precipitate. Later stage splaying calcite mosaics found in the massive tufa facies (Fig. 3.33C, 6.3D) probably precipitated from standing pore fluids.

The banded isopachous cements, sparry fringes and mosaic cements are found in all of the tufa facies, and, locally, heavy cementation produced the massive facies by obscuring primary textures. Interestingly, one thin section of massive facies tufa contained relic textures – cross-sections through microbial columns (Fig. 3.34). Thus, even highly weathered tufa, that looks featureless in the field, may retain information about primary precipitation patterns. However, infiltration of meteoric water and precipitation of these secondary cements may also have obliterated primary isotopic signatures (Chapter 4).

Calcite cement growth is permitted by delivery of  $\text{Ca}^{2+}$  and  $\text{CO}_3^{2-}$  ions. In the case of primary cements, these were derived from the spring water. After activity ceased at the fossil spring vents, dissolution of pre-deposited tufa supplied ions for later stage cement growth. The loss of surface textures in the massive and granular tufa facies speaks for indiscriminate dissolution of surface exposed carbonate across the fossil tufa deposit. Beneath this surface layer, void spaces in sparry and bi-terminal crystals, corroded crystal cores, and hollow spar crystals may have been generated by discriminating dissolution of less stable mineral phases from the tufa. High Mg-calcite, for example, is more prone to dissolution and recrystallization than its lower energy, low-Mg calcite counterpart (Walter, 1986). Dissolution of less stable mineral phases may provide an important carbonate source for secondary mineral precipitates.

Not all of the re-distributed carbonate mineralogy is sequestered by cement growth; SEM and thin section investigations also revealed the presence of micro-scale mineral precipitates. Micritic coatings wrap around void spaces, coat sparry calcite crystals and chasmo-/endo-lithic filamentous microbes, and locally, fill primary filament casts. There are three types of micrite in the fossil Miette tufa: twinned fibre calcite blades, filiform micro-rod fibre micrite, and nodular micrite.

The twinned fibre calcite blades are found in granular and stromatolitic tufa in the upper tufa ledge. The crystals (4-5 x 0.5  $\mu\text{m}$ ) are usually straight or gently bowed, have blunt ends, and consist of two parallel cylindrical crystals (Fig. 6.4). They are identical to the “2-lobed composite fibre crystals” described by Jones and Kahle (1993) and the “coupled monocrystalline rods” designated MA1 and MA3 by Verrecchia and Verrecchia (1994). The crystals are randomly arranged in porous meshworks and are commonly associated with mucus, bacterial bodies, and fungal hyphae (Fig. 6.4).

The origin of these crystals has been attributed to biologically induced calcite precipitation in the interior of fungal hyphae, subsequent to which random crystal orientations are achieved by decay of the hyphal sheaths (Phillips and Self, 1987; Verrecchia and Verrecchia, 1994). The mucus or gel-like material associated with twinned fibre calcite blades in the Miette fossil tufa may have been produced by bacteria using fibre crystal forming fungi as a food source. The mucus may also compliment fungal processes to promote the growth of the crystal blades since the adsorption of organic molecules to a crystal can inhibit growth in certain directions, leading to elongated crystal habits (cf. Verrecchia and Verrecchia, 1994). Alternately, the fibre calcite crystals may have been produced without biological mediation. Fibre calcite crystals have been produced experimentally by inorganic precipitation (Jones and Kahle, 1993); they are found in the surfaces of microbial mats and soils where rapid evaporation controls water chemistry (Chafetz *et al.*, 1985; Jones and Kahle, 1993; Pentecost *et al.*, 1997); and, ion poisoning may produce distinctively elongate crystal morphologies (James, 1972; Folk, 1974). The critical requirement for the formation of fibre calcite crystals seems to be the presence of pore fluids highly saturated in  $\text{CaCO}_3$  (James, 1972) and if “...biogenic/abiogenic factors are important, as seems to be common, it is because they directly or indirectly modify the [pore] fluid and create conditions suitable for the

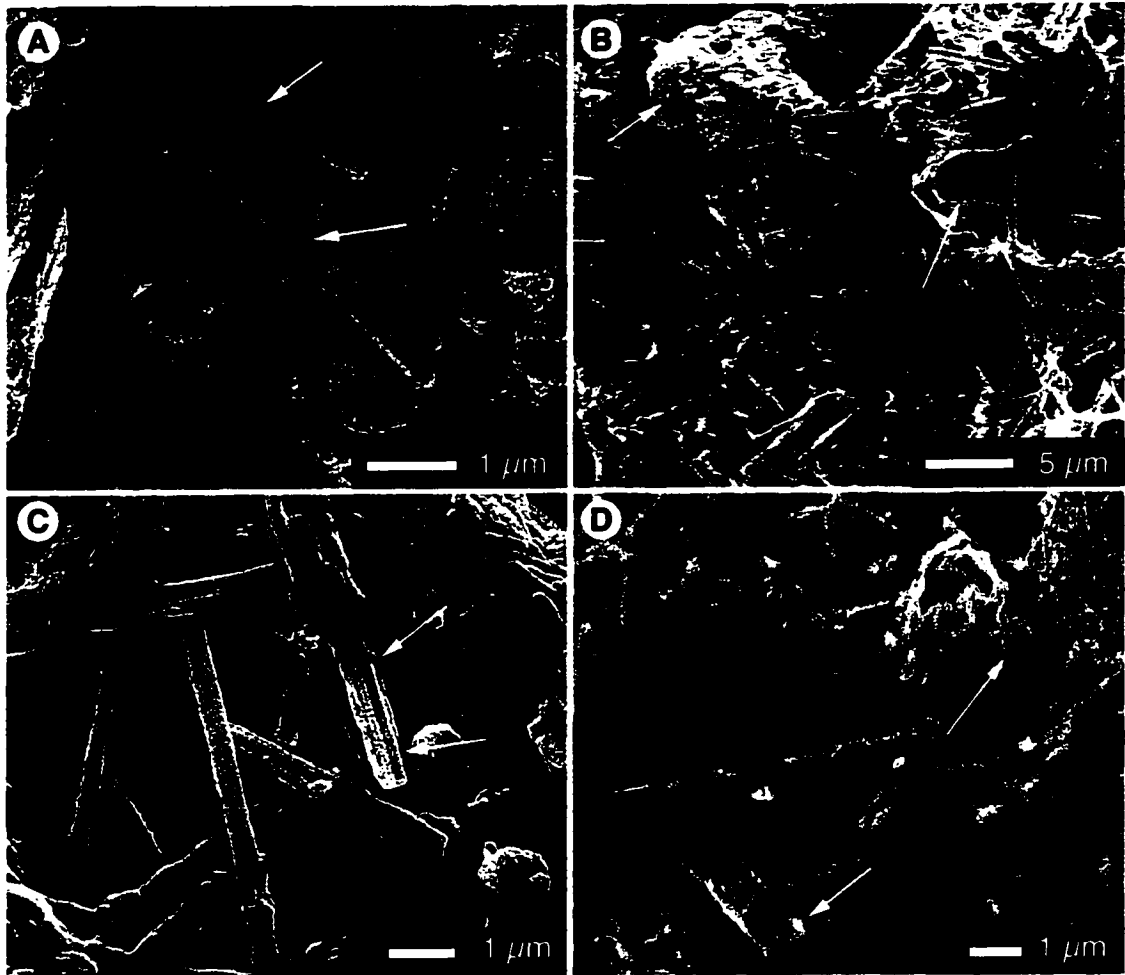


**Figure 6.4**

SEM images of coupled fibre calcite crystals from granular tufa sample M12 from MS4. (A) Isolated crystal emerging from mucus containing bacteria (arrows). (B) Random meshwork of crystals in open pore space between corroded calcite crystals (arrows). (C) Detail of crystals from previous image; note the presence of parallel striations running lengthwise along the flat surface of each crystal twin (arrows). (D) Detail of a coupled crystal emerging from bacterial mucus with a pocket of micro-rod fibre micrite nearby (arrows).

precipitation of fibre... crystals” (Jones and Kahle, 1993). Fibre calcite crystals are found in divergent diagenetic settings (from arid desert calcretes to moist cave deposits, and in both phreatic and vadose settings) that are geographically widespread, and are a common constituent of subaerial terrestrial carbonates (Jones and Kahle, 1993; Verrecchia and Verrecchia, 1994). They have been described in fossil tufa situated above modern ground water tables (Janssen *et al.*, 1999) and in the upper layers of actively calcifying microbial mats at the Pammukle Travertine, Turkey (Pentecost *et al.*, 1997).

Filliform micro-rod fibre micrite (monocrystal M, cf. Verrecchia and Verrecchia, 1994) is the most abundant secondary mineral form in the fossil Miette tufa and it was found in every facies examined, usually in association with mucus gels (Fig. 6.5). The crystals are small (0.1 to 1  $\mu\text{m}$  x 50 to 150 nm), approximately cylindrical (though some taper apically), have rounded crystal ends, and are rarely straight along their length. Curving, bundled micro-rods form “tangential needle fibre” sheets that coat larger calcite crystal faces and siliceous microfossils (cf. Jones and Kahle, 1993). The rods also form bridges that span cavities, and, locally, tubular voids or “doughnuts” (Fig. 6.5A, B, D). This arrangement is termed an “alveolar texture” and its origin has been attributed to the precipitation of the micro-rods on and about roots and microbial filaments whose subsequent decay leaves the rounded structures unsupported (Phillips and Self, 1987). The micro-rods themselves are thought to be nucleated by crystallites formed inorganically in extracellular mucus, or to form around calcified bacteria (Verrecchia and Verrecchia, 1994). Some of the porous sheet networks the Miette micro-rods form could be explained by precipitation about rootlets or filaments, but other micro-rod structures seem to mimic shapes defined by desiccated mucus sheets (Fig. 6.5B), indicating that filaments/rootlets may not have been required for structural support. Locally, the micro-rods also form nest-like bundles and conical “volcano” structures that look like congregations of sociable worms (Fig. 6.5C). This structural arrangement is described by Verrecchia and Verrecchia (1994) who attributed its genesis to reorganization of micro-rods by circulating solutions such that they are progressively concentrated around pore edges or air bubbles. If the mucus associated with the micro-rod crystals in the Miette tufa is critical to their genesis, nest and volcano micro-rod arrangements could also be derived from the spatial arrangement of bacterial colonies, or globular mucus masses.

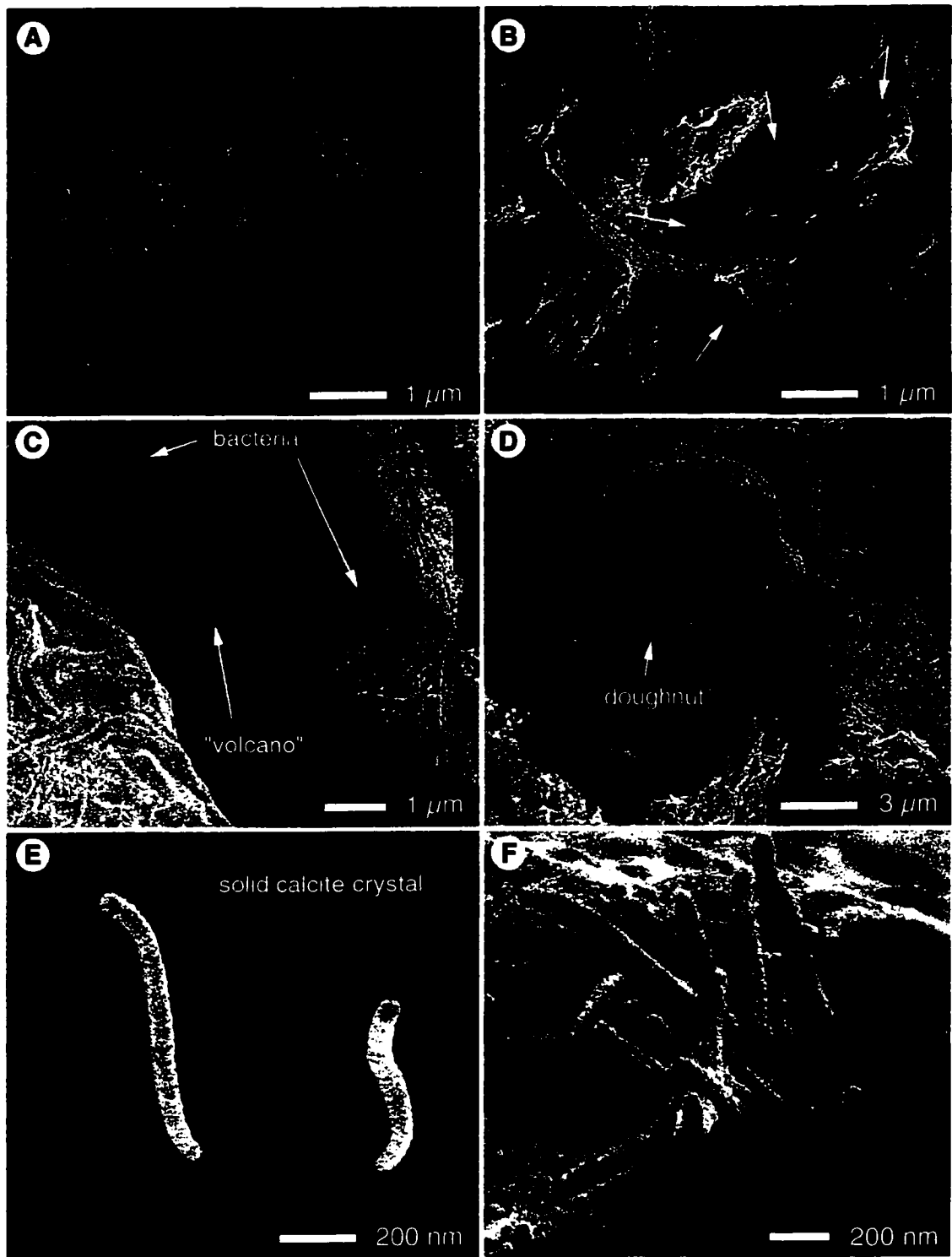


**Figure 6.5**

SEM images of micro-rod micrite. (A) Random mesh of micro-rods in porous laminar sample M24 from MS6. (B) Micritised mucus strands(?) form curtains in void spaces in porous laminar tufa sample M53. (C) Micro-rod "volcano" surrounded by bacteria and mucus - from sample M53. (D) Micro-rod "doughnut" from sample M53. (E) Free standing micro-rods found on solid crystal faces in sample M53. (F) Tongue shaped, twinned, apically tapering micro-rod micrite from porous laminar tufa sample M9 found at MS4.

Most of the micro-rods in the fossil Miette tufa are bi-terminal, but a few were found attached to larger crystal faces at one end. These crystals are very small (usually less than 0.5  $\mu\text{m}$  long) and reach out from the substrate in multiple directions forming fingers and fans of “standing worms” (Fig. 6.5E, F). In several instances, these tiny crystals are twinned, and apically tapering, taking on the appearance of outstretched tongues (Fig. 6.5F). It is possible that these crystals were supported by mucus during growth, which degraded, leaving free-standing structures. Alternately, they may have grown subaqueously, supported by surrounding hydrostatic pressures (similar to larger scale subaqueous helictite growth described by Davis *et al.* (1990)).

Anhedral to subhedral nodular micrite is found capping calcite crystal ends, encrusting endolithic and chasmolithic microbes, and back-filling primary filament casts throughout the fossil Miette tufa (Fig. 6.6). The nodular micrite is presumably an “inorganic” precipitate from carbonate saturated fluids. Where it fills cavities (Fig. 6.6E), it may be detrital; where it forms rinds on larger crystals (Fig. 6.6F), it probably formed from solution; and, where it is found coating young filaments (Fig. 6.6A-C), it may be recrystallized. Although the small size of the crystallites did not allow elemental investigation, some of the crystals found on “calcifying” endolithic and chasmolithic filaments (Fig. 6.1F, 6.6A-C) may have been calcium oxalate. Verrecchia *et al.* (1993) found that filament mineralization in calcretes is initiated by the formation of rhombohedral calcium oxalate, which has commonly been misidentified as calcite. Calcium oxalate recrystallizes to calcite with diagenesis (Verrecchia *et al.*, 1993), and the nodular micrite found on filaments in the Miette tufa may represent an early stage of recrystallization. Alternately, if formation of the fibre and micro-rod micrite is biologically mediated, then the nodular micrite may simply be the product of micritic precipitation free of direct biological control.

Minute dodecahedral (a rhombic prism terminating in two pyramids) and rhombic crystals were also found in bryophyte tufa and mineralized wood at MNN. The crystals are euhedral (2-3  $\mu\text{m}$  wide), intergrown with calcite and micrite or borne on siliceous microfossils, and are associated with bacterial mucus and body fossils (Fig. 6.7, 3.29D). The dodecahedral and rhombic crystals are respectively identical to crystals of

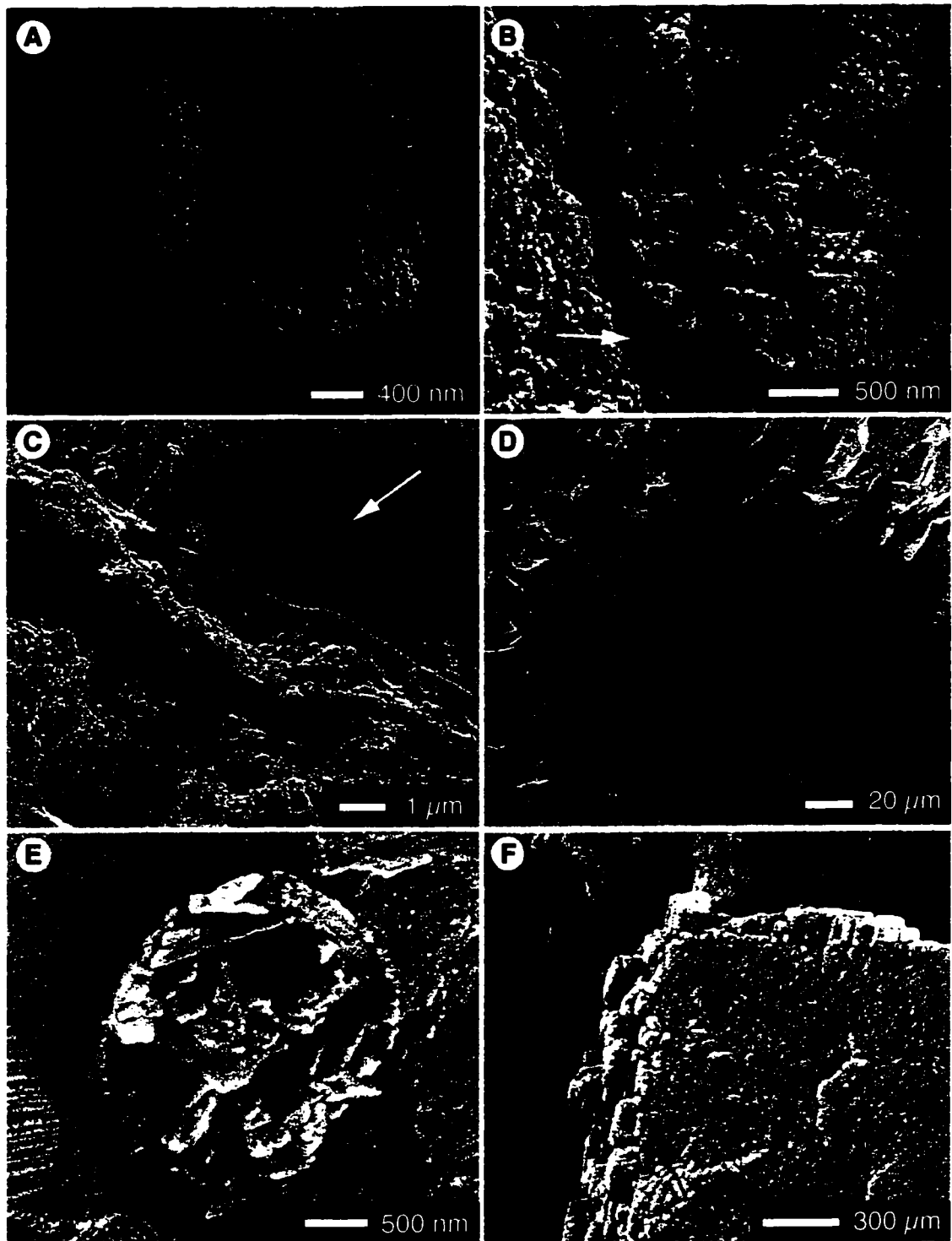


**Figure 6.6**

SEM images of nodular and rhombic micrite. (A) Nodular micrite encrusted chasmolithic filament overlying an unmineralised chasmolithic filament from sheet tufa sample M53 collected at MN3. (B,C) Varying degrees of encrustation by nodular micrite on chasmolithic filaments. Some micro-rod micrite is also present in B and C (arrows). (D) Nodular micrite capping sparry calcite lining pore spaces in porous laminar tufa sample M24 from MS6. (E) Rhombic micrite backfilling a filament cast in mineralised wood sample M60 from MNN2. (F) Rhombic micrite rind on large calcite crystals in bryophyte tufa sample M59 from MNN1.

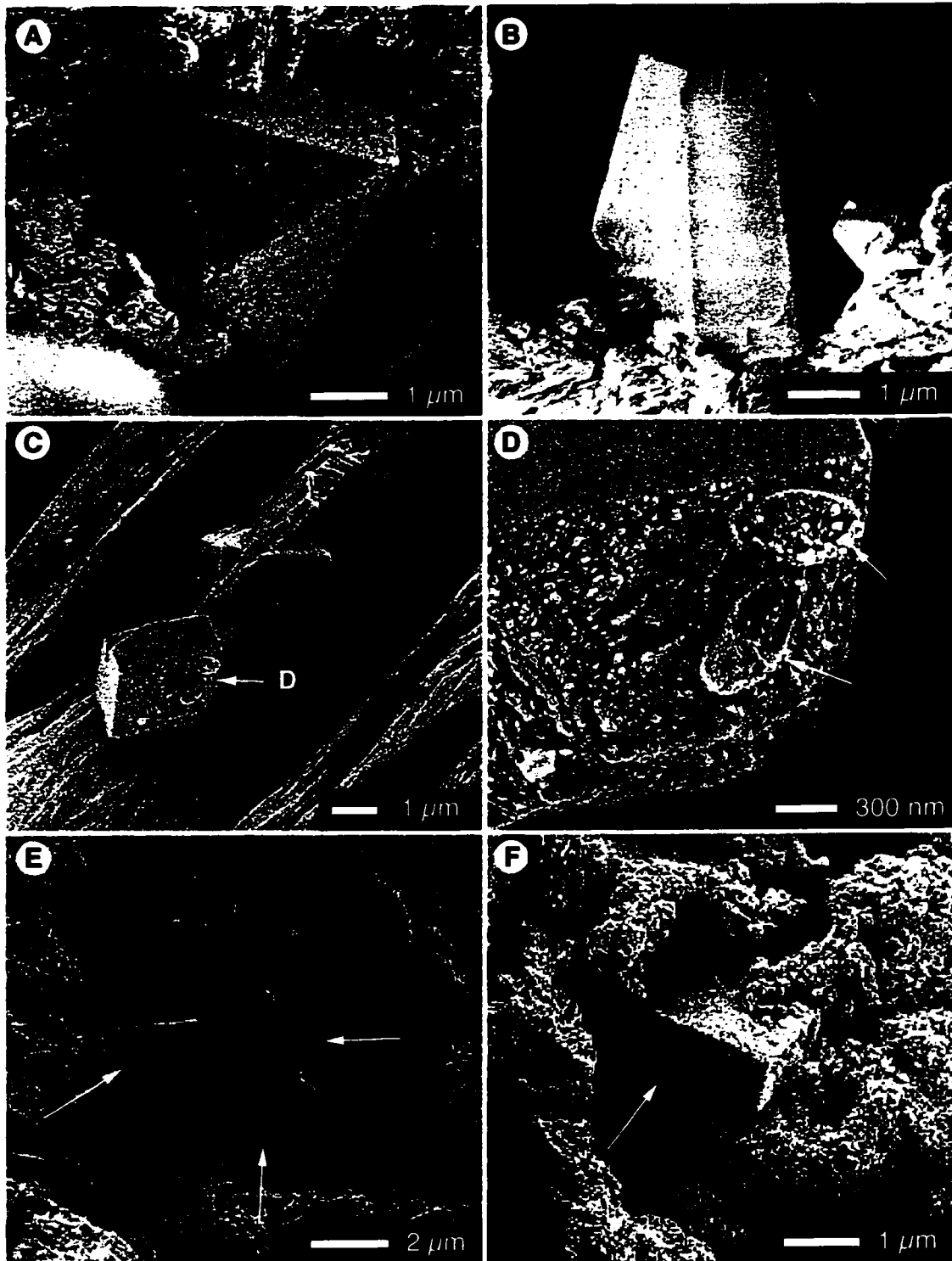


**Figure 6.7**

SEM images of dodecahedral and rhombic calcium oxalate crystals found in mineralised wood and bryophyte tufa from the north end of the Miette tufa exposure (MNN): (A) Calcium oxalate crystal skirted by mucus (arrow). (B) Side view of dodecahedral crystal structure. (C) Calcium oxalate crystals intergrown with etched calcite and hosting bacterial body fossils. (D) Detail of bacterial body fossils. (E, F) Rhombic calcium oxalate surrounded by micro-rod fibre micrite (E) and nodular micrite (F).



polyhydrate calcium oxalate ( $\text{CaC}_2\text{O}_4 \cdot (2 + x)\text{H}_2\text{O}$ ) and monohydrate calcium oxalate (whewillite) described by Verrecchia *et al.* (1993). Calcium oxalate crystals are common constituents of calcretes formed in the presence of organic exudates. Species of lichens, seeds, and filamentous fungi excrete oxalic acids which react with available  $\text{Ca}^{2+}$  in the environment or in cell walls, forming calcium oxalate salts (Lewin and Charola, 1981; Verrecchia *et al.*, 1993). In the Miette tufa the dodecahedral calcium oxalate crystals found associated with the mineralized bryophytes and wood are commonly skirted by mucus and host bacterial body casts. The formation of these crystals may have been instigated by the chemical exudates of the bacteria. Alternately, the bacteria may have been colonizing other organisms, such as filamentous fungi, whose exudates promoted mineral precipitation. Ca-oxalate crystals were extracted from actively growing moss travertines (a.k.a. bryophyte tufa) by Freytet and Verrecchia (1995) proving that they can be produced as primary components of bryophyte dominated spring deposits. The growth of Ca-oxalate crystals in the Miette tufa may have taken place during tufa growth, or the crystals may be relics of the tufa's exposure on a forested hill slope during which time it was colonized by plants, lichens, fungi, and, almost certainly, many bacteria. The fact that the dodecahedral crystals are found favours the latter scenario because polyhydrate calcium oxalate is metastable. It is altered to more stable monohydrate calcium oxalate by epitactic growth, and eventually this is changed to calcium carbonate with diagenesis "...probably as a result of soil microfauna and bacterial activities" (Verrecchia *et al.*, 1993).

The reason for the difference in habit between calcium oxalate in the south (nodular coatings on filaments) and north (euhedral crystals) end of the fossil tufa deposit is unknown, but may be related to the relative proportions of bacteria and fungi inhabiting the rock: tufa collected from the north end of the deposit contained abundant bacteria, bacterial mucus, and large euhedral calcium oxalate crystals; tufa collected from the south end of the deposit contained fewer bacteria, abundant fungal hyphae and spore clusters, and calcium oxalate (if present) is found only as anhedral to subhedral crystals borne by microbial filaments.

The micrite and calcium oxalate formed from carbonate rich waters that derived their mineral load from dissolution of surrounding tufa. The percolation of water through

pore spaces results in saturation with carbonate mineral phases, and, if the water is allowed to pass through the tufa without redepositing its mineral load, calcite is precipitated at its point of exit from the tufa. Where the fossil Miette tufa forms overhangs, such as in the former spring vent pool “caves” and beneath displaced boulders, carbonate has been locally redeposited as speleothems including moon-milk rinds, cave popcorn, and miniature stalagmites and stalactites.

### 6.5 *Summary*

The fossil Miette tufa has been subject to extensive change since deposition as the result of environmental stresses, biological colonization, and various mineralogical changes during diagenesis. The original porosity of the tufa was reduced by the deposition of cements, the (possibly biologically mediated) growth of micrite and calcium oxalate, and the calcification of endolithic and chasmolithic microbes. Frost and root wedging, dissolution, and infiltration of humic acids and the metabolic by-products of microbes weakened the tufa and, locally, obliterated surface textures. These processes were most efficient in surface exposed layers of the tufa such that the cross-sections of tufaceous strata provided by fracture and disarticulation of the spring mound yield the best view of the original tufa facies.

## 7 Conclusions

At the modern Miette Hot Springs:

- (1) There is currently no tufa growth.
- (2) The spring flow paths are dominantly populated by species of *Oscillatoria* and *Phormidium* and a *Cymbella* dominated diatom assemblage.
- (3) Precipitates of gypsum and elemental sulphur are found in the spring flow paths with lesser quantities of microcrystalline calcite and strontianite.
- (4) Precipitation is induced by inorganic cooling and degassing but photosynthetic microbes growing in the spring water influence the  $\delta^{13}\text{C}$  of the carbonate mineral precipitates, intercellular mucus in microbial mats supports suspended mineral growth, gypsum and sulphur nucleated in suspension are accumulated by adherence to the surfaces of microbial sheaths, and diatom mucus is associated with crystal corrosion.

At the fossil Miette Hot Springs:

- (1) A line of hot thermal springs (50-65°C at the vents) that perched ~30 m above the bed of Sulphur Creek supported tufa growth on an unstable slope for ~2000 years, beginning during a moist climate interval in the Neoglacial.
- (2) The hot thermal springs had similar chemistry to the modern Miette Hot Springs but had higher hydrologic head (and possibly higher vent temperature), which maximized  $\text{CO}_2$  loss at the vent, promoting carbonate mineral precipitation.
- (3) A warm thermal spring at MNN supported tufa growth concurrently with or subsequent to activity at the hot thermal springs to its south.
- (4) Variation in the topography of the flow path produced six distinct tufa morphotypes.
- (5) Variations in the topography, rate of precipitation, style and rate of flow, water temperature, and biological species present produced eight distinct primary facies in the fossil tufa. Two other facies formed through diagenetic alteration of primary textures.

- (6) Precipitation from the fossil spring water was driven by inorganic degassing but precipitation on and about filamentous microbes and bryophyte colonies produced biologically mediated textures.
- (7) As tufa growth diminished at the fossil springs (~2500 years BP), spring vents migrated to progressively lower elevations, emerging through and undercutting pre-deposited tufa. These later stage spring waters precipitated gypsum and strontianite in pore spaces in the fossil tufa they emerged through.
- (8) Since deposition, the fossil Miette tufa has been subject to diagenetic change and the tufa deposit has been disarticulated by landslide activity.

Combining observation of the modern and fossil Miette Hot Springs, the following conclusions can be drawn:

- (1) Spring activity at the Miette Hot Springs site is a persistent feature of Sulphur Creek Valley.
- (2) The Miette Hot Springs respond to regional changes in moisture with an increased volume of flow at their vents, which may result in a shift from dominant precipitation of gypsum and strontianite to dominant precipitation of calcium carbonate.

## WORKS CITED

- Andrews, J.E., Riding, R. and Dennis, P.F. 1997. The stable isotope record of environmental and climatic signals in modern terrestrial microbial carbonates from Europe. *Palaeogeography, Palaeoclimatology, Palaeoecology*, **129**: 171-189.
- Arp, G., Reimer, A. and Reitner, J. 2001. Photosynthesis-induced biofilm calcification and calcium concentrations in Phanerozoic oceans. *Science*, **292**: 1701-1704.
- Arp, G., Theil, V., Reimer, A., Michaelis, W. and Reitner, J. 1999. Biofilm exopolymers control microbialite formation at thermal springs discharging into the alkaline Pyramid Lake, Nevada, USA. *Sedimentary Geology*, **126**: 159-176.
- Bachu, S. and Hitchon, B. 1996. Regional-scale flow of formation waters in the Williston Basin. *American Association of Petroleum Geologists Bulletin*, **80**: 248-264.
- Baird, D.M. 1963. Jasper National Park: Behind the mountains and glaciers. *Miscellaneous Report 6, The Geological Survey of Canada: Ottawa*.
- Bartley, J.K. 1996. Actualistic taphonomy of cyanobacteria: implications for the Precambrian fossil record. *Palaios*, **11**: 571-586.
- Bauld, J. 1981. Geobiological role of cyanobacterial mats in sedimentary environments and production and preservation of organic matter. *BMR Journal of Australian Geology and Geophysics*, **6**: 307-317.
- Beaudoin, A.B., Wright, M. and Ronaghan, B. 1996. Late Quaternary landscape history and archeology in the "Ice-Free Corridor." Some recent results from Alberta. *Quaternary International*, **32**: 113-126.
- Borneuf, D. 1983. Earth Sciences Report 82-3: Springs of Alberta. Alberta Research Council, National Resources Division, Groundwater Development.
- Braithwaite, C.J.R. 1979. Crystal textures of recent fluvial pisolites and laminated crystalline crusts in Dyfed, South Wales. *Journal of Sedimentary Petrology*, **49**(1): 181-194.
- Brandon, L.V. 1965. Groundwater hydrology and water supply in the District of Mackenzie, Yukon Territory, and adjoining parts of British Columbia. *Geological Survey of Canada, Paper 64-39*. 102p.
- Brock, T.D. 1978. *Thermophilic Microorganisms and Life at High Temperatures*. Springer-Verlag: New York.
- Brues, C.T. 1927. Animal life in hot springs. *Quaternary Review of Biology*, **2**(2): 181-203.

- Buczynski, C. and Chafetz, H.S. 1991. Habit of bacterially induced precipitates of calcium carbonate and the influence of medium viscosity on mineralogy. *Journal of Sedimentary Petrology*, **61**: 226-233.
- Canter-Lund, H. and Lund, J. 1995. *Freshwater Algae – Their microscopic world explored*. Bio Press Ltd: Bristol, England.
- Casanova, J. and Renaut, R. 1987. Les stromatolites du milieu hydrothermal. *In* Le demi-graben de Baringo-Bogoria, Rift Gregory, Kenya: 30,000 ans d'histoire hydrologique et sedimentaire. *Edited by* Tiercelin, J.J. and Vincens, A. Centres de Recherches Exploration – Production Elf- Aquitaine, Bulletin 11, p. 484-490.
- Castanier, S., Le Metayer-Lecrel, G. and Perthuisot, J. 1999. Ca-carbonates precipitation and limestone genesis – the microbiogeologist point of view. *Sedimentary Geology*, **126**: 9-23.
- Castenholz, R.W. 1969. Thermophilic blue green algae and the thermal environment. *Bacteriological Reviews*, **33**(4): 476-504.
- Castenholz, R.W. 1973. Ecology of blue-green algae in hot springs. *Botanical Monographs*, **9**: 379-414.
- Castenholz, R.W. 1976. The effect of sulfide on the bluegreen algae of hot springs. I. New Zealand and Iceland. *Journal of Phycology*, **12**: 54-68.
- Cecile, M.P. and Jones, L.D. 1979. Note on radioactive barite sinter, Bonnet Plume map area, District of Mackenzie. Geological Survey of Canada, Paper 79-1B. 416.
- Chafetz, H.S. and Folk, R. 1984. Travertines: depositional morphology and the bacterially constructed constituents. *Journal of Sedimentary Petrology*, **54**(1): 289-316.
- Chafetz, H.S. and Guidry, S.A. 1999. Bacterial shrubs, crystal shrubs, and ray-crystal shrubs: bacterial vs. abiotic precipitation. *Sedimentary Geology*, **126**: 57-74.
- Chafetz, H.S., Wilkinson, B.H. and Love, K.M. 1985. Morphology and composition of non-marine carbonate cements in near-surface settings. *SEPM Special Publication* 36: 337-347.
- Chafetz, H.S., Rush, P.F. and Utech, N.M. 1991a. Microenvironmental controls on mineralogy and habit of CaCO<sub>3</sub> precipitates: an example from an active travertine system. *Sedimentology*, **38**: 107-126.

- Chafetz, H.S., Utech, N.M. and Fitzmaurice, S.P. 1991b. Differences in the  $\delta^{18}\text{O}$  and  $\delta^{13}\text{C}$  signatures of seasonal laminae comprising travertine stromatolites. *Journal of Sedimentary Petrology*, **61**: 1015-1028.
- Cohen, Y., Jorgensen, B.B., Padan, E. and Shilo, M. 1975. Sulphide-dependent anoxygenic photosynthesis in the cyanobacterium *Oscillatoria limnetica*. *Nature*, **257**: 489-492.
- Collins English Dictionary – Millenium edition. 1999. HarperCollins Publishers: Glasgow.
- Criss, R.E. and Taylor Jr., H.P. 1986. Meteoric-hydrothermal systems. *In Valley, Edited by J.W., Taylor Jr., H.P. and O'Neil, J.R. Stable Isotopes in High Temperature Geological Processes. Reviews in Mineralogy*, **16**. Mineralogical Society of America: Chelsea, Michigan, p. 373-422.
- Davis, D.G., Palmer, M.V. and Palmer, A.N. 1990. Extraordinary subaqueous speleothems in Lechuguilla. *NSS Bulletin*, **52**: 70-86.
- Defarge, C., Trichet, J., Maurin, A. and Hucher, M. 1994. Kopara in Polynesian atolls: early stages of formation of calcareous stromatolites. *Sedimentary Geology*, **89**: 9-23.
- Doemel, W.N. and Brock, T.D. 1977. Structure, growth, and decomposition of laminated algal-bacterial mats in alkaline hot springs. *Applied and Environmental Microbiology*, **34** (4): 433-452.
- Dowling, D.B. 1911. Coal fields of Jasper Park, Alta. Summary Report of the Geological Survey of Canada, 150-168.
- Elworthy, R.T. 1926. Hot springs in western Canada; their radioactive and chemical properties. Institute of Petroleum: London.
- Emeis, K.C., Richnow, H.H. and Kempe, S. 1987. Travertine formation in Plitvice National Park, Yugoslavia: chemical versus biological control. *Sedimentology*, **34**: 595-609.
- Folk, R.L. 1974. The natural history of crystalline calcium carbonate: effect of magnesium content and salinity. *Journal of Sedimentary Petrology*, **44**(1): 40-53.
- Folk, R.L. 1994. Interaction between bacteria, nannobacteria, and mineral precipitation in hot springs in central Italy. *Geographie Physique et Quaternaire*, **48**: 233-246.
- Ford, T.D. and Pedley, H.M. 1996. A review of tufa and travertine deposits of the world. *Earth-Science Reviews*, **41**: 117-175.

- Forester, R.M. 1991. Ostracode assemblages from springs in the western United States: implications for paleohydrology. *Memoirs of the Entomological Society of Canada*, **155**: 181-201.
- Fouke, B.W., Farmer, J.D. Des Marias, D.J. and Discipulo, M.K. 1997. Integrated inorganic and organic controls on the mineralogy and geochemistry of modern travertines, Mammoth Hot Springs, Yellowstone National Park. Abstracts with Programs – Geological Society of America, **29**: 130.
- Freytet, P. and Verrecchia, E.P. 1995. Discovery of Ca-oxalate crystals associated with fungus in moss travertines (byoherms, freshwater heterogeneous stromatolites). *Geomicrobiology Journal*, **13**: 117-127.
- Gadd, B. 1999. *Handbook of the Canadian Rockies* (2<sup>nd</sup> edition). Corax Press: Jasper, Canada.
- Gandolfi, A., Todeschi, E.B.A., Rossi, V. and Menozzi, P. 2001. Life history traits in *Darwinula Stevensoni* (Crustacea: Ostracoda) from southern European populations under controlled conditions and their relationship with genetic features. *Journal of Limnology*, **60**(1): 1-10.
- Grasby, S. 1998. Controls on the occurrence and chemistry of thermal springs in the Canadian Cordillera. *Reservoir*, **25**(3): 8.
- Grasby, S.E. and Hutcheon, I. 2001. Controls on the distribution of thermal springs in the southern Canadian Cordillera. *Canadian Journal of Earth Science*, **38**: 427-440.
- Grasby, S.E., Hutcheon, I. and Krouse, H.R. 2000a. Influence of water-rock interaction of the chemistry of thermal springs in western Canada. *Applied Geochemistry*, **15**: 439-454.
- Grasby, S.E., Osadetz, K., Betcher, R. and Render, F. 2000b. Reversal of the regional-scale flow system of the Williston basin in response to Pleistocene glaciation. *Geology*, **28**(7): 635-638.
- Griffiths, H.I., Pillidge, K.E., Hill, C.J., Evans, J.G. and Learner, M.A. 1996. Ostracod gradients in a calcareous stream: Implications for the palaeoecological interpretation of tufas and travertines. *Limnologica*, **26** (1): 49-61.
- Gulley, A.L. 1993. Rabbitkettle Hotsprings, Nahanni National Park Reserve, N.W.T.: a hydrogeological study. Masters thesis, Ottawa-Carleton Geoscience Centre, Carleton University.



- Guo, L., Andrews, J., Riding, R., Dennis, P. and Dresser, Q. 1996. Possible microbial effects on stable carbon isotopes in hot spring travertines. *Journal of Sedimentary Research*, **66**: 468-473.
- Guo, L. and Riding, R. 1998. Hot-spring travertine facies and sequences, Late Pleistocene, Rapolano Terme, Italy. *Sedimentology*, **45**: 163-180.
- Haug, G.H., Huchen, K.A., Sigman, D.M., Peterson, L.C. and Rohl, U. 2001. Southward migration of the Intertropical Convergence Zone through the Holocene. *Science*, **293**: 1304-1308.
- Henning, G.J., Grun, R. and Brunnacker, K. 1983. Speleothems, travertines, and paleoclimates. *Quaternary Research*, **20**: 1-29.
- Hern. J.D. 1989. Study and interpretation of the chemical characteristics of natural water. USGS Water Supply Paper 2254, 3<sup>rd</sup> edition.
- Heusser, C.J. 1956. Postglacial environments in the Canadian Rocky Mountains. *Ecological Monographs*, **26**(4): 263-302.
- Hinman, N.W. and Lindstrom, R.F. 1996. Seasonal changes in silica deposition in hot spring systems. *Chemical Geology*, **132**: 237-246.
- Hoffman, P. 1975. A search for early life. *Geos*, **Winter**: 12-14.
- James, N.P. 1972. Holocene and Pleistocene calcareous crust (caliche) profiles: criteria for subaerial exposure. *Journal of Sedimentary Petrology*, **42**: 817-836.
- Janssen, A., Swennen, R., Podoor, N. and Keppens, E. 1999. Biological and diagenetic influence in Recent and fossil tufa deposits from Belgium. *Sedimentary Geology*, **126**: 75-95.
- Janssens, J.A. 1990. Ecology of peatland bryophytes and palaeoenvironmental reconstruction of peatlands using fossil bryophytes. *Limnological Research Centre Contribution no. 346*.
- Jones, B. and Kahle, C.F. 1993. Morphology, relationship, and origin of fibre and dendrite calcite crystals. *Journal of Sedimentary Petrology*, **63**(6): 1018-1031.
- Jones, B. and Renaut, R.W. 1998. Origin of platy calcite crystals in hot-spring deposits in the Kenya Rift valley. *Journal of Sedimentary Research*, **68**(5): 913-927.
- Jones, B., and Renaut, R.W. 1996a. Skeletal crystals in calcite and trona from hot spring deposits in Kenya and New Zealand. *Journal of Sedimentary Research*, **66**(1): 265-274.

- Jones, B. and Renaut, R.W. 1996b. Influence of thermophilic bacteria on calcite and silica precipitation in hot springs with water temperatures above 90 degrees C; evidence from Kenya and New Zealand. *Canadian Journal of Earth Sciences*, **33**(1): 72-83.
- Jones, B., Renaut, R.W., Rosen, M.R. and Ansdell, K.M. 2002. Coniform stromatolites from geothermal systems, North Island, New Zealand. *Palaios*, **17**: 84-103.
- Jones, B., Renaut, R.W. and Rosen, M.R. 2001. Microbial construction of siliceous stalactites at geysers and hot springs: examples from the Whakarewarewa Geothermal Area, North Island, New Zealand. *Palaios*, **16**: 73-94.
- Jones, B., Renaut, R.W. and Rosen, M.R. 1998. Microbial biofacies in hot-spring sinters: a model based on Ohaaki Pool, North Island, New Zealand. *Journal of Sedimentary Research*, **68**(3): 413-434.
- Jones, B., Renaut, R.W. and Rosen, M.R. 1997. Vertical zonation of biota in microstromatolites associated with hot springs, North Island, New Zealand. *Palaios*, **12**: 220-236.
- Jones, B., Renaut, R.W. and Rosen, M.R. 1996. High-temperature (>90°C) calcite precipitation at Waikite Hot Springs, North Island, New Zealand. *Journal of the Geological Society, London*, **153**: 481-496.
- Kallio, P. and Karenlampi, L. 1975, Photosynthesis in mosses and lichens. *In* Photosynthesis and Productivity in Different Environments. *Edited by* J.P. Cooper. Cambridge University Press: Cambridge, p. 393-423.
- Kazmierczak, J. and Kempe, S. 1990. Modern cyanobacterial analogs of Paleozoic stromatoporoids. *Science*, **250**: 1244-1248.
- Kearney, M.S., and Luckman, B.H. 1987. A mid-Holocene vegetational and climatic record from the supalpine zone of the Maligne Valley, Jasper National Park, Alberta (Canada). *Palaeogeography, Palaeoclimatology, Palaeoecology*, **59**(4): 227-242.
- Kerr, R.C. and Turner, J.S. 1996. Crystallization and gravitationally controlled ponding during the formation of mound springs, terraces, and "black smoker" flanges. *Journal of Geophysical Research*, **101**: 125-137.
- Kim, S-T. and O'Neil, J.R. 1997. Equilibrium and nonequilibrium oxygen isotope effects in synthetic carbonates. *Geochimica et Cosmochimica Acta*, **61**(16): 3461-3475.
- Knoll, A.H. and Barhoorn, E.S. 1975. Precambrian eukaryotic organisms; a reassessment of the evidence. *Science*, **190**: 52-54.

- Konhauser, K.O., Phoenix, V.R., Bottrell, S.H., Adams, D.G. and Head, I.M. 2001. Microbial-silica interactions in Icelandic hot spring sinter; possible analogues for some Precambrian siliceous stromatolites. *Sedimentology*, **48**(2): 415-433.
- Lewin, S.Z. and Charola, A.E. 1981. Plant life on stone surfaces and its relation to stone conservation. *Scanning Electron Microscopy*, **1**: 563-568.
- Lepitzki, D. and Lepitzki, B. 2001. Preliminary resource reconnaissance of the invertebrates of some of Banff's thermal springs. Heritage Resource Conservation (Aquatics), Banff National Park.
- Levson, V. and Rutter, N.W. 1985. The last glacial in Jasper National Park. Program with Abstracts, Canqua Symposium on the Paleoenvironmental Reconstruction of the Late Wisconsin Deglaciation and the Holocene, 39.
- Love, M.L., and Chafetz, H.S. 1988. Diagenesis of laminated travertine crusts, Arbuckle Mountains, Oklahoma. *Journal of Sedimentary Petrology*, **58**(3): 441-445.
- Luckman, B.H. 1986. Reconstruction of Little Ice Age events in the Canadian Rocky Mounatins. *Geographie physique et Quaternaire*, **40**(1): 17-28.
- MacDonald, G.M. and Case, R.A. 2000. Biological evidence of multiple temporal and spatial scales of hydrological variation in the western interior of Canada. *Quaternary International*, **67**: 133-142.
- McDonald, J. 1978. Hotsprings of Western Canada: A Complete Guide. Labrador Tea Company: Vancouver, Canada.
- Miette Water Chemistry Report. 1989. Analytical Report Submitted to the Miette Hot Springs Resort by Norwest Labs, Edmonton.
- Miette Water Chemistry Report. 2000. Analytical Report Submitted to the Miette Hot Springs Resort by Norwest Labs, Edmonton.
- Merz, M.U.E. 1992. The biology of carbonate precipitation by cyanobacteria. *Facies*, **26**: 81-102.
- Merz-Preiß, M. and Riding, R. 1999. Cyanobacterial tufa calcification in two freshwater streams: ambient environment, chemical thresholds and biological processes. *Sedimentary Geology*, **126**: 103-124.
- Monty, C.L.V., 1976. The origin and development of cryptalgal fabrics. *In* *Stromatolites: Amsterdam, Elsevier, Developments in Sedimentology 20. Edited by Walter, M.N., p193-250.*
- Mountjoy, E.W. 1959. Miette, West of Fifth Meridian, Alberta. Geological Survey of

Canada, Map 40-1959.

- Mussieux, R. and Nelson, M. 2000. A Traveller's Guide to Geological Wonders in Alberta. The Provincial Museum of Alberta: Edmonton, p. 127.
- O'Neil, J.R., Clayton, R.N. and Mayeda, T.K. 1969. Oxygen isotope fractionation in divalent metal carbonates. *Journal of Chemical Physics*, **51**(12): 5547-5558.
- Osborn, G. and Luckman, B.H. 1988. Holocene glacier fluctuations in the Canadian Cordillera (Alberta and British Columbia). *Quaternary Science Reviews*, **7**(2): 115-128.
- Pannella, G.T.D. 1976. Geophysical inferences from stromatolite lamination. *In* *Stromatolites: Amsterdam, Elsevier, Developments in Sedimentology 20. Edited by Walter, M.N., 497-518.*
- Patrick, E. 1977. Ecology of freshwater diatoms. *In* *The biology of diatoms. Botanical Monographs # 13. Edited by Werner, D., Blackwell Scientific Publications: London, 285-332.*
- Pedley, H.M. 1990. Classification and environmental models of cool freshwater tufas. *Sedimentary Geology*, **68**: 143-154.
- Pedley, H.M. 1992. Freshwater (phytoherm) reefs: the role of biofilms and their bearing on marine reef cementation. *Sedimentary Geology*, **79**: 255-274.
- Pedley, M., Andrews, J., Ordonez, S., Garcia del Cura, M.A., Martin, J.G. and Taylor, D. 1996. Does climate control the morphological fabric of freshwater carbonates? A comparative study of Holocene barrage tufas from Spain and Britain. *Palaeogeography, Palaeoclimatology, Palaeoecology*, **121**: 239-257.
- Pentecost, A. 1978. Blue-green algae and freshwater carbonate deposits. *Proceedings of the Royal Society of London*, **200**: 43-61.
- Pentecost, A. 1999. The origin and development of the travertines and associated thermal waters at Matlock Bath, Derbyshire. *Proceedings of the Geologists' Association*, **110**: 217-232.
- Pentecost, A., Bayari, S. and Yesertener, C. 1997. Phototrophic microorganisms of the Pamukkle Travertine, Turkey: their distribution and influence on travertine deposition. *Geomicrobiology Journal*, **14**: 269-283.
- Pentecost, A. and Bauld, J. 1988. Nucleation of calcite on the sheaths of cyanobacteria using a simple diffusion cell. *Geomicrobiology Journal*, **6**: 129-135.

- Pentecost, A. and Riding, R. 1986. Calcification in cyanobacteria. *In* Biomineralisation in Lower Plants and Animals. Systematics Association Special Volume, 30. Clarendon Press: New York. P. 73-90.
- Pentecost, A. and Spiro, B. 1990. Stable carbon and oxygen isotope composition of calcites associated with modern freshwater cyanobacteria and algae. *Geomicrobiology Journal*, **8**: 17-26.
- Pfennig, N. 1989. Metabolic diversity among the dissimilatory sulfate-reducing bacteria. *Antonie Van Leeuwenhoek*, **56**: 127-138.
- Phillips, S.E. and Self, P.G. 1987. Morphology, crystallography and origin of needle-fibre calcite in Quaternary pedogenic calcretes of South Australia. *Australian Journal of Soil Research*, **25**: 429-444.
- Prescott, G.W. 1970. How to know the freshwater algae, 3<sup>rd</sup> ed. The pictured Key Nature Series, Wm. C. Brown Company Publishers: Dubuque, Iowa.
- Pritchard, G., Williams, D.D. and Danks, H.V. 1991. Insects in thermal springs. *In* Arthropods of Springs, With Particular Reference to Canada, Memoirs of the Entomological Society of Canada, p.89-106.
- Proctor, M.C.F. 2000. Physiological Ecology. *In* Bryophyte Biology. Edited by Shaw, A.J. and Goffinet, B. Cambridge University Press: Cambridge, U.K.
- Reeder, S.W., Hitchon, B., and Levinson, A.A. 1972. Hydrogeochemistry of the surface waters of the Mackenzie River drainage basin, Canada – I. Factors controlling inorganic composition. *Geochimica et Cosmochimica Acta*, **36**: 825-865.
- Renaut, R.W., Jones, B. and Tiercelin, J-J. 1998. Rapid *in situ* silicification of microbes at Loburu Hot Springs, Lake Bogoria, Kenyan Rift Valley. *Sedimentology*, **45**: 1083-1103.
- Renaut, R.W. and Jones, B. 1997. Controls on aragonite and calcite precipitation in hot spring travertines at Chemurkeu, Lake Bogoria, Kenya. *Canadian Journal of Earth Sciences*, **34**: 801-818.
- Riding, R. 1991. Calcified cyanobacteria. *in* Riding, R. (ed.). Calcareous Algae and Stromatolites. Springer-Verlag: Berlin, p. 55-87.
- Rippka, R., Deruelles, J., Waterbury, J.B., Herdman, M. and Stanier, R.Y. 1979. Generic Assignments, strain histories and properties of pure cultures of cyanobacteria. *Journal of General Microbiology*, **111**: 1-61.
- Round, E.E., Crawford, R.M. and Mann, D.G. 1990. The diatoms – biology and morphology of the genera. Cambridge University Press: Cambridge, p. 107-117.

- Ryves, D.B., Juggins, S., Fritz, S.C. and Battarbee, R.W. 2001. Experimental diatom dissolution and the quantification of microfossil preservation in the sediments. *Palaeogeography, Palaeoclimatology, Palaeoecology*, **172**: 99-113.
- Sauchyn, D.J. and Beaudoin, A.B. 1998. Recent environmental change in the southwestern Canadian plains. *The Canadian Geographer*, **42**(4): 337-353.
- Schneider, J. 1976. Biological and inorganic factors in the destruction of limestone coasts. *Contributions to Sedimentology*, **6**, 112p.
- Scholle, P.A. 1978. A colour illustrated guide to carbonate rock constituents, textures, cements, and porosities. AAPG Memoir 27. Rodgers Litho Press: Tulsa, Oklahoma.
- Simonsen, R. 1987. Atlas and catalogue of the diatom types of Freidrich Hustedt, Volume 2 – Atlas, Plates 1-139. Stuttgart/J. Cramer: Berlin.
- Spaulding, S.A. and Kociolek, J.P. 1998. The diatom genus *Orthoseira*: Ultrastructure and morphological variation in two species from Madagascar with comments on nomenclature in the genus. *Diatom Research*, **13**(1): 133-147.
- Squair, C.A. 1988. Surface karst on Grand Cayman Island, British West Indies. Master's Thesis, Department of Geology, University of Alberta.
- Tazaki, K., Miyata, K., Belkova, N. and Asada, R. 2001. Sr-rich microbial mats at Zhemchug hot springs, southwest Lake Baikal, Russia. *The Science Reports of Kanazawa University*, **46**(1): 67-78.
- Turi, B. 1986. Stable isotope geochemistry of travertines. *In* The terrestrial environments, B - Handbook of environmental isotope geochemistry, **2**. Edited by Fritz, P. and Fontes, J.C., p. 207-238.
- Vance, R.E., Beaudoin, A.B. and Luckman, B.H. 1995. The paleoecological record of 6ka BP climate in the Canadian prairie provinces. *Geographie physique et Quaternaire*, **49**(1): 81-98.
- van Everdingen, R.O. 1970. The Paint Pots, Kootenay National Park, British Columbia; acid spring water with extreme heavy-metal content. *Canadian Journal of Earth Sciences*, **7**(3): 831-852.
- van Everdingen, R.O. 1972. Thermal and Mineral Spring in the Southern Rocky Mountains of Canada. Water Management Service, Department of the Environment, Environment Canada.

- van Everdingen, R.O. 1980a. Investigations at Miette Hot Springs, Jasper National Park, Alberta: Preliminary report. Hydrology Research Division, National Hydrology Research Institute, Calgary, Alberta.
- van Everdingen, R.O. 1980b. Investigations at Miette Hot Springs, Jasper National Park, Alberta: Analytical Results. Hydrology Research Division, National Hydrology Research Institute, Calgary, Alberta.
- van Everdingen, R.O. 1980c. Investigations at Miette Hot Springs, Jasper National Park, Alberta: Recommendations for continuing measurements and considerations for redevelopment. Hydrology Research Division, National Hydrology Research Institute, Calgary, Alberta.
- van Everdingen, R.O. 1983. Dirty-water events at Rocky Mountain Hot Springs and their correlation with other short-lived phenomena. *Canadian Journal of Earth Sciences*, **21**: 997-1007.
- van Everdingen, R.O. 1986. Miette and Radium Hot Springs – results of periodic sampling May 1984 – February 1985. National Hydrology Research Institute, Environment Canada, Calgary, Alberta.
- van Everdingen, R.O. 1991. Physical, chemical, and distributional aspects of Canadian springs. *Memoirs of the Entomological Society of Canada*, **155**: 7-28.
- Verrecchia, E.P., Dumont, J-L. and Verrecchia, K.E. 1993. Role of calcium oxalate biomineralisation by fungi in the formation of calcretes: a case study from Nazareth, Isreal. *Journal of Sedimentary Research*, **63**(5): 1000-1006.
- Verrecchia, E.P. and Verrecchia, K.E. 1994. Needle-fibre calcite: a critical review and a proposed classification. *Journal of Sedimentary Research*, **A64**(3): 650-664.
- Viles, H.A. 1987. Blue-green algae and terrestrial limestone weathering on Aldabra Atoll: an SEM and light microscope study. *Earth Surface Processes and Landforms*, **12**: 319-330.
- Villeneuve, V. and Pienitz, R. 1998. Composition diatomifere de quatre sources thermals au Canada, en islande et au Japon. *Diatom Research*, **13**(1): 149-175.
- Vinson, D.K. and Rushforth, S.R. 1989. Diatom species composition along a thermal gradient in the Portneuf River, Idaho, USA. *Hydrobiologia*, **185** (1): 41-54.
- Walter, L.M. 1986. Relative efficiency of carbonate dissolution and precipitation during diagenesis: a progress report on the role of solution chemistry. *The Society of Economic Paleontologists and Mineralogists*.

- Walter, M.R. 1976. Hot-spring sediments in Yellowstone National Park. *In Stromatolites: Developments in Sedimentology 20*, Elsevier: Amsterdam. *Edited by* Walter, M.R., 489-498.
- Walter, M.R., Bauld, J. and Brock, T.D. 1976. Microbiology and morphogenesis of columnar stromatolites (*Conophyton*, *Vaccerrilla*) from hot springs in Yellowstone National Park. *In Stromatolites: Amsterdam, Elsevier, Developments in Sedimentology 20. Edited by* Walter, M.R., p. 497-518.
- Walter, M.R., Desmarais, D., Farmer, J.D., and Hinman, N.W. 1996. Lithofacies and biofacies of mid-Paleozoic thermal spring deposits in the Drummond Basin, Queensland, Australia. *PALOIS*, **11**: 497-518.
- Weed, W.H. 1889. Formation of travertine and siliceous sinter by the vegetation of hot springs. United States Geological Survey Annual Report. 9; Pages 613-676.
- Wickstrom, C.E. and Castenholz, R.W. 1985. Dynamics of cyanobacterial and ostracod interactions in an Oregon hot spring. *Ecology*, **66**(3): 1024-1041.
- Woodsworth, G. 1997. *Hotsprings of Western Canada*. Gordan Soles Book Publishers Ltd.: West Vancouver, Canada.



<p><b>UNICELLULAR</b></p> <p>Cells single or in colonial aggregates held together by additional outer cell wall layers</p>	<p><b>Reproduction by binary fission or budding</b></p> <p><b><i>Synechococcus</i></b></p> <ul style="list-style-type: none"> <li>- cells ovate to rod-shaped</li> <li>- unsheathed</li> <li>- thylakoids present</li> <li>- division in one plane</li> <li>- 1- 30 µm in length</li> <li>- slight blue-green hue</li> </ul>	<p><b><i>Gloeocapsa</i></b></p> <ul style="list-style-type: none"> <li>- spherical cells</li> <li>- division in two or three planes at right angles</li> <li>- thylakoids present</li> <li>- sheath present, may be concentric layers of sheath mucilage encasing multiple cells</li> </ul>
	<p><b>Reproduction by multiple fission yielding small daughter cells (baeocytes)</b></p> <p><b><i>Xenococcus</i></b></p> <ul style="list-style-type: none"> <li>- sub-spherical cells joined to neighbours forming cell masses which may be pseudo-filamentous in one plane</li> <li>- common epiphytes on filamentous algae (1)</li> </ul>	
<p><b>FILAMENTOUS</b></p> <p>Trichome straight, no branching or false branching</p> <p>Trichome composed of vegetative cells - no heterocysts or akinetes - grows by intercalary cell division</p> <p>Reproduction by forming hormogonia</p>	<p><b>Trichome unsheathed</b></p> <p><b><i>Oscillatoria</i></b></p> <ul style="list-style-type: none"> <li>- cells disc-shaped (2) to isodiametric or cylindrical (1, 3)</li> <li>- no constriction between cells, contain visible gas vesicles</li> <li>- trichomes are solitary or intermingled, not aligned</li> <li>- 1.5 - 30+ µm cell diameter</li> </ul>	<p>subdivision <i>Limnothrix</i>:</p> <ul style="list-style-type: none"> <li>- thin filaments</li> <li>- slight tapering with swollen apical cell</li> <li>- contain large gas vesicles concentrated at ends of cells (3)</li> </ul>
	<p><b>Trichome sheathed</b></p> <p><b><i>Phormidium</i></b></p> <ul style="list-style-type: none"> <li>- sheathed trichomes, 1.5 ~ 5 µm cell diameter</li> <li>- cells isodiametric to cylindrical</li> <li>- some constriction between cells</li> <li>- form sticky, resistant mats without erect tufts (1)</li> <li>- may form loose coils of one or more filaments (3)</li> <li>- distinguished from <i>Lyngbya</i> by having a "stickier" sheath (1)</li> </ul>	

**APPENDIX 1** - Summary of key features used to identify genera of cyanobacteria in microbial mats from the modern Miette Hot Springs. Some genera are poorly defined, thus controversial taxonomic indicators are followed by the source material in which they are described: 1- Prescott (1970), 2- Rippka *et al.* (1979), 3- Canter-Lund and Lund (1995).

## Appendix 2

Stable carbon and oxygen isotope values measured for successive laminae in stromatolitic tufa (sample M24 belongs to the dense laminar tufa facies, samples M13 and M22 belong to the porous laminar tufa facies, and sample M9 represents a transitional facies) and bulk sample measurements for a suite of samples collected along a down slope transect.

\* d = dark coloured laminae with flat-lying microbial structures

p = light coloured laminae with upright microbial structures

d/p = a pocket of dark coloured tufa with flat-lying microbial structures contained within a light coloured lamina with upright microbial structures.

M# = sample i.d. letter = subsampling lamina	type of lamina*	$\delta^{13}\text{C}$ PDB ( $\pm$ 0.41)	$\delta^{18}\text{O}$ SMOW ( $\pm$ 0.11)
M24-b	d	3.27	8.40
c	p	3.12	7.76
c'	d/p	3.25	7.99
d	d	2.93	7.39
e	p	2.76	6.97
f	d	4.02	8.70
g	p	2.83	7.09
M13-a	d	1.87	9.64
b	p	2.03	7.72
c	d	2.05	7.93
d	p	2.04	6.90
e	d	1.91	7.77
f	p	2.13	7.32
g	d	2.09	7.31
M22-b	d	3.22	8.48
c	p	3.15	8.28
d	d	2.75	8.24
e	p	2.76	7.43
f	d	3.19	8.73
g	d	3.19	8.15
h	p	3.09	7.86
i	d	3.11	8.66
j	p	3.40	8.82
M9-a	d	2.16	7.09
b	d	2.41	6.37
c	p	2.30	6.41
d	p	0.88	6.50
e	d	2.26	6.28
f	p	2.21	6.35
g	d	2.32	6.35
h	p	2.61	6.94
i	d	1.75	6.55
j	p	2.37	6.31
k	d	2.21	5.77
M2	n/a	3.04	7.68
M4	n/a	2.80	8.79
M5	n/a	2.83	8.11
M10	n/a	2.46	5.56
M11	n/a	2.91	6.82
M14	n/a	2.04	7.42
M17	n/a	2.74	6.78
M18	n/a	2.61	7.87
M19	n/a	2.63	7.97
M27	n/a	3.37	8.05
M28	n/a	3.35	7.49
M29	n/a	3.32	7.95